

NOTE TO USERS

This reproduction is the best copy available.

UMI[®]

UNIVERSITY OF OKLAHOMA

GRADUATE COLLEGE

AXIAL LOAD CAPACITY OF COLD-FORMED STEEL SECTIONS

A DISSERTATION

SUBMITTED TO THE GRADUATE FACULTY

in partial fulfillment of the requirements for the

degree of

Doctor of Philosophy

By

Chris C. E. Ramseyer

Norman, Oklahoma

2006

UMI Number: 3203326

Copyright 2005 by
Ramseyer, Chris C. E.

All rights reserved.

UMI[®]

UMI Microform 3203326

Copyright 2006 by ProQuest Information and Learning Company.
All rights reserved. This microform edition is protected against
unauthorized copying under Title 17, United States Code.

ProQuest Information and Learning Company
300 North Zeeb Road
P.O. Box 1346
Ann Arbor, MI 48106-1346

AXIAL LOAD CAPACITY OF COLD-FORMED STEEL SECTIONS

**A DISSERTATION APPROVED FOR THE
SCHOOL OF CIVIL ENGINEERING AND ENVIRONMENTAL SCIENCE**

BY

Kyran D. Mish, Chair

Benjamin Wallace

Kanthasamy K. Muraleetharan

Gerald A. Miller

Curtis C. McKnight

Jinsong Pei

©Copyright by CHRIS C. E. RAMSEYER 2006

All Rights Reserved.

Acknowledgements

I wish to thank the following individuals and groups for their support. Star Building Systems for providing funding and materials for the project. Dennis Watson and Pat Toney of Star Building Systems have been very helpful with their ideas for the test setup and experimental procedure.

I would like to thank my friends at Fears Structural Engineering Laboratory, University of Oklahoma for helping me with the tests and sharing their opinions. Without the friendship and support of Beth Brueggen and Vinay Thottunkal I would not have found this journey quite as enjoyable. I would like to thank Mike Schimitz's for having been helpful with setting up the testing equipment and instrumentation and for helping to ensure our safety in the lab.

I would like to express my appreciation to Dr. Kim Mish for being my advisor and chair of my Defense committee. He has been a true mentor through the entire process of earning my doctorate. I would like to thank Dr. Ben Wallace, Dr. K.K. Muraleethran, Dr. Curtis McKnight, Dr. Gerald Miller and Dr. Jinsong Pei for giving up hours of their time to act as members of my committee and I would also like to thank them for their helpful comments.

Finally, I would also like to thank my wife, Karen Barker, for her support and encouragement throughout this research. Without her good natured support none of the work would have been possible.

Dedication

To

Karen Barker

Thanks for all the wonderful years together!

Table of Contents

Acknowledgements	iv
Dedication.....	v
List of Figures.....	xiv
List of Tables	xviii
Abstract.....	xxi
Chapter 1 Introduction.....	1
1.1 Summary of Problem.....	4
1.1.1 Purlins	4
1.1.2 Built-up Members	5
1.2 Objective of Research.....	7
1.2.1 Purlins	7
1.2.2 Built-up Members	7
1.3 Scope of Research.....	7
1.3.1 Purlins	7
1.3.2 Built-up Members	8
Chapter 2 Background and Literature Review	9
2.1 Background.....	9
2.1.1 Purlins	9

2.1.1.1 Through-fastened Roof	12
2.1.1.2 Standing Seam Roof.....	13
2.1.2 Built-up Members	17
2.1.2.1 Joists	17
2.1.2.2 Compression Elements.....	20
2.2 Literature Review	22
2.2.1 Purlins	22
2.2.1.1 Elastic Buckling of Cold-Formed Steel Compression Members	22
2.2.1.2 AISI Specification (2002)	28
2.2.1.3 Direct Strength Method.....	32
2.2.1.4 Empirical Studies of Purlin Struts.....	35
2.2.1.4.1 Simaan and Pekoz.....	35
2.2.1.4.2 Dimos and Sudharmapal.....	37
2.2.1.4.3 Hatch, Murray and Ellifritt	37
2.2.1.4.4 Fisher, Kaehler and Glaser	39
2.2.1.4.5 Stolarczyk and Fisher	43
2.2.1.4.6 Summary of Empirical Studies of Purlin Struts	44
2.2.2 Built-up Members	44
2.2.2.1 Bleich.....	45
2.2.2.2 Zandonini.....	48

2.2.2.3 Aslani and Goel	48
2.2.2.4 Sherman and Yura	49
2.2.2.5 AISI <i>Specification C4.5</i> (2002)	51
2.2.2.6 Eccentric Intermediate Connections.....	53
Chapter 3 Purlin Testing Program.....	54
3.1 Purlins with Standing Seam Roofing.....	55
3.1.1 Tests with Four Purlins	55
3.1.1.1 Test Objective and Description	55
3.1.1.2 Instrumentation and Data collected.....	61
3.1.1.3 Test Procedure.....	62
3.1.2 Tests with Two Purlins and Without Lateral Restraint.....	64
3.1.2.1 Test Objective and Description	64
3.1.2.2 Instrumentation and Data collected.....	68
3.1.2.3 Test Procedure.....	69
3.1.3 Tests with Two Purlins with Lateral Restraint	69
3.1.3.1 Test Objective and Description	69
3.1.3.2 Instrumentation and Data collected.....	73
3.1.3.3 Test Procedure.....	74
3.2 Purlins with No Roofing.....	74

3.2.1 Tests with Two Purlins but without Lateral Restraint	75
3.2.1.1 Test Objective and Description	75
3.2.1.2 Instrumentation and Data collected.....	79
3.2.1.3 Test Procedure.....	80
3.2.2 Tests with Two Purlins and Lateral Restraint.....	81
3.2.2.1 Test Objective and Description	81
3.2.2.2 Instrumentation and Data collected.....	85
3.2.2.3 Test Procedure.....	85
Chapter 4 Built-up Member Testing Program.....	86
4.1 Tests with Fixed End Conditions.....	86
4.1.1 Test Objective and Description.....	87
4.1.2 Instrumentation and Data collected.....	89
4.1.3 Test Procedure.....	89
4.2 Tests with Pinned End Conditions.....	90
4.2.1 Test Objective and Description.....	91
4.2.2 Instrumentation and Data collected.....	93
4.2.3 Test Procedure.....	93
Chapter 5 Test Results.....	94
5.1 Purlins with Standing Seam Roof Panel.....	94

5.1.1 Tests with Four Purlins	94
5.1.1.1 12 inch deep purlins	94
5.1.1.2 14 inch deep purlins	95
5.1.2 Tests with Two Purlins and no Lateral Restraint.....	96
5.1.2.1 12 inch deep purlins	97
5.1.2.2 14 inch deep purlins	98
5.1.3 Tests with Two Purlins and Lateral Restraint.....	98
5.1.3.1 12 inch deep purlins	98
5.1.3.2 14 inch deep purlins	99
5.2 Purlins with No Roofing.....	99
5.2.1 Tests with Two Purlins and no Lateral Restraint.....	100
5.2.2 Tests with Two Purlins and Lateral Restraint.....	102
5.3 Built-up Members.....	105
5.3.1 Tests with Fixed End Conditions.....	105
5.3.2 Tests with Pinned End Conditions.....	108
Chapter 6 Discussion of Test Results.....	116
6.1 Purlins with Standing Seam Roofing.....	116
6.1.1 Tests with Four Purlins	117
6.1.2 Tests with Two Purlins and No Lateral Restraint.....	118

6.1.3 Tests with Two Purlins and Lateral Restraint.....	118
6.2 General discussion of experimental purlin capacities	119
6.3 Calculation of the Purlin Design Capacity	123
6.4 Comparison of Purlin Experimental to Theoretical Design Values	125
6.4.1 Two purlin tests without lateral restraint but with roof panel.....	125
6.4.1.1 Direct Strength Method (2004)	127
6.4.1.2 AISI <i>Specification</i> (2002).....	130
6.4.1.3 Fisher's Method (1993).....	131
6.4.2 Two Purlin Tests with Lateral Restraint and roof panel	132
6.4.2.1 Direct Strength Method (2004)	133
6.4.2.2 AISI Specifications (2002).....	134
6.4.3 Tests with Two Purlins without Lateral Restraint or roof panel.....	136
6.4.3.1 Direct Strength Method (2004)	137
6.4.3.2 AISI Specifications (2002).....	138
6.4.4 Tests with Two Purlins Without roof Panel but with Lateral Restraint	139
6.4.4.1 Direct Strength Method (2004)	140
6.4.4.2 AISI Specifications (2002).....	141
6.4.5 Comparison of Experimental and AISI (2004) Capacities	142

6.4.6 Comparison of Purlin Experimental to Theoretical Design Values.....	143
6.5 Built-up Members.....	145
6.5.1 Tests with Fixed End Conditions.....	145
6.5.1.1 Tests without intermediate stitch welding.....	146
6.5.1.2 Tests with a stitch weld on one side at mid-length	148
6.5.1.3 Tests with stitch welds on one side at third points.....	149
6.5.1.4 Tests with stitch welds on both sides at third points.....	149
6.5.1.4 Comparison of Experimental and Theoretical Capacities.....	149
Chapter 7 Conclusions and Recommendations.....	154
7.1 Conclusions.....	154
7.1.1 Purlins	154
7.1.2 Built-up Members	156
7.2 Recommendations.....	157
7.2.1 Purlins	157
7.2.2 Built-up Members	158
References	160
APPENDIX A - Section Properties of Purlin Test Specimens	163
APPENDIX B - Purlin Axial Load Vs Axial Deflection Plots.....	165
APPENDIX C - Purlin Direct Strength Method Plots	183

APPENDIX D - Purlin AISI Effective Method Capacity Calculation	188
APPENDIX E - Section Properties of Built-up Test Specimens	197
APPENDIX F - 55" – 1 5/8" Built-up Member, Fixed End, Load vs. Deflection Plots	199
APPENDIX G - 55" – 1 5/8" Built-up Member, Pinned End Load vs. Deflection Plots	210
APPENDIX H - 71" – 1 5/8" Built-up Member, Pinned End Load vs. Deflection Plots	215
APPENDIX I - 71" – 2 ½" Built-up Member, Pinned End Load vs. Deflection Plots	228

List of Figures

Figure 2.11 (a) A Typical Metal Building.....	10
Figure 2.12 (b) Double Purlin Strut.....	11
Figure 2.23 Cross Section Detail of Through Fastened Roof.....	13
Figure 2.34 Cross Section Detail of Standing Seam Roof.....	14
Figure 2.45 (a) Clip Mounted On a Purlin (b) Roof Panel Attached To Clip.....	14
Figure 2.56 (a) Unseamed (b) Seamed - Cross-Section of Standing Seam Roof	16
Figure 2.67 Bar Joist vs. Cold-Formed Joist – elevation view	19
Figure 2.78 Bar Joist vs. Cold-Formed Joist – Section view	19
Figure 2.89 First Web Member of Cold-Formed Joist – Elevation view.....	21
Figure 2.910 Buckling Modes of Cold-Formed Steel Zee's.....	23
Figure 2.1011 Post Buckling Strength Model.....	25
Figure 2.1112 Stress Distribution in Stiffened Compression Elements.....	27
Figure 2.1213 Cold-Formed Zee Section Dimensions.....	33
Figure 2.1314 Direct Strength Method Flow Chart	34
Figure 3.115 Test Configurations.....	54
Figure 3.216 Test Set Up.....	56
Figure 3.317 Cee Channel In Between Purlins To Prevent Lateral Sway	57
Figure 3.418 Plan View of Test Setup (4 Purlin Test).....	59
Figure 3.519 Test Supports and Spreader Beam	60
Figure 3.620 Four Purlin Test Setup without Roof Panel.....	61

Figure 3.721	LVDT Placement	62
Figure 3.822	Plan View of Test Setup (2 Purlin w/o Lateral Restraint)	66
Figure 3.923	Test Supports and Spreader Beam	67
Figure 3.1024	Two Purlin Test without Lateral Restraint	68
Figure 3.1125	Plan View of Test Setup (2 Purlin w/ Lateral Restraint)	70
Figure 3.1226	Test Supports and Spreader Beam	71
Figure 3.1327	Lateral Restraints	72
Figure 3.1428	Measurement of Lateral Force Using Load Cell	73
Figure 3.1529	Plan View of Test Setup (2 Purlin w/o Lateral Restraint)	76
Figure 3.1630	Test Supports and Spreader Beam	77
Figure 3.1731	Two Purlin Test with out Lateral Restraint	78
Figure 3.1832	Plan View of Test Setup (2 Purlin with Lateral Restraint)	82
Figure 3.1933	Test Supports and Spreader Beam	83
Figure 3.2034	Two Purlin Test with Lateral Restraint.....	84
Figure 4.1 35	Web member pairs	87
Figure 4.236	Specimen with fixed end condition ready for testing	88
Figure 4.337	Specimen with pinned end condition ready for testing.....	92
Figure 5.138	Local Buckling Of the Web Due To Axial Compression.....	95
Figure 5.239	Purlins Undergoing Large Side Sway.....	96
Figure 5.340	Local Buckling along Entire Length of Two-Purlin Test.....	97
Figure 5.441	Local Buckling of Top Flange	99
Figure 5.542	Global failure of unrestrained test of purlins with no roof panel	101

Figure 5.643 Distortional failure for restrained test of purlins with no roof panel	103
Figure 5.744 Distortional and Local failure for restrained test of purlins with no roof panel.....	104
Figure 5.845 Ultimate buckling loads of built-up column test specimens.....	107
Figure 5.946 Ultimate buckling loads w/ pinned ends, 1 ⁵ / ₈ " sections, 55" Long .	109
Figure 5.1047 Ultimate buckling loads w/ pinned ends, 1 ⁵ / ₈ " section, 71" Long..	110
Figure 5.1148 Ultimate buckling loads w/ pinned ends, 1 ⁵ / ₈ " section, 71" Long.	111
Figure 5.1249 Ultimate buckling loads w/ pinned ends, 1 ⁵ / ₈ " section, 71" Long.	112
Figure 5.1350 Ultimate buckling loads w/ pinned ends, 2 ¹ / ₂ " section, 71" Long.	113
Figure 5.1451 Ultimate buckling loads w/ pinned ends, 2 ¹ / ₂ " section, 71" Long.	114
Figure 5.1552 Ultimate buckling loads w/ pinned ends, 2 ¹ / ₂ " section, 71" Long.	115
Figure 6.153 Capacity Comparison of a Single Purlin with Roof Panel.....	116
Figure 6.254 Capacity Comparison of a Single Purlin.....	119
Figure 6.355 Capacity Comparison due to bracing.....	120
Figure 6.456 Capacity comparison of 12Z100 purlins due to section stability	121
Figure 6.557 Capacity comparison of 12Z100 purlins due to section stability	122
Figure 6.658 Capacity comparison of 12Z100 purlins.....	123
Figure 6.759 Experimental Capacity Vs Theoretical Capacity.....	127
Figure 6.860 Stress Vs Half Wavelength of 12Z80 Specimen	128
Figure 6.961 Experimental Capacity Vs Theoretical Capacity.....	133
Figure 6.1062 Experimental Capacity Vs Theoretical Capacity.....	137

Figure 6.1163	Experimental Capacity Vs Theoretical Capacity	140
Figure 6.1264	Experimental vs. AISI C4.7 Capacities	143
Figure 6.1365	Unrestrained Experimental vs. Design Capacities.....	144
Figure 6.1466	Restrained Experimental vs. Design Capacities	144
Figure 6.1567	Deformed shape of paired members with no stitch welds	147
Figure 6.1668	Buckling of typical specimen with no stitch welding.....	147
Figure 6.1769	Buckling of specimen with stitch welding on one side	148
Figure 6.1870	Typical elastic buckling curves used with DSM	152

List of Tables

Table 2.21 Section Properties Deemed Important By Simaan and Fisher	40
Table 2.32 Summary of Previous Tests Performed On Cold-Formed Zee sections	44
Table 3.13 Test Section Properties (Four Purlin Tests)	57
Table 3.24 Test Section Properties (Two Purlin w/o Lateral Restraint)	68
Table 3.35 Test Section Properties (Two Purlin w/ Lateral Restraint & roof panel)	72
Table 3.46 Test Section Properties (Two Purlin w/o Lateral Restraint or Roof Panel).....	79
Table 3.67 Test Section Properties (Two Purlin w/ Lateral Restraint w/o Roof Panel).....	85
Table 5.18 Axial Capacity of a Single Purlin in Tests with Standing Seam Roofing	94
Table 5.29 Axial Capacity of A Single Purlin in Tests without Roof Panel.....	100
Table 5.310 Average ultimate buckling loads w/ fixed ends	106
Table 5.411 Ultimate buckling loads w/ pinned ends, 1 ⁵ / ₈ " section, 55" Long	109
Table 5.512 Ultimate buckling loads w/ pinned ends, 1 ⁵ / ₈ " section, 71" Long	110
Table 5.613 Ultimate buckling loads w/ pinned ends, 1 ⁵ / ₈ " section, 71" Long	111
Table 5.714 Ultimate buckling loads w/ pinned ends, 1 ⁵ / ₈ " section, 71" Long	112
Table 5.815 Ultimate buckling loads w/ pinned ends, 2 ¹ / ₂ " section, 71" Long ...	113
Table 5.916 Ultimate buckling loads w/ pinned ends, 2 ¹ / ₂ " section, 71" Long	114

Table 5.10	17 Ultimate buckling loads w/ pinned ends, 2½" section, 71" Long..	115
Table 6.1	18 Experimentally Calculated Design Capacities of a Single Purlin (4 Purlin Test).....	124
Table 6.2	19 Experimentally Calculated Design Capacities of a Single Purlin (Tests with no roof panel or lateral restraint).....	125
Table 6.3	20 Comparison of Experimental and Theoretical Capacities.....	126
Table 6.4	21 Comparison of Experimental and DSM (2004) Values.....	129
Table 6.5	22 Geometric Restriction of AISI (2002) & DSM (2004).....	130
Table 6.6	23 Geometric Restrictions of Fisher (1993).....	131
Table 6.7	24 Comparison of Experimental and Theoretical Capacities.....	132
Table 6.7	25 Comparison of Experimental and DSM (2004) Capacities.....	134
Table 6.8	26 Comparison of Experimental and AISI (2002) Capacities.....	135
Table 6.9	27 Comparison of Experimental and Theoretical Capacities.....	136
Table 6.10	28 Comparison of Experimental and DSM (2004) Capacities.....	138
Table 6.11	29 Comparison of Experimental and AISI (2002) Capacities.....	139
Table 6.12	30 Comparison of Experimental and Theoretical Capacities.....	139
Table 6.10	31 Comparison of Experimental and DSM (2004) Capacities.....	141
Table 6.11	32 Comparison of Experimental and AISI (2002) Capacities.....	142
Table 6.12	33 Design phi-factors and buckling capacities of selected built-up configurations.....	146
Table 6.13	34 Experimental vs. theoretical capacities.....	150

Abstract

Columns, or compression elements, are fundamental structural elements that exist in all but a few types of structures. Columns, or compression elements, made from cold-formed steel are fairly new products that have not been well studied. The code for the design of cold-formed steel built-up members is based on eleven hot-rolled tests while the code for cold-formed deep purlin design is based on three tests.

Cold-formed steel strut purlins are important compression members in metal building wind bracing systems. They are generally located under the roof panel either in the braced bay or between the end wall and the first wind-braced bay in the building. Cold-formed Zee and Cee sections are typically used for strut purlins. The axial capacities of these members are often controlled by local and distortional buckling. These buckling modes can lead to a substantial reduction in the load-bearing capacity of these members. The current trend towards deeper, more slender sections makes this stability problem even more critical.

The current criteria for calculating the axial load capacity of cold-formed Zee section strut purlins is based upon experimental studies conducted with sections up to 10 inches deep and 25 feet long, with h/t ratios between 100 and 135. This study investigates 12 and 14 inch deep strut purlins that are 30 to 40 feet long, with h/t ratios between 120 and 150. The results of full-scale testing of roof systems were compared to the theoretical capacities of the current AISI

Specification and the Direct Strength Method. With strut purlins with no lateral bracing, it was found that the current design method is unconservative for sections with depths greater than 10 inches, and the Direct Strength Method tends to yield similar unconservative capacities. For the strut purlins with lateral bracing it was found that the current methods are marginally unconservative for deep Zee purlins and become increasingly unconservative for the heaviest 14 inch deep Zee purlins. Similar unconservative results are seen when the experimental results for built-up members are compared to the AISI Specification and the Direct Strength Method.

Chapter 1 Introduction

Humanity has been concerned with safe structures for our known history. The Code of Hammurabi, an early Babylonian king, dates from around 1780 B.C. and is the earliest complete code of law that is known to mankind. The 228th through 233rd "laws of justice" in the Code deal with the construction of houses. For example number 229 states "If a builder build(s) a house for some one, and does not construct it properly, and the house which he built fall(s) in and kill(s) its owner, then that builder shall be put to death" (King 1998).

The column is the fundamental element in resisting collapse under gravity loads. This is true in both man-made and natural structures, in buildings and bridges or trees and plants. For approximately the next 3500 years our understanding of columns was based upon crude "rules of thumb" and craft hall design theory. These methods were plagued by unexpected failures, because the stability of compression members was not understood. Which, following the Code of Hammurabi, surely would have resulted in the unfortunate demise of more than a few builders.

Our modern history of column theory dates to Leonard Euler, who published his famous column formula in 1744 A.D. in the appendix of a paper on maxima and minima which has become known as the "Elastica" (Euler 1744). Euler's method of solving for equilibrium of the deformed (i.e. buckled) member to establish a theoretical buckling threshold was revolutionary, and this approach forms the basis of all compression member design today. However, his critical

elastic global buckling load illuminated only one of many column stability issues. According to Dr. Galambos, known today as the father of Load and Resistance Factored Design (LRFD) for typical steel construction, "The theoretical developments since (Euler) represent some of the finest achievements in the discipline of applied mechanics" (Galambos, 1998). However, many column stability issues remain poorly understood and are addressed only through empirical observations. Local and distortional buckling of cold-formed steel members remain especially poorly understood.

In modern hot rolled steel design, Euler's equation has been modified due to empirical data and reformed into design equations. The design equations are based on the work of the Column Research Council (CRC) and the Structural Stability Research Council (SSRC) the predecessor of the CRC. These design equations are based on an initial out-of-straightness equal to $1/1500$ (Bjorhovde 1972 & 1988, Galambos 1998, & Tide 1985) and are empirically derived from tests where global buckling was the sole failure mode.

To address other failure modes the AISC code (AISC 2001) divides columns into "slender" and "non-slender". Typical column design is "non-slender", fails due to global buckling and is not sensitive to more complex local buckling modes. The hot-rolled steel design *Specification* (AISC 2001) does include limited provisions for slender columns in an appendix. This procedure uses a reduction factor Q_s to reduce the design strength using the typical, "non-slender" column capacity equations to accommodate "slender" columns and is

limited to local buckling failure modes where the critical element is stiffened and under uniform stress. These provisions are rarely used in practice. There are few hot rolled sections available that are slender and therefore sensitive to local buckling. Only 59 of 276 wide flange shapes listed in Chapter 1 of the AISC Manual of Steel Construction (2001) are sensitive to local buckling if the yield strength of the material is not more than 36 ksi. These sections are very rarely used as columns because they have been optimized to be very efficient as beams, but are inefficient as columns. It would be fair to say that most structural engineers avoid "slender" steel column design.

In general, cold-formed members are more difficult to design than conventional hot-rolled members. This is because of their thinness, cold formed residual stresses and because of the lack of section standardization. Unlike hot-rolled members, cold-formed members can be manufactured in small quantities of unusual shapes. The thinness of the material leads to a tendency for more complicated local and distortional buckling modes to control the design. As a result, the compression member provisions in the governing cold-formed steel design provisions (AISI 2002) must be much more extensive than those in the AISC provisions for hot-rolled steel. Specifically, the cold-formed provisions must account for global, distortional, and local buckling modes, and the interactions between these modes.

This dissertation describes the investigation of two important issues that are beyond the level of current understanding, in the design of cold-formed steel compression members:

- 1) the capacity of long, deep Zee purlins
- 2) the capacity of Cee sections used as built-up members

While these issues are not directly related to each other, they are related to the larger issue of thin-walled column behavior where the failure mode is not limited to global buckling.

1.1 Summary of Problem

In the last five years there has been an increasing demand in the market place for buildings that have a bay spacing larger than historically possible with cold-formed purlins but still shorter than economical "long bay" construction with bar joists. The metal building industry has pursued a solution to this by considering building with longer, deeper cold-formed purlins or with cold-formed steel joists. Both of these options are presently being sold or developed by metal building manufacturers, but both products present significant, unaddressed compression member design issues.

1.1.1 Purlins

If the longer, deeper cold-formed purlins are accepted as an economical solution to bay spacing in the 30 to 40 foot range, these sections will also be required to act as axial strut purlins. Strut purlins transfer wind loads on an end

wall into the rod bracing system and act as columns. Current design procedures are not suitable for the analysis and design of these compression members, especially when they are used with a standing seam roof. These sections fall outside the limitations of the existing cold-formed steel design specification (AISI *Specification* 2002), and they are beyond the scope of previous research (Fisher et al 1993, Hatch et al 1991). Because of their increased slenderness, deeper cold-formed Zee sections are more susceptible to local and distortional buckling modes than their relatively compact predecessors.

1.1.2 Built-up Members

If the cold-formed steel joists are accepted as an economical solution to bay spacing in the 30 to 60 foot range, many elements must act in compression. Joists, at their simplest, can be analyzed as trusses. As such, each element of the truss acts as a two force member, either in tension or compression. While there is little redundancy within a joist to redistribute the load away from an unstable member, the design of these elements is well within the scope of the existing cold-formed steel design specification (AISI *Specifications* 2002).

In general, manufacturers would like to build cold-formed joists with the same web section through out the joist. This would simplify the construction process and also make it less likely for a catastrophic error due to switching two members that are similar in every aspect except thickness. The problem with this approach lies in the behavior of trusses. Under a typical uniform roof load, the

shear force on the joist as a whole increases as the bearing area is approached. These global shear forces are carried by the web members in tension and compression. The web member closest to the bearing seat at each end of the joist must resist the highest axial loading. Using a member thickness adequate for this most highly loaded web member leads to excess material in the joist. However, using two web members at this critical location reduces the required thickness of the web section throughout the joist, resulting in a significant economic advantage.

To improve the structural efficiency of this pair of web members they can be welded to one another at discrete points. By doing so they become, what AISC defines as "built-up members." In 2001, when this research was initiated, the existing cold-formed steel design specification (*AISI Specification 1997*) did not include provisions for built-up members. Since then the specification has been amended to include these members. However, this revision is based on existing research that is limited to hot-rolled steel members, and when the AISI task force voted to adopt the built-up member provision they also voted to initiate research to verify that the provision was accurate for cold formed sections. The task force also planned to significantly revise the built-up member provision at the next code cycle based upon their agreed upon research. Unfortunately the planned research, that the task force used to support the adoption of the revision, was never funded (Schafer 2005). This research addresses these deficiencies.

1.2 Objective of Research

1.2.1 Purlins

The primary objective of this research is to develop a method for estimating the axial load capacities of cold-formed Zee members with deeper sections than previously studied. A secondary objective is to determine if the AISI (American Iron and Steel Institute) equations for standing seam roof systems are valid for use with sections deeper than 10 inches. This research will examine if equations previously developed for through-fastened roof panel can be used to predict the axial load capacities of strut purlins with standing seam roof systems.

1.2.2 Built-up Members

The primary objective of this research is to develop a method for estimating the axial load capacities of built-up cold-formed members connected by discrete stitch welds. A secondary objective is to determine if the current AISI equations for built-up members, adopted in 2002 are valid.

1.3 Scope of Research

1.3.1 Purlins

Three different types of test configurations with roof panel are considered in this research. The tests were conducted using 12 and 14 inch deep Zee sections with two different thicknesses of each. The 12 inch deep sections were 30 foot long, and the 14 inch deep sections were 40 foot long. The members were loaded axially since a strut purlin functions as a member resisting axial load. Five tests of each member type with roof panel were considered which resulted in a total of

twenty tests. There were twelve tests with four purlins, four tests with two purlins without lateral restraints and four tests with two purlins with lateral restraints.

Two different types of test configurations without roof panel are considered in this research. Each set up is tested with members having two different depths and two different thicknesses per depth, or four distinct member types. The members were loaded axially in a similar manner to a strut purlins' function as part of a structural, lateral load resisting system. Seven or Eight tests of each member type without roof panel were considered which resulted in a total of thirty tests. There were fifteen tests with two purlins without lateral restraints and fifteen tests with two purlins with lateral restraints.

1.3.2 Built-up Members

The testing program for the built-up members involved a total of sixty tests with fixed end rotation and eighty tests with pinned end rotation. Various discrete stitch-welded configurations are tested and two different member lengths are tested. Stitch configurations include one sided welds and welded on both sides. The specimens tested are 1 5/8" x 1 5/8" lipped cees that were tested at 55 inches and 71 inches in length. All specimens were welded on both sides at the top and bottom of the built-up member.

Chapter 2 Background and Literature Review

2.1 Background

Approximately seventy percent of all new low rise nonresidential buildings in the United States are metal buildings. These structures can be used in multiple ways. They are used as warehouses, shopping centers, schools, barns, office buildings, casinos, and churches. Metal buildings are structurally efficient and can be constructed in a very short time when compared to traditional steel or reinforced concrete buildings. This efficiency makes them very economical. Additionally, metal buildings give the end user total design flexibility. Figure 2.1 shows a typical metal building consisting of primary (metal frames and columns) and secondary (purlins and girts) structural members.

For the last five years, there has been a growing demand for buildings with long bays between the frames. This has been documented by a growth of sales in "long bay" buildings by Star Building Systems, the third largest manufacturer of metal buildings in the United States. To economically span the longer bay spacing requires much deeper Zee purlins or cold-formed joists.

2.1.1 Purlins

Historically, 8 inch deep Zee purlins were "typical"; today, 12 inch deep Zee purlins are common, and 14 inch Zee purlins are being manufactured (Toney 2003). In addition to resisting gravity or uplift loads, metal buildings must also resist lateral loads due to wind or seismic events. Some of the roof purlins, called "strut purlins," are part of the wind bracing system of the building. They are

1. Applied Wind Load
 2. Endwall Column with Wind Load
 3. Purlin Strut
 4. Double Strut
 5. Rods (Roof)
 6. Eave Strut
 7. Rods (Wall)
- Note: Arrows show the load path*

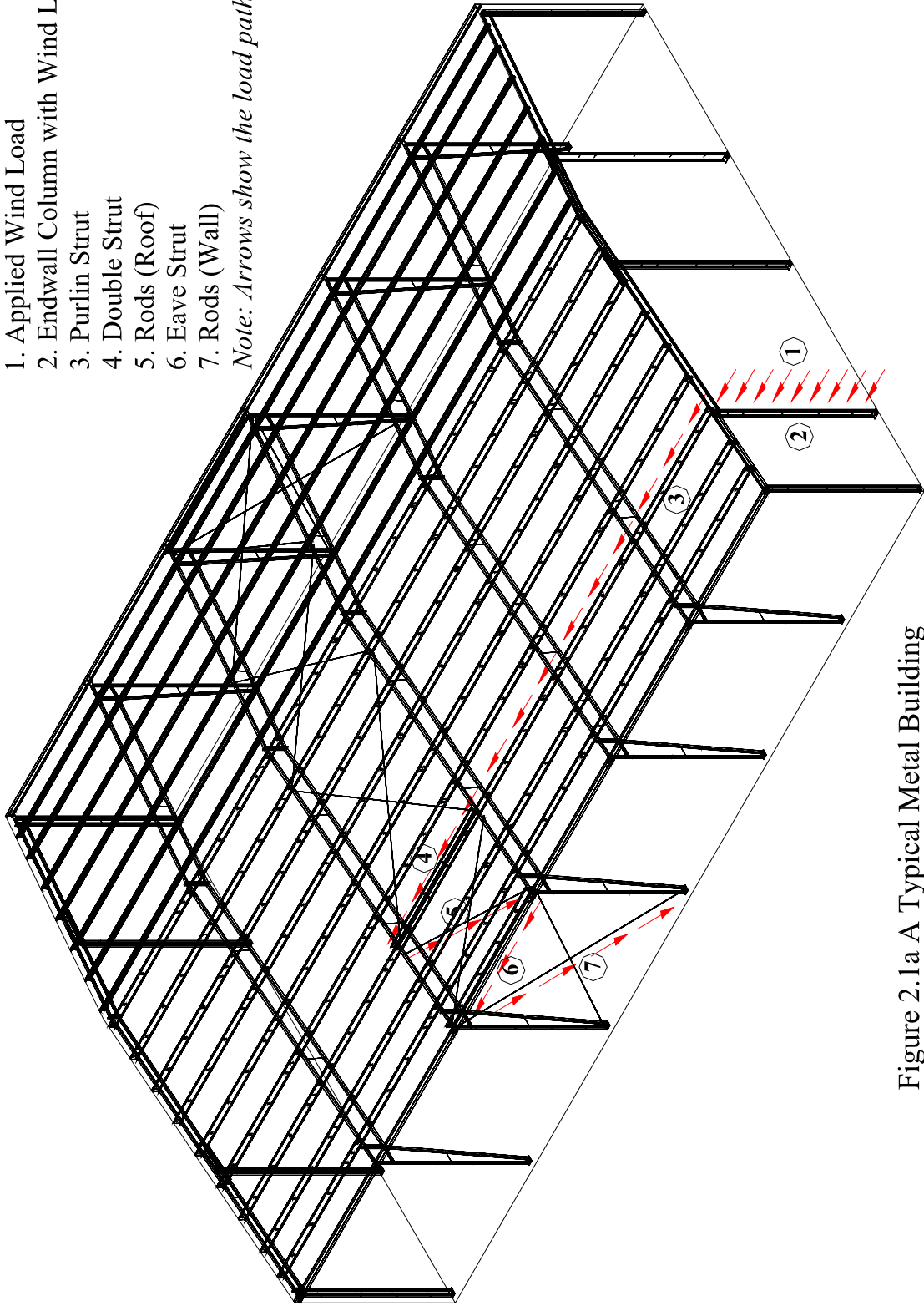


Figure 2.1a A Typical Metal Building

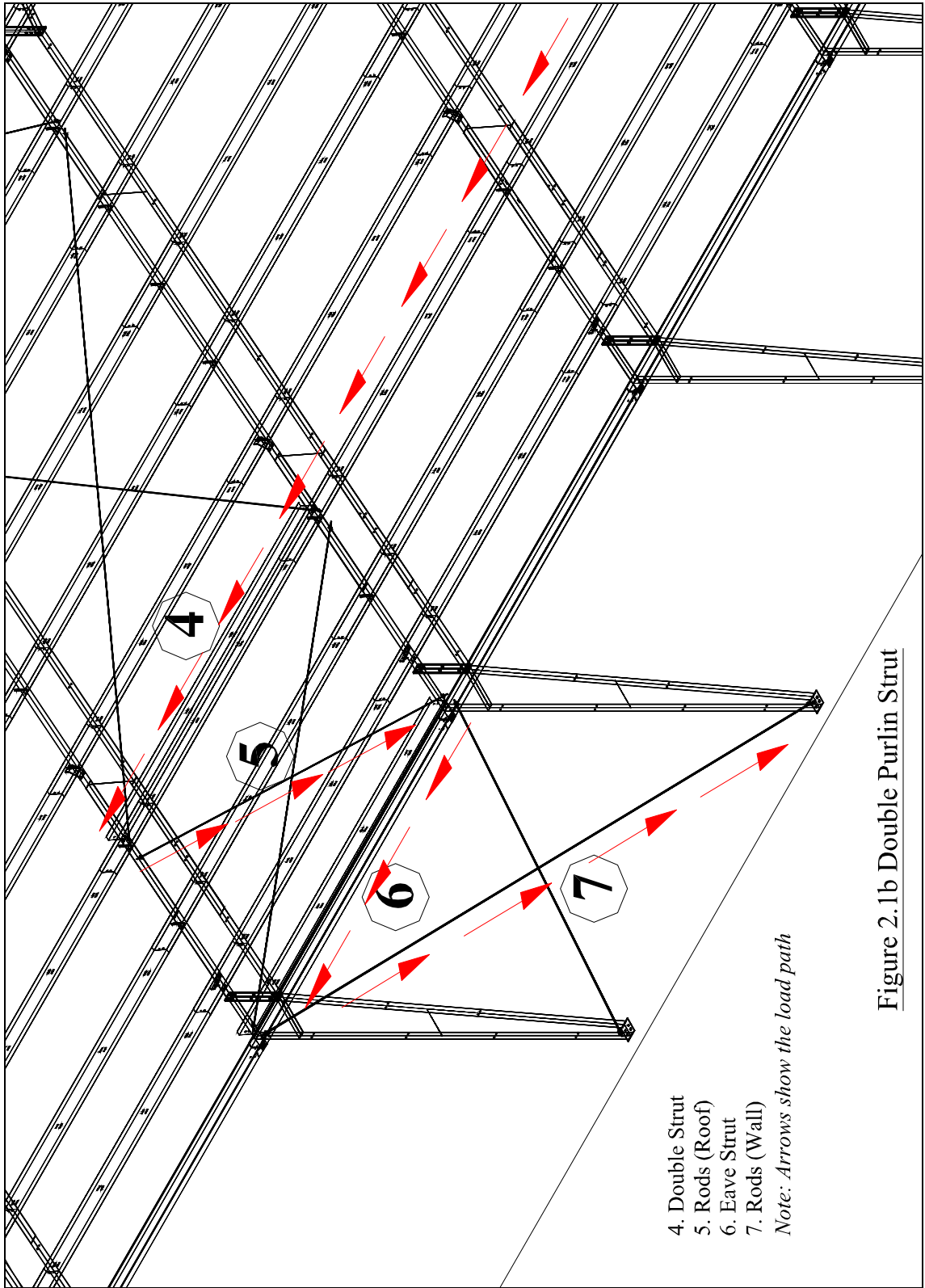


Figure 2.1b Double Purlin Strut

named this because they are designed to carry axial loads in a roof system and to differentiate them from standard, flexure only, purlins.

Strut purlins are required for structural stability. They are typically made from cold-formed Zee sections and are located in the braced bay or between the end wall and the first wind-braced bay in the building. Strut purlins carry the wind load from the end wall to the braced frame in axial compression. They are attached to the roof panel in the same way as a typical purlin supporting the roof and are designed to carry combined axial and bending loads. In some cases the roof panel acts as a diaphragm and its in-plane stiffness provides the purlin some restraint against lateral-torsional buckling.

There are two common roof systems that are used in metal buildings: through-fastened and standing seam. Through-fastened roofs have been used since metal buildings first came into the market in the 1940's. Standing seam roofs have many advantages over through-fastened roofs, and they have slowly increased their market share in the metal building industry the 1970's

2.1.1.1 Through-fastened Roof

In a through-fastened roof, the steel roof panel is attached directly to the purlin with self tapping screws, as shown in Figure 2.2. The direct attachment of the roof panel to the purlins gives the roof system additional rigidity, which increases its strength and stability. Through-fastened roof systems do have some disadvantages. When the roof is installed, the steel panels are punctured. A

neoprene washer is built into the screw is intended to provide weather tightness around the hole. However, thermal effects (expansion and contraction of the roof) cause the roof panel to move, which can cause the screw hole to elongate. Over time, the holes can become larger than the washers on the screws, leading to leaks and corrosion. Also, the neoprene washers eventually deteriorate and fail, leading to another avenue for leaks. Another disadvantage of through-fastened roof systems is that the roof insulation must be discontinuous. It can only be installed between the purlins. This makes installing the roof system more labor-intensive, and it decreases the energy efficiency of the roof.

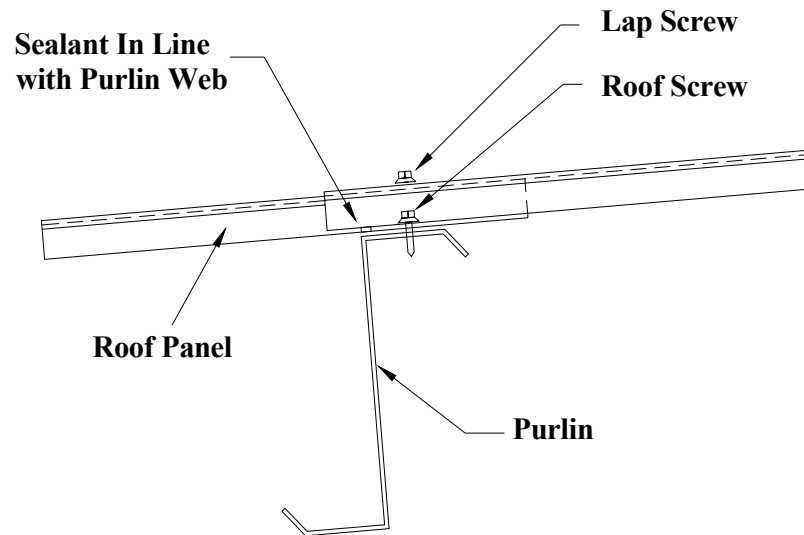


Figure 2.2 Cross Section Detail of Through Fastened Roof
Courtesy: Star Building Systems

2.1.1.2 Standing Seam Roof

Standing seam roof systems were developed to address the weathering problems associated with through-fastened roof systems. A standing seam roof panel is not directly attached to the purlins. This is shown in Figure 2.3. The panel

is elevated above the purlins on a metal clip. This offset allows the insulation to be continuous over the purlins. The batts are compressed between the purlin and the roof panel in the space provided by the clips. The thickness and style of this clip vary according to the manufacturer, but several generalizations can be made.

Figure 2.4 shows a typical metal clip used by Star Building Systems.

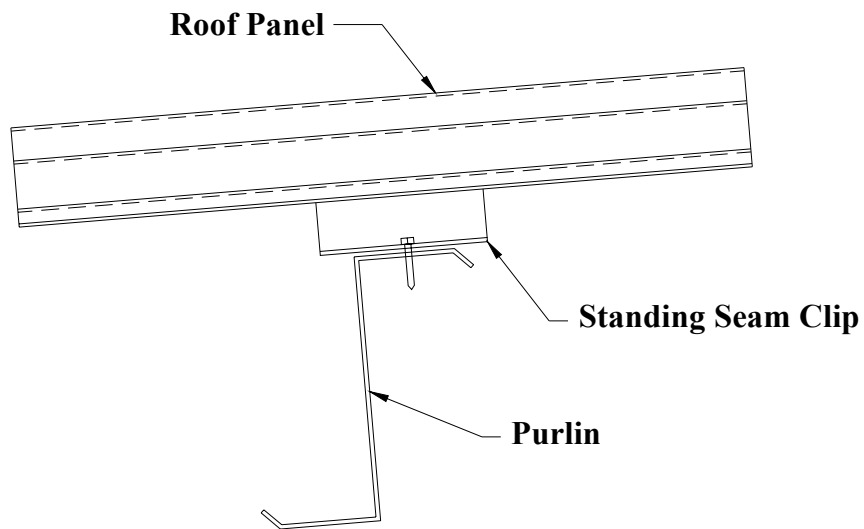


Figure 2.3 Cross Section Detail of Standing Seam Roof
 Courtesy: Star Building Systems

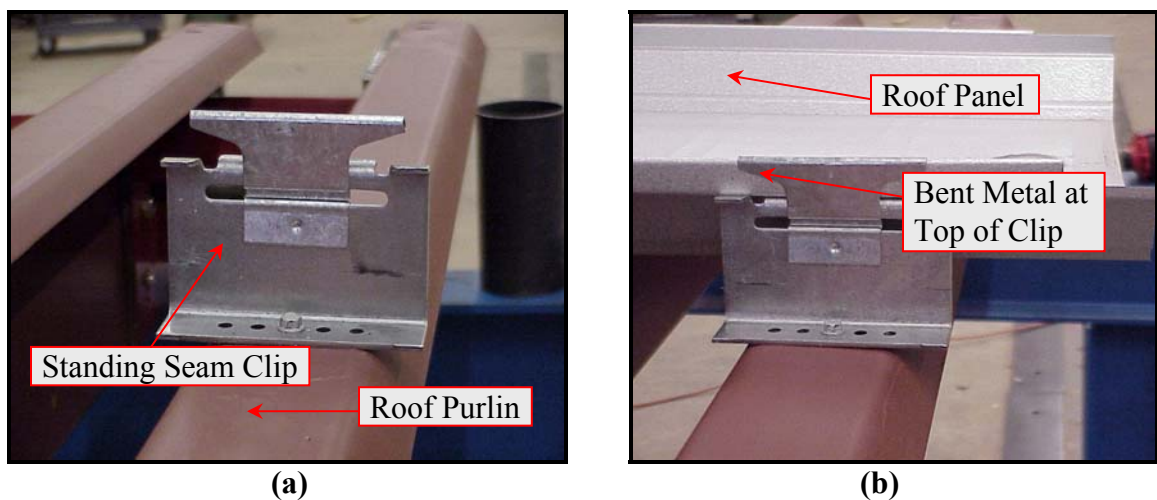


Figure 2.4 (a) Clip Mounted On a Purlin (b) Roof Panel Attached To Clip

A standing seam roof system is installed in several steps. The clip is snapped onto the "Male Rib" of the roof panel and attached to the purlin with screws. The "Female Rib" of the next panel is snapped over the "Male Rib" and clip assembly. Figure 2.5 (a) shows the unseamed cross-section of the standing seam roof. The two roof panels and the clip are then crimped together; producing the finished seamed cross-section shown in Figure 2.5 (b). The folded seam is weather tight and firmly attached to the structural framing system via the panel clip. The standing seam clips permit the steel roof panel to move or "float" over the structure. This movement reduces the problems associated with thermal expansion and contraction of the roof. Additionally, there are no holes drilled in the metal roof, which enhances water tightness and eliminates corrosion of the roof system.

There is one significant drawback to a standing seam roof system. Because the roof panel is not directly attached to the purlins, it is conservatively assumed that the roof panel does not impart any rigidity to the structure. Additional material is usually required in the secondary roof framing members for structural rigidity and stability. Although standing seam roofs have taken a considerable share in the metal building market, very little research has been done to study the actual load carrying capacities of members supporting a standing seam roof. The metal building industry accepts that there is a significant structural difference between through-fastened and standing seam roof systems, but in most cases research using through-fastened systems is applied to standing seam systems without accounting

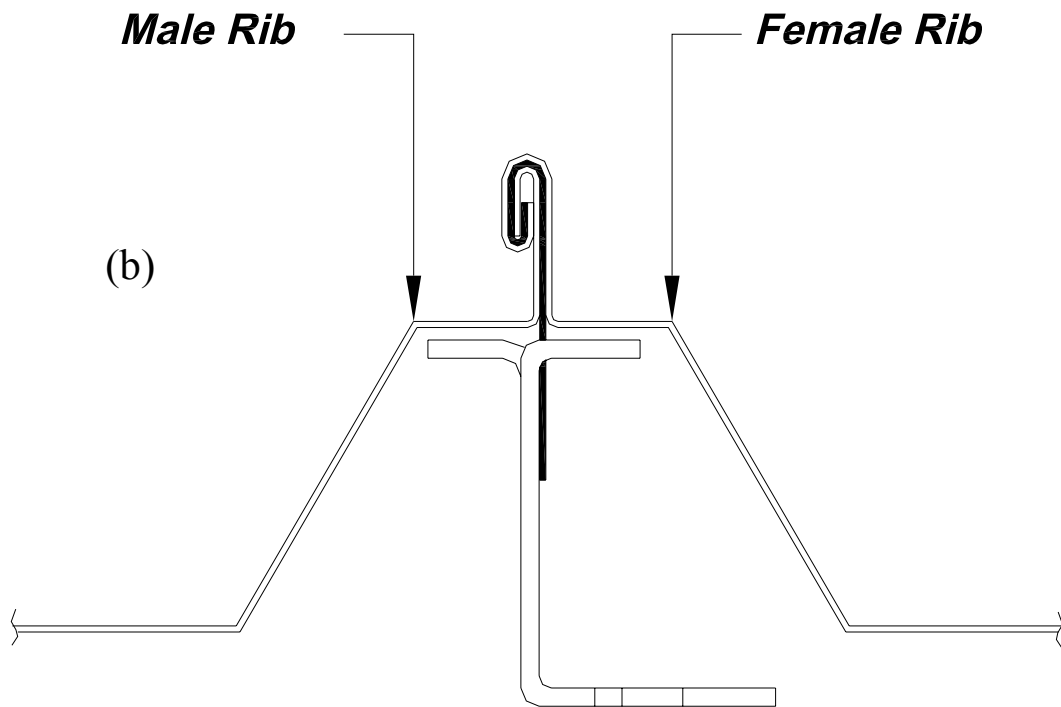
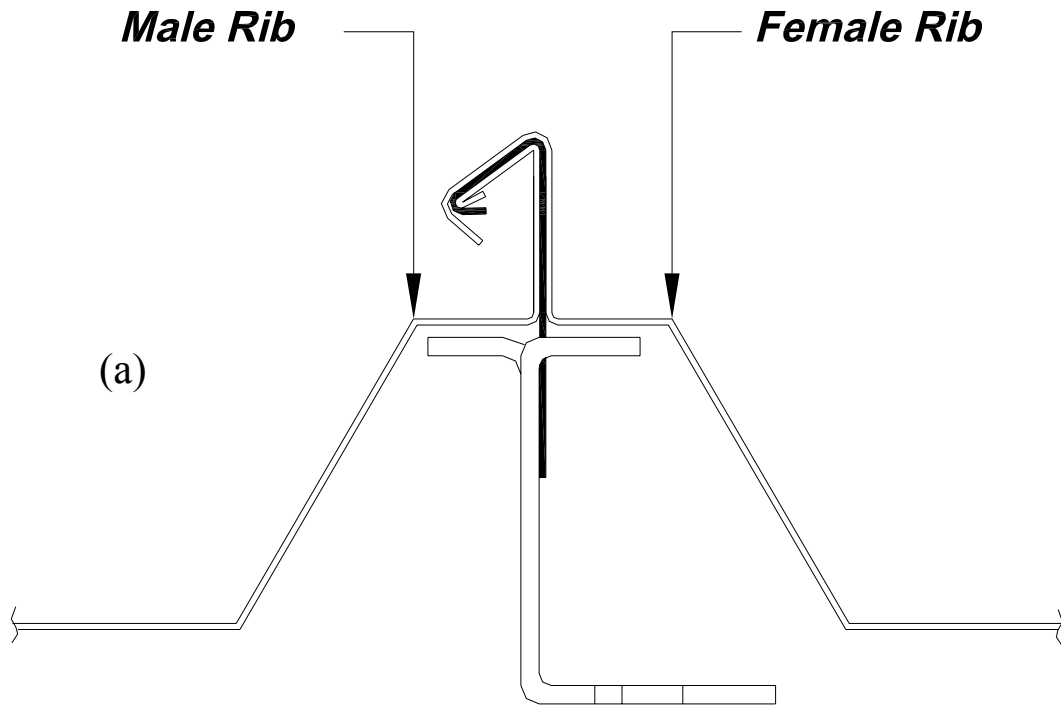


Figure 2.5 (a) Unseamed (b) Seamed - Cross-Section of Standing Seam Roof

for these differences. For example, Fisher et al (1993) suggests that their method developed for through-fastened roof can be directly applied to standing seam roofs but no standing seam roof systems were tested in this research.

2.1.2 Built-up Members

As mentioned earlier, for the last five years, there has been a growing demand for buildings with long bays between the frames. To economically span the longer bay spacing requires much deeper purlins or cold-formed joists. Having discussed purlins we will now turn our attention to cold-formed joists and the use of built-up members in their construction.

2.1.2.1 Joists

Steel joists are structural load-carrying members with an open web system which supports floors and roofs utilizing hot-rolled or cold-formed steel and is designed as a simple span member. They are an extremely efficient use of material when compared to most flexural load-carrying members.

Open web hot-rolled steel joists have been used since at least 1928 when the Steel Joist Institute, the group that sets the standards for joist construction was founded. The K-Series were primarily developed to provide structural support for floors and roofs of buildings. K-Series Joists are light in weight - they possess an exceptionally high strength-to-weight ratio in comparison with other building materials. Coupled with their low price per pound, they contribute significantly to lower building costs. An additional economy stemming from their light weight is the fact that the structural materials supporting the joists, such as beams and Joist

Girders, columns, and the foundations themselves, can therefore be lighter, leading to even greater economy. These advantages and features have resulted in their wide use and acceptance throughout the United States and other countries.

The earliest documented use of cold-formed joists dates to the 1950's. This early cold-formed joist was rather robust and was designed to allow the roofer to nail the roof panel into a crimped valley on the top edge of the joist. The nail did not penetrate the joist; it was simply wedged into the groove. The roofer had to place the nail within a 1/8th of an inch tolerance to make this system work. This product was never popular and was taken off the market in less than ten years. In June of 2001, Star Building Systems initiated a line of research investigating the engineering challenges of manufacturing cold-formed joists. In 2003 American and the NCI group of companies started selling cold-formed joists in the U.S. market. This competition from a new product led to a significant reduction in the cost of hot-rolled joists. It is obvious from the market reaction that cold-formed joists, with a greater higher strength-to-weight ratio, are leading to lower cost when compared to hot-rolled steel joists.

Figure 2.6 and 2.7 show typical elevation and section views of examples of a hot-rolled and cold-formed steel joist. There is very little difference in the elevation and or layout of the two joist types. They have been manufactured in many common truss geometries such as Pratt, Warren etc. Figure 2.7 highlights the differences between these products. Hot-rolled joist is generally made from hot-rolled angles and extruded rod while the cold formed joist is totally made from

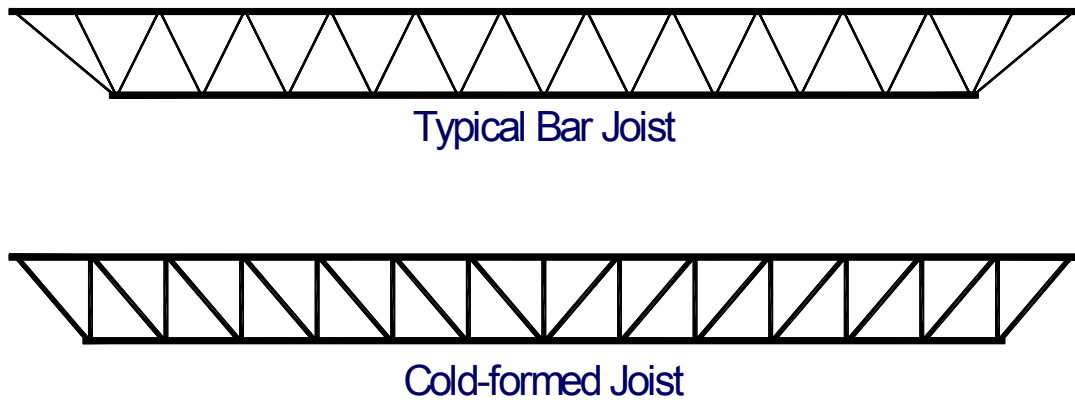


Figure 2.6 Bar Joist vs. Cold-Formed Joist – elevation view

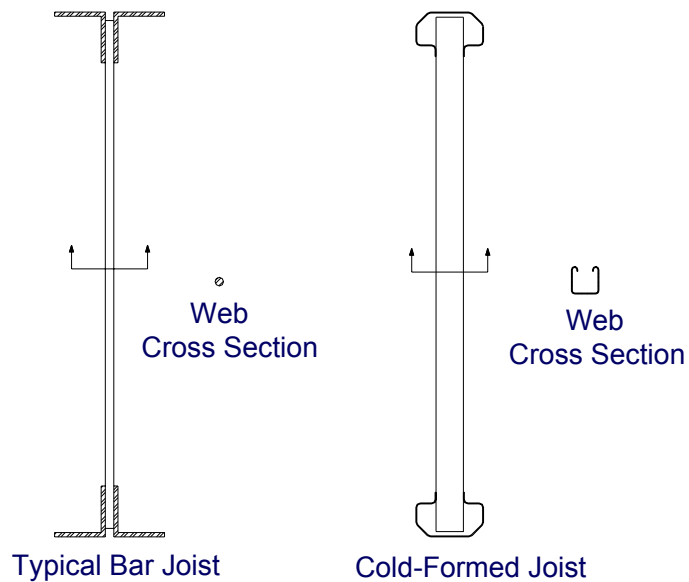


Figure 2.7 Bar Joist vs. Cold-Formed Joist – Section view

folded plate. So by using material even more efficiently, cold-formed steel joists can potentially be manufactured even more economically than hot-rolled steel joists. Cold-formed steel joists possess an exceptionally high strength-to-weight ratio very similar to or greater than hot-rolled steel joists. Additionally, cold-

formed steel generally has a lower price per pound than hot-rolled, which can contribute significantly to lower building costs.

2.1.2.2 Compression Elements

Let's compare a uniformly loaded simply supported prismatic beam to an open web joist for bending. The top fiber of the simply supported beam will be in compression and the bottom fiber of is in tension similar to the joist, where the top chord is in compression and the bottom chord is in tension. At mid-span the moment due to the load is the largest and the compressive or tensile stress related to this moment is greatest at mid-span in both structures. So in both cases, optimizing for bending tends to occur at mid-span and the optimized section is used for the entire joist length.

Now let's compare a uniformly loaded simply supported prismatic beam to an open web joist for shear. At mid-span the shear force is zero and it linearly increases towards both reaction points. In the prismatic beam these shear forces are carried by the depth of the section (in a W section it would be the web) with the area at the neutral axis providing the greatest resistance. In the joist the web members resist the shear forces. Since the shear force is greatest close to the reaction area of the joist and beam this is the area of greatest concern for shear. In a prismatic or wide flange beam this optimization for shear is the same for the entire length of the member. This is not true with open web joists where every web member can be optimized. In general a joist manufacturer is not likely to

optimize every web member because the chance of making a mistake in manufacturing is fairly high and the cost of failure is also high. That being said there is still a desire to improve the efficiency of the joist and improve profits. To do this, without manufacturing mistakes due to varying thickness of the elements, is possible by using built-up members at the highest stressed web locations.

Figure 2.8 identifies the first diagonal web member with a blue dashed box. This member is the most severely loaded web member in compression due to uplift loading. The first vertical web member, which is shown in Figure 2.8 as a built-up member, is the most severely loaded web member in compression member due to gravity loading. By using two members instead of one at these locations, or a selected number of additional neighboring locations, it may be possible to manufacture a more efficient joist safely.

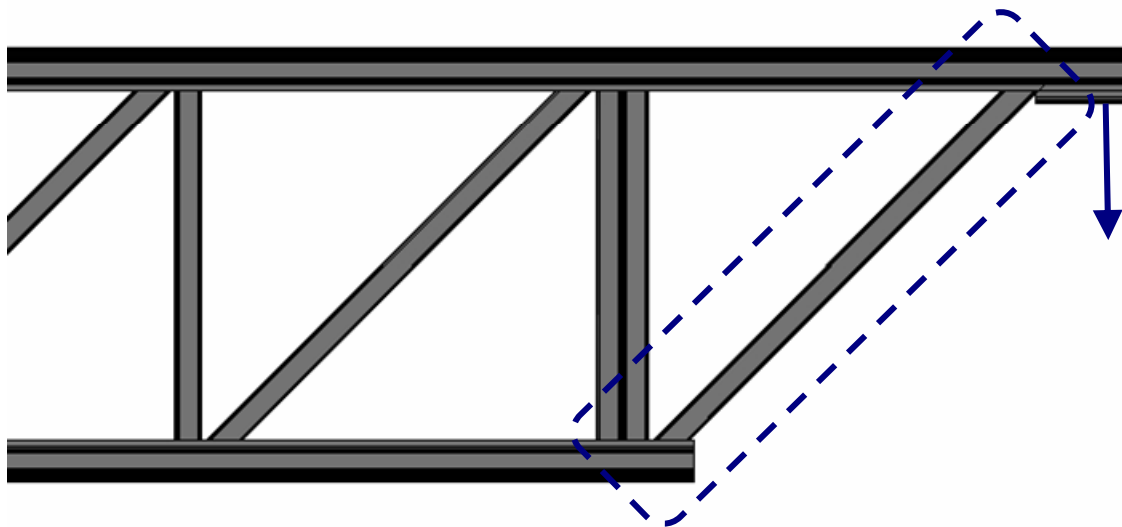


Figure 2.8 First Web Member of Cold-Formed Joist – Elevation view

In hot-rolled design, local and distortional buckling modes rarely control the capacity of structural shapes. In cold-formed design, however, local and

distortional buckling often controls the capacity of compression members. With cold-formed built-up members in compression that are in contact it is likely that the interaction between members could affect the local, distortional and global buckling capacities.

2.2 Literature Review

2.2.1 Purlins

2.2.1.1 Elastic Buckling of Cold-Formed Steel Compression Members

Analysis of cold-formed steel compression members differs significantly from analysis of hot-rolled steel. One major difference is that cold-formed steel sections are more susceptible to certain elastic buckling modes. Schafer (2002) defines elastic buckling as “a phenomenon that occurs when the change in energy associated with out-of-plane deformation response to an in-plane load is equal to the change in energy for in-plane response to the same in-plane load.” Lets consider normal elastic global buckling of a perfect column, i.e. Euler buckling. As an axial load is applied to the column, initially the column responds elastically by shortening concentrically. This is an example of an in-plane response to an in-plane load. When the load is increased to P_{cr} , the critical Euler buckling load, the midpoint of the column suddenly move 90° to the applied load. This is an example of an out-of-plane response to an in-plane load. As P_{cr} is incrementally approached, the energy required to cause axial (in-plane) deformation and the energy required to cause global (out-of-plane) deformation become more similar. At the critical load these energy values are equal. This analogy can be extended to

all other elastic buckling modes since this energy relationship defined the critical buckling load for all modes.

Elastic buckling can be divided into three relevant buckling modes depending on the portion of the section that becomes unstable. These modes are: local, distortional and lateral-torsional or “global” buckling. Figure 2.9 shows the

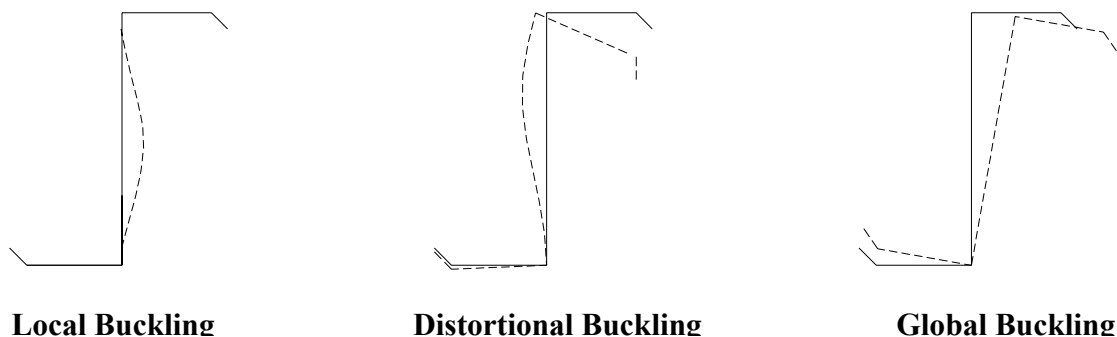


Figure 2.9 Buckling Modes of Cold-Formed Steel Zee's

deformations associated with each type of buckling. Most hot-rolled steel sections are stocky enough that local and distortional buckling do not occur.

Local buckling is characterized by the buckling of individual plate elements in a section. It occurs at a short wavelength and the buckling of one element does not affect other elements in the section. It can occur in any of the elements of the section, not just the web section as shown in Figure 2.9. There is significant distortion of the section, which involves rotation but no translation at the fold lines of the member.

According to Schafer (2002), distortional buckling occurs when there is both translation and rotation at the fold line of the member. It takes place due to

the distortion of a portion of the cross-section while other portions, such as the flange or lip of a section, remain rigid. The wavelength of distortional buckling is generally intermediate between that of local buckling and global buckling (Schafer 2002). Distortional buckling, with its rotation at the fold line of the member, is not seen in the hot-rolled sections due to the increase restraint provided by fillets common in these sections. It has become a concern in recent years with the use of thinner materials that do not provide adequate restraint at the fold. This type of buckling tends to be more of a problem with Cee shapes.

Global buckling occurs when the entire cross-section buckles. It involves translation (i.e. Euler buckling), rotation (i.e. Torsional buckling) or both (i.e. Flexural-Torsional buckling). No distortion exists in any of the elements in this buckling mode. It is sometimes termed “rigid-body” buckling because any given cross-section moves as a rigid body without any distortion of the cross-section (Davies 2000).

A stiffened compression element in a cold-formed member will not collapse when it reaches its local buckling stress. It continues to carry additional load beyond the buckling load as a result of the redistribution of stress. This phenomenon is known as post buckling strength and is a very important aspect of cold-formed steel design, especially for stiffened compression elements with large width/thickness ratios. The theory of post buckling as explained in section B2 of the *AISI Specification and Commentary* (2002) is based on the research of Winter (1970).

Winter modeled a square plate that is uniformly compressed in one direction and simply supported along the two edges parallel to this stress. This initial condition is shown in Figure 2.10 (a). Figure 2.10 (b) shows Winter's model applied to the web of a zee section, which is restrained on both edges by the flanges. Since it is difficult to visualize the performance of such two dimensional elements loaded along the edges, Winter proposed replacing the plate with bars in the longitudinal and transverse directions. In Figure 2.10 the longitudinal bars are represented by the red dashed lines and the transverse bars are represented by the blue dashed lines. Let's consider the longitudinal bars first. Since the plate is uniformly compressed, each of the longitudinal bars represents a column loaded with a force of P/n , where P is the total load on the plate and n is the number

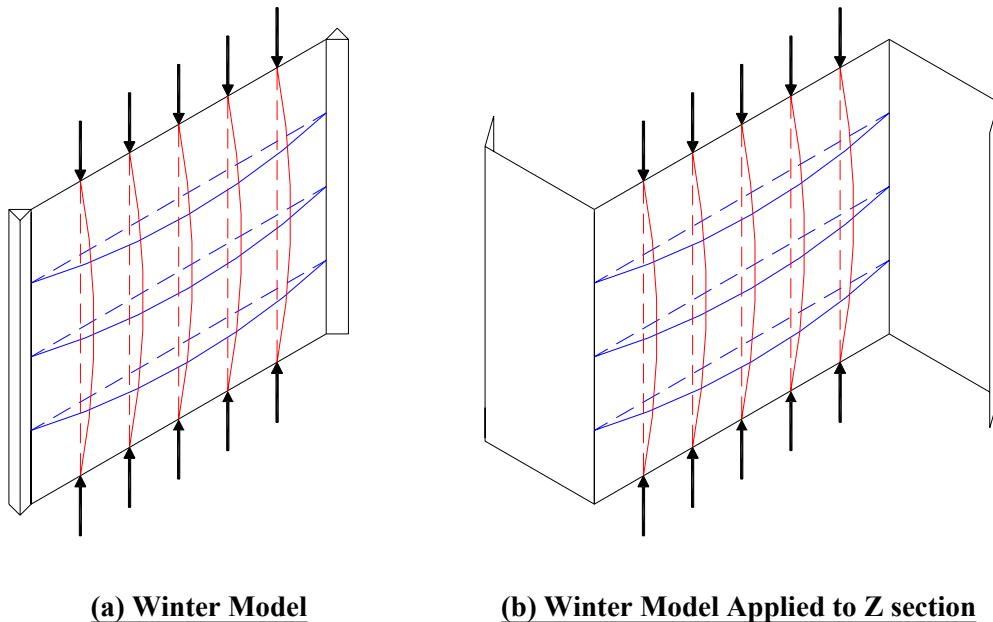


Figure 2.10 Post Buckling Strength Model

of longitudinal bars in the model. As the load is gradually increased the compression stress in each of these bars will reach the critical column buckling value (i.e. Euler buckling load) and all five bars will tend to buckle simultaneously. The buckled shape is represented by the solid red lines. If these struts were simple columns, unsupported except at the ends, they would simultaneously collapse through an unrestrained and increasing large deflection.

Now let's consider the longitudinal and transverse bars at the same time. The transverse bars are represented by the dashed blue lines when no load is present. And let's attach the longitudinal and transverse bars together where ever they cross one another. Now when the longitudinal bars are loaded to the critical column buckling value they do not simultaneously collapse through unrestrained and increasing deflection. As the longitudinal struts begin deflecting at their critical column buckling stress, the transverse bars that are connected to them begin to stretch to accommodate the imposed deflection. The stretched shape of the transverse bars is represented by the solid blue lines. Like any structural material, steel resists stretching, and by so doing exerts a restraining effect on the deflections of the longitudinal bars. In other words, the longitudinal bars carry additional load even after reaching their buckling stress. Therefore in a cold-formed steel section under a uniform compressive load, a redistribution of stresses takes place, which results in an increase in its load carrying capacity which is called, post buckling strength. *AISI Specifications (2002)* uses the post buckling strength of the stiffened compression elements for design purposes.

Another consequence of the model is that the longitudinal bar (strips of the plate) closest to the center, which deflect the most, "get away from the load," and hardly participate in carrying any additional load after the critical column buckling value is reached. The longitudinal bars (strips of plate) closest to the edges, held straight by the transverse bars, continue to resist increasing load with hardly any increasing deflection. For the plate, this means that the uniformly distributed compression stress re-distributes itself in a manner shown in Figure 2.11. This behavior is the foundation of the effective area method of the *AISI Specification* (2002), where the complex stress behavior of the section is simplified, in this case, to two uniform stress regions adjacent to the supported edges. This is very similar to the Whitney stress block theory used in concrete design.

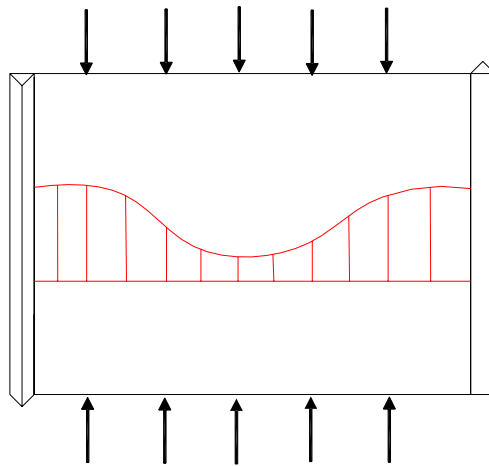


Figure 2.11 Stress Distribution in Stiffened Compression Elements

2.2.1.2 AISI Specification (2002)

The AISI *Specification for Cold-Formed Steel Structural Members* (2002) uses the effective width concept for both the stiffened and unstiffened elements of a section to find its resistance to local and global buckling due to uniform and non-uniform stress gradients. The effective area method considers the elements forming a cross-section in isolation, thus minimizing the interaction between the elements. This semi-empirical approach is based on the results obtained from many years of testing typical cold-formed sections and comparing them to idealized plates using Winter's (1970) model. As sections become more complex and additional edges and intermediate stiffeners are added, calculating the effective width becomes much more complex. Additionally the interaction between the elements become more significant making the analysis much less accurate.

In order to maximize strength-to-weight ratios cold-formed sections have become more slender and more complex in recent years. They are now very different from the sections which were used to calibrate the effective width equations. Distortional buckling rarely, if ever, controlled in these historical sections so this buckling mode was not included in the effective width method. In some cases the effective width method now overestimates a section's resistance to local buckling. This is evident from comparison of values obtained with the AISI effective width method to the the tests done by Schafer (2002), Fisher et al (1993)

& Hatch, et al (1991). It has become necessary to find a more general approach to determining a section's resistance to local and distortional buckling modes.

Calculating the capacity of a cold-formed member subjected to an axial load is described in Chapter C4 of the *AISI Specification* (2002). Individual member capacities are determined as a function of the member's resistance to local buckling, global buckling and yielding. The capacity of a concentrically loaded compression member is given by:

$$P_n = A_e F_n \quad (\text{AISI Eq. C4-1})$$

Where

A_e = effective area calculated at stress F_n .

F_n = combined resistance to buckling yielding calculated as follows:

$$\text{For } \lambda_c \leq 1.5 \quad F_n = \left(0.658^{\lambda_c^2}\right) F_y \quad (\text{AISI Eq. C4-2})$$

$$\text{For } \lambda_c > 1.5 \quad F_n = \left(\frac{0.877}{\lambda_c^2}\right) F_y \quad (\text{AISI Eq. C4-3})$$

Where

$$\lambda_c = \sqrt{\frac{F_y}{F_e}}$$

F_e = the least of the elastic flexural, torsional and torsional-flexural

buckling stress determined according to Sections C4.1 through C4.4

F_y = the specified minimum yield point of the type of steel used determined according to Section F3, A7.2 and A2.3.2

The effective width for a member without intermediate stiffener is calculated as:

$$b = w \quad \text{when } \lambda \leq 0.673 \quad (\text{AISI Eq. B2.1-1})$$

$$b = \rho w \quad \text{when } \lambda > 0.673 \quad (\text{AISI Eq. B2.1-2})$$

Where

w = flat width of element

$$\rho = \left(\frac{1 - 0.22}{\lambda} \right) \lambda \quad (\text{AISI Eq. B2.1-3})$$

$$\lambda = \text{slenderness factor} = \sqrt{\frac{f}{F_{cr}}}$$

$$F_{cr} = k \frac{\pi^2 E}{12(1 - \mu^2)} \left(\frac{t}{w} \right)^2$$

Where

t = thickness of uniformly compressed stiffened element

μ = Poisson's ratio of steel

$f = F_n$ = buckling stress in compression element as calculated by C4-2

& C4- 3

E = modulus of elasticity

k = plate buckling coefficient

= 4.0 for four sides simply supported in uniform compression

(Stiffened edges)

Section F1 of the *AISI Specification* (2002) gives the criteria for accepting experimental capacities of cold-formed steel members or systems. It also provides equations for determining an appropriate factor of safety (Ω) for ASD (Allowable Stress Design) or resistance factor (ϕ) for LRFD (Load Resistance and Factor Design). The factors Ω & ϕ are calculated using

$$\phi = C_{\phi} (M_m F_m P_m) e^{-\beta_0 \sqrt{V_M^2 + V_F^2 + C_P C_P^2 + V_Q^2}}$$

And

$$\Omega = \frac{\phi}{1.6}$$

Where

C_{ϕ} = calibration constant = 1.52

M_m = mean value of material factor, M, listed in Table F1 for the type component involved

F_m = mean value of fabrication factor, F, listed in Table F1 for the type of component involved

P_m = mean value of professional factor, P, for tested component = 1.0

β_0 = target reliability index = 2.5 for structural members and 3.5 for connections

V_m = coefficient of variation of material factor listed in Table F1 for type of component involved

V_f = coefficient of variation of fabrication factor listed in Table F1 for type
of component involved

C_p = correction factor listed = $(1+1/n) m / (m-2)$ for $n \geq 4$, and 5.7 for $n = 3$

V_p = coefficient of variation of test results, but not less than 60%

m = degrees of freedom = $n-1$

n = number of tests

V_Q = coefficient of variation of load effect = 0.21

e = natural logarithmic base = 2.718...

The *AISI Specification* (2002) states that evaluation of test results shall be made on the basis of the average value of test data from a minimum of three identical specimens. If the deviation of any individual test result from the average value obtained from all tests exceeds 15%, then more tests need to be performed.

2.2.1.3 Direct Strength Method

Finite strip analysis has been developed as a direct method to calculate the elastic buckling strength of an entire cross section and overcome the inefficiency of the current AISI method. Schafer (2002) has implemented this method in an alternate design method called the Direct Strength Method (DSM). The DSM has been accepted by the *AISI Committee on Specifications* as a rational alternate design method. It accounts for the interaction of elements in local buckling (e.g. web/flange interaction), and distortional buckling is treated explicitly in the design process.

Like the procedure in the current AISI *Specification* (2002), the direct strength method was calibrated against tests done by Kwon and Hancock (1992), Lau and Hancock (1987), Loughlan (1979), Miller and Pekoz(1994), Mulligan (1983), Polyzois et al. (1993) and Thomasson (1978) for Zee sections in axial compression. This calibration confirms its effectiveness for members meeting the following limitations.

- 1) $76 < \mathbf{h/t} < 137$
- 2) $30 < \mathbf{b/t} < 56$
- 3) $0 < \mathbf{d/t} < 36$
- 4) $1.5 < \mathbf{h/b} < 2.7$
- 5) $0.00 < \mathbf{d/b} < 0.73$
- 6) $\theta \sim 50$ degree
- 7) $\mathbf{E/F_y} \sim 50$ ksi

Figure 2.12 defines the dimensions in these limitations.

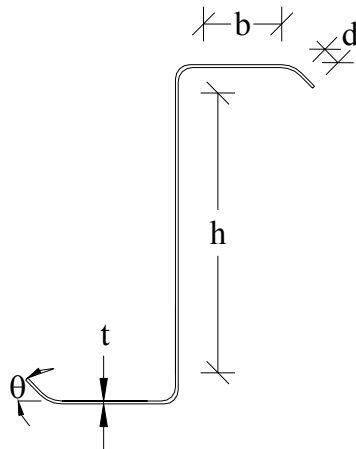


Figure 2.12 Cold-Formed Zee Section Dimensions.

The Direct Strength Method calculates the member capacity differently than the *AISI Specification*. It uses the finite strip method for calculating buckling loads rather than using the effective width method which the *AISI Specification* uses. The steps involved in the calculation of a member capacity using the Direct Strength Method are shown in Figure 2.13

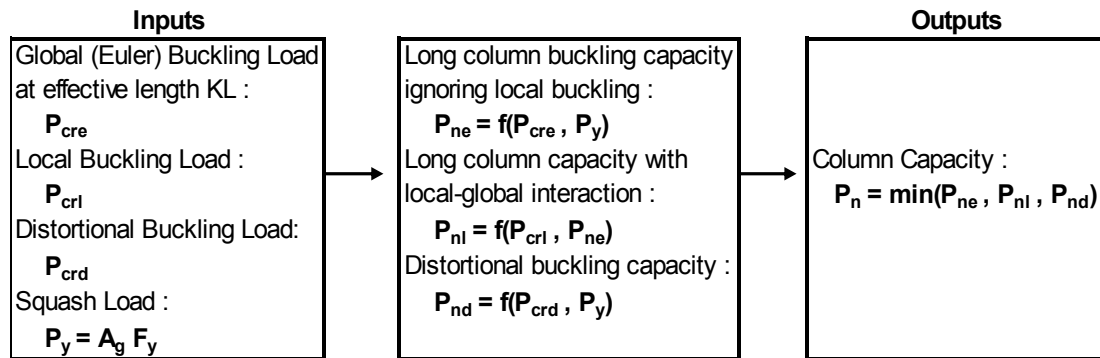


Figure 2.13 Direct Strength Method Flow Chart
(Schafer, 2002)

Currently, under the consistent with the “any rational analysis” clause of the *AISI Specifications* (2002) section A1.1 (b) , the Direct Strength Method can be used for members that fall outside its stated limitations, but a reduced load reduction factor ϕ (LRFD) or an increased safety factor Ω (ASD) must be used (Schafer 2002). A drawback in the Direct Strength is that it does not account for any connections. Each member is analyzed separately as a single member. Thus, our ability to calculate the capacity of sections in a system needs further improvement.

2.2.1.4 Empirical Studies of Purlin Struts

A significant amount of research has been conducted concerning the axial buckling behavior of cold-formed steel sections, but no studies were identified in the literature on axial load capacities of Zee sections with a depth greater than 10 inches, and only five tests at a depth of 10 inches were found.

2.2.1.4.1 Simaan and Pekoz

Simaan and Pekoz (1976) studied the axial capacity of diaphragm-braced Cee and Zee sections. Simaan and Pekoz predicted the axial capacity of Cee and Zee sections with flanges braced by diaphragms on one and both sides, using an energy method approach. The following equation predicts the critical buckling load for a Zee section braced on one side and simply supported at the ends:

$$\begin{aligned}
 & P^3 - P^2 \left[P_x + P_y + Q + P_\phi + \frac{1}{r_o^2} \left(Q \frac{d^2}{4} + \frac{FL^2}{n^2 \pi^2} \right) \right] \\
 & + P \left\{ (P_y + Q)P_z - P_{xy}^2 + (P_y + Q + P_y) \left[P_\phi + \frac{1}{r_o^2} \left(Q \frac{d^2}{4} + \frac{FL^2}{n^2 \pi^2} \right) \right] - \frac{1}{r_o^2} \left(Q \frac{d}{2} \right)^2 \right\} \\
 & - \left[(P_y + Q)P_x - P_{xy}^2 \right] \left[P_\phi + \frac{1}{r_o^2} \left(Q \frac{d^2}{4} + \frac{FL^2}{n^2 \pi^2} \right) \right] + \frac{1}{r_o^2} P_x \left(Q \frac{d}{2} \right)^2 = 0
 \end{aligned}$$

Where

P_x = Euler buckling load about the x-axis

P_y = Euler buckling load about the y-axis

P = Buckling Load

Q = Shear rigidity of the diaphragm bracing

P_{ϕ} = Torsional buckling load

$$r_o^2 = I_p/A$$

I_p = Polar moment of inertia about the shear center

A = Cross-sectional area

d = Overall dimension of web (depth of section)

F = Rotational restraint by diaphragm bracing

n = Number of half-sine waves into which the column may buckle, or the n^{th} term of the series

L = Length of the column

For a given section with known shear rigidity of the diaphragm bracing (Q) and the rotational restraint of the diaphragm bracing (F) values, the lowest root of the cubic equation results in the critical buckling load.

The analytical results were then verified experimentally. They presented the results of their theoretical and experimental work and suggested a design procedure. Their testing program consisted of eleven assemblies, each using two steel studs 12 feet long and 3.07 inches deep with wallboard attached on either one or both sides. The spacing of the studs was 2 feet at the ends; the studs were simply supported about their y-axis, fixed about their x-axis, and restrained against twisting. The loads were applied directly to the studs with a hydraulic testing machine. Cee sections with thicknesses varying from 0.062 to 0.106 inches and Zee sections with a thickness of 0.106 inches were tested. They concluded that when using wallboards as bracing, the load-carrying capacity of the cold-formed

section increases significantly. Based on this research, they developed an analytical formulation for the behavior of diaphragm-braced thin-walled open sections. Computer programs were then developed to simplify the use of their formulation for designing wall studs.

2.2.1.4.2 Dimos and Sudharmapal

Dimos and Sudharmapal (1990) studied the ultimate capacity of cold-formed steel Zee sections with sloping edge stiffeners under axial load. They evaluated the AISI design criteria for cold-formed sections with sloping edge stiffeners and compared the calculated design values to experimental data obtained from their tests. This testing was limited to simple column tests and does not include any system effects. The tests consisted of forty-six Zee sections, varying in length from 1.5 to 8.0 feet and 3.397 to 4.283 inches deep. The sections were loaded in direct compression. They concluded that, "basing the ultimate capacity of sections with unstiffened flanges on the local buckling capacity of the flanges leads to a very conservative estimate of the members' capacity". Dimos and Sudharmapal further recommended that "for Zee sections this requirement be lifted and the allowable load be based on the post-buckling capacity of the flanges".

2.2.1.4.3 Hatch, Murray and Ellifritt

Hatch et al. (1991) evaluated the strength of strut-purlins with Zee and Cee sections attached to a through fastened roof panel. They pursued an experimental

investigation to verify that strut-purlin strength could be predicted using the interaction equation in the then-current AISI *Specification* (1986).

They performed an initial series of five interaction tests with varying combinations of uplift and axial loads on roof systems supported by 8 inch deep Zee-purlin sections. The axial load carrying capacity of the purlins was determined from a near zero uplift moment test, and the uplift moment load carrying capacity was determined from a zero axial load test. Through extensive literature review as noted in their report, Hatch et al (1991), found an empirically based method for determining uplift loading capacity. To verify the method's applicability to strut-purlins, a series of eight axial load tests was conducted. The test specimens consisted of 7 and 10 inch deep Cee sections and 10 inch deep Zee sections. Rotational stiffness tests were also done. Finally, two sets of five interaction tests were conducted using 10 inch Zee and Cee sections to evaluate the accuracy of the interaction equation and the method of determining uplift and axial load capacities. These are the only axial load tests involving 10 inch deep Zee-purlin sections reported in the literature.

Hatch et al. concluded that the axial capacity of a strut-purlin can vary by up to 100% depending on the deck-to-purlin fastener location. This duplicates the conclusions of Willis and Wallace (Willis 1990) at the University of Oklahoma. Hatch et al. recommended that further testing needed to be conducted to determine the effect of “average” fastener locations as found in field conditions. He further

recommended that additional study be concentrated on attaining a simpler method for determining strut-purlin axial capacity.

2.2.1.4.4 Fisher, Kaehler and Glaser

Fisher et al. (1993) conducted tests on cold-formed Cee and Zee sections to determine their axial capacity. He developed an equation for the axial load capacity of Cee and Zee sections with one flange connected to a through fastened roof or wall panel. His studies were built upon earlier research done by Simaan (1973) and axial load tests reported by Hatch, et al (1991).

Fisher's testing consisted of six full scale tests using 8 inch deep Cee and Zee sections. The base test consisted of two 25-foot long opposed Zee sections with a twenty-six gauge screw down panel. This panel was similar to a through-fastened roof connected to one of the flanges of each section. To determine the effect of purlin continuity on axial load capacity, a two span system was tested. Each span was 25 feet long, and the purlins were lapped 2 feet on each side of the center of support. The remaining four tests were done using two different types of standing seam roof panels. All of the Zee sections had a nominal thickness of 0.075 inches.

Simaan (1976) had created a very complicated design equation for the axial buckling capacity of Cee and Zee wall studs attached to gypsum wallboard. Fisher conducted a parametric study of the variables used in Simaan's equation in order to simplify the equation. He used Simaan's equation to calculate the axial load

capacities of sections he had tested and compared these analytical results with his test results. Table 2.2 shows the variables Simaan and Fisher considered in developing their equations.

Fisher concluded that the section depth, flange width, member thickness and rotational stiffness of the deck to flange connection could not be eliminated from the equation, but the remaining seven variables could be ignored if certain practical limitations were applied.

Table 2.2 Section Properties Deemed Important By Simaan and Fisher

	<u>Simaan (1976)</u>	<u>Fisher et al. (1993)</u>
1	Section Depth	Section Depth
2	Flange Width	Flange Width
3	Member Thickness	Member Thickness
4	Rotational Stiffness of the Deck to Flange Connection	Rotational Stiffness of the Deck to Flange Connection
5	Member Length	<i>N/A</i>
6	Form Factor (Q)	<i>N/A</i>
7	Allowable Diaphragm Strain	<i>N/A</i>
8	Diaphragm Shear Rigidity	<i>N/A</i>
9	Allowable Purlin Rotation	<i>N/A</i>
10	Yield Stress	<i>N/A</i>
11	Fastener Spacing	<i>N/A</i>

His justification for eliminating certain variables is summarized below.

- a) *Member Length*: Critical stress should be based on the lower bound critical stress for lengths typically encountered. Thus member length is not a parameter in the equation formulation presented.
- b) *Form Factor*: A specimen's form factor is defined by its shape and size. The critical stress does not change if the form factor is greater than 0.5. The members studied had a form factor nearly equal to one, so it was not significant
- c) *Allowable Diaphragm Strain*: If allowable strain is more than 0.002 in./in., the allowable diaphragm strain has negligible effect on the critical stress. Through-fastened metal roof systems generally meet this provision.
- d) *Diaphragm Shear Rigidity*: As long as a minimum rigidity of approximately 500 kips/inch/inch exists, the variation in shear rigidity has a negligible effect on the critical stress. Most through-fastened metal panels meet this requirement.
- e) *Allowable Purlin Rotation*: Based on the tests done by Hatch (1991), under the direction of Fisher, purlin rotation varied from approximately 0.2 to 0.3 radians for 7 to 10 inch deep purlins. For this range of allowable purlin rotation, only a small variation in critical stress occurred.
- f) *Yield Stress*: Elastic buckling is independent of yield stress, so there is no effect on critical stress due to changing the yield stress from 33 to 60 ksi.
- g) *Fastener Spacing*: The critical stress does not change with fastener spacing over the range that was tested (3 to 36 inches).

Fisher (1993) then developed a simplified formula, which seems to be based on a log based regression analysis, for calculating axial load capacities as:

$$P_u = (0.79x + 0.54) (1.7t + 0.93) (2.5b - 1.63h + 22.8) A$$

Where,

P_u = the required axial strength

x = fastener distance from the web centerline divided by the flange width

t = section thickness, inches

b = flange width, inches

h = section depth, inches

A = full unreduced cross-sectional area at the member

Fisher (1993) verified the capacities obtained from the above equation using the results of his tests. Several limitations were included on the section properties such as depth, span length, thickness and fastener spacing. He restricted the use of his equation to calculating the axial load capacity for Cee and Zee sections with through-fastened roof panel. He suggested that an equation for sections with standing seam panels can be obtained experimentally by obtaining the critical axial stress for the thickest section of any given depth series. The weak axis load capacity may then be calculated using the smaller value of this stress or the stress obtained from his equation for any section with the same depth and flange width.

2.2.1.4.5 Stolarczyk and Fisher

Stolarczyk and Fisher (2001) conducted tests on cold-formed Zee sections attached to standing seam roof panels to determine their axial capacity. Due to the lack of an analytical solution for the flexural buckling strength of Zee purlins attached to a standing seam roof, designers of metal buildings are required by code to conduct Uplift Base Tests to determine the capacity of the purlin and roof system. Because the Uplift Base Test is already required by the code, they reasoned that it would be beneficial if the axial load capacity of the Zee purlin could also be determined by from the same test data. Stolarczyk et al. hypothesized that the axial strength of Zee purlins could be obtained by applying a factor or factors to the results of the flexural Uplift Base Tests.

The axial load capacity was determined by developing a relationship between the flexural uplift buckling strength and the axial buckling strength in the Zee purlin. This relationship was investigated using finite element models and by conducting a parametric study. At the conclusion of the parametric study, three confirmatory tests were conducted to verify the finite element results. A relationship is provided that relates the axial buckling strength in the Zee purlin to the flexural uplift buckling strength.

2.2.1.4.6 Summary of Empirical Studies of Purlin Struts

Table 2.3 summarizes the parameters of sections used by the researchers in the past. It is interesting to note that prior to 1991, no research was done to determine the axial capacity of a cold-formed Zee purlin attached to a roof deck. And it wasn't until 2001 that the relationship between the axial capacity of a cold-formed Zee purlin attached to a standing seam roof was investigated. And that investigation was limited to 3 tests. The total number of full scale tests on the axial capacity of Zee purlins completed prior to this investigation is twelve.

Table 2.3 Summary of Previous Tests Performed On Cold-Formed Zee sections

Researcher (year)	No. of Tests	Roof System	Depth (inch)	Thickness (inch)	Length (feet)
Simaan & Pekoz (1976)	11	Wallboard	3.07	0.106	12
Dimos et al. (1990)	46	None	3.397- 4.283	0.076 - 0.081	1.5 - 8
Hatch et al. (1991)	3	Through-fastened	10	0.058 - 0.075	15 - 25
Fisher et al. (1993)	6	Through-fastened	8	0.075	25
Stolarczyk et al. (2001)	3	Standing Seam	8 & 8.5	0.10 & 0.12	23 & 30

2.2.2 Built-up Members

When built-up member are created with discontinuous connections between the individual parts, the shear flexibility is greatly increase when compared to a section with continuous connections between the individual parts. As a result of this decreased stiffness the member's critical buckling load also decreases.

Analysis and design procedures must account for this behavior in order to provide reasonable, conservative results and design. A significant portion of the experimental work done to validate this theory was done using hot-rolled sections.

2.2.2.1 Bleich

Bleich developed an equation in 1952 to calculate the modified slenderness ratio of hinged-end battened columns. The derivation is based on the energy condition that the transition from stable to unstable equilibrium of any elastic system is characterized by,

$$V - W = 0$$

Where V is the strain energy due to deflection and W is the work done by the external axial force P . The elastic strain energy of a deformed battened column consists of:

1. The energy due to axial force in the two individual components.
2. The energy due to local bending of the two individual components.
3. The energy due to local bending of the battened plates.

The first term can be interpreted as the strain energy due to overall bending of the column. Bleich points out that the third term is small and can be neglected compared to the other two terms. This assumption is more accurate in the case of stitched columns because the stitches can be considered more rigid compared to the batten plates. Considering each segment of the member between two stitches as a panel, Bleich summed the strain energy of all panels to calculate the total

strain energy. The classical assumption of inflection points being located at the mid-point of all transverse and longitudinal member segments is used in the derivation process.

Based on the above approach, Bleich derived the following equation for modification of the slenderness ratio of a hinged-end battened column:

$$\left(\frac{KL}{r}\right)_m = \sqrt{\left(\frac{L}{r}\right)_o^2 + \frac{\pi^2 I_o}{24 I_{ib}} \left(\frac{a}{r}\right)^2}$$

Where:

$\left(\frac{KL}{r}\right)_m$ = Modified effective slenderness of the composite member

$\left(\frac{L}{r}\right)_o$ = Overall slenderness ratio of the composite member

I_o = Moment of inertia of the section about the buckling axis, neglecting the moment of inertia of individual components

$$\text{about their own centroidal axis} = 2 \left[A_i \left(\frac{h}{2} \right)^2 \right] = \frac{A_i h^2}{2}$$

A_i = Cross sectional area of each individual component

h = Distance between the centroids of individual components

I_{ib} = Moment of inertia of individual components about their own centroidal axis parallel to the axis of buckling = $2A_i (r_{ib})^2$

a = The distance between batten plates or stitches

Replacing $\left(\frac{1}{r}\right)^2$ with $\frac{2A_i}{I_t}$ gives:

$$\left(\frac{KL}{r}\right)_m = \sqrt{\left(\frac{L}{r}\right)_o^2 + \frac{\pi^2 I_o}{24 I_{ib}} \left(\frac{a}{1}\right)^2 \frac{2A_i}{I_t}}$$

Where:

$$I_t = \text{Moment of inertia of the composite section about the axis of buckling} = 2A_i r^2$$

Replacing I_{ib} with $r_{ib}^2 A_i$ leads to:

$$\left(\frac{KL}{r}\right)_m = \sqrt{\left(\frac{L}{r}\right)_o^2 + \frac{\pi^2 I_o}{24 r_{ib}^2 A_i} \left(\frac{a}{1}\right)^2 \frac{2A_i}{I_t}}$$

Which simplifies to:

$$\left(\frac{KL}{r}\right)_m = \sqrt{\left(\frac{L}{r}\right)_o^2 + \frac{\pi^2}{12} \left(\frac{a}{r_{ib}}\right)^2 \frac{I_o}{I_t}}$$

Bleich indicated that in a battened column section the distance between the centroids of individual components is large compared to the radius of gyration of the individual components. Because of this, in calculating the total moment of inertia I_t , the individual moment of inertia may be neglected in comparison with the $2\left[A_i\left(\frac{h}{2}\right)^2\right]$ term. This approximation leads to:

$$I_t = 2I_b + 2\left[A_i\left(\frac{h}{2}\right)^2\right] \approx 2A_i\left(\frac{h}{2}\right)^2 \approx I_o$$

$$\text{Or } \frac{I_o}{I_t} = 1$$

Bleich introduced this simplification into the equation and simplified it as:

$$\left(\frac{KL}{r}\right)_m = \sqrt{\left(\frac{L}{r}\right)_o^2 + \frac{\pi^2}{12}\left(\frac{a}{r_{ib}}\right)^2}$$

This is the equation suggested by Bleich for modification of the slenderness ratio of hinged-end battened columns to account for the detrimental effect of shear flexibility on the member strength.

2.2.2.2 Zandonini

In the early 1980's Zandonini (1985) performed a series of experiments and confirmed that for built-up sections with intermediate connectors that are snug-tight bolted, Bleich's equation could be modified to account for any boundary condition. As an additional simplification he noted that $\frac{\pi^2}{12}$ is nearly equal to one and dropped this term. His equation:

$$\left(\frac{KL}{r}\right)_m = \sqrt{\left(\frac{KL}{r}\right)_o^2 + \left(\frac{a}{r_i}\right)^2}$$

was eventually adopted by AISC as equation E4-1 of the specification.

2.2.2.3 Aslani and Goel

Aslani and Goel (1991) build upon the work of Bleich and Zandonini. They confirmed that Bleich's equation for general end conditions can be given as:

$$\left(\frac{KL}{r}\right)_m = \sqrt{\left(\frac{KL}{r}\right)_o^2 + \frac{\pi^2}{12} \left(\frac{a}{r_{ib}}\right)^2 \frac{I_o}{I_t}}$$

They then reviewed the assumption of $\frac{I_o}{I_t}$ noting that this quantity decreases as the distance between the two components becomes smaller. For a general case, the exact expression for the ratio can be derived in terms of the separation ratio

$\alpha = \frac{h}{2r_{ib}}$ And the ratio of $\frac{I_o}{I_t}$ can be derived to be equal to $\frac{\alpha^2}{\alpha^2 + 1}$ Substituting this

into Bleich's equation and using $\pi=3.14$ results in:

$$\left(\frac{KL}{r}\right)_m = \sqrt{\left(\frac{KL}{r}\right)_o^2 + 0.82 \frac{\alpha^2}{1 + \alpha^2} \left(\frac{a}{r_{ib}}\right)^2}$$

which was eventually adopted by AISC as equation E4-2 of the specification for intermediate connectors that are welded or fully tensioned bolted.

2.2.2.4 Sherman and Yura

Sherman and Yura (1998) performed experimental research to determine the number of intermediate connectors required on hot-rolled built-up members. The number of intermediated bolts required for built-up double angle compression members varied among different steel design standards. They performed eleven elastic tests and one inelastic test of full scale double-angle members with bolted end connections. In addition to the number in intermediate connectors, the variables included the installation tightness of the end and intermediate bolts, the faying surface condition at the end and the size of the intermediate fillers. The

results showed that preventing shear slip in the end connection is the most important factor in developing the capacity of the built-up member. This is reflected in the *AISI Specification (2002) C4.5* criteria number two which requires an end connection that prevents shear slip at the ends of the member.

Sherman and Yura's test results showed a trend of increasing capacity with an increasing number of intermediate connectors and with the tightness of the intermediate bolts. This verified the *AISC Specification* criteria. However, in their opinion, the increases due to additional connectors are not great and the single value predicted by Eurocode 3 was determined to be reasonable. For the case considered, Eurocode 3 would require fourteen intermediate connectors, while the tests showed little increase in strength when the number of connectors was increased from 2 to 5. The *AISC specification E.4* allowed as few as two intermediate connectors on the sections tested. With five intermediate connectors the tests and the *AISC specification* indicate that the full elastic buckling strength of the member is essentially achieved.

Sherman and Yura propose the following equation for determining the shear transfer force in the end connection for which slip is to be prevented.

$$V_{\text{total}} = 0.008PL \frac{Q}{I}$$

Where:

P = Member axial load

L = Member length

Q = First moment of area on one component about the axis of buckling of the built-up member

I = Moment of Inertia about the axis of buckling

They note that it is important to realize that the connection does not have to be designed as slip-critical for the full member load. Only the shear transfer force in the buckled mode must be developed with no slip. This is reflected in the *AISI Specification* (2002) C4.5 criteria number three which requires the shear connector to resist 2.5% of the member axial load (P).

2.2.2.5 *AISI Specification C4.5 (2002)*

Section C4.5 of the 2001 *AISI Specification* deals with Built-Up Members in compression composed of two sections in contact. According to this section, "if the buckling mode involves relative deformations that produce shear forces in the connectors between shapes," the effective length is to be modified to:

$$\left(\frac{KL}{r}\right)_m = \sqrt{\left(\frac{KL}{r}\right)_o^2 + \left(\frac{a}{r_i}\right)^2} \quad (\text{AISI Eq. C4.5-1})$$

Where:

$\left(\frac{KL}{r}\right)_o$ = Overall slenderness ratio of entire section about built up member axis

a = Intermediate fastener or spot weld spacing

r_i = Minimum radius of gyration of full unreduced cross-sectional area of an individual shape in a built-up member

In addition, the fastener spacing (a) shall satisfy the following three criteria:

(1)

$$\frac{a}{r_i} \leq 0.5 \left(\frac{KL}{r} \right)_o \quad (\text{Commentary C4.5})$$

According to the *AISI Commentary* this is to prevent flexural buckling of the individual shapes between the intermediate connectors. The *Commentary* goes on to say that this spacing is "consistent with the previous edition of the *AISI Specification* with the $\frac{1}{2}$ factor included to account for any one of the connectors becoming loose or ineffective." As such, this is considered a conservative spacing requirement.

(2) The ends of a built-up compression member shall be connected by a weld having a length not less than the maximum width of the member or by connectors spaced longitudinally not more than 4 diameters apart for a distance equal to 1.5 times the maximum width of the member. This criteria is to prevent shear slip in the end connection.

(3) Each discrete connector shall be capable of transmitting a longitudinal shear force of 2.5% of the total force in the built-up member. The total

force considered is the unfactored force for ASD and the factored force for LRFD.

The *commentary* goes on to say that "the provision in Specification Section C4.5 has been substantially taken from research in hot-rolled built-up members connected with bolts or welds." They also note that the hot-rolled provisions have been extended to include other fastener types common in cold-formed steel construction, such as screws. When the AISI committee for columns petitioned for adoption of C4.5 they had intent to support research in this area to validate equation C4.5-1. Unfortunately, funding for this research was never allocated by AISI (Schafer 2005). No research for built-up members in compression composed of two sections in contact has been completed prior to this work.

2.2.2.6 Eccentric Intermediate Connections

With the continued automation of the steel industry, fabricators are showing increased interest in robotic welding and single step assembly. In single step assembly the product is not rotated or flipped during the assembly process. This manufacturing process requires that all flat or horizontal welding processes must be made from one side of the product. To use built-up members in this manufacturing process the intermediate welds would be located on one side only, eccentric to the composite member. This is not specifically excluded by the AISI *Specification*, rather the specification is silent on this issue. It is not a type of built-up member that has been studied and reported in the literature.

Chapter 3 Purlin Testing Program

Three different types of test configurations with roof panel and two without roof panel are considered in this research. Figure 3.1 shows an elevation view of the purlins cross-section for the five test configurations. The tests were conducted using 12 and 14 inch deep Zee sections with two different thicknesses of each. The 12 inch deep sections were 30 feet long, and the 14 inch deep sections were 40 feet long. The members were loaded axially along the zee purlins shown in Figure 3.1. After an extensive literature review we can state that these configurations have never been tested. They are unique in: 1) purlin depth and length, 2) the use of bracing similar to that used in typical current practice, & 3) the inclusion of a standing seam roof panel in an axially loaded Zee purlins.

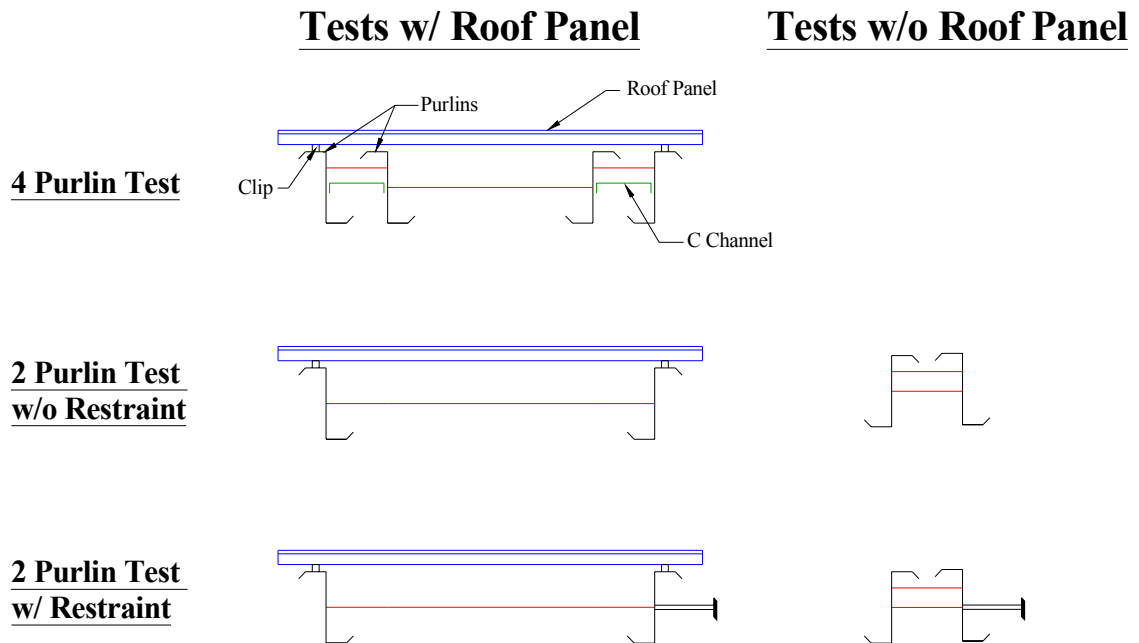


Figure 3.1 Test Configurations

3.1 Purlins with Standing Seam Roofing

All strut purlins are connected directly to a roof system. While the primary contribution of this roof system to the structure is weather tightness there is considerable thought that the interaction of the roof clips and panel affects the behavior of the purlins. If this is true then, as with many aspects of metal buildings, they would act as a system. These tests were designed to experimentally quantify the axial capacity of the double strut purlins with interaction with the roof clips and panel.

3.1.1 Tests with Four Purlins

3.1.1.1 Test Objective and Description

This testing configuration duplicates a portion of a typical full-scale roof system. Each test consisted of two pairs of two purlins with a 24 gauge standing seam roof panel attached. The roof clip used in this test had a 1 inch offset and is the standard slide clip for Star Building Systems. No roof insulation was installed in this test. This setup is shown in Figure 3.2.

The outside purlins are considered "roof strut" purlins and the inside purlins are considered "double strut" purlins by the metal building industry. There was an 11 inch space between the purlins in each pair. This is the standard distance used by Star Building Systems. The roof panels were attached to the top flange of the outside (strut purlin) purlin with standing seam clips and the inside (double strut) purlin is not. The clips elevated the roof panel 1.0 inch above the

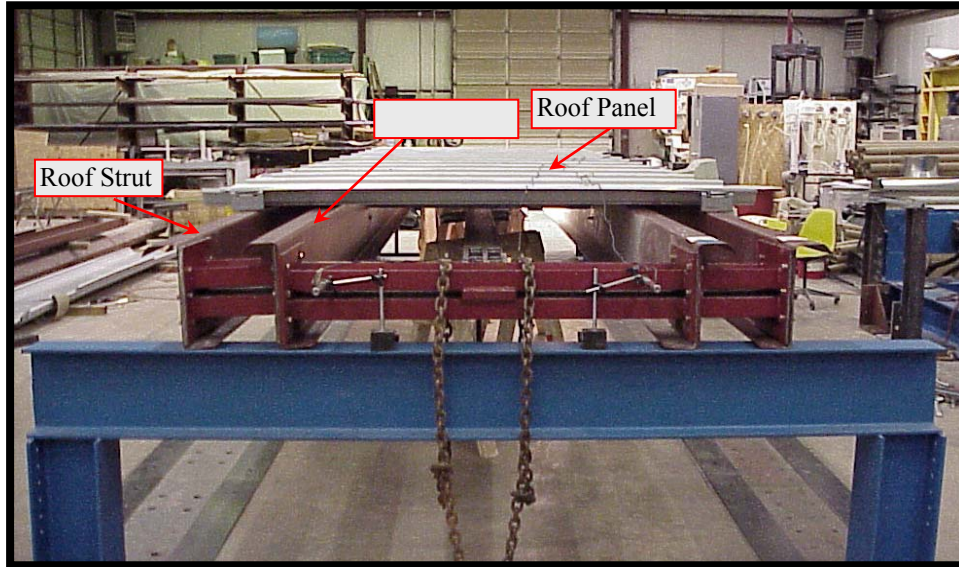


Figure 3.2 Test Set Up

purlin flange. The clips were attached to the purlins with self-drilling screws at 24 inches on center. Sag angles were attached to the purlins at three points to brace each pair of purlins which are shown in Figure 3.3. These bracing points are at the third points of the purlins if three feet at each end of the purlin is ignored. This is Star Building System's standard bracing locations. During the preliminary tests, large lateral deflections of the purlin and roof system were observed due to the long span and high slenderness ratio. At the sponsors request this deflection problem was reduced by adding a press broke, cold-formed Cee channel between the purlins in each pair. Each channel had an 11 inch web and a 3 inch flange and was 12 ft. long. The channels were centered on the length of the purlin spans and attached to the purlins with bolts at the center and each end of the channel. This channel is shown Figure 3.3.

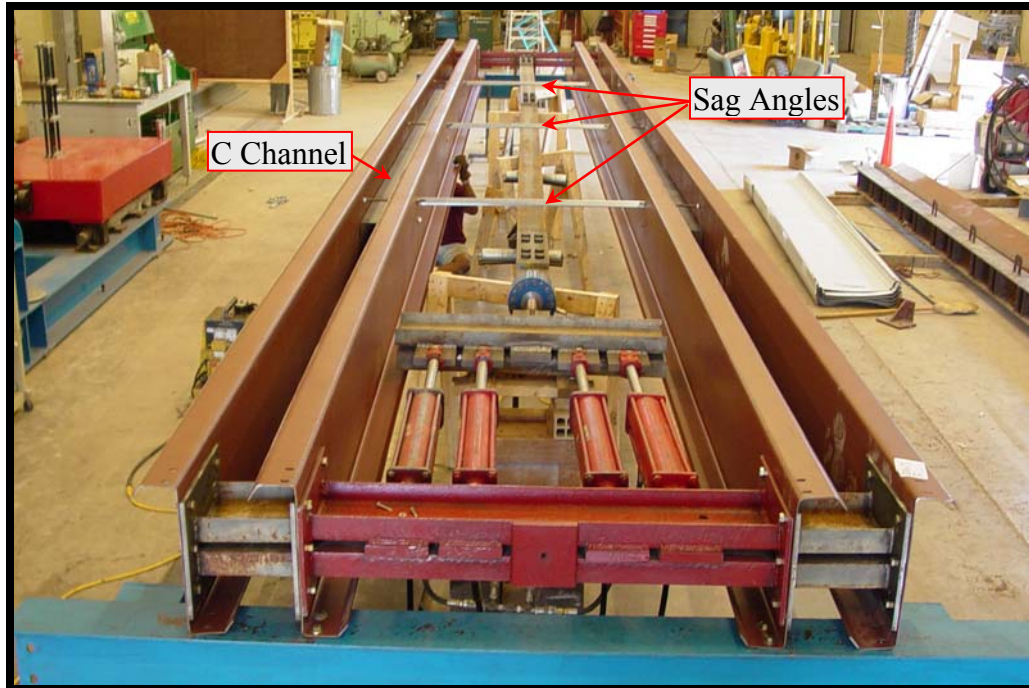


Figure 3.3 Cee Channel In Between Purlins To Prevent Lateral Sway

Both 12 inch and 14 inch deep purlins were tested in this setup. The 12 inch deep purlins were 30 foot long, and the 14 inch deep purlins were 40 foot long. Table 3.1 shows properties of the purlins tested in this series.

Table 3.1 Test Section Properties (Four Purlin Tests)

Section	Depth (in)	Thickness (in)	Area (in ²)	Length (ft)	Wt/ft (lbs)	Number of Tests
12Z080	12	0.080	1.65	30	5.59	3
12Z100		0.100	2.07		7.03	3
14Z080	14	0.080	1.85	40	6.29	3
14Z134		0.134	3.14		10.68	3

The purlins were supported on each end by a support frame connected to the reaction floor. Details of the test setup can be seen in Figures 3.4, 3.5 & 3.6. They were bolted to the frame at one end in order to provide stability and the other end was free to allow for axial shortening of the specimens. A safety chain was loosely connected between the free end spreader beam and the support frame. This was done to prevent the specimen from dangerous, large displacements when failure of the specimen occurred. The safety chain can be seen in Figure 3.6, which also shows the test setup before the roof panel was installed. The saw-horses in Figure 3.6 support the tension strap during set up and the initial steps of the test. As force is applied to the tension strap it lifts off of the saw-horses and becomes a frictionless, two force tension element.

Force was applied to the specimens using four 4 inch bore hydraulic cylinders connected in parallel. Each cylinder had a maximum capacity of 27 kips. A spreader beam consisting of three pieces at one end of the test setup transferred force from the hydraulic cylinders to the strut purlins. A similar spreader beam was used at the other end of the purlins. These spreader beams were made with two C8x11.5 channels welded back to back and spaced one inch apart. The spreader beams were connected with a 1 inch x 6 inch steel plate "connection strap" which acted as a tension element during the test.

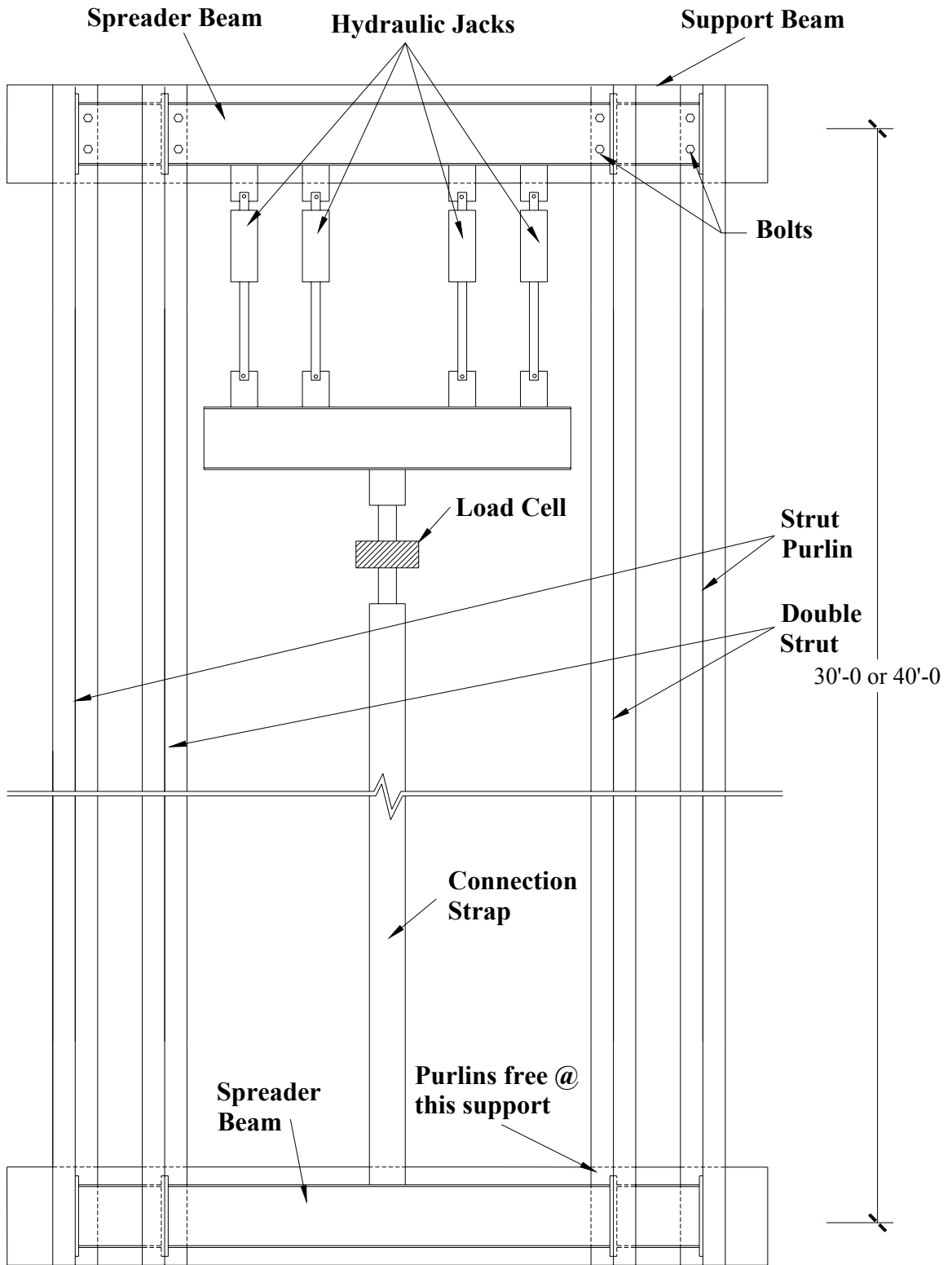
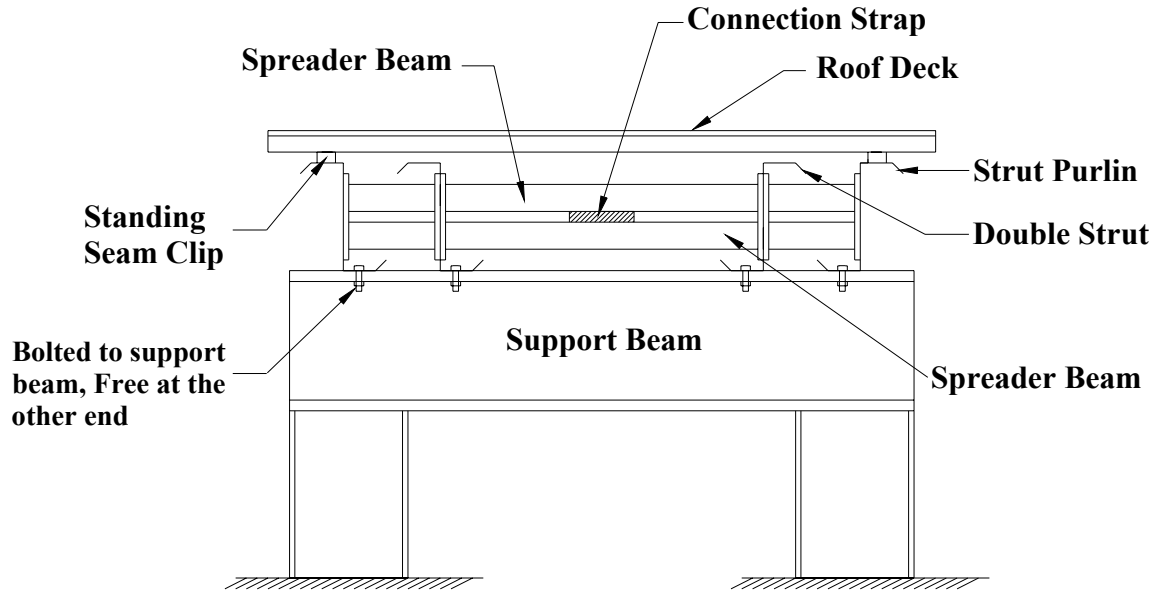
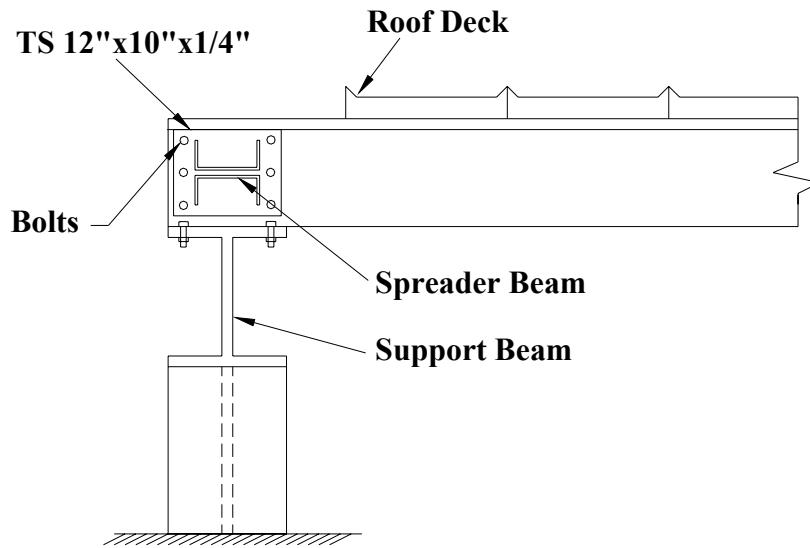


Figure 3.4 Plan View of Test Setup (4 Purlin Test)



End View



Sideview

Figure 3.5 Test Supports and Spreader Beam

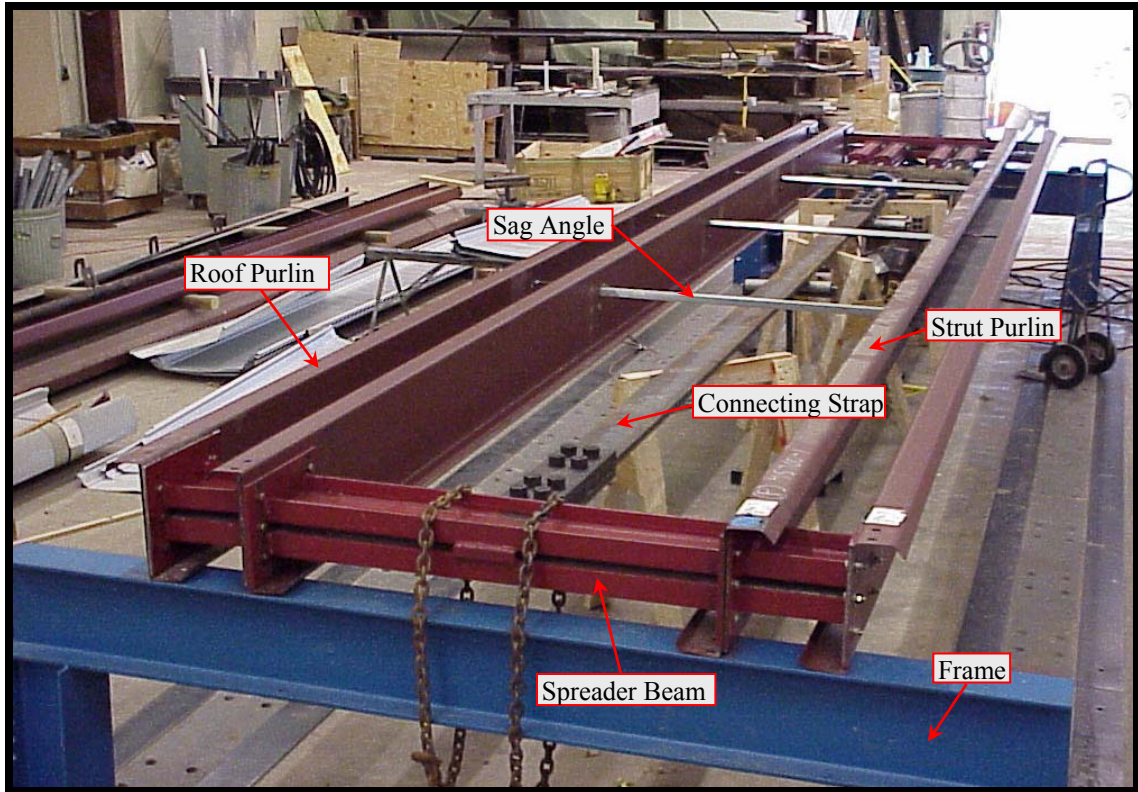


Figure 3.6 Four Purlin Test Setup without Roof Panel

3.1.1.2 Instrumentation and Data collected

Load was measured with a 100 kip capacity load cell in line with the connecting strap. Two Linear Variable Displacement Transducers (LVDT's) were used to measure the longitudinal deflection of the specimen during testing. They are shown in Figure 3.7.

The LVDT's had spring-loaded plungers to bear against the specimen and had a maximum usable stroke of approximately 0.7 inches. Beyond this point, the LVDT signal remains constant as the test continues. The LVDT's were positioned to maximize their useful travel. Measurements were taken at each end of the spreader beam so that any rotation of the system could be recorded. The specimens

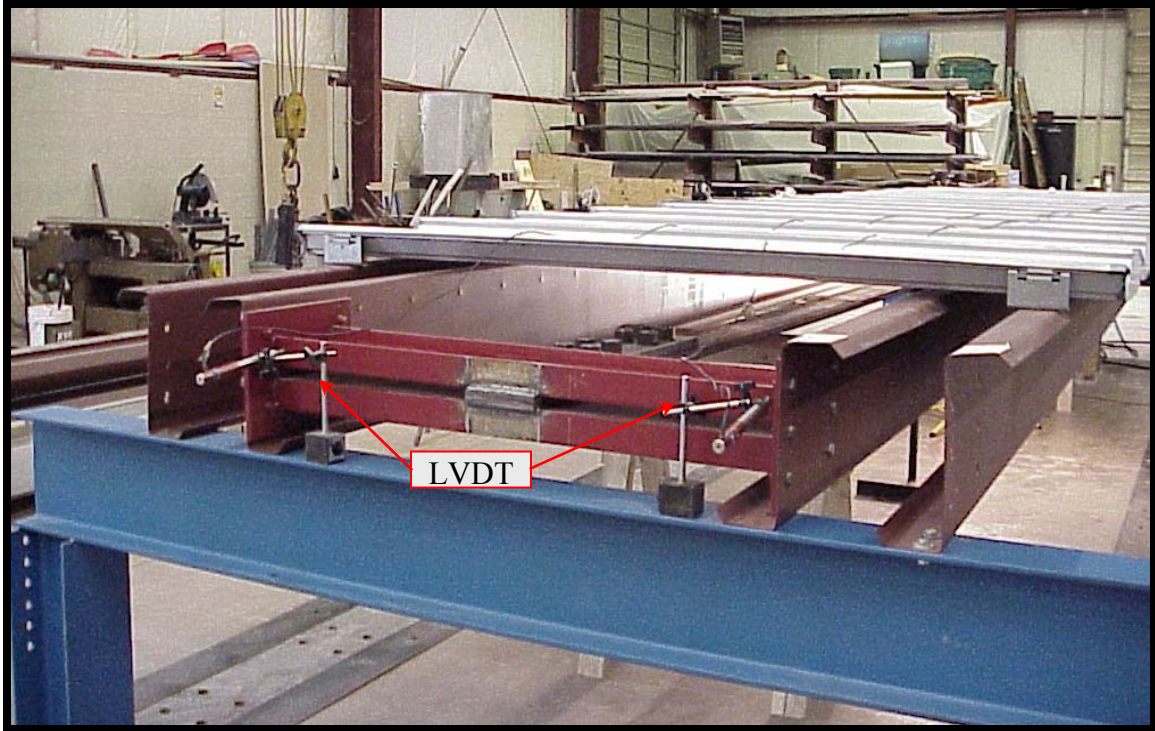


Figure 3.7 LVDT Placement

were numbered sequentially for identification. Data from each test was stored in a computer file with the file name matching to the specimen. Data was plotted as load vs. LVDT displacement. Data from the same configuration and loading are printed on a common plot. Plots for all tests are included in Appendix B.

3.1.1.3 Test Procedure

Each specimen was installed in the testing frame and attached to the spreader beams using six, $\frac{1}{2}$ inch diameter A307 bolts at each connection. All bolts were snug tightened. Care was taken so that the purlins and hydraulic cylinders were arranged symmetrically. This ensured that the same load was applied to each purlin and that significant moments were not introduced into the

system. The sag angles and channels were installed to restrain the purlins against relative displacement, and the roof panel was installed.

The location of each LVDT on the specimen was measured and recorded. The data acquisition system was initialized while there was slack in the tension strap, ensuring that the data acquisition system's initial definition of zero load was correct. An electric-powered hydraulic pump was used to load the strut purlins. The rate of loading was manually controlled. A constant rate of loading was maintained by coordinating the hydraulic pump with the readings on the computer monitor. The monitor displayed the purlins axial shortening and load on the section. The specimen was loaded slowly so that a sufficient number of data points could be collected and the behavior of the system could be carefully observed. The real-time display of load vs. axial shortening was carefully monitored during each test to help determine when the specimen behavior was changing so that significant behavior could be observed as it occurred. The test was terminated when the monitor indicated that the specimen was no longer accepting additional load, indicating that the specimen had reached its maximum axial capacity. A time of ten minutes actual loading was typical. Peak loads were printed out on the computer printer, and all data was stored on disk after each test. Failure modes of the specimens were noted and documented with photographs.

3.1.2 Tests with Two Purlins and Without Lateral Restraint

The purlin tests with standing seam roofing were large and expensive. They required a lot of time to set up, a fair amount of equipment and the roof panel and clips had to be new for each test. Because of these constraints only a limited number of tests were possible. Originally only the four purlin tests had been planned but as we constructed the first tests we realized that by elevating the test off the floor we could remove the inner double strut purlin and have one test of a single strut. Since all of the tests remain in the elastic range reloading the purlins would be ok. With the four purlin test we had initially decided to test the worst case scenario of no lateral restraint provided by the eave strut. We duplicated this with the two purlin test but we also decided to test it with lateral bracing provided by the strong floor. This would provide us with information that would help us to bracket the conditions found on a real building.

3.1.2.1 Test Objective and Description

The goal of this test was to check the behavior of purlins when acting independently as a "purlin strut" rather than in pairs as "double purlin struts". This test was also desirable because it allowed us to compare our data with the tests done previously by Fisher et al (1993). Each test consisted of only the outer purlin of each pair spaced 5 feet 8 inch apart. The purlins were attached to one another at three points by 3/8" diameter rods. The replacement of the sag angles with the more flexible threaded rods was due to the increased distance between the purlins

which could not be spanned by the sag angles. The testing apparatus from the tests with four purlins was used for this test. Figures 3.8, 3.9 and 3.10 show details of this test setup. The three pieces of spreader beam used in the four purlin test were bolted together to span the 5 feet 8 inches separating the purlins. This detail can be seen in Figures 3.7 and 3.9. The roof panels were attached to the top flanges of the purlins with standing seam clips in the same manner as the four purlin test. Table 3.2 lists the purlins tested in this series.

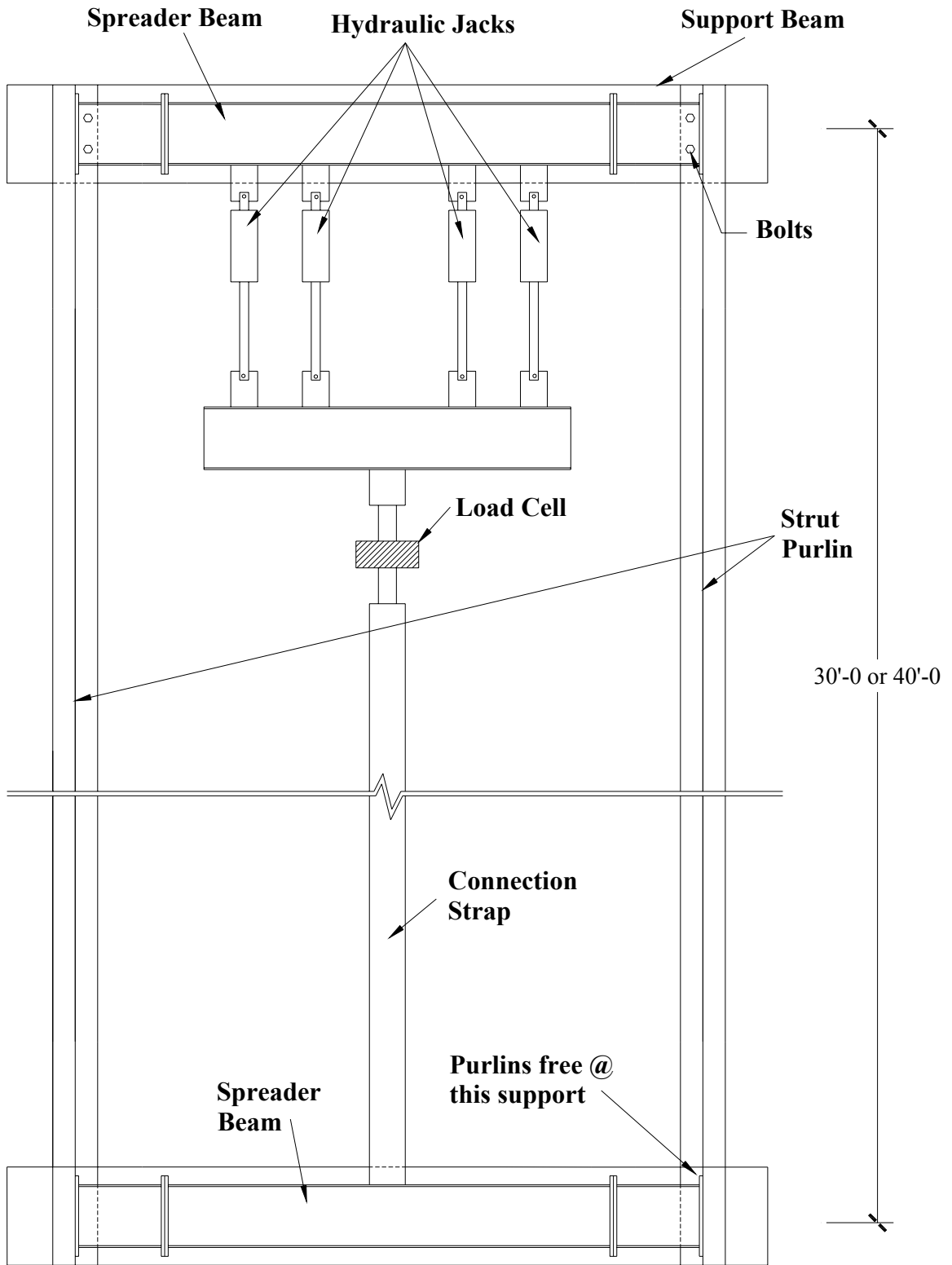


Figure 3.8 Plan View of Test Setup (2 Purlin w/o Lateral Restraint)

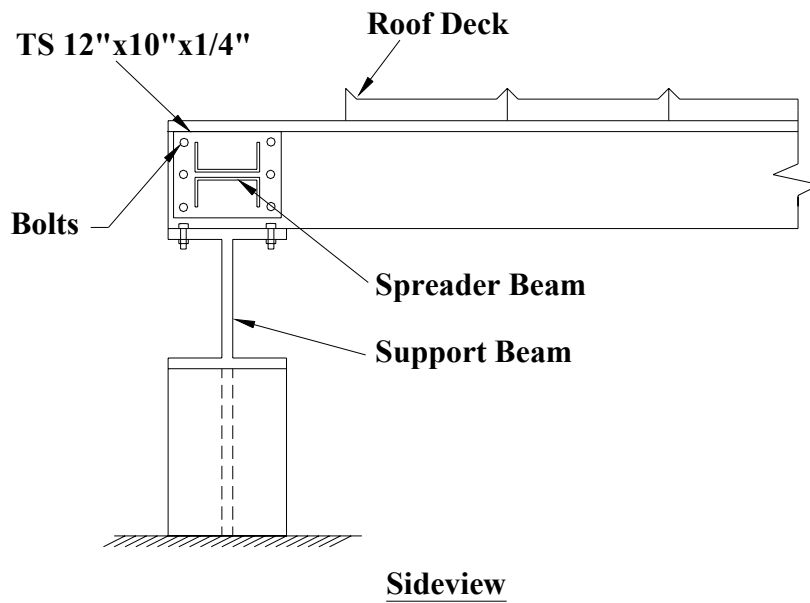
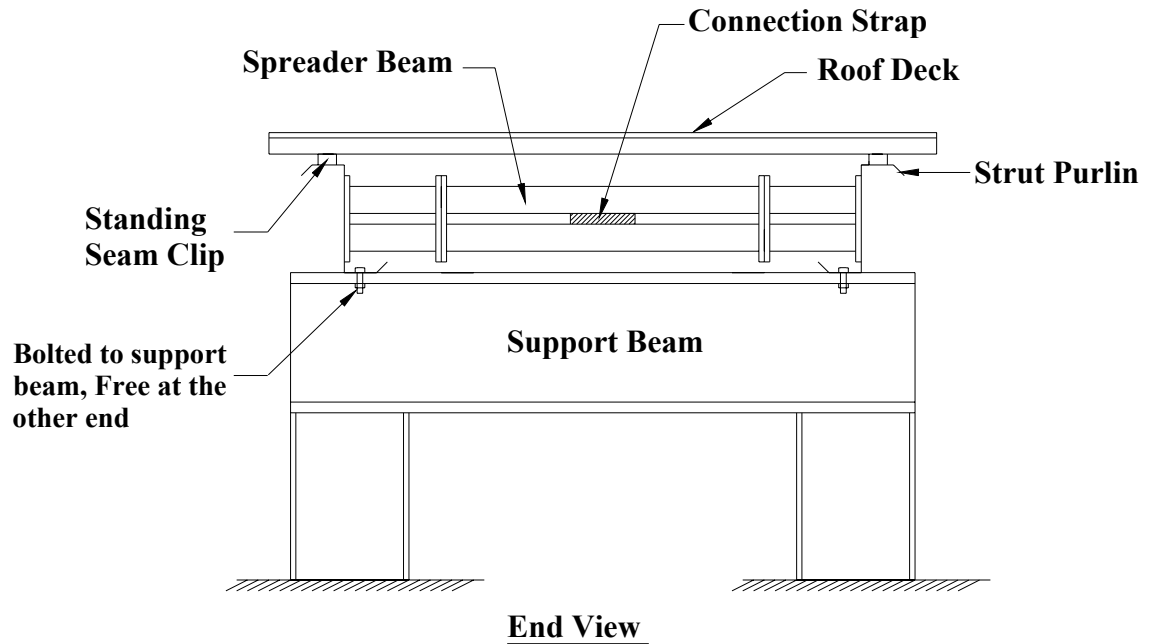


Figure 3.9 Test Supports and Spreader Beam



Figure 3.10 Two Purlin Test without Lateral Restraint

Table 3.2 Test Section Properties (Two Purlin w/o Lateral Restraint)

Section	Depth (in)	Thickness (in)	Area (in ²)	Length (ft)	Wt/ft (lbs)	Number of Tests
12Z080	12	0.080	1.65	30.00	5.59	1
12Z100		0.100	2.07		7.03	1
14Z080	14	0.080	1.85	40.00	6.29	1
14Z134		0.134	3.14		10.68	1

3.1.2.2 Instrumentation and Data collected

The specimens in this group of tests were instrumented identically to the specimens in the tests with four purlins. Load-displacement plots for all tests are included in Appendix B.

3.1.2.3 Test Procedure

The testing procedure for this group of tests was identical to the procedure followed when testing the specimens with four purlins.

3.1.3 Tests with Two Purlins with Lateral Restraint

3.1.3.1 Test Objective and Description

This series of tests was a modification of the tests with two purlins and no external lateral bracing. The purpose of this modification was to measure the increase in the capacity as a result of bracing the system globally against lateral deformations. In an actual building, the sag angles are partially restrained to some degree by both eave strut and peak connections. The two purlin test without lateral restraint assumed that the eave strut and peak has zero stiffness and does not restrain buckling of the purlins. This test, with the lateral restraint provided by a strong floor and a small amount of steel linkage models the restraint provided by an eave strut and peak that are nearly infinitely stiff. In real construction the stiffness of the eave strut falls somewhere between these two extreme values. The results of these tests bracket all possible conditions found in practice.

In this test, the threaded rods were replaced by hot rolled angles, because the threaded rods were very flexible and would not be able to provide adequate bracing between the purlins. The purlins were braced at the same locations as in the previous tests. One side of the brace system was attached to the reaction floor to prevent any lateral movement of the system. Figures 3.11, 3.12 and 3.13 show

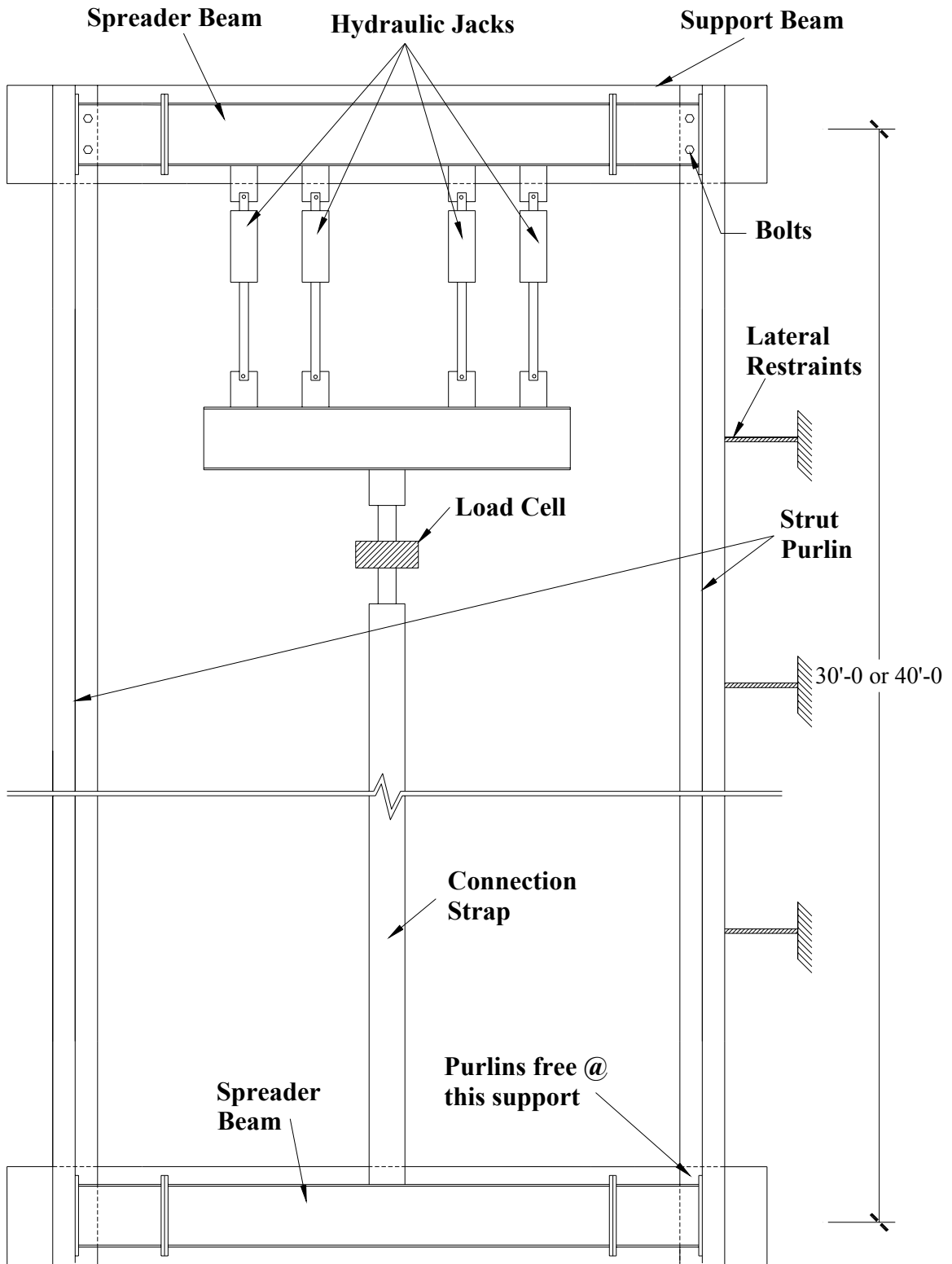


Figure 3.11 Plan View of Test Setup (2 Purlin w/ Lateral Restraint)

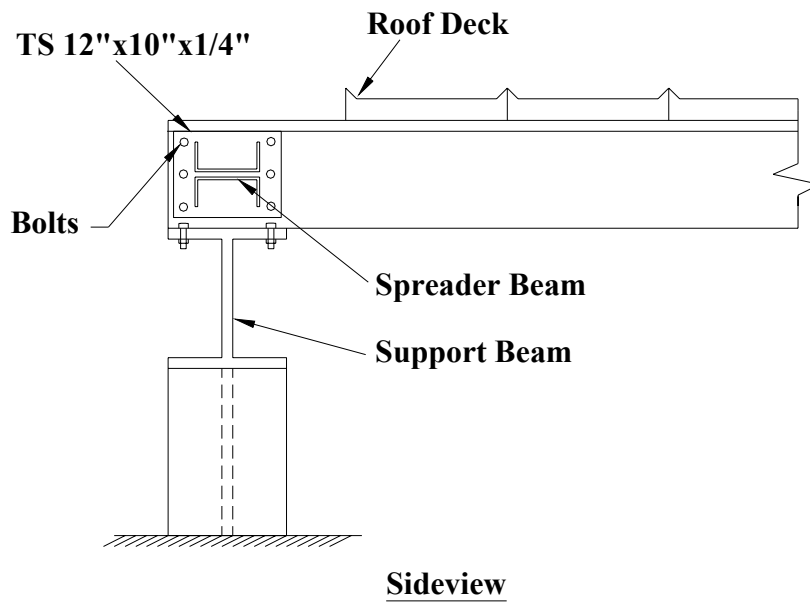
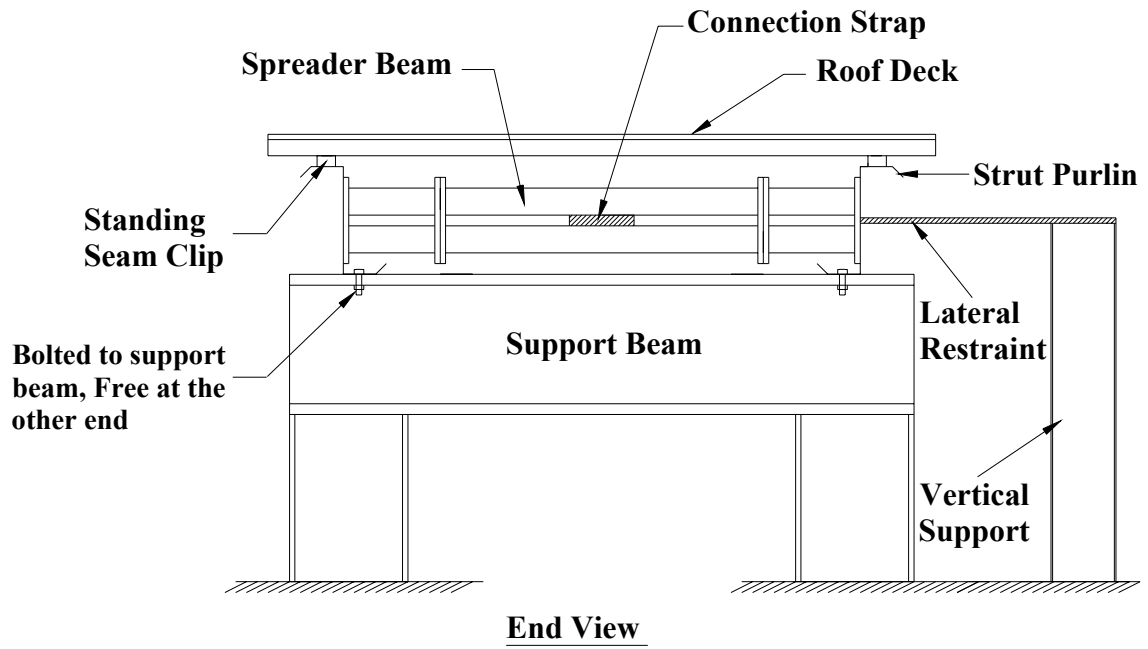


Figure 3.12 Test Supports and Spreader Beam

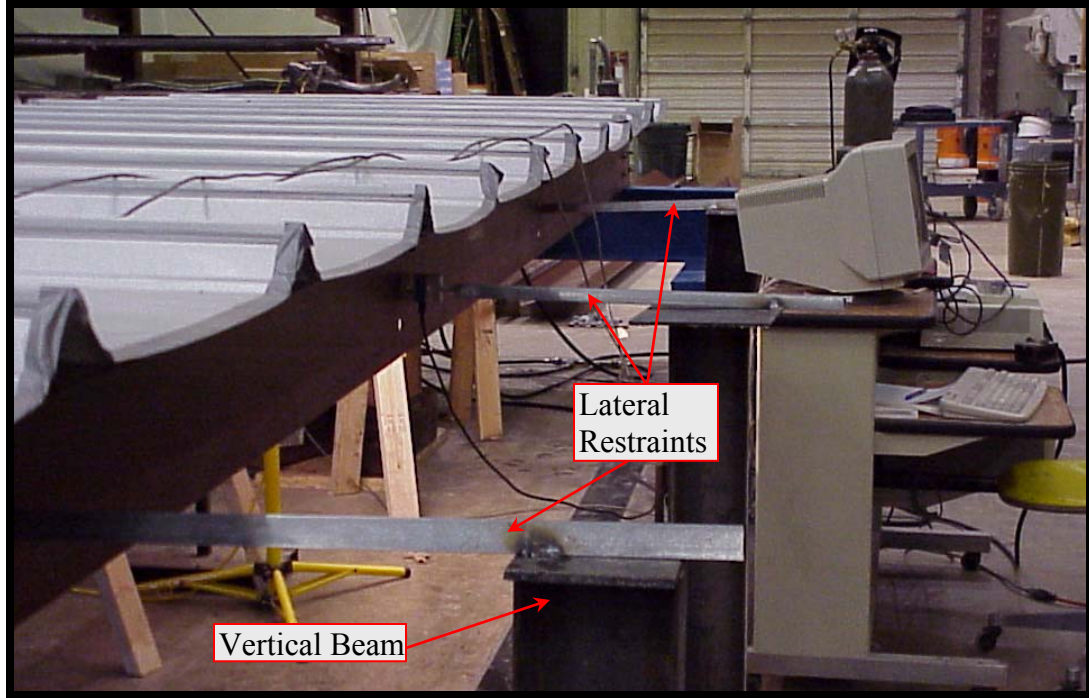


Figure 3.13 Lateral Restraints

details of this test configuration. The external bracing was provided by attaching a second set of sag angles to the outside or opposite side of the purlin, directly below the sag angles bracing the purlins to one another, as shown in Figure 3.12. The sag angles were then connected to a vertical beam bolted to the reaction floor. The remainder of the test setup was identical to the tests with two purlins and no external lateral restraint. Table 3.3 lists the purlins tested in this series.

Table 3.3 Test Section Properties (Two Purlin w/ Lateral Restraint & roof panel)

Section	Depth (in)	Thickness (in)	Area (in ²)	Length (ft)	Wt/ft (lbs)	Number of Tests
12Z080	12	0.080	1.65	30	5.59	1
12Z100		0.100	2.07		7.03	1
14Z080	14	0.080	1.85	40	6.29	1
14Z134		0.134	3.14		10.68	1

3.1.3.2 Instrumentation and Data collected

The specimens in this group of tests were instrumented almost identically to the specimens in the tests with four purlins. The only difference is that the lateral force on the center restraint was measured with a 4 kip capacity load cell located on the sag angle that was anchored to the strong floor. This load cell is shown in Figure 3.14. Load-displacement plots for all tests are included in Appendix B.

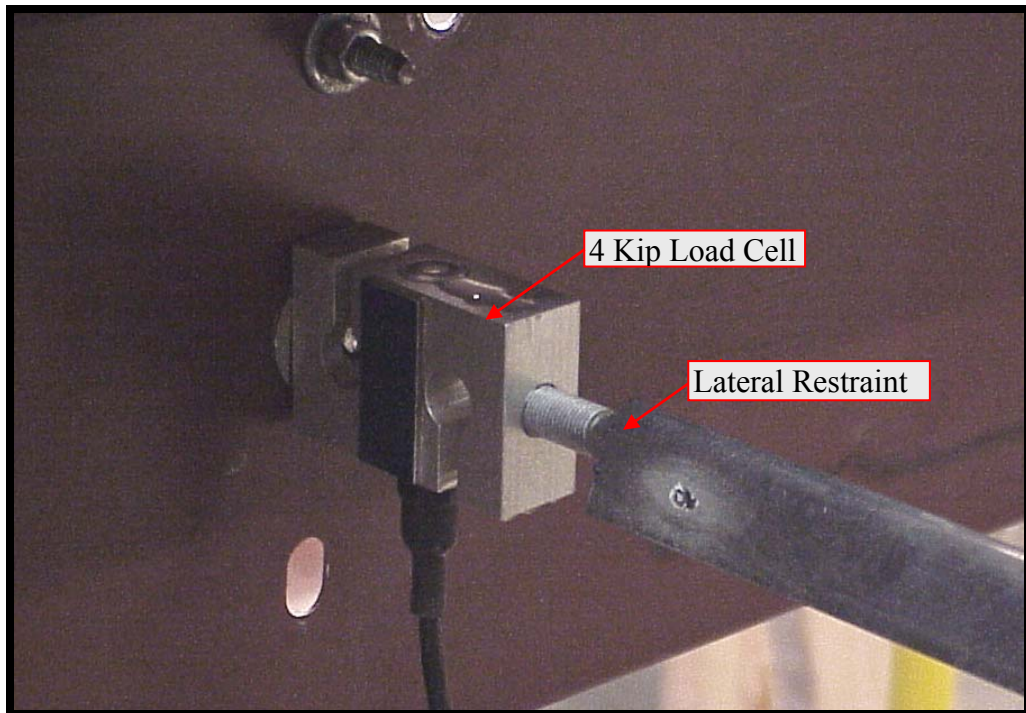


Figure 3.14 Measurement of Lateral Force Using Load Cell

3.1.3.3 Test Procedure

The testing procedure for this group of tests was almost identical to the procedure followed when testing the specimens with four purlins. The only variation was recording of the lateral load on the center sag angle.

3.2 Purlins with No Roofing

After the purlin tests with standing seam roofing were completed and the data was reviewed it became clear that: 1) we had an extremely limited amount of data, 2) the data hinted at some interesting possibilities & 3) that purlin tests without roof panel might be able to shed some light on the problem. While the effect of the interaction of the panel clip and panel with the purlin was not included in these tests, their results provided additional information. This included a comparison which helps quantify the effect of the interaction with the roof panel.

We had tested the two purlin test with and without lateral bracing. Because of this it was decided that the purlin tests with no roof panel would also be tested with and without lateral bracing. The test with no lateral restraint models the condition of no stiffness provided by the eave strut, while the test with the lateral restraint provided by a strong floor models the condition of almost infinite stiffness provided by the eave strut. In the real world the stiffness that the eave strut provides would fall somewhere between these two tests. Essentially these tests will bracket all possible real world conditions as far as the bracing conditions.

3.2.1 Tests with Two Purlins but without Lateral Restraint

3.2.1.1 Test Objective and Description

As mentioned earlier this test models the condition of no stiffness provided by the eave strut. It does not model the interaction of the panel clip and panel. The test objective was to try to quantify the affect of the panel clip and panel on the axial capacity of a Zee purlin with no stiffness provided by the eave strut.

A test consisted of two purlins attached to each other at each end and spaced 11 inches apart by the small spreader elements used in the purlins with standing seam roof tests. The purlins were attached to one another at three points by 3/8" diameter rods in the middle hole of a punched hole group. These were located at Star Building Systems standard brace points, located at the third points of the purlins if three feet at each end of the purlin is ignored. During the preliminary test, a very small nominal capacity was achieved. We noted that the Zee purlins had buckled globally and the cross section of the Zee had rotated. This totally free rotation is impossible to achieve in a building due to the attachment of panel clips or screw down panel. To provide a small amount of stability to the cross section a second 3/8" diameter rod was installed at each brace point in the top hole of a punched hole group.

Figures 3.15, 3.16 and 3.17 show details of this test configuration. Table 3.4 lists the purlins tested in this series.

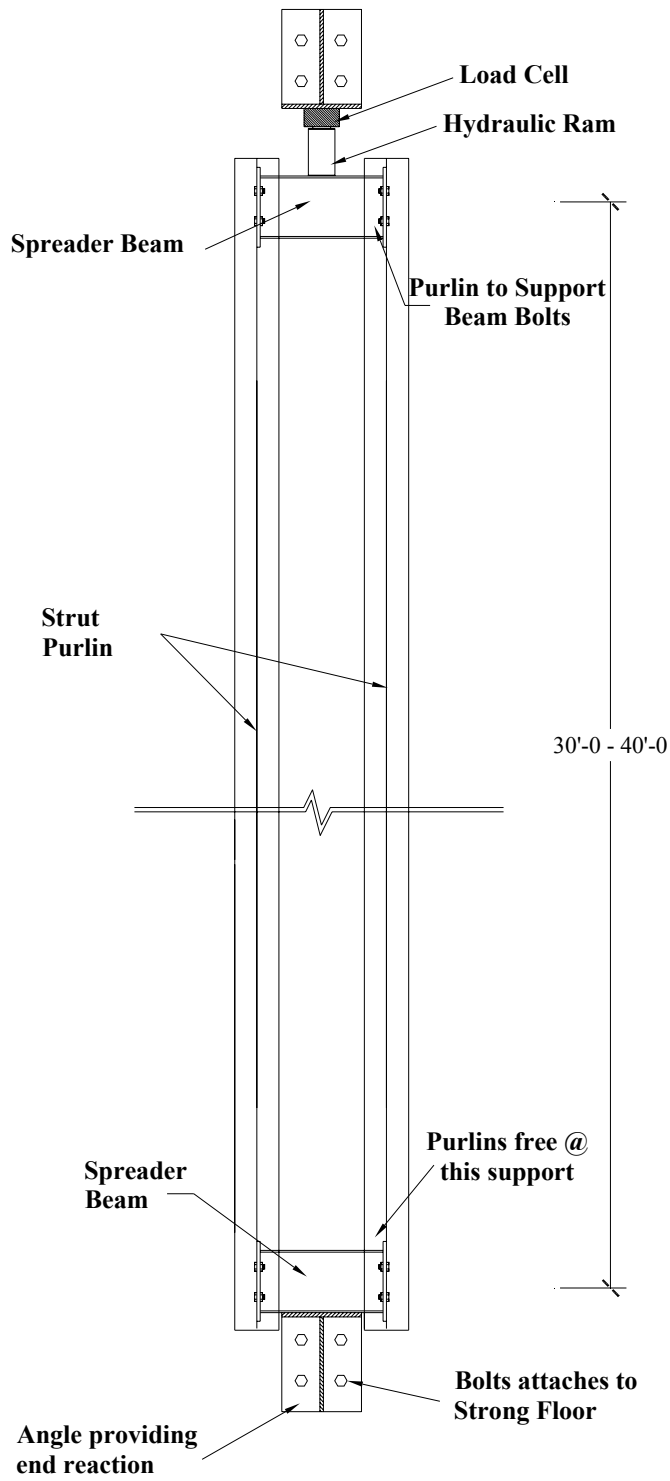
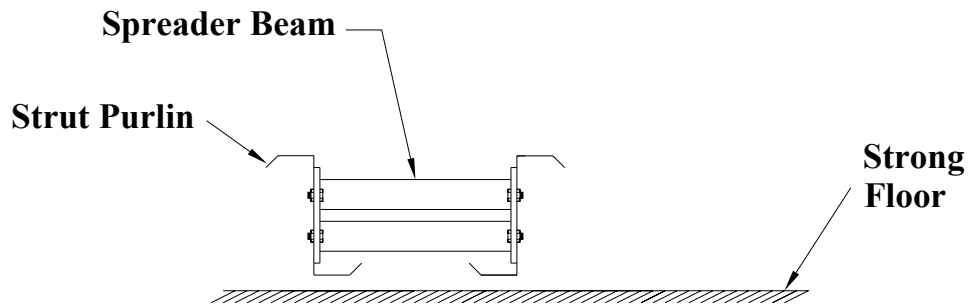
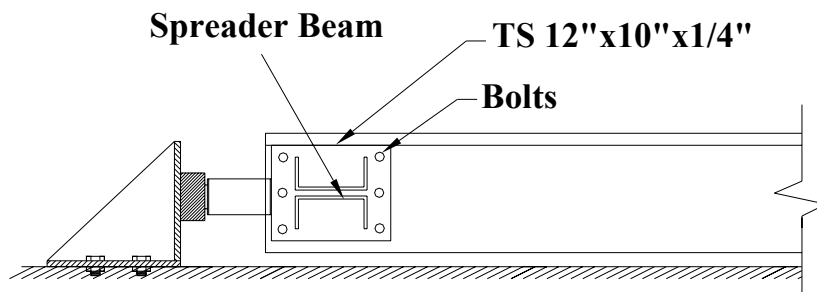


Figure 3.15 Plan View of Test Setup (2 Purlin w/o Lateral Restraint)



End View (End reaction not shown for clarity)



Side View

Figure 3.16 Test Supports and Spreader Beam



Figure 3.17 Two Purlin Test with out Lateral Restraint

Table 3.4 Test Section Properties (Two Purlin w/o Lateral Restraint or Roof Panel)

Section	Depth (in)	Thickness (in)	Area (in²)	Length (ft)	Wt/ft (lbs)	Number of Tests
12Z080	12	0.080	1.65	30	5.59	4
12Z100		0.100	2.07		7.03	4
14Z080	14	0.080	1.85	40	6.29	4
14Z134		0.134	3.14		10.68	3

3.2.1.2 Instrumentation and Data collected

Load was measured with a 100 kip capacity load cell in line with the purlin, resting on a wood platform. Two Linear Variable Displacement Transducers (LVDT's) were used to measure the longitudinal deflection of the specimen during testing. One is shown in Figure 3.7 between the purlins.

The LVDT's have spring-loaded plungers to bear against the specimen and had a maximum usable stroke of approximately 0.7 inches. After this point, the LVDT signal remains constant as the test continues. The LVDT's were positioned to maximize their useful travel. Measurements were taken on each side of the spreader beam. The specimens were numbered sequentially for identification. Data from each test was stored in a computer file with the file name matching the specimen. Data was plotted as load vs. LVDT displacement. Data from the same

configuration and loading are printed on a common plot. Plots for all tests are included in Appendix B.

3.2.1.3 Test Procedure

Each specimen was attached to the spreader beams using six, ½ inch diameter A307 bolts at each connection. All bolts were snug tightened. Care was taken so that the purlins and hydraulic cylinders were arranged symmetrically. This ensured that the same load was applied to each purlin and that significant moments were not introduced into the system.

The location of each LVDT on the specimen was measured and recorded. The data acquisition system was initialized while there was no load on the hydraulic cylinder, ensuring that the data acquisition system's initial definition of zero load was correct. An hand-powered hydraulic pump was used to load the strut purlins. The monitor displayed the axial shortening and load of the section. The specimen was loaded slowly so that a sufficient number of data points could be collected and the behavior of the system could be carefully observed. The real-time display of load vs. axial shortening was carefully monitored during each test to help determine when the specimen behavior was changing so that significant behavior could be observed as it occurred. The test was terminated when the monitor indicated that the specimen was no longer accepting additional load, indicating that the specimen had reached its maximum axial capacity. A time of ten minutes for loading was typical. Peak loads were printed out on the computer

printer, and all data was stored on disk after each test. Failure modes of the specimens were noted and documented with photographs.

3.2.2 Tests with Two Purlins and Lateral Restraint

3.2.2.1 Test Objective and Description

As mentioned earlier this test models the condition of almost infinite stiffness provided by the eave strut. It does not model the interaction of the panel clip and panel. The test objective was to try to quantify the affect of the panel clip and panel on the axial capacity of a Zee purlin with extremely high stiffness provided by the eave strut.

These tests were almost identical to the two purlins, no panel or lateral restraint tests. The only variation was the lateral restraint at the brace points that was attached to the strong floor.

Figures 3.18, 3.19 and 3.20 show details of this test configuration. Table 3.6 lists the purlins tested in this series.

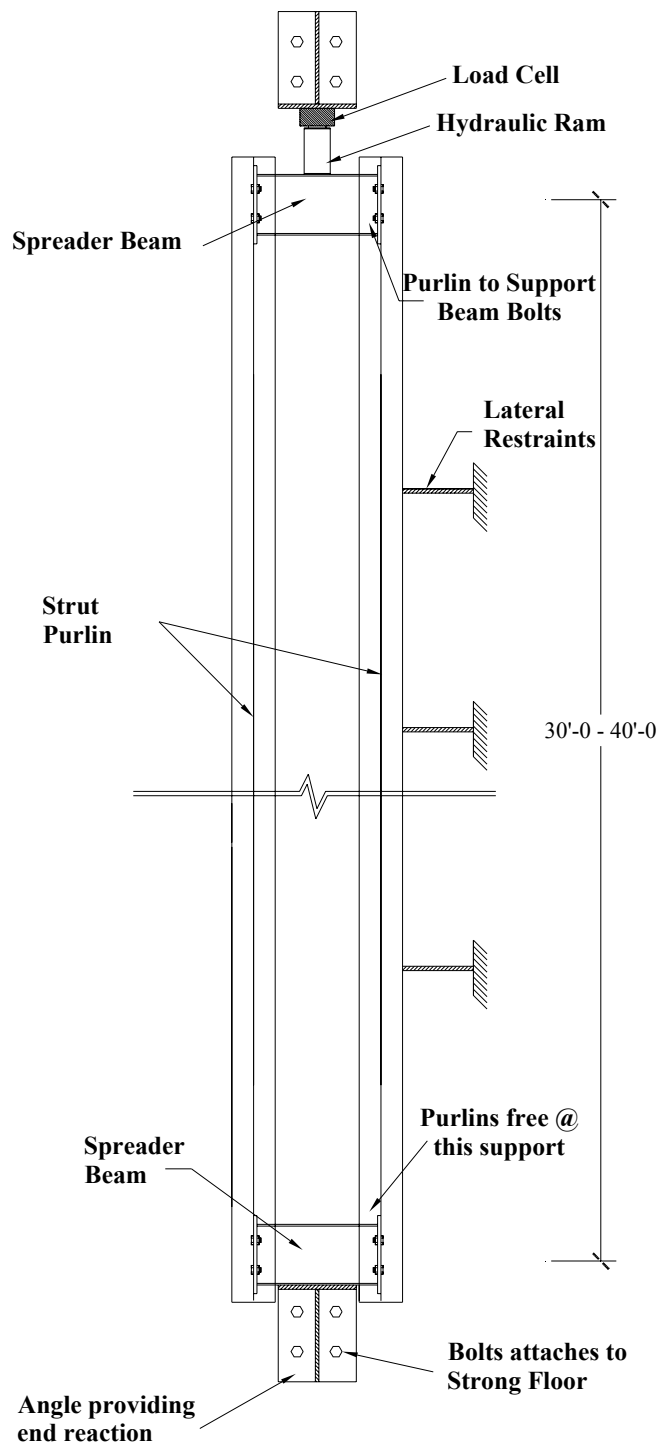
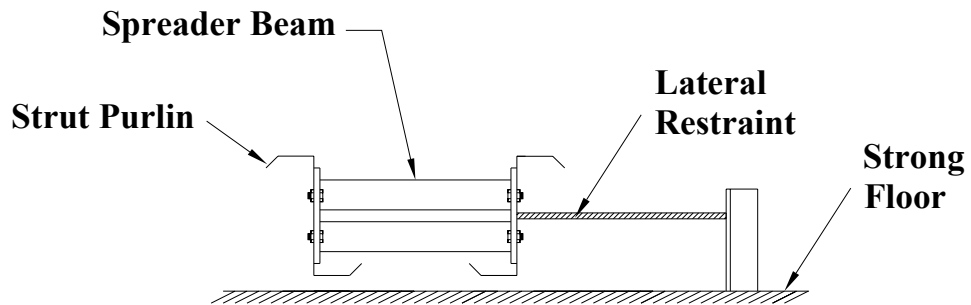
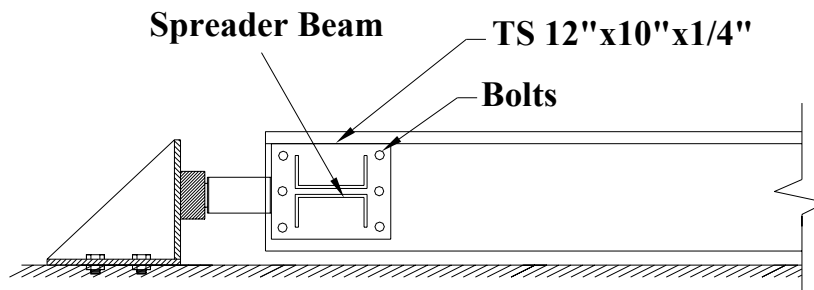


Figure 3.18 Plan View of Test Setup (2 Purlin with Lateral Restraint)



End View (End reaction not shown for clarity)



Side View

Figure 3.19 Test Supports and Spreader Beam

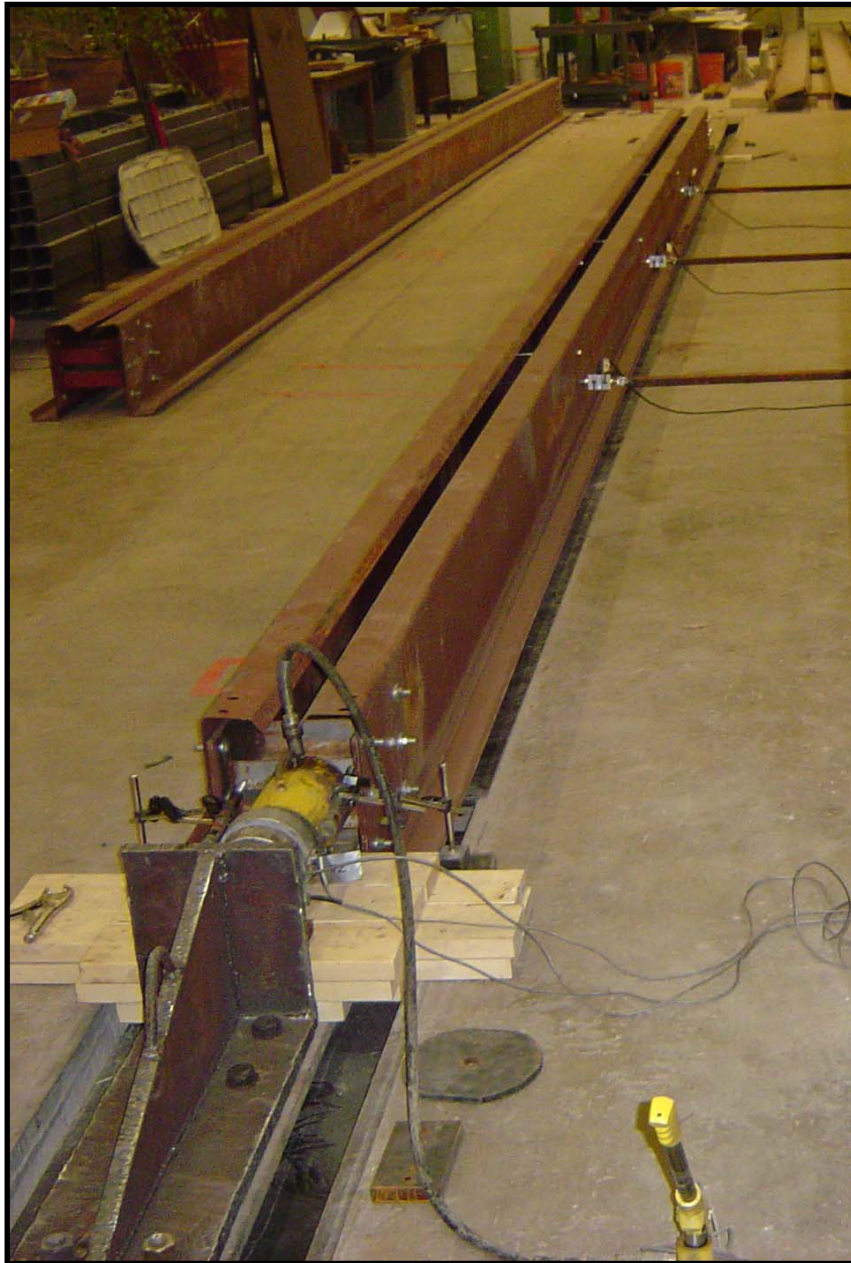


Figure 3.20 Two Purlin Test with Lateral Restraint

Table 3.6 Test Section Properties (Two Purlin w/ Lateral Restraint w/o Roof Panel)

Section	Depth (in)	Thickness (in)	Area (in²)	Length (ft)	Wt/ft (lbs)	Number of Tests
12Z080	12	0.080	1.65	30	5.59	4
12Z100		0.100	2.07		7.03	4
14Z080	14	0.080	1.85	40	6.29	4
14Z134		0.134	3.14		10.68	3

3.2.2.2 Instrumentation and Data collected

The specimens in this group of tests were instrumented almost identically to the specimens in the tests with two purlins, no panel or lateral restraint. The only difference is that the lateral force on the three restraints was measured with a 4 kip capacity load cell located on the tubes that was anchored to the strong floor. These load cells are shown in Figure 3.14 & 3.20. Load-displacement plots for all tests are included in Appendix B.

3.2.2.3 Test Procedure

The testing procedure for this group of tests was almost identical to the procedure followed when testing the specimens with two purlins, no panel or lateral restraint. The only variation was recording of the lateral load on the lateral restraints.

Chapter 4 Built-up Member Testing Program

This research is broken into two distinct groups of tests: tests with a fixed end condition and tests with a pinned end condition. Since the built-up member design equation is a modification of KL/r all three terms will be used as variables during this investigation. The effective length factor K , is natural division of the research since it is determined by the boundary conditions of the test and only these two boundary conditions are easily reproducible in the lab and they bracket the entire spectrum of partially restrained connections.

4.1 Tests with Fixed End Conditions

All of the specimens tested were made from two 1 $\frac{5}{8}$ inch square lipped C sections with a $\frac{3}{8}$ inch lip. Figure 4.1 shows typical built-up sections created for this research. Three nominal material thicknesses were studied: 0.064 in., 0.080 in., and 0.100 in. All specimens in this series were 55 $\frac{1}{2}$ in. long. Five welding patterns were investigated:

- 1) welding the members to one another only at their ends
- 2) adding a stitch weld at mid-length on only one side of the member
- 3) adding stitch welds at mid-length on both sides of the member
- 4) adding stitch welds at the third points on one side of the member.
- 5) adding stitch welds on both sides of the members at the third points

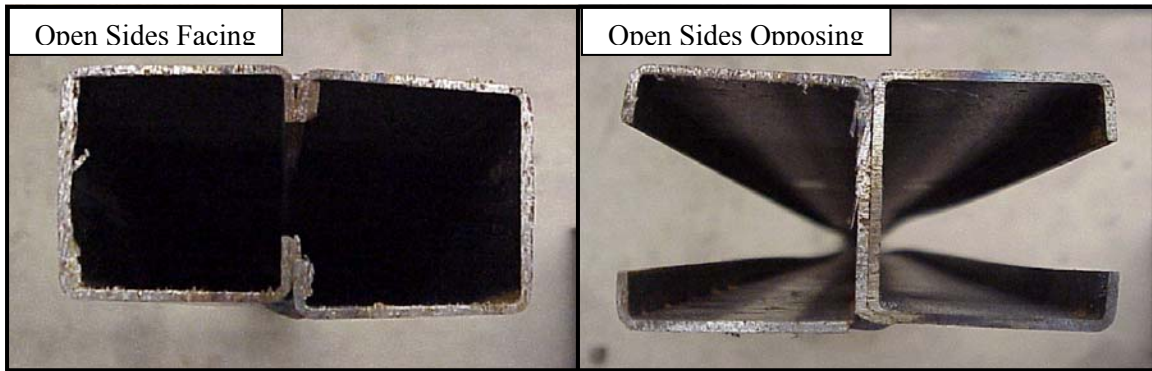


Figure 4.1 Web member pairs

The intermediate stitch welds were approximately 1 ½ in. long. Additionally, the members were connected at their ends with 1 in. long flared groove welds in all specimens. Assuming an effective length factor $K=1.0$ and solving equation AISI Equation C4.5-1 found in section 2.2.2.5 for the maximum spacing of the intermediate fastener, a_{max} , for the sections tested, it was found that $a_{max} = 0.42 * \text{Length}$. Only welding patterns #4 & #5 meet this criterion. Or using $K=0.5$ and solving for the maximum allowed spacing a_{max} , using AISI Equation C4.5-1 it was found that $a_{max} = 0.84 * \text{Length}$. Welding pattern #1 does not meet this criterion. Partial restraint of the ends was assumed in finding the third points. The centers of the welds were located 20.75 in. from each end, and were spaced 14 in. apart. Single members were also tested in order to confirm the accuracy of the analyses, including confirmation of the end fixity.

4.1.1 Test Objective and Description

This group of tests had two objectives. The first objective was to compare the buckling behavior of pairs of web members to the buckling behavior of single

web members. The second objective was to determine the effect of different welding patterns on the critical axial load of a pair of built-up members.

The specimens were placed vertically in a testing frame. To ensure that the load would bear uniformly on the test specimen, the ends of the members were ground flat, and a pivoting head was used to accommodate any remaining out-of-true of the specimen ends. Friction caused this head to become fixed under load. Load was then applied from the top using a hydraulic cylinder and a manual pump. A time of ten minutes actual loading time was typical. Figure 4.2 shows a specimen ready for testing.



Figure 4.2 Specimen with fixed end condition ready for testing

4.1.2 Instrumentation and Data collected

For most of the specimens, load was measured using a 50 kip load cell. For the 0.100 in. thick specimens with stitch welds on both sides and the specimens with stitch welds at third points, load was measured using a 100 kip load cell. An LVDT was used to measure the axial displacement of the specimen during testing. This LVDT had a spring-loaded plunger to bear against the specimen. Readings from the load cell and LVDT were recorded using a PC controlled data acquisition system.

The specimens were numbered sequentially for identification. Data from each test was stored in a computer file with the file name matched to the specimen. Data was plotted as load vs. LVDT displacement. Data from the same configuration and loading are printed on a common plot. Plots for all tests are included in Appendix E.

4.1.3 Test Procedure

Each specimen was placed in the frame and centered under the loading cylinder. A very small load (1-2 pounds) was applied to keep the specimen from falling over. The data acquisition system was then initialized. The specimen was loaded slowly until failure. A time of ten minutes actual loading was typical. Failure modes of the specimens were noted and documented with photographs.

4.2 Tests with Pinned End Conditions

The specimens tested were made from two 1 5/8 or 2 1/2 inch square lipped C sections with a 3/8 inch lip. Figure 4.1 shows typical built-up sections created for this research. Three nominal material thicknesses were studied: 0.064 in., 0.080 in., and 0.100 in. Specimens in this series were 55 1/2 in. and 71 in. long. Seven welding patterns were investigated:

- 1) welding the members only at their ends
- 2) adding a stitch weld at mid-length on only one side of the member
- 3) adding stitch welds at mid-length on both sides of the member
- 4) adding stitch welds at the third points on one side of the member.
- 5) adding stitch welds on both sides of the members at the third points
- 6) adding stitch welds at the sixth points on one side of the member.
- 7) adding stitch welds on both sides of the members at the sixth points

The intermediate stitch welds were approximately 1 1/2 in. long. Additionally, the members were connected at their ends with 1 in. long flared groove welds in all specimens. Assuming an effective length factor $K=1.0$ and solving for the maximum spacing of the intermediate fastener, a_{max} , for the sections tested, it was found that $a_{max} = 0.42 * \text{Length}$. Only welding patterns #4, #5, #6 & #7 meet this criterion. Single members were also tested in order to confirm the accuracy of the analyses for this simple case.

4.2.1 Test Objective and Description

This group of tests had three objectives. The first and second objectives were the same as the fixed end condition tests: 1) to compare the buckling behavior of pairs of web members to the buckling behavior of single web members and 2) to determine the effect of different welding patterns on the critical axial load of a pair of built-up members. The third objective was to be able to compare and contrast the end boundary condition.

The specimens were placed vertically in a testing frame. To ensure that the load would bear uniformly on the test specimen, the ends of the members were ground flat, and a pivoting head was used to accommodate any remaining out-of-true of the specimen ends. Friction did not cause this head to become fixed under load. Load was then applied from the top using a hydraulic cylinder and a manual pump. A time of ten minutes actual loading time was typical. . Figure 4.3 shows a specimen ready for testing.

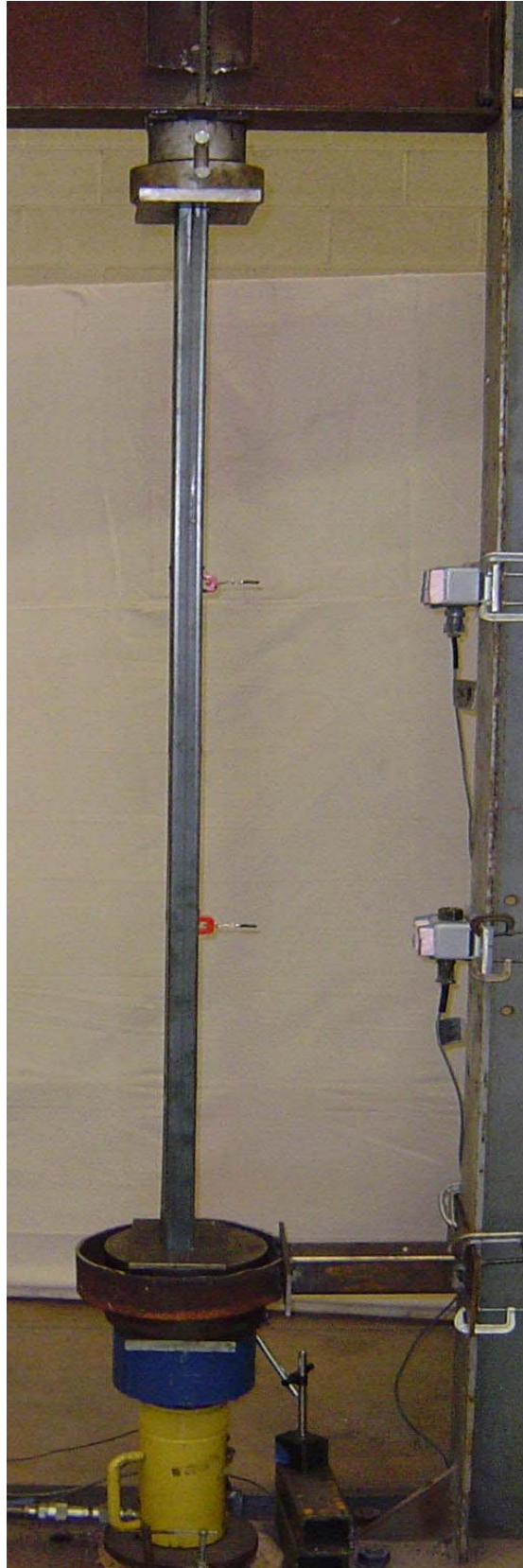


Figure 4.3 Specimen with pinned end condition ready for testing

4.2.2 Instrumentation and Data collected

For all of the specimens with pinned end boundary conditions, load was measured using a 100 kip load cell. An LVDT was used to measure the axial displacement of the specimen during testing. This LVDT had a spring-loaded plunger to bear against the specimen. Two wire-pots were used to measure the transverse displacement at the third points. Readings from the load cell, LVDT and wire-pots were recorded using a PC controlled data acquisition system.

The specimens were numbered sequentially for identification. Data from each test was stored in a computer file with the file name matched to the specimen. Data was plotted as load vs. LVDT displacement. Data from the same configuration and loading are printed on a common plot. Plots for all tests are included in Appendix F.

4.2.3 Test Procedure

Each specimen was placed in the frame and centered under the loading cylinder. A very small load (1-2 pounds) was applied to keep the specimen from falling over. The data acquisition system was then initialized. The specimen was loaded slowly until failure. A time of ten minutes actual loading was typical. Failure modes of the specimens were noted and documented with photographs.

Chapter 5 Test Results

5.1 Purlins with Standing Seam Roof Panel

A summary of the failure load of each test is shown in Table 5.1. These loads are per purlin i.e. the load to fail a single purlin.

Table 5.1 Axial Capacity of a Single Purlin in Tests with Standing Seam Roofing

Length	Test Specimen	Four Purlin Tests		Two Purlin Tests	
		Capacity (kips)	Average Capacity (kips)	Capacity Without Lateral Restraint (kips)	Capacity With Lateral Restraint (kips)
30 ft.	12 Z 080	12.73 12.46 12.85	12.68	12.11	18.02
	12 Z 100	15.53 15.98 16.05	15.85	15.58	29.61
40 ft.	14 Z 080	8.51 8.20 8.50	8.40	8.43	20.94
	14 Z 134	15.52 15.51 15.47	15.50	12.24	30.25

5.1.1 Tests with Four Purlins

5.1.1.1 12 inch deep purlins

The 12 feet long Cee channel bolted between the outer and inner purlins was effective for controlling the lateral sway of the system. Failure of the specimen was due to local buckling of the inner purlins. Local buckling waves in the purlin web (i.e. oil canning) were observed, and are shown in Figure 5.1

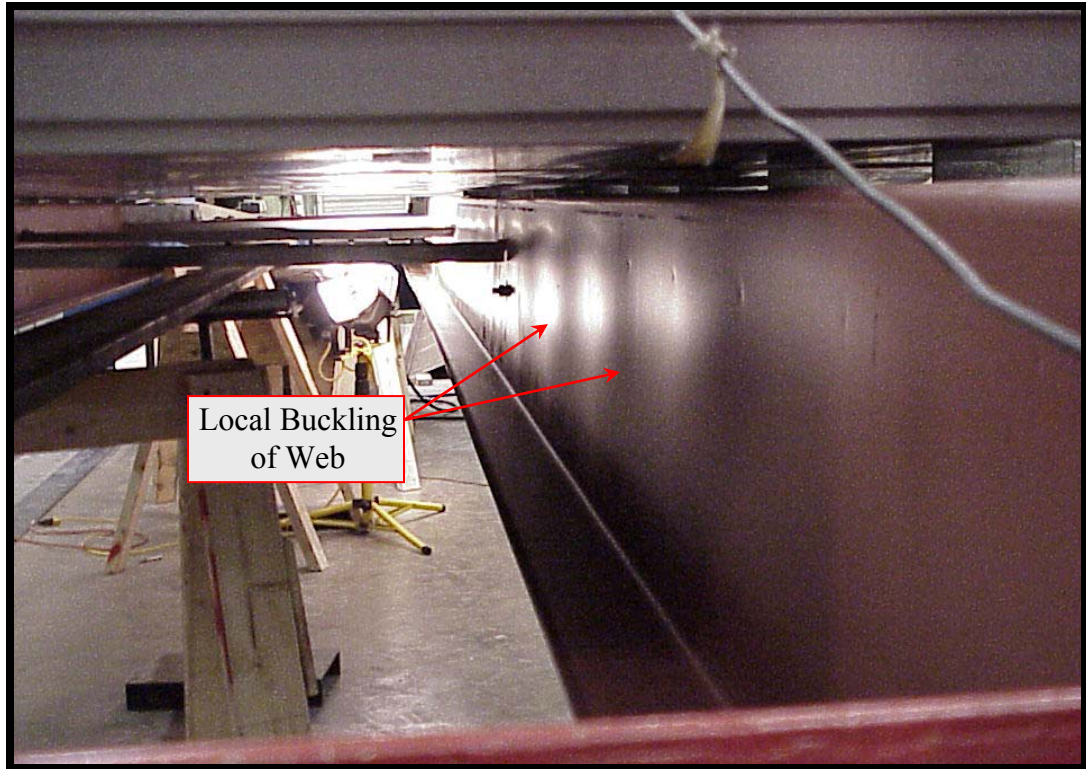


Figure 5.1 Local Buckling Of the Web Due To Axial Compression

This deformation was the first indication of failure due to axial compression of the purlin. The center to center distance between the peaks of the waves was found to be approximately 19 inches. The half wavelength is 9.5 inches. The waves did not form, or minimally formed, in the area laterally restrained by the channels.

5.1.1.2 14 inch deep purlins

The tests with 14 inch purlins were dominated by high lateral deflections due to their high slenderness. The Cee channel bolted between the outer and inner purlins was extended to a total length of 18 feet. Local buckling was observed at loads as low as 5 kip. Loading was terminated when the side sway deflection equaled 3.25 inches which is approximately $L/150$. Figure 5.2 shows a test in

progress with purlins undergoing large amounts of side sway. Local deformations can be seen in both the web and flange lip of the purlin.



Figure 5.2 Purlins Undergoing Large Side Sway

5.1.2 Tests with Two Purlins and no Lateral Restraint

The aim of this test was to check the behavior of purlins when acting as strut purlins rather than as double struts in the case of the four-purlin tests. These tests without lateral restraint, models a condition where the eave strut and sag rod system provides no stability to the system.

5.1.2.1 12 inch deep purlins

The tests were carried out with only the roof purlins braced by a threaded metal rod ($3/8''$ diameter) in place of sag angles. These specimens began showing a noticeable amount of lateral deflection at a total load of 21 kips or 10.5 kips per purlin. A maximum capacity of 12.11 kips per purlin was recorded at a lateral deflection of 3.5 inches with the 0.080 inch thick purlin and 15.58 kips with the 0.100 inch thick purlin. Local buckling was observed throughout the length of the test specimen, as shown in Figure 5.3.

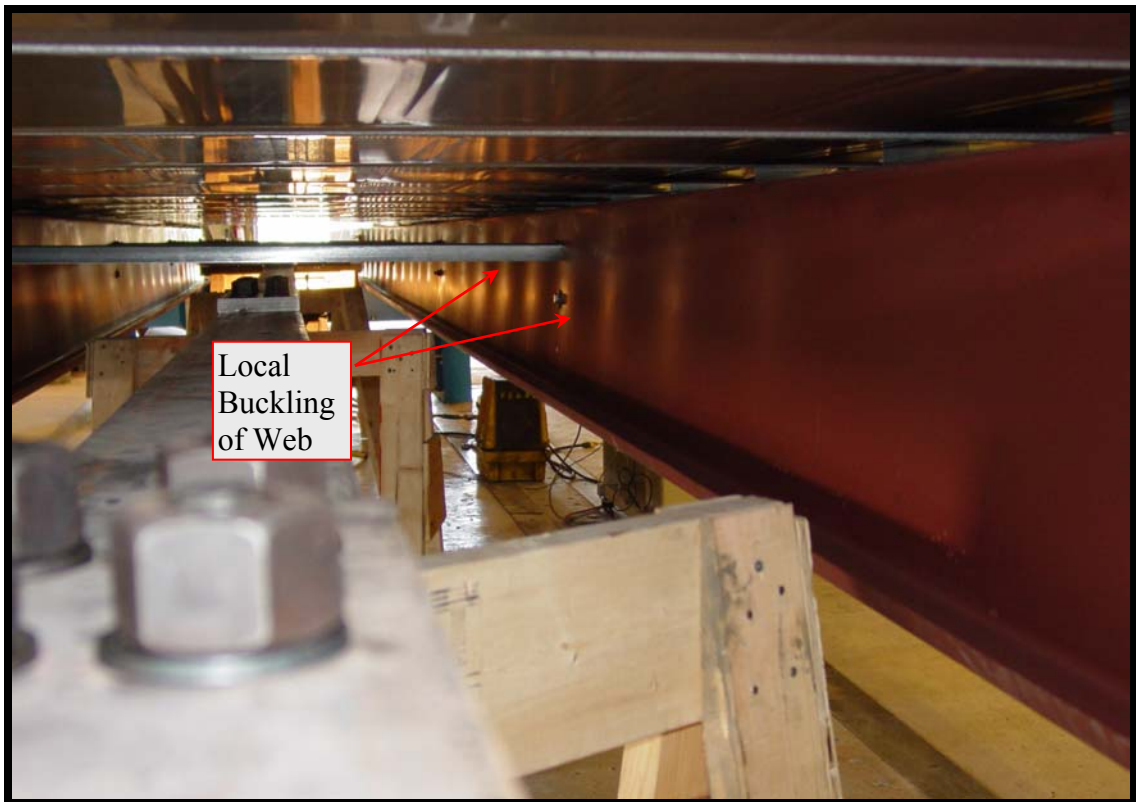


Figure 5.3 Local Buckling along Entire Length of Two-Purlin Test

5.1.2.2 14 inch deep purlins

The tests were carried out with only the roof purlins braced by a threaded metal rod (3/8" diameter) in place of sag angles. The maximum capacity obtained was 8.43 kips for the 0.080 inch thick purlin and 12.24 kips for the 0.134 inch thick purlin.

5.1.3 Tests with Two Purlins and Lateral Restraint

The aim of this test was to check the behavior of purlins when acting as strut purlins rather than as double struts in the case of the four-purlin tests. With lateral restraint models a condition where the eave strut and sag rod system provides nearly infinite stability to the system.

5.1.3.1 12 inch deep purlins

The threaded rod used in the tests without lateral restraint was replaced with a hot rolled angle. The maximum lateral force measured at the middle sag angle in the 0.080 and 0.100 inch thick specimen were 384 lbs and 585 lbs respectively. The 0.080 thick purlins failed at a load of 18.02 kips and the 0.100 thick purlins failed at a load of 29.61 kips. One of the failures occurred due to inelastic local buckling of the top flange. It was located at 25.5 inches from the central sag angle restraint, as shown in Figure 5.4

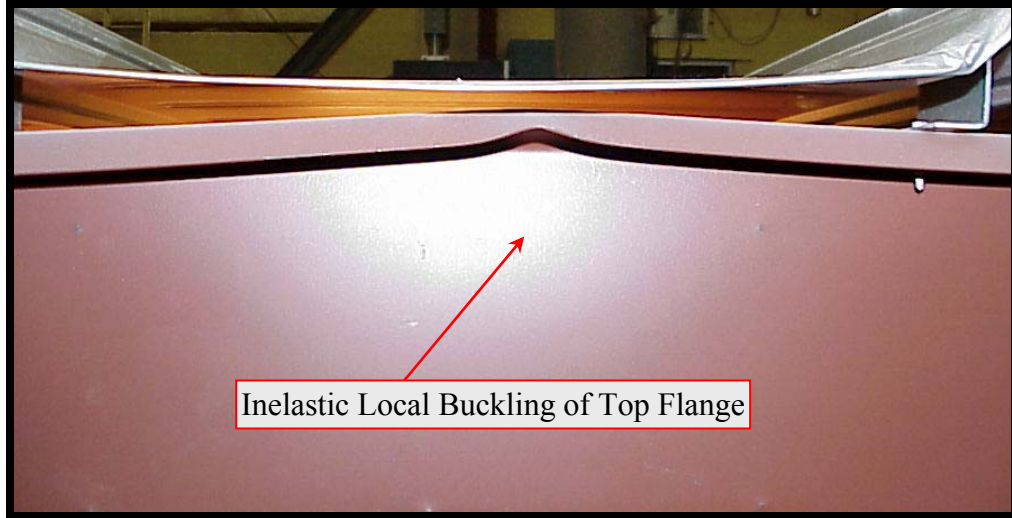


Figure 5.4 Local Buckling of Top Flange

5.1.3.2 14 inch deep purlins

The threaded rod used in the tests without lateral restraint was replaced with a hot rolled angle. The 0.080 thick purlins failed at a load of 20.94 kips and the 0.134 thick purlins failed at a load of 30.25 kips. The maximum lateral force measured in the 0.080 and 0.134 inch thick specimen were 737 lbs and 546 lbs respectively.

5.2 Purlins with No Roofing

A summary of the failure load of each test is shown in Table 5.2. These loads are per purlin i.e. the load to fail a single purlin. The purlins used in this series of tests were previously used in the “Purlins with Standing Seam Roofing” tests described in section 5.1. The purlins were inspected for damage prior to testing and any nicks and dings were worked out of the sections. These tests were performed on purlins with two sets of rods at each of the brace points.

Table 5.2 Axial Capacity of A Single Purlin in Tests without Roof Panel

Length	Test Specimen	Two Purlin Tests			
		Capacity Without Lateral Restraint (kips)	Average Capacity Without Lateral Restraint (kips)	Capacity With Lateral Restraint (kips)	Average Capacity With Lateral Restraint (kips)
30 ft.	12 Z 080	8.02 10.01 8.70 9.60	9.08	13.50 19.05 18.90 21.20	18.16
	12 Z 100	12.05 11.40 14.11 12.45	12.50	22.15 26.50 27.50 29.48	26.41
40 ft.	14 Z 080	5.04 5.74 5.46 4.82	5.26	20.00 19.22 19.12 22.21	20.14
	14 Z 134	14.44 10.04 11.38	11.95	45.98 45.08 47.03	46.03

5.2.1 Tests with Two Purlins and no Lateral Restraint

As mentioned in section 3.2.1 all tests were performed with two rods at each brace point. Figure 5.5 shows a typical failure mode for these tests. Every test failed by elastic global or "euler" buckling. Figure 5.5 shows a lateral deflection at midspan of approximately 4 inches.



Figure 5.5 Global failure of unrestrained test of purlins with no roof panel

5.2.2 Tests with Two Purlins and Lateral Restraint

As mentioned in section 3.2.1.1 the first test performed in this test series was tested with only one rod, at mid-depth of the section, at each of the brace points. This test was performed with a pair of 12Z100 purlins. The resulting capacity of a single purlin with lateral restraint was 17.30 kips. All additional tests were performed with two rods at each brace point. Every test failed by elastic distortional with some sections also showing signs of local buckling. Figure 5.6 shows a typical distortional failure mode for these tests. Figure 5.7 shows the interaction of distortional and local buckling failure. Note the local buckling failure of the web section in the foreground while the flanges give indications of distortional buckling. A few of these test failed do to abrupt formation of inelastic buckling of one of the flanges after formation of elastic distortional buckling.



Figure 5.6 Distortional failure for restrained test of purlins with no roof panel



Figure 5.7 Distortional and Local failure for restrained test of purlins with no roof panel


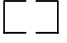

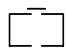
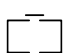



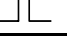
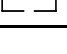


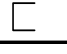
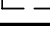
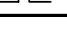
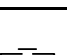


5.3 Built-up Members

5.3.1 Tests with Fixed End Conditions

Average maximum loads attained for each group of specimens are presented in Table 5.3. Figure 5.8 shows the scatter of the data points for each material thickness and orientation.

All of the specimens tested were made from two 1 $\frac{5}{8}$ inch square lipped C sections with a $\frac{3}{8}$ inch lip. Three nominal material thicknesses were studied: 0.064 in., 0.080 in., and 0.100 in. All specimens in this series were 55 $\frac{1}{2}$ in. long. Five welding patterns were investigated and are represented in Table 5.3 and Figure 5.8 by small diagrams.

Table 5.3 Average ultimate buckling loads w/ fixed ends

Thickness	Orientation	Capacity (kips)	Average Capacity (kips)	Orientation Description
0.100		13.10 12.60 12.17	12.62	Single member
		30.25 35.29 38.36	34.63	Two members, open sides facing, welded at ends only
		32.71 35.38 35.52	34.54	Two members, open sides opposing, welded at ends only
		43.65 37.81 34.21	38.56	Two members, open sides facing, stitch weld on one side at mid-length
		46.25 52.85 42.41	47.17	Two members, open sides facing, stitch welds on both sides at mid-length
	 3	52.56 55.91	54.24	Two members, open sides facing, stitch welds on one side at third points
0.080		6.99 10.90 8.08	8.66	
		22.43 18.20 20.56	20.40	
		22.76 22.93 23.00	22.90	
		24.56 35.43 32.31	30.77	
		43.04 39.30 36.07	39.47	
	 3	25.08 30.35		
	 3	34.75 35.81	35.28	Two members, open sides facing, stitch welds on both sides at third points
0.064		9.00 4.54 5.15	6.23	
		14.06 17.73 20.02	17.27	
		18.06 19.00 17.39	18.15	
		26.26 22.10 20.23	22.86	
		25.48 26.56 25.10	25.71	

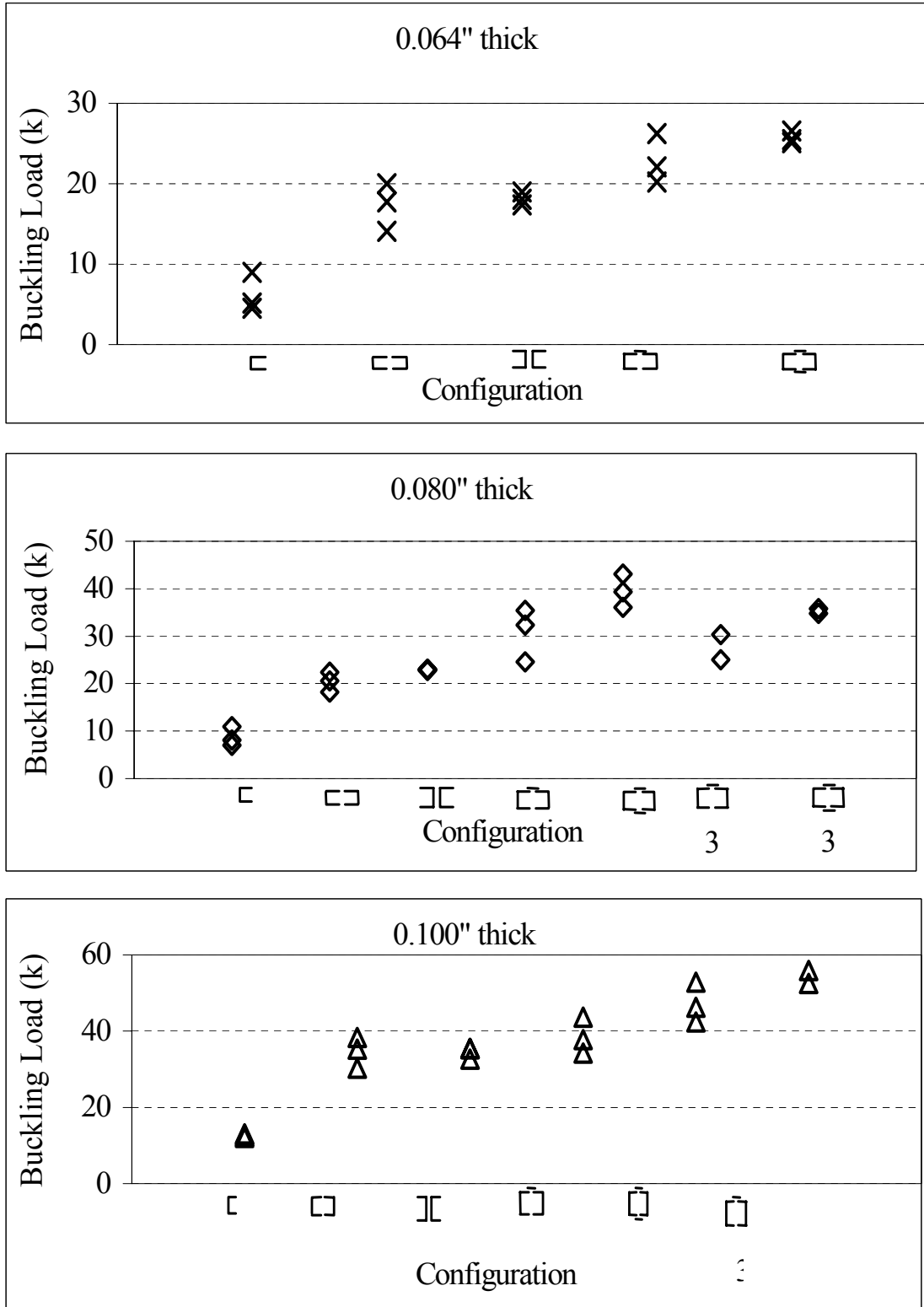



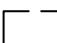

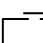
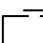
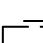
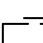
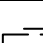
Figure 5.8 Ultimate buckling loads of built-up column test specimens

5.3.2 Tests with Pinned End Conditions

Average maximum loads attained for each group of specimens are presented in Table 5.4 through Table 5.10. Figure 5.9 through 5.15 shows the scatter of the data points for each material thickness and orientation.

All of the specimens tested were made from two 1 $\frac{5}{8}$ inch or 2 $\frac{1}{2}$ inch square lipped C sections with a $\frac{3}{8}$ inch lip. Three nominal material thicknesses were studied: 0.064 in., 0.080 in., and 0.100 in. All specimens in the first series were 55 $\frac{1}{2}$ in. long, all other series were 71 in. long. Seven welding patterns were investigated and are represented in Table 5.4 through Table 5.10 and Figure 5.9 through 5.15 by small diagrams.

Table 5.4 Ultimate buckling loads w/ pinned ends, 1⁵/₈" section, 55" Long

Thickness	Orientation	Capacity (kips)	Average Capacity (kips)	Orientation Description
0.080		7.64	7.64	Single member
		23.40	23.40	Two members, open sides facing, welded at ends only
		35.23 28.54	31.89	Two members, open sides facing, stitch weld on one side at mid-length
		39.41	39.41	Two members, open sides facing, stitch welds on both sides at mid-length
		30.75	30.75	Two members, open sides facing, stitch welds on one side at third points
		39.20	39.20	Two members, open sides facing, stitch welds on both sides at third points
		33.29 30.88 28.48	30.88	Two members, open sides facing, stitch welds on one side at sixth points
		36.96	36.96	Two members, open sides facing, stitch welds on both sides at sixth points

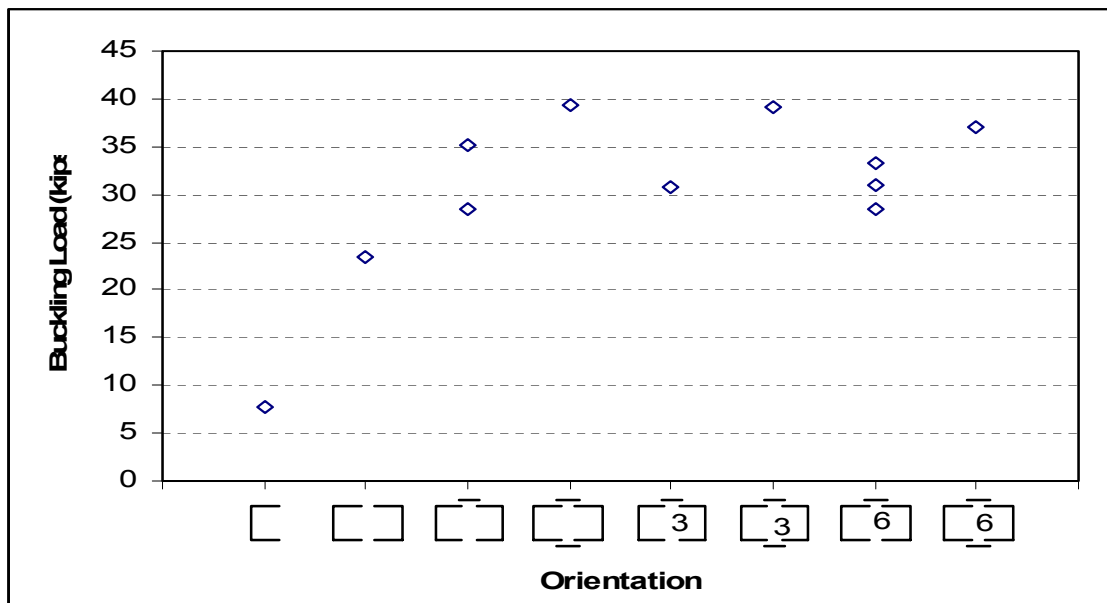

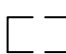
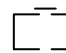
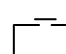
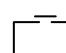
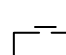
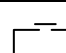
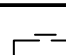


Figure 5.9 Ultimate buckling loads w/ pinned ends, 1⁵/₈" sections, 55" Long

Table 5.5 Ultimate buckling loads w/ pinned ends, 1⁵/₈" section, 71" Long

Thickness	Orientation	Capacity (kips)	Average Capacity (kips)	Orientation Description
0.100		10.09 8.81 8.67	9.19	Single member
		24.82 30.37 23.43	26.21	Two members, open sides facing, welded at ends only
		31.31 31.45 34.87	32.54	Two members, open sides facing, stitch weld on one side at mid-length
		46.56 48.36 44.16	46.36	Two members, open sides facing, stitch welds on both sides at mid-length
		36.39 36.22 36.53	36.38	Two members, open sides facing, stitch welds on one side at third points
		49.18 51.58 48.68	49.81	Two members, open sides facing, stitch welds on both sides at third points
		40.06 42.84 39.96	40.95	Two members, open sides facing, stitch welds on one side at sixth points
		52.68 54.99 43.16	50.28	Two members, open sides facing, stitch welds on both sides at sixth points

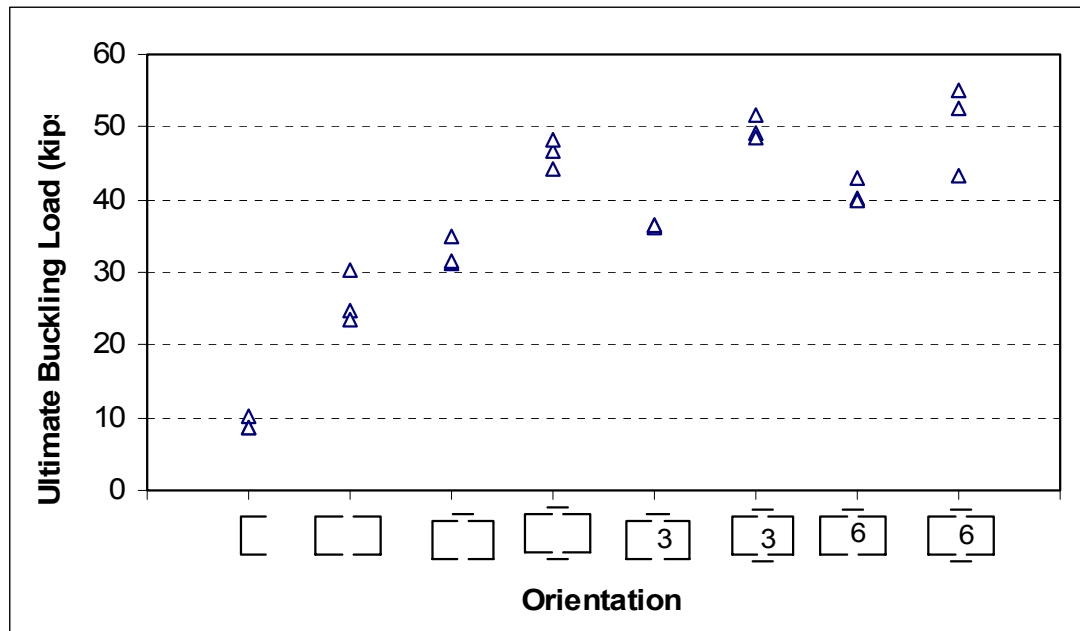

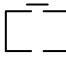

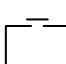
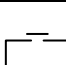
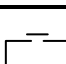



Figure 5.10 Ultimate buckling loads w/ pinned ends, 1⁵/₈" section, 71" Long

Table 5.6 Ultimate buckling loads w/ pinned ends, 1⁵/₈" section, 71" Long

Thickness	Orientation	Capacity (kips)	Average Capacity (kips)	Orientation Description
0.080		5.42	5.42	Single member
		34.30 24.62 21.53	26.82	Two members, open sides facing, stitch weld on one side at mid-length
		32.11 33.32 31.17	32.20	Two members, open sides facing, stitch welds on both sides at mid-length
	 3	20.59 22.25 21.72	21.52	Two members, open sides facing, stitch welds on one side at third points
	 3	28.86 36.02 33.88	32.92	Two members, open sides facing, stitch welds on both sides at third points
	 6	31.35 30.16 28.34	29.95	Two members, open sides facing, stitch welds on one side at sixth points
	 6	34.41 25.61 36.14	32.05	Two members, open sides facing, stitch welds on both sides at sixth points

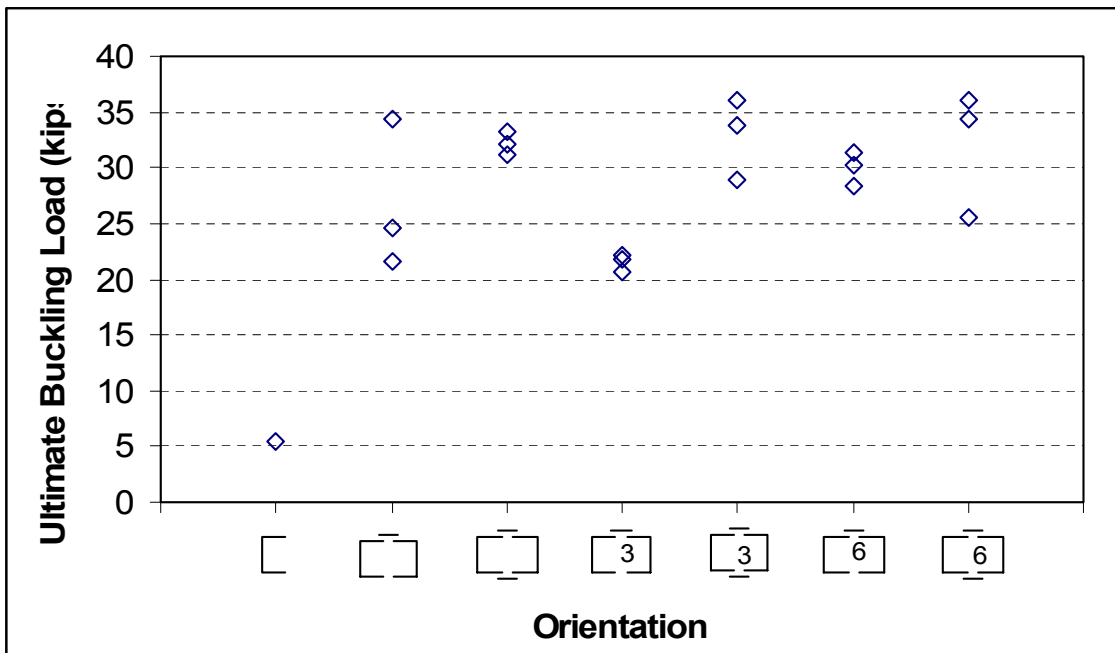

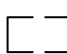
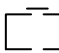
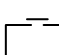
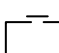
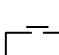

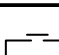


Figure 5.11 Ultimate buckling loads w/ pinned ends, 1⁵/₈" section, 71" Long

Table 5.7 Ultimate buckling loads w/ pinned ends, 1⁵/₈" section, 71" Long

Thickness	Orientation	Capacity (kips)	Average Capacity (kips)	Orientation Description
0.064		2.33 3.43 4.34	3.37	Single member
		11.83 14.53 11.66	12.67	Two members, open sides facing, welded at ends only
		16.45 16.43 18.72	17.20	Two members, open sides facing, stitch weld on one side at mid-length
		21.54 23.08 24.78	23.13	Two members, open sides facing, stitch welds on both sides at mid-length
	 3	16.78 14.71 13.21	14.90	Two members, open sides facing, stitch welds on one side at third points
	 3	30.03 33.87 33.22	32.37	Two members, open sides facing, stitch welds on both sides at third points
	 6	17.34 16.98 18.26	17.53	Two members, open sides facing, stitch welds on one side at sixth points
	 6	31.24 30.20 27.02	29.49	Two members, open sides facing, stitch welds on both sides at sixth points

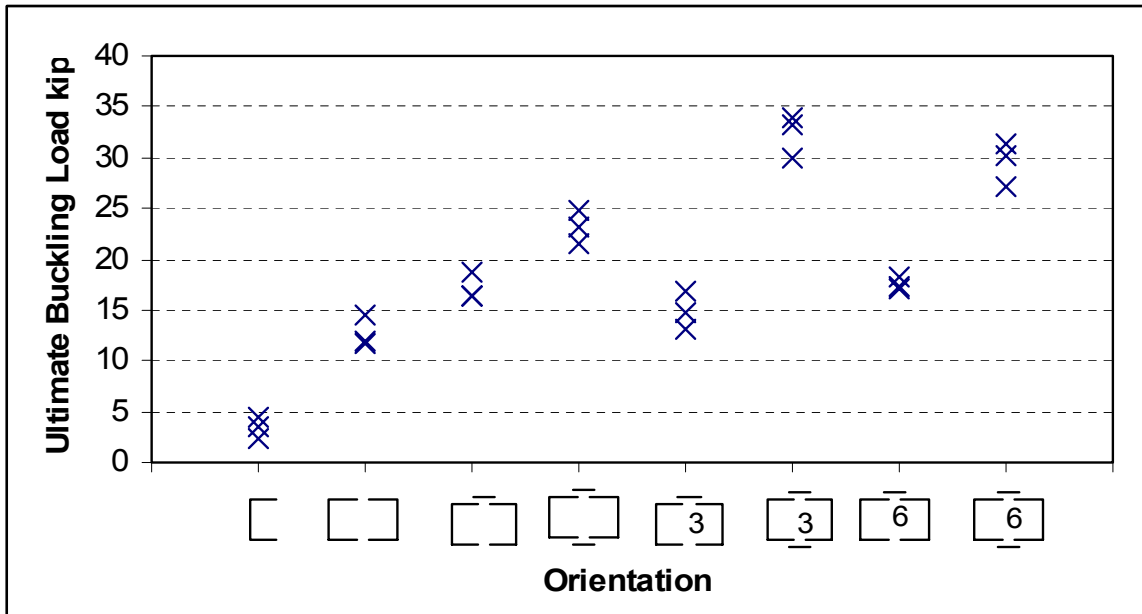

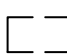
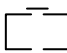
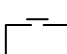
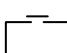
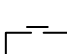
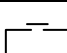



Figure 5.12 Ultimate buckling loads w/ pinned ends, 1⁵/₈" section, 71" Long

Table 5.8 Ultimate buckling loads w/ pinned ends, 2½" section, 71" Long

Thickness	Orientation	Capacity (kips)	Average Capacity (kips)	Orientation Description
0.100		23.11 23.09 18.88	21.69	Single member
		63.23 61.99 64.19	63.14	Two members, open sides facing, welded at ends only
		72.13 81.04 69.89	74.35	Two members, open sides facing, stitch weld on one side at mid-length
		97.57 88.73 90.04	92.11	Two members, open sides facing, stitch welds on both sides at mid-length
		80.48 77.99 79.10	79.19	Two members, open sides facing, stitch welds on one side at third points
		97.82 97.28 97.94	97.68	Two members, open sides facing, stitch welds on both sides at third points
		76.10 82.17 74.96	77.74	Two members, open sides facing, stitch welds on one side at sixth points
		82.22 88.25 90.11	86.86	Two members, open sides facing, stitch welds on both sides at sixth points

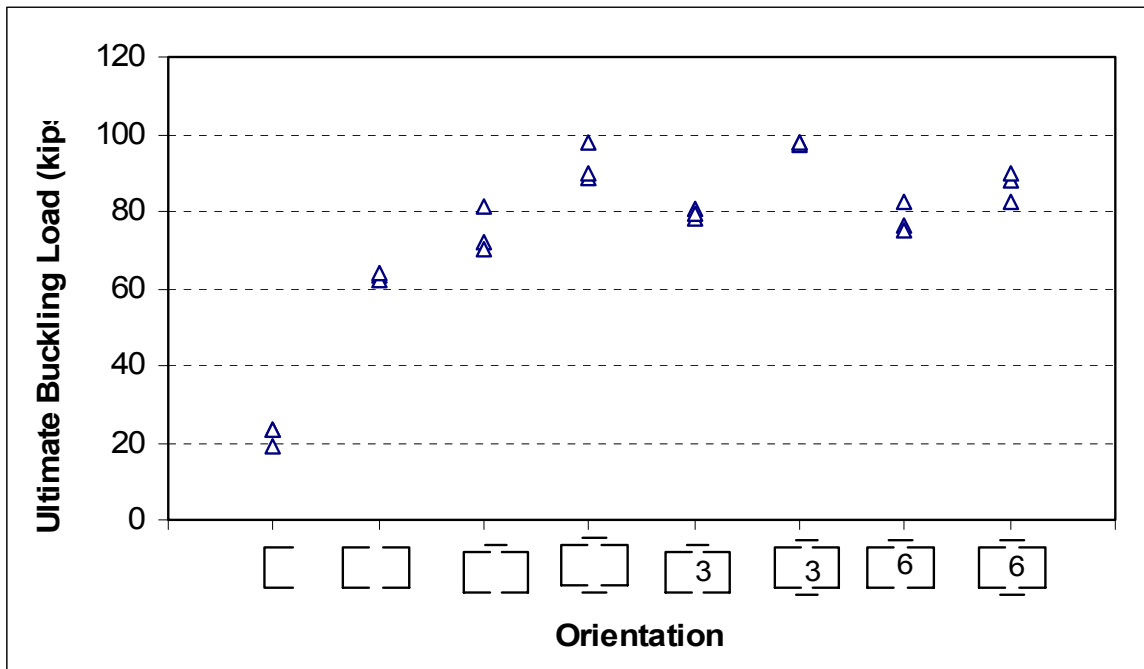

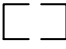
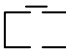
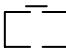
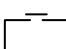
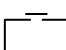
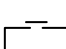
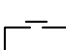


Figure 5.13 Ultimate buckling loads w/ pinned ends, 2½" section, 71" Long

Table 5.9 Ultimate buckling loads w/ pinned ends, 2½" section, 71" Long

Thickness	Orientation	Capacity (kips)	Average Capacity (kips)	Orientation Description
0.080		14.11 14.55 15.10	14.59	Single member
		40.06 41.45 43.90	41.80	Two members, open sides facing, welded at ends only
		43.39 47.47 47.59	46.15	Two members, open sides facing, stitch weld on one side at mid-length
		53.57 51.09 47.61	50.76	Two members, open sides facing, stitch welds on both sides at mid-length
	 3	44.23 44.57 43.35	44.05	Two members, open sides facing, stitch welds on one side at third points
	 3	45.90 53.94 54.69	51.51	Two members, open sides facing, stitch welds on both sides at third points
	 6	47.19 49.34 48.84	48.46	Two members, open sides facing, stitch welds on one side at sixth points
	 6	54.95 55.78 54.51 50.75	54.00	Two members, open sides facing, stitch welds on both sides at sixth points

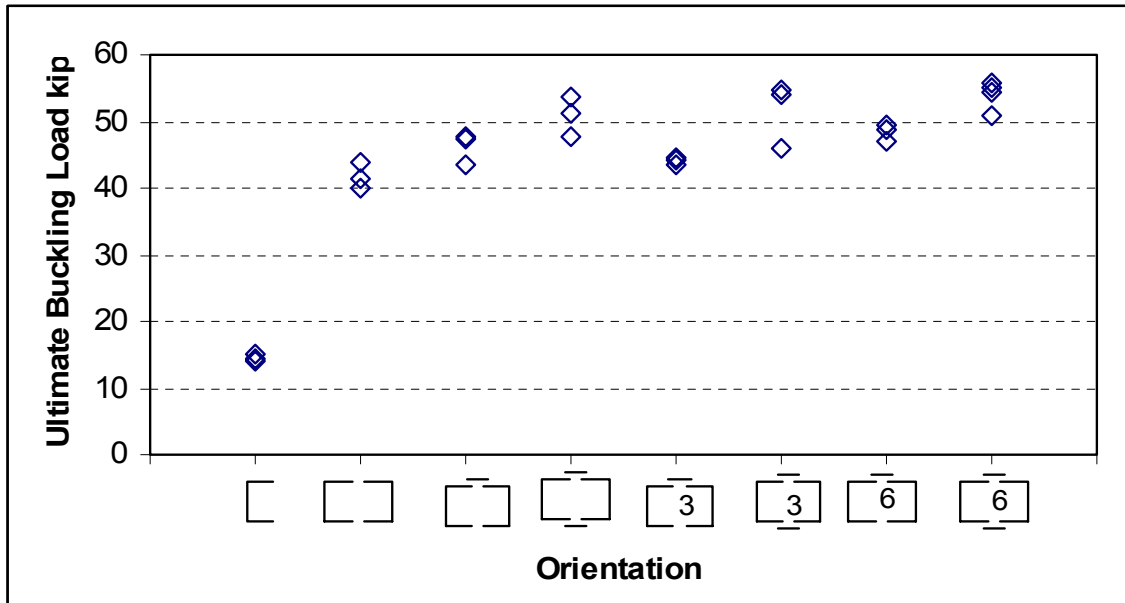

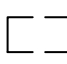
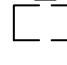
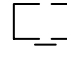
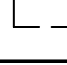
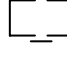
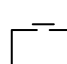



Figure 5.14 Ultimate buckling loads w/ pinned ends, 2½" section, 71" Long

Table 5.10 Ultimate buckling loads w/ pinned ends, 2½" section, 71" Long

Thickness	Orientation	Capacity (kips)	Average Capacity (kips)	Orientation Description
0.064		8.96 10.02 10.26	9.75	Single member
		30.21 26.60 29.80	28.87	Two members, open sides facing, welded at ends only
		29.50 35.88 31.63	32.34	Two members, open sides facing, stitch weld on one side at mid-length
		34.78 41.85 39.24	38.62	Two members, open sides facing, stitch welds on both sides at mid-length
	 3	33.10 33.91 35.77	34.26	Two members, open sides facing, stitch welds on one side at third points
	 3	39.52 38.13 41.21 40.78	39.91	Two members, open sides facing, stitch welds on both sides at third points
	 6	35.85 35.54 37.86 35.65	36.23	Two members, open sides facing, stitch welds on one side at sixth points
	 6	36.33 42.07 40.67	39.69	Two members, open sides facing, stitch welds on both sides at sixth points

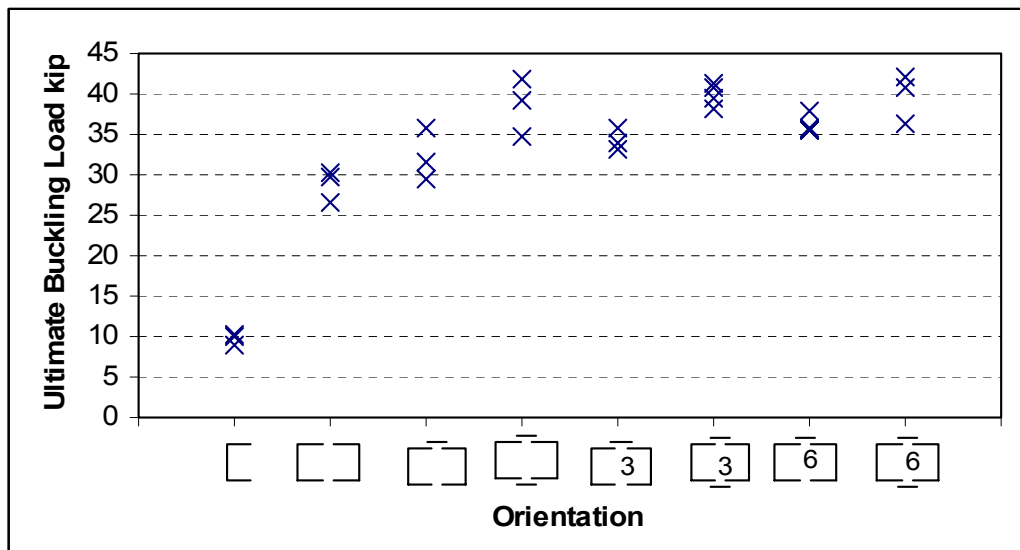


Figure 5.15 Ultimate buckling loads w/ pinned ends, 2½" section, 71" Long

Chapter 6 Discussion of Test Results

6.1 Purlins with Standing Seam Roofing

Figure 6.1 shows the average single purlin capacity for each series of tests. The test results show that there is a minimal difference in the experimental capacity of a single purlin with a channel placed in between the strut purlin and the double strut. This can be seen in Figure 6.1 when comparing the four purlin tests, which have a channel and the two purlin tests without lateral restraint, which do not have a channel. There is one exception, a significant change in the capacities of the two test setups can be seen with the 14Z134 specimen. The capacity of the purlins can more than double when provided with lateral restraint. This can be seen in Figure 6.1 when comparing the two purlin tests with and without lateral restraint.

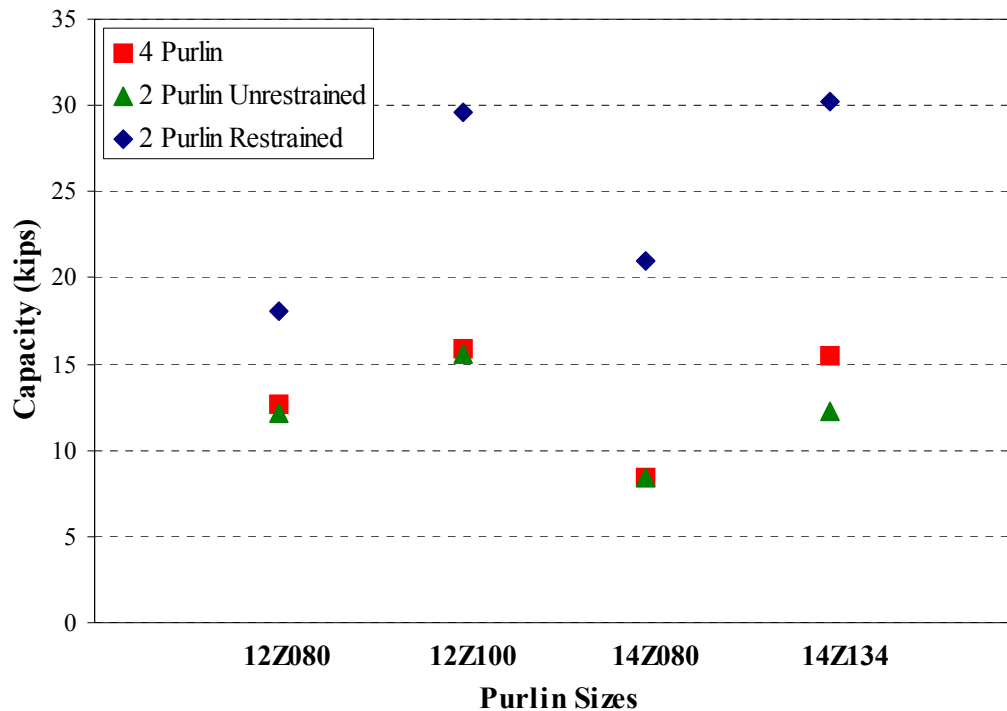


Figure 6.1 Capacity Comparison of a Single Purlin with Roof Panel

The actual lateral restraint on a metal building falls somewhere between the two purlin test with no lateral restraint and the two purlin test with lateral restraint. This is the difference between no global lateral restraint and total fixity of the global lateral restraint. The typical metal building falls somewhere in between these two extremes.

6.1.1 Tests with Four Purlins

The results from the four purlin tests showed that the restraint due to the Cee channel between the strut purlin and double strut does affect the capacity of specimen and sometimes by a significant amount as seen in case of 14Z134 specimen. As we would expect, slenderness of the specimen was the key issue in all the specimens tested. All of the 12 inch specimens failed due to local buckling in the web. In general, the channel placed between the strut purlin and the double strut, in the four purlin test, increased the lateral stability to the strut purlins resulting in a minimal increase of their capacity. There was one exception observed in the 0.134 inch thick 14 inch deep section, where there was a significant increase in the capacity. In all of the tests with 14 inch purlins, large lateral deflections were observed, which combined with the high slenderness ratio restricted their axial load capability. The failure mode in these sections was due to local buckling.

6.1.2 Tests with Two Purlins and No Lateral Restraint

In three of the four tested configurations, these tests had similar failure modes and loads as the tests with four purlins. However, as discussed in the previous section, there was a large difference in the capacity of the 14Z134 specimens in the four purlin test and the two purlin test without lateral restraint. In this case the two purlin test with no lateral restraint had 26.63% less capacity in comparison to the four purlin test. This difference can be attributed to the action of the Cee channel placed in between the strut purlin and the roof purlin in the four purlin test. The channel restricted the lateral deflection to an extent and reduced the tendency for web buckling, thereby allowing more force to be transferred axially. These results point out that the channel may sometimes be useful in reducing the lateral deflection and increase the axial capacity of the purlins.

6.1.3 Tests with Two Purlins and Lateral Restraint

The tests with global lateral restraints reinforced the earlier observation that providing proper lateral restraint can increase the purlin capacity significantly. This can be seen by comparing the results of the two purlin tests without lateral restraint to the two purlin test with lateral restraint. The lateral restraint reduces the effective length of the purlin, increasing the Euler buckling load of the strut purlin. Global lateral bracing of the system increased the capacity of the 12 inch purlins by 49%-90% and the 14 inch purlins by 247%-249%. Specimens in this test setup

were the only specimens to fail due to local buckling of the flange, as shown in Chapter 5 Figure 5.2.

6.2 General discussion of experimental purlin capacities

Figure 6.2 shows the average single purlin capacity for each series of tests with and with out roofing. The solid filled data points represent the average capacity of a single purlin with standing seam roofing attached. The hollow data points represent the average capacity of a single purlin with out roofing. The red data points represent the capacity of a single purlin from the double strut four

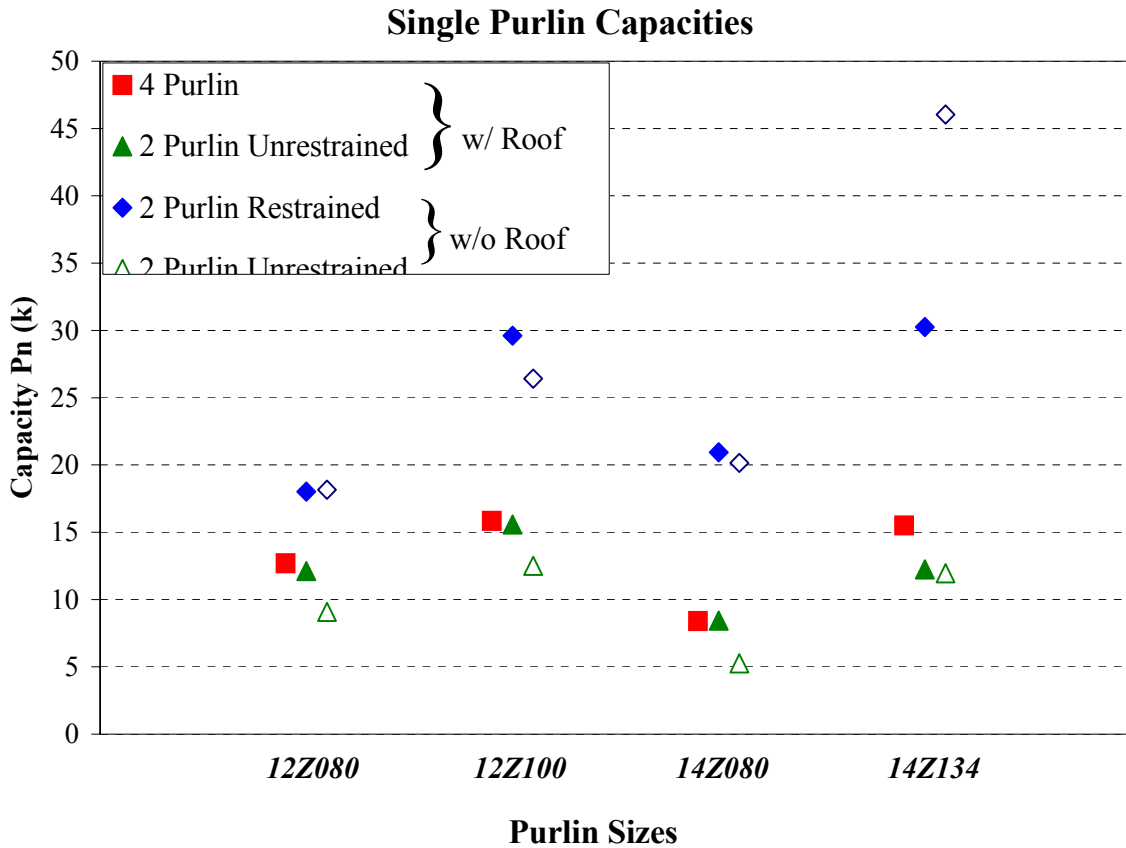


Figure 6.2 Capacity Comparison of a Single Purlin

purlin tests, while the green represent the unrestrained two purlin tests and the blue the restrained two purlin tests.

In Figure 6.3 you will note that global bracing always improves the axial capacity of a purlin. This is illustrated by the red ovals and arrows. Figure 6.3 also shows that the capacity is sensitive to the rigidity of the bracing. The unrestrained capacities represent zero global bracing and the restrained capacities, since the braces are attached to a strong floor, represent almost 100% global bracing. These two extremes bracket the rigidity of possible bracing conditions. The actual restraint provided would obviously fall somewhere within this range.

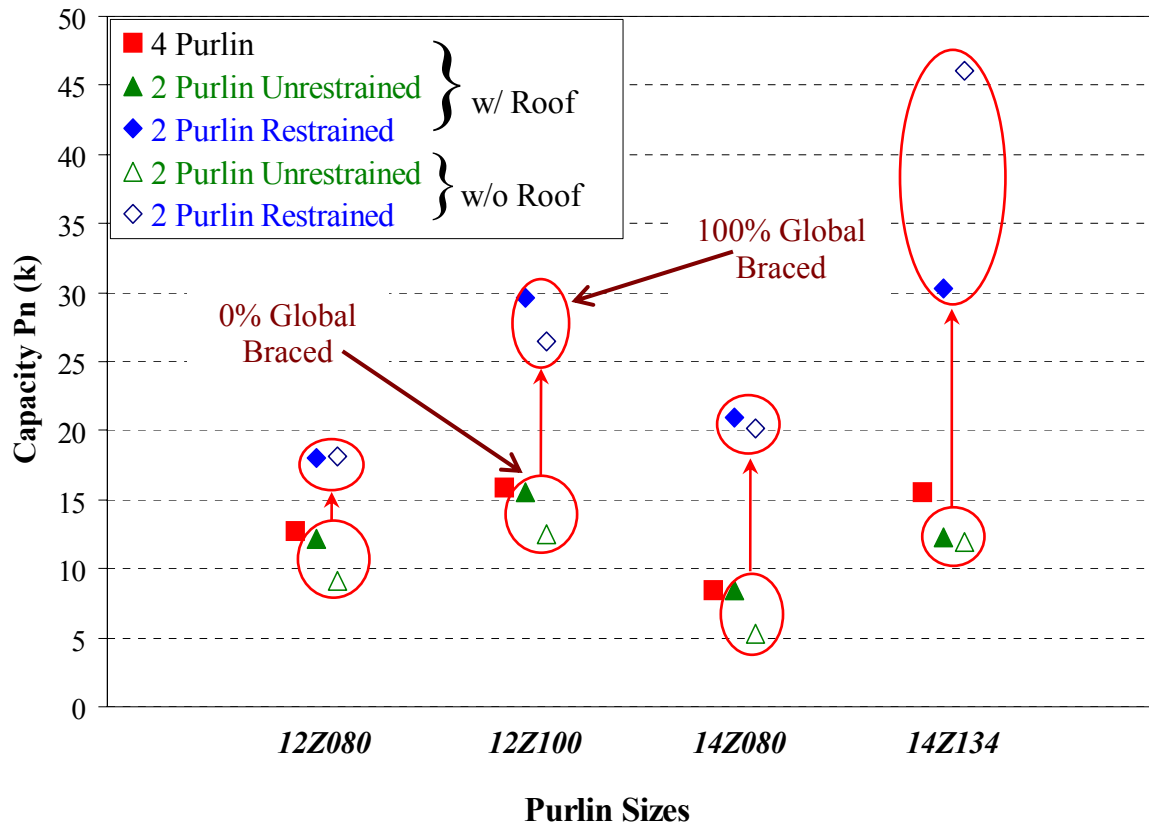


Figure 6.3 Capacity Comparison due to bracing

Figure 6.4 illustrates that increasing the stability of the purlin at the brace location increases the axial capacity of the purlin. These test results are for twelve inch deep purlins with a thickness of 0.100 inches, typically called a 12Z100. The purlins were all 30 feet long, with three brace locations. The top row in this figure illustrates the increase when no lateral restraint is provided at the brace points and the bottom row illustrates the increase when lateral restraint is provided. The sections shown in the left column of this figure illustrate tests performed with no roof panel while the sections on the right included a standing seam roof system. All sag rods or the equivalent are shown in red. These are provided at the standard brace locations.

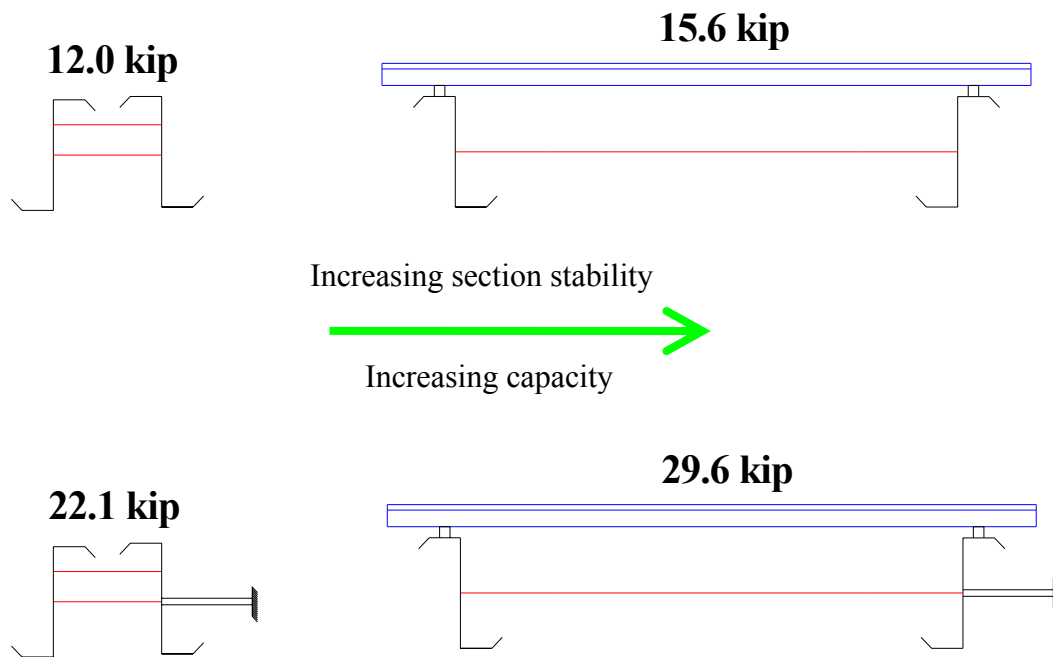


Figure 6.4 Capacity comparison of 12Z100 purlins due to section stability

Figure 6.5 illustrates that increasing the stability of the purlin at the brace location and increasing global bracing at the brace location increases the axial capacity of the purlin. These test results are for the same sections discussed in Figure 6.4. Both Figures 6.4 and 6.5 illustrate that increasing the stability of the purlin at the brace location increases the axial capacity of the purlin. This "stability" at the brace location includes controlling translation and rotation of the sections. In these tests resistance to translation is provided by the global bracing located at three points along the length of the purlin. Resistance to rotation is provided by several different mechanisms. In the tests with out roof panel rotation is resisted at the discrete brace points by the use of two rods relatively bracing the purlins. In the tests with roof panel the clip connection to the top flange of the

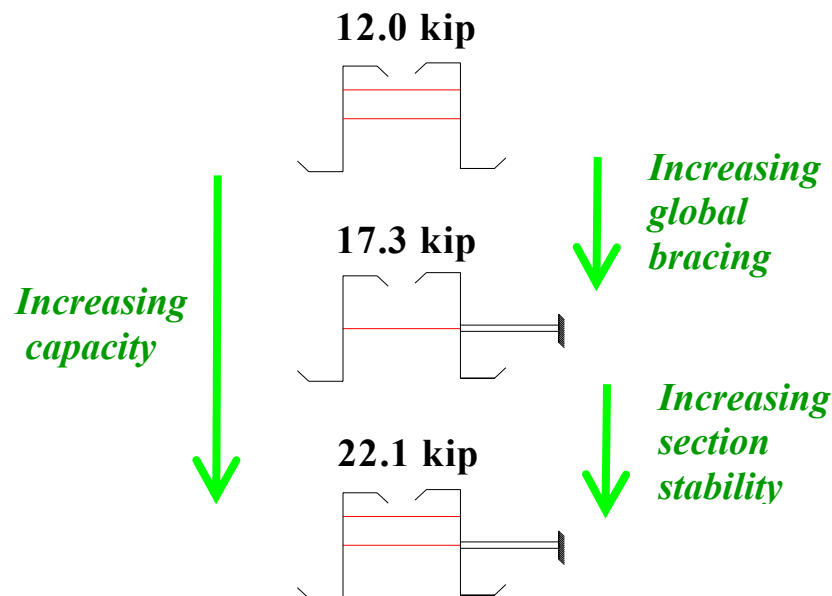


Figure 6.5 Capacity comparison of 12Z100 purlins due to section stability

purlin every two feet provides part of the rotational resistance while the sag rod at the discrete brace points provides the remainder. This is shown in Figure 6.6.

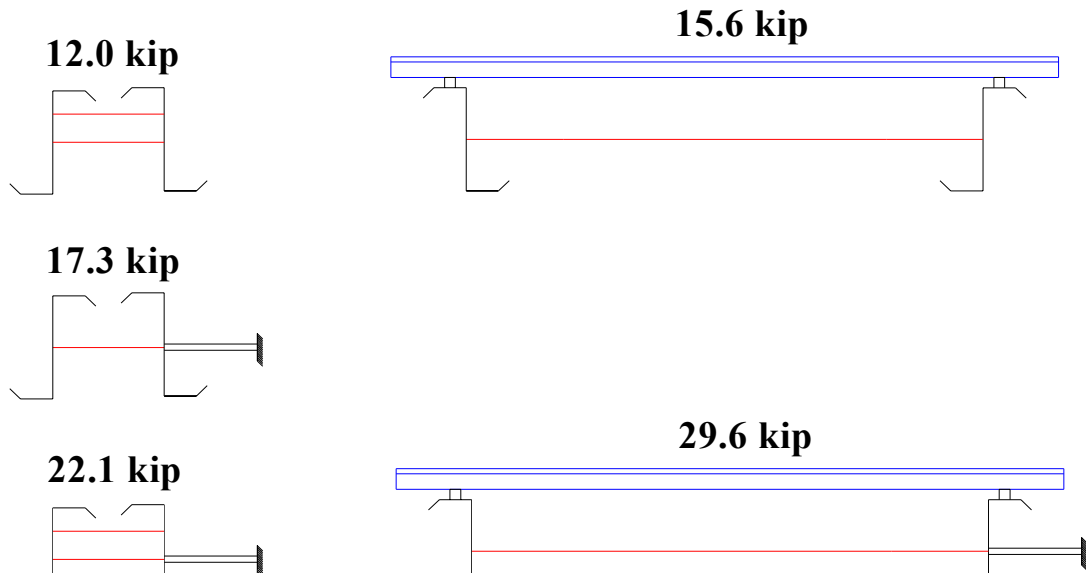


Figure 6.6 Capacity comparison of 12Z100 purlins

6.3 Calculation of the Purlin Design Capacity

Phi factors for each group of purlins in the four purlin test series were calculated according to the provisions of Chapter F of the *AISI Specifications* (2002). In all cases, the four purlin test results were clustered tightly enough that the maximum allowable phi-factor for $n = 3$ tests was obtained. For selecting the values and coefficients of variation for the material factor and fabrication factor (M_m , F_m , V_M , and V_F), it was assumed that the purlins were “concentrically loaded

compression members” type of component. Table 6.1 shows the LRFD design capacities calculated for the purlin struts tested from the four purlin test.

**Table 6.1 Experimentally Calculated Design Capacities of a Single Purlin
(4 Purlin Test)**

Purlin Size	Average Ultimate Axial Capacity (kips)	Phi (ϕ)	Design Axial Capacity (kips)
12 Z 080	12.68	0.75	9.51
12 Z 100	15.85	0.75	11.89
14 Z 080	8.40	0.75	6.30
14 Z 134	15.50	0.75	11.63

In the 4 purlin test the values shown are for struts braced relative to each other and are not globally braced. For all other tests with roof panel only one test was performed per each thickness. The *AISI Specifications (2002)* states that there needs to be a minimum of three tests in order to obtain a phi factor. Because of this no other design values are calculated for these tests.

Table 6.2 shows the LRFD design capacities calculated for the purlin struts tested from the purlins without roof panel tests. In all but two cases, the purlin with out roof panel test results were clustered tightly enough that the maximum allowable phi-factor was obtained. In these two cases the +/- 15% deviation limit is exceeded and a Φ factor can not be calculated with out additional testing. These two cases are shown in red.

**Table 6.2 Experimentally Calculated Design Capacities of a Single Purlin
(Tests with no roof panel or lateral restraint)**

Purlin Size	Average Ultimate Axial Capacity (kips)	Phi (ϕ)	Design Axial Capacity (kips)
12 Z 080	9.08	0.75	6.81
12 Z 100	12.50	0.75	9.38
14 Z 080	5.26	0.75	3.95
14 Z 134	11.95	0.47	N.A.

(Tests with lateral restraint, but no roof panel)

Purlin Size	Average Ultimate Axial Capacity (kips)	Phi (ϕ)	Design Axial Capacity (kips)
12 Z 080	18.16	0.57	N.A.
12 Z 100	26.41	0.75	19.81
14 Z 080	20.14	0.75	15.11
14 Z 134	46.03	0.75	34.52

6.4 Comparison of Purlin Experimental to Theoretical Design Values

6.4.1 Two purlin tests without lateral restraint but with roof panel

Table 6.3 compares the capacities obtained from the two purlins tests without lateral restraint but with roof panel to the capacities determined by other methods. Fisher's method has been compared only with the two purlin tests

without lateral restraint since it resembles the set up that he used (Fisher et. al 1993). Figure 6.7 shows the same values in graphical form.

**Table 6.3 Comparison of Experimental and Theoretical Capacities
(2 Purlin Test without Lateral Restraint but with roof panel)**

Purlin Size	Single Purlin Capacity P_n (kips)			
	Experimental	Fisher (1993)	AISI (2002)	DSM (2004)
12Z080	12.11	17.95	7.91	9.13
12Z100	15.57	23.03	11.18	11.91
14Z080	8.43	15.46	5.78	6.28
14Z134	12.24	27.85	12.00	11.98

The calculated design values are conservative when compared to the experimental values with an exception to Fisher's method which is highly unconservative. It should be noted that all of the theoretical methods place limitations on the strut purlin geometry and/or restraint that are not satisfied by the specimens tested.

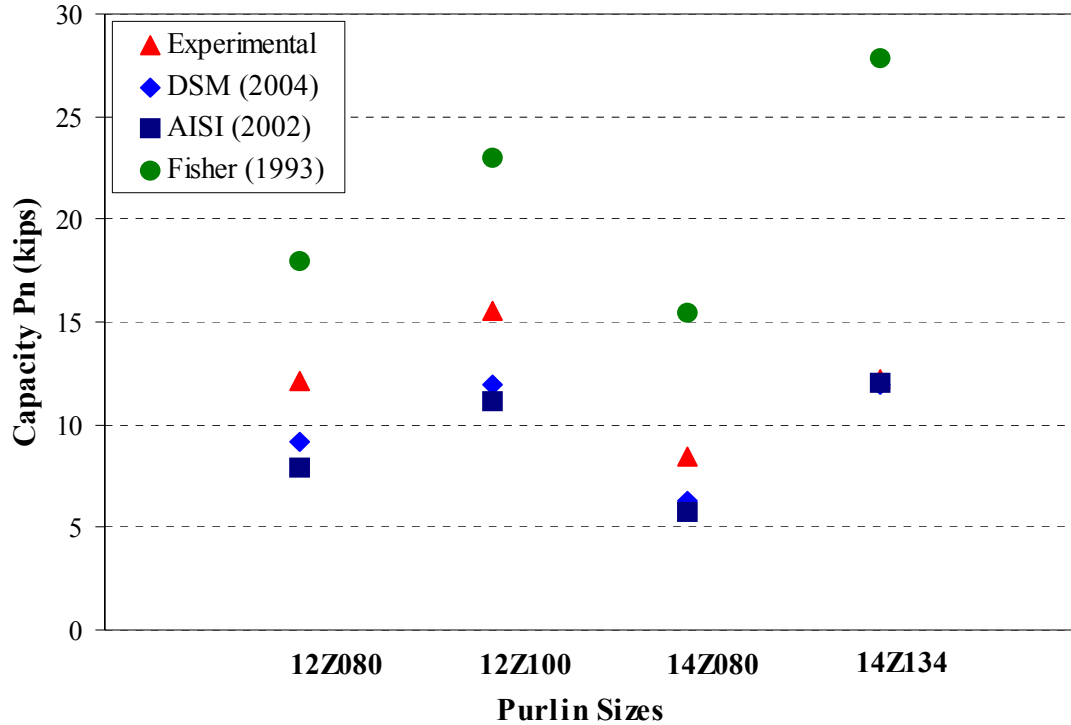


Figure 6.7 Experimental Capacity Vs Theoretical Capacity

6.4.1.1 Direct Strength Method (2004)

Figure 6.8 shows a graph of a typical stress vs. half wave length plot of a typical test specimen using Direct Strength Method (DSM). The analysis was done with the 12Z80 specimen with an effective length of 234 inches. This effective length is derived at by using an effective length factor (K) equal to 0.65. The graph points out that, the stress in the specimen due to local buckling and global buckling lay in close proximity, when compared to distortional buckling. The stress values at each mode of buckling are used in an interaction equation and the capacity of the specimen due to the different modes of buckling is calculated. The lowest of the three is taken as the capacity of the section. The DSM analysis of the

test specimens shows that the axial capacity is very sensitive to global buckling which is a function of the effective length factor (K) which varies according to the boundary conditions. Any change in the effective length affects the capacity significantly and yet the boundary conditions are subject to debate since they are rarely ideal i.e. classical examples.

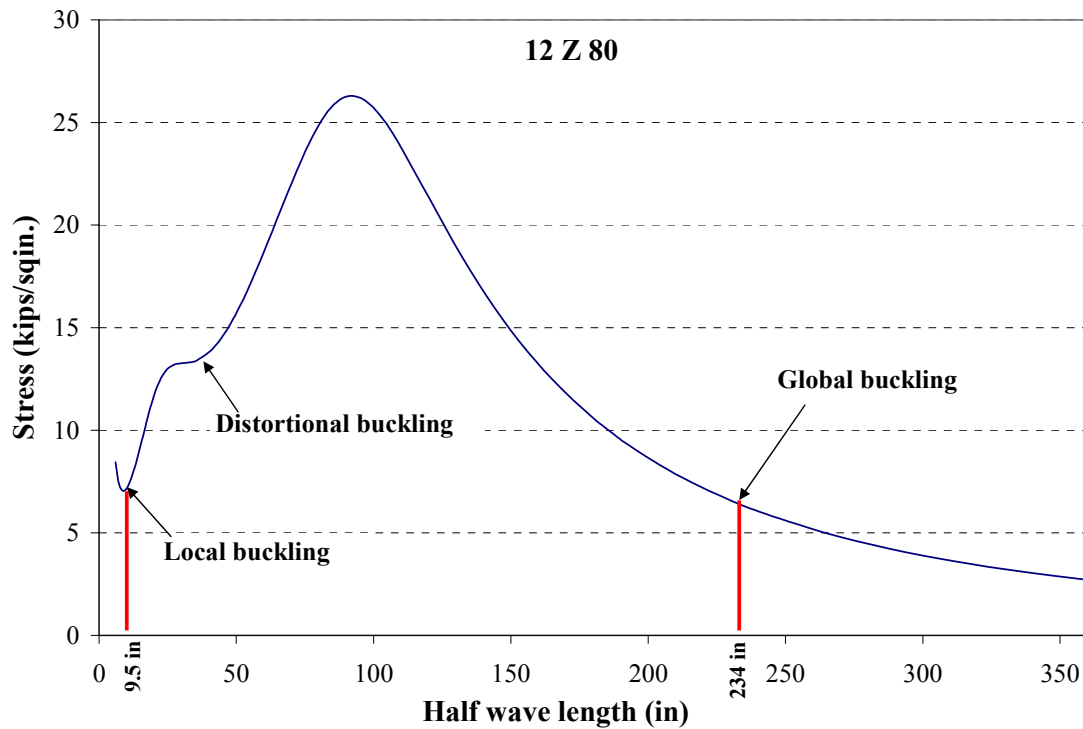


Figure 6.8 Stress Vs Half Wavelength of 12Z80 Specimen

Table 6.4 compares the axial capacity of a single purlin obtained experimentally with the ones obtained by Direct Strength Method. The Direct Strength Method resulted in design values 2% to 34% lower than the experimental testing. The 14Z134 strut purlin was the only one with a difference less than 2.5%. The differences in the capacity values may be due to 1) a weakness in the DSM method or 2) an increase in the experimental capacity due to system effects

from the standing seam roof. One difficulty with any analysis method is modeling the restraint due to the standing seam roof system. Currently no such method is available, so no restraint is usually assumed to ensure conservatism.

**Table 6.4 Comparison of Experimental and DSM (2004) Values
(Two Purlin Test without Lateral Restraint but with roof panel)**

Test Specimen	Thickness (inch)	Experimental Capacity (kips)	DSM Capacity (kips)	% Difference
12 Z 080	0.080	12.11	9.13	-32.64%
12 Z 100	0.100	15.57	11.91	-30.73%
14 Z 080	0.080	8.43	6.28	-34.24%
14 Z 134	0.134	12.24	11.98	-2.17%

Both the effective width method in the current *AISI Specifications (2002)* and the Direct Strength Method (2004) are limited to purlins meeting certain geometric restrictions. Table 6.5 summarizes these restrictions and compares them to the sections tested in this research. Values that are in violation are highlighted in red.

When calculating the design value ϕP_n using the Direct Strength Method, Schafer (2002) notes that a phi factor of 0.80 should be used consistent with the clause A1.1 (b) of *AISI Specifications (2002)*, instead of the normal 0.85. This

reduction in the ϕ factor would make his design capacity more conservative.

Because Direct Strength Method uses a theoretically based approach to determine

Table 6.5 Geometric Restriction of AISI (2002) & DSM (2004)

Size Restrictions	12Z080	12Z100	14Z080	14Z134
$76 < h/t < 137$	150	120	175	105
$30 < b/t < 56$	40.6	32.5	43.8	26.1
$0 < d/t < 36$	16.0	13.7	16.4	11.6
$1.5 < h/b < 2.7$	3.7	3.7	4.0	4.0
$0.00 < d/b < 0.73$	0.394	0.422	0.374	0.446
$\theta \sim 50^\circ$	50°	50°	50°	50°

buckling capacities, the design values obtained do approach the values obtained by the globally restrained testing program for the 12 inch Zee purlins tested and the lightest 14 inch Zee purlin tested. It is promising that the half wavelengths for local buckling modes predicted by the finite strip analysis is similar to the half wavelengths observed in the laboratory. An effective length factor of 0.65 was used to determine the critical global buckling stress on the sections. This determination was based on the K value obtained from the American Institute of Steel Construction (AISC) design manual.

6.4.1.2 AISI Specification (2002)

The AISI values for the 12 inch purlins are found to be unconservative when compared to the capacities obtained experimentally. An effective length factor (K) of 0.65 was used for the analysis.

6.4.1.3 Fisher's Method (1993)

Fisher's method resulted in design values 48% to 128% greater than the experimental results. This may be due to large number of parameters Fisher removed from Simaan's method or due to our tests violating his analysis limitations. Table 6.6 summarizes these restrictions and compares them to the sections tested in this research. Values shown in red are in violation of his limitations. It should be noted that for the twelve inch deep sections only the fastener spacing limitation was violated. It should also be noted that most roof panel on the market today uses a 24 inch fastener spacing, in essence violating one of Fishers geometric restrictions.

Table 6.6 Geometric Restrictions of Fisher (1993)

Size Restrictions	12Z080	12Z100	14Z080	14Z134
Depth \leq 12	12	12	14	14
Span \leq 30	30	30	40	40
Fastener Spacing = 12 in.	24	24	24	24
Thickness \leq 0.125 inch	0.080	0.100	0.080	0.134

Fisher has stated in his recommendations that the equation he developed cannot be used for calculating the capacity of Zee members with a standing seam roof system attached to one flange. However, he also says that the capacity of Zee sections with standing seam panels can be obtained in an alternate way. First, the critical axial stress for the thickest section of any given depth series needs to be

found experimentally. Then, the weak axis capacity of the section should be calculated using the smaller value of the critical axial stress obtained experimentally and the value obtained from his equation developed for Zee sections with through-fastened roof panel. This critical stress can be used for purlins in the depth series of any length and thickness. In essence Fisher modifies his totally analytical approach with a quasi experimental/analytical, approach to deal with the system effects of standing seam roofs.

6.4.2 Two Purlin Tests with Lateral Restraint and roof panel

Table 6.7 compares the capacities obtained from the two purlins tests with lateral restraint and roof panel. Figure 6.9 shows the same values in graphical form.

**Table 6.7 Comparison of Experimental and Theoretical Capacities
(2 Purlin Tests with Lateral Restraint and roof panel)**

Purlin Size	Single Purlin Capacity P_n (kips)		
	Experimental	AISI (2002)	DSM (2004)
12Z080	18.02	38.48	21.26
12Z100	29.61	54.99	34.45
14Z080	20.94	31.24	18.73
14Z134	30.25	67.16	57.02

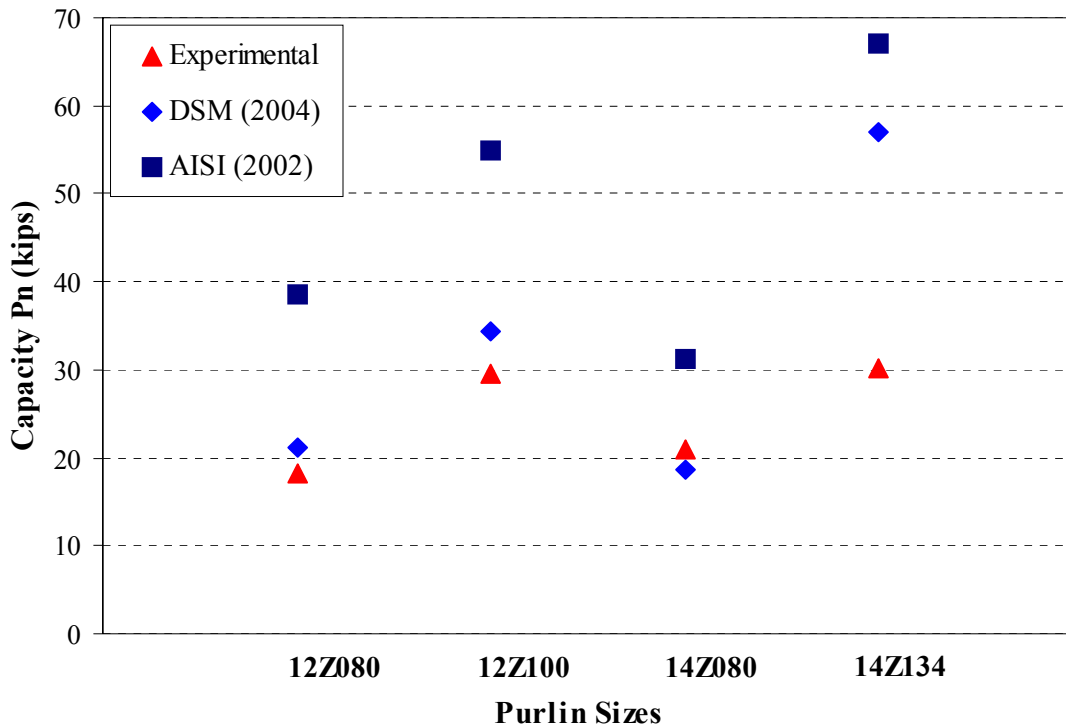


Figure 6.9 Experimental Capacity Vs Theoretical Capacity

Fisher's method could not be used to compare the values since there was no provision to incorporate the lateral restraint conditions. The theoretical values calculated using AISI (2002) and Direct Strength Method are unconservative, with an exception to the 14Z80 specimen where the values obtained by Direct Strength Method is conservative and almost identical to the tested capacity.

6.4.2.1 Direct Strength Method (2004)

The analysis of purlins with lateral restraint was similar to section 6.4.1.1 the section dealing with analysis of purlins without lateral restraint. An effective length factor (K) of 1.0 was used for the analysis, This represents a purlin section between lateral brace points. A length of specimen equal to 6 ft and 9ft. was used

for 12 inch and 14 inch specimens respectively. Table 6.7 compares the axial capacity of a single purlin obtained by Direct Strength Method to the experimental capacity. The Direct Strength Method capacity of a 14Z134 specimen was 89% greater than the tested capacity. This may be due to a weakness in the Direct Strength method when used for sections that are deeper and thicker.

It should be noted that only the restraints due to the lateral supports were considered for the analysis since there was no way of modeling the restraints due to the standing seam roof in Direct Strength Method.

Table 6.7 Comparison of Experimental and DSM (2004) Capacities (2 Purlin Tests with Lateral Restraint and roof panel)

Purlin Size	Experimental (kips)	DSM (2004) (kips)	% Difference
12Z080	18.02	21.26	-17.98
12Z100	29.61	34.45	-16.35
14Z080	20.94	18.73	10.55
14Z134	30.25	57.02	-88.50

6.4.2.2 AISI Specifications (2002)

When determining the axial capacity using the AISI method (2002) an appropriate effective length factor (K) and the unbraced length (L), between lateral restraint locations was used. An unbraced length of 6 feet with a K factor of 1.0 was used in the analysis of 12 inch deep purlins. An unbraced length of 9 feet with a K factor of 1.0 was used in the analysis of 14 inch deep purlins. These

values are similar to those used in the Direct Strength Method analysis. These sections, located in the middle of the purlin span between lateral brace points, are the controlling lengths for each purlin size.

Table 6.8 compares the values of a single purlin obtained experimentally and that calculated using the AISI Effective Width method. Values obtained from the Effective width method were found to be 49 % to 122 % higher than the ones obtained from testing. Figure 6.9 shows the same values in graphical form.

Table 6.8 Comparison of Experimental and AISI (2002) Capacities (2 Purlin Tests with Lateral Restraints)

Purlin Size	Experimental (kips)	AISI Specifications (kips)	% Difference
12Z080	18.02	38.48	-113.54
12Z100	29.61	54.99	-85.71
14Z080	20.94	31.24	-49.19
14Z134	30.25	67.16	-122.02

Unlike the Direct Strength Method, the Effective Width Method used by the AISI *Specifications* (2002) is empirically based. This makes any deviation from the dimensions used to develop the method very problematic. Because of this the AISI *Specifications* (2002) cannot be used to calculate the capacity of laterally restrained purlins, due to highly unconservative results.

6.4.3 Tests with Two Purlins without Lateral Restraint or roof panel

Table 6.9 compares the capacities obtained from the two purlins tests without lateral restraint or roof panel. Figure 6.10 shows the same values in graphical form. The theoretical values calculated using AISI (2002) and Direct Strength Method are unconservative for all cases.

**Table 6.9 Comparison of Experimental and Theoretical Capacities
(2 Purlin Tests without Lateral Restraint or Roof Panel)**

Purlin Size	Single Purlin Capacity P_n (kips)		
	Experimental	AISI (2002)	DSM (2004)
12Z080	9.08	23.51	12.53
12Z100	12.50	32.40	17.16
14Z080	5.26	18.74	8.65
14Z134	11.95	41.00	19.37

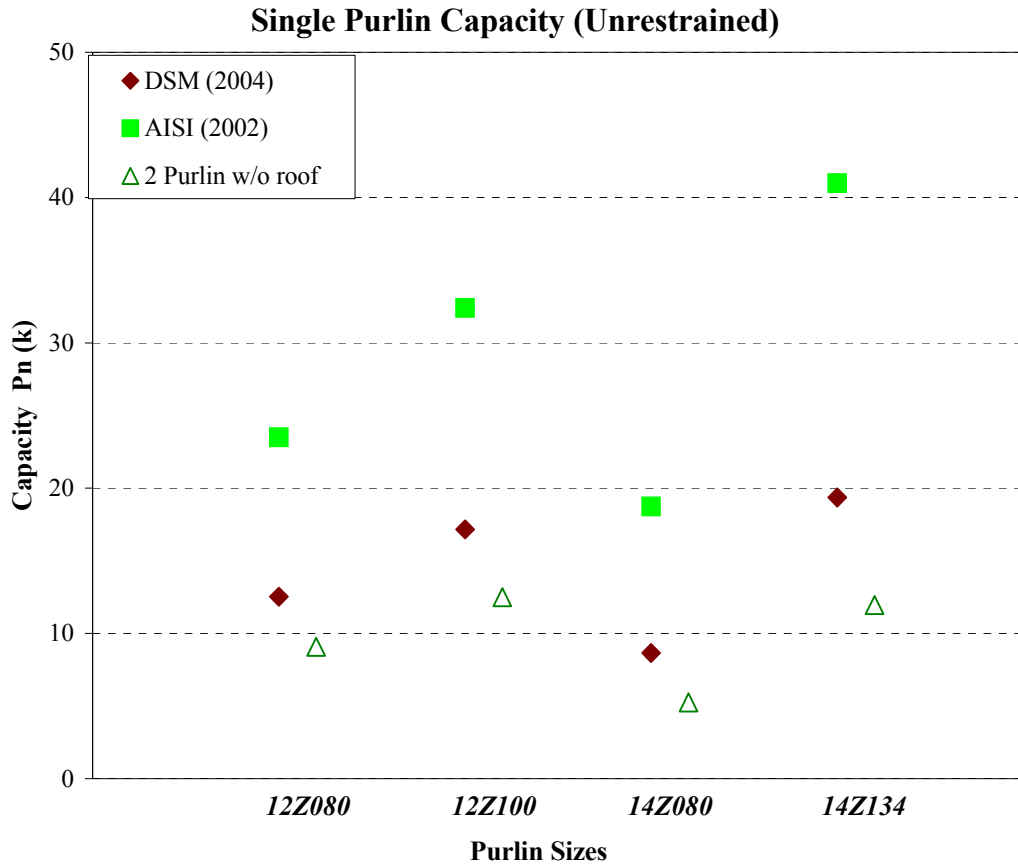


Figure 6.10 Experimental Capacity Vs Theoretical Capacity

6.4.3.1 Direct Strength Method (2004)

The analysis of purlins with lateral restraint was similar to section 6.4.1.1, the section dealing with analysis of purlins without lateral restraint. An effective length factor (K) of 1.0 was used for the analysis, This represents a purlin section between lateral brace points. A length of specimen equal to 30 ft and 40 ft. was used for 12 inch and 14 inch specimens respectively. Table 6.10 compares the axial capacity of a single purlin obtained by the Direct Strength Method to the experimental capacity. The Direct Strength Method capacity of a 14Z080 specimen was 64% greater than the tested capacity. This may be due to a

weakness in the Direct Strength method when used for sections that are deeper and thicker.

Table 6.10 Comparison of Experimental and DSM (2004) Capacities (2 Purlin Tests with Lateral Restraints)

Purlin Size	Experimental (kips)	DSM (2004) (kips)	% Difference
12Z080	9.08	12.53	-38.00
12Z100	12.50	17.16	-37.28
14Z080	5.26	8.65	-64.45
14Z134	11.95	19.37	-62.09

6.4.3.2 AISI Specifications (2002)

When determining the axial capacity using the AISI method (2002) an appropriate effective length factor (K) and the unbraced length (L), between lateral restraint locations was used. An unbraced length of 30 feet with a K factor of 1.0 was used in the analysis of 12 inch deep purlins. An unbraced length of 40 feet with a K factor of 1.0 was used in the analysis of 14 inch deep purlins. Table 6.11 compares the values of a single purlin obtained experimentally and that calculated using AISI Effective Width method. Values obtained from the Effective width method were found to be 159 % to 256 % higher than the ones obtained from testing. Figure 6.10 shows the same values in graphical form.

**Table 6.11 Comparison of Experimental and AISI (2002) Capacities
(2 Purlin Tests with Lateral Restraints)**

Purlin Size	Experimental (kips)	AISI Specifications (kips)	% Difference
12Z080	9.08	23.51	-158.92
12Z100	12.50	32.40	-159.20
14Z080	5.26	18.74	-256.27
14Z134	11.95	41.00	-243.10

6.4.4 Tests with Two Purlins Without roof Panel but with Lateral Restraint

Table 6.12 compares the capacities obtained from the two purlins tests without roof panel but with lateral restraint. Figure 6.11 shows the same values in graphical form. The theoretical values calculated using AISI (2002) and Direct Strength Method are unconservative, with an exception to the 14Z80 specimen where the values obtained by Direct Strength Method is conservative and almost identical to the tested capacity.

**Table 6.12 Comparison of Experimental and Theoretical Capacities
(2 Purlin Tests without roof panel but with Lateral Restraint)**

Purlin Size	Single Purlin Capacity P_n (kips)		
	Experimental	AISI (2002)	DSM (2004)
12Z080	18.16	38.48	21.26
12Z100	26.41	54.99	34.45
14Z080	20.14	31.24	18.73
14Z134	46.03	67.16	57.02

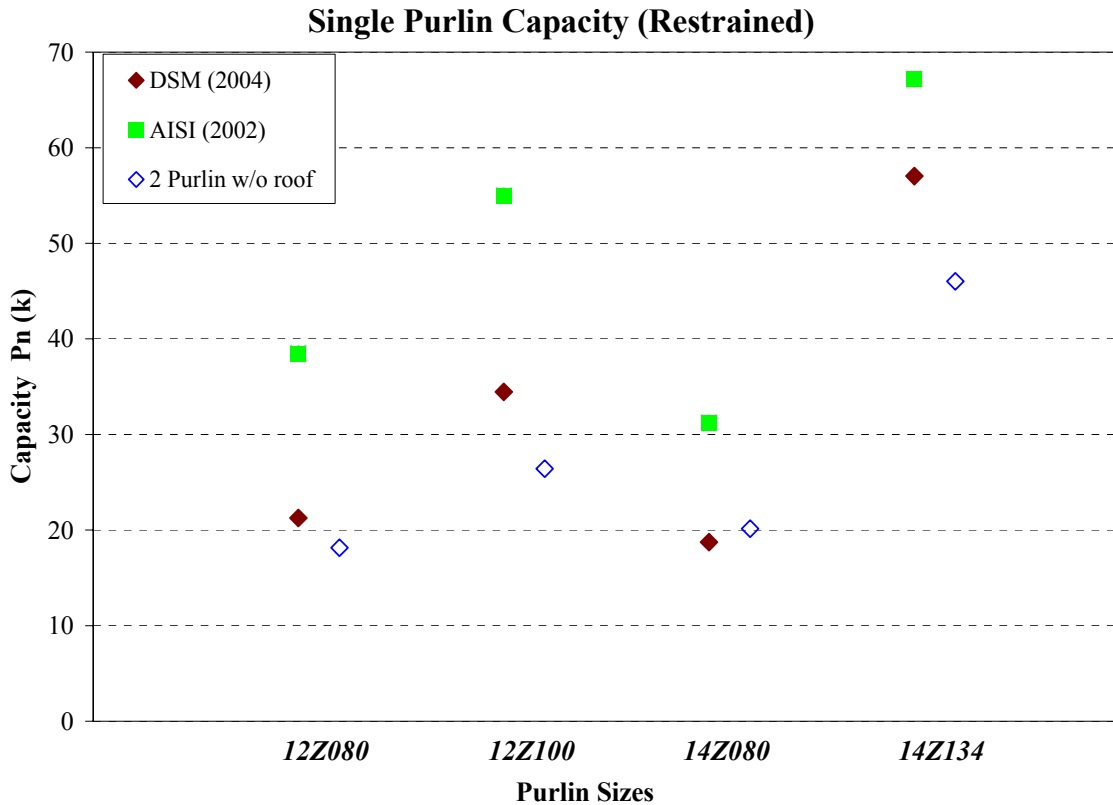


Figure 6.11 Experimental Capacity Vs Theoretical Capacity

6.4.4.1 Direct Strength Method (2004)

The analysis of purlins with lateral restraint was similar to section 6.4.2.1 the section dealing with analysis of purlins with lateral restraint. An effective length factor (K) of 1.0 was used for the analysis, This represents a purlin section between lateral brace points. A length of specimen equal to 6 ft and 9ft. was used for 12 inch and 14 inch specimens respectively. Table 6.10 compares the axial capacity of a single purlin obtained by Direct Strength Method to the experimental capacity. The Direct Strength Method capacity of a 14Z080 specimen was 64% greater than the tested capacity. This may be due to a weakness in the Direct Strength method when used for sections that are deeper and thicker.

**Table 6.10 Comparison of Experimental and DSM (2004) Capacities
(2 Purlin Tests without roof panel but with Lateral Restraint)**

Purlin Size	Experimental (kips)	DSM (2004) (kips)	% Difference
12Z080	18.16	21.26	-17.07
12Z100	26.41	34.45	-30.44
14Z080	20.14	18.73	7.00
14Z134	46.03	57.02	-23.88

6.4.4.2 AISI Specifications (2002)

When determining the axial capacity using the AISI method (2002) an appropriate effective length factor (K) and the unbraced length (L), between lateral restraint locations was used. An unbraced length of 6 feet with a K factor of 1.0 was used in the analysis of 12 inch deep purlins. An unbraced length of 9 feet with a K factor of 1.0 was used in the analysis of 14 inch deep purlins. These values are similar to those used in the Direct Strength Method analysis. These sections, located in the middle of the purlin span between lateral brace points, are the controlling lengths for each purlin size.

Table 6.11 compares the values of a single purlin obtained experimentally and that calculated using AISI Effective Width method. Values obtained from the Effective width method were found to be 46 % to 112 % higher than the ones obtained from testing. Figure 6.11 shows the same values in graphical form.

**Table 6.11 Comparison of Experimental and AISI (2002) Capacities
(2 Purlin Tests with Lateral Restraints)**

Purlin Size	Experimental (kips)	AISI Specifications (kips)	% Difference
12Z080	18.16	38.48	-111.89
12Z100	26.41	54.99	-108.22
14Z080	20.14	31.24	-55.11
14Z134	46.03	67.16	-45.90

6.4.5 Comparison of Experimental and AISI (2004) Capacities

In March of 2005 AISI published a supplement to the 2002 Specification. C4.7 of this supplement is a new method of calculating the axial capacity of compression member having one flange fastened to a standing seam roof. Figure 6.12 illustrates the theoretical axial capacity using C4.7 and compares it to the experimental data. It is easily seen that the AISI Design Method C4.7 2004 is unconservative except when the bracing is extremely rigid.

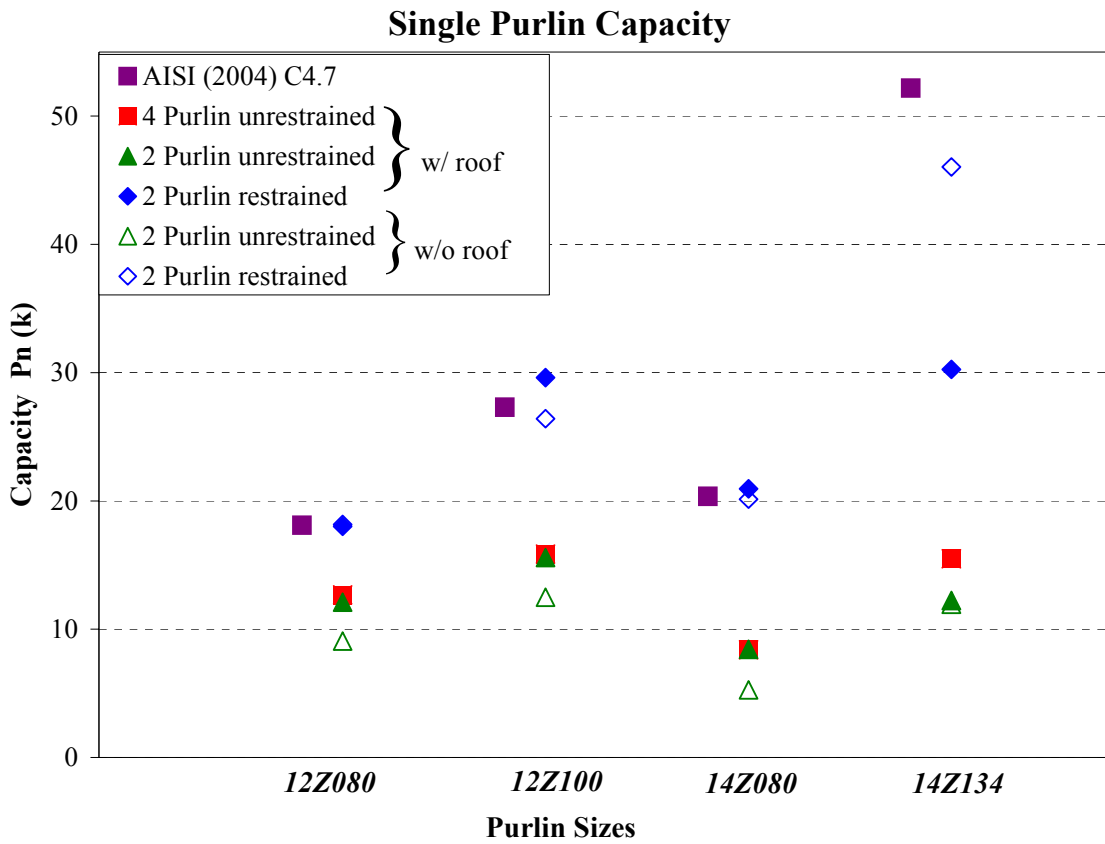


Figure 6.12 Experimental vs. AISI C4.7 Capacities

6.4.6 Comparison of Purlin Experimental to Theoretical Design Values

Figure 6.13 and Figure 6.14 compare and contrast the purlin experimental capacities, with and with out roof panel to the various theoretical design values.

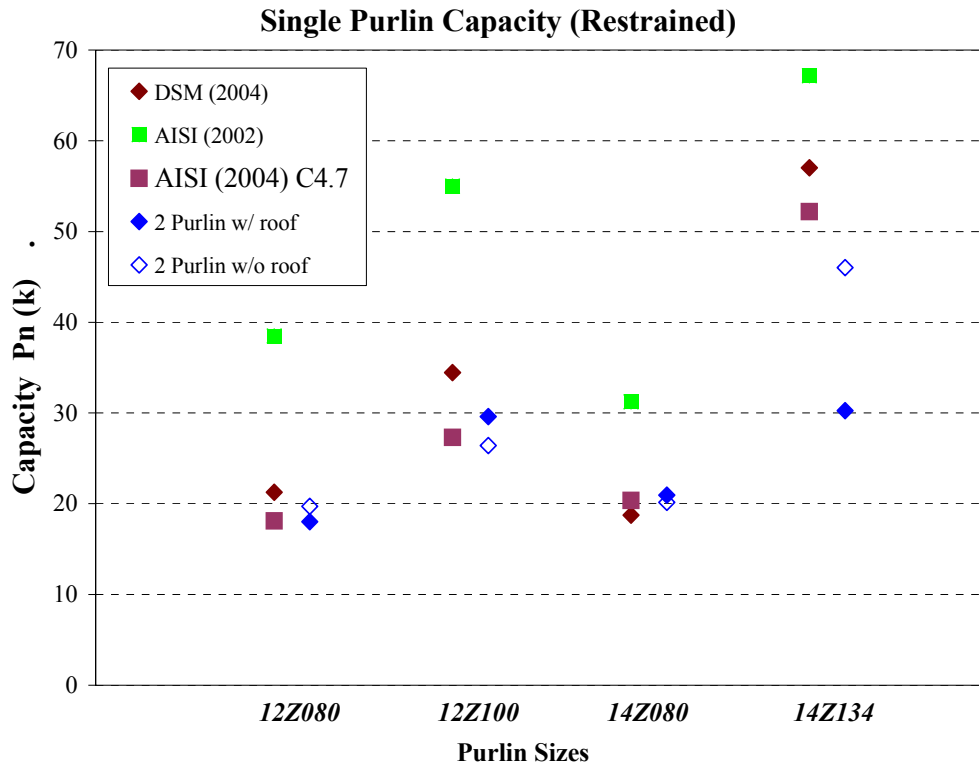


Figure 6.13 Unrestrained Experimental vs. Design Capacities

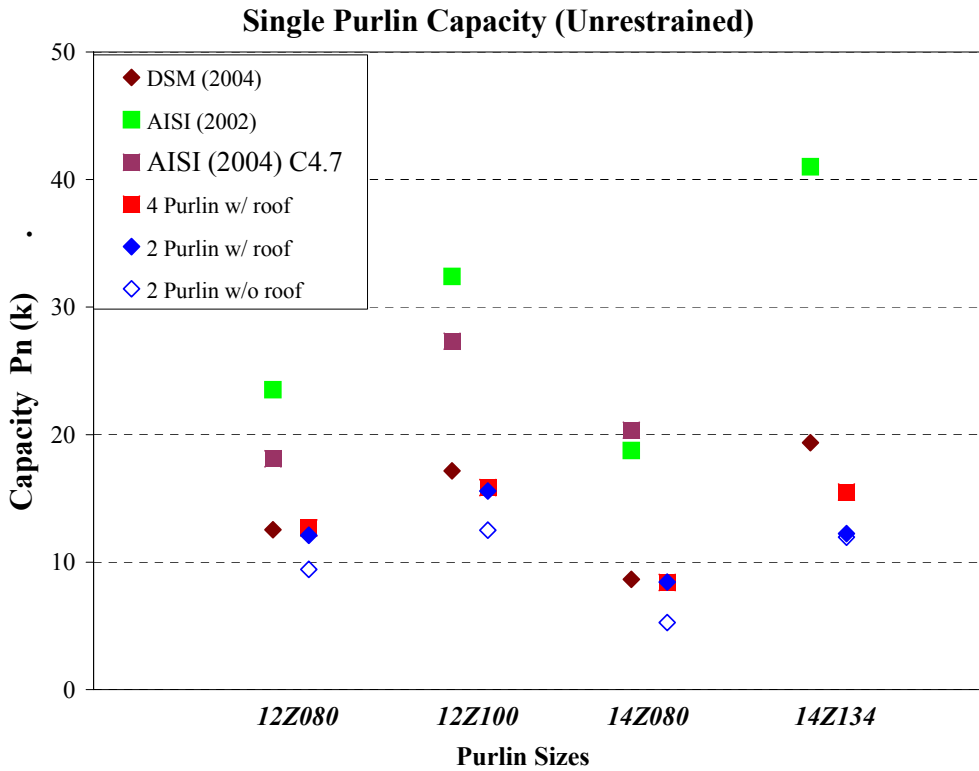


Figure 6.14 Restrained Experimental vs. Design Capacities

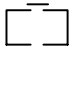
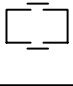
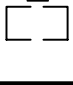
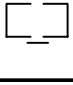
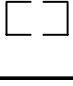
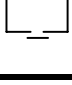
6.5 Built-up Members

6.5.1 Tests with Fixed End Conditions

The 2001 *Specification* was used to calculate a design buckling capacity for some of the configurations tested. All of the conditions of Chapter F, “Tests for Special Cases,” concerning the number of tests and the scatter of the data points were met by these tests. Equation F1.1-2 was used to calculate the phi-factor for each configuration. The results of these calculations are given in Table 6.12.

It was found that welding on only one side of the pair provides a surprising amount of restraint against relative rotation of the members. Also, welding the members together at the mid-points, which is not acceptable according to the *Specification*, created a specimen with a higher capacity than welding them together at third-points, which is acceptable according to the *Specification*. This behavior seems to be because the welding at the mid-points restrains the members relative to one another at the point of maximum curvature in the buckled shape.

Table 6.12 Design phi-factors and buckling capacities of selected built-up configurations.

Thickness	Orientation	Buckling Load (k)		ϕ	ϕR_n (k)		
		Results	Average				
0.100		43.65	38.56	0.648	25.0		
		37.81					
		34.21					
		46.25	47.17				
		52.85					
		42.41					
0.080		24.56	30.77	0.485	14.9		
		35.43					
		32.31					
		43.04	39.47			0.755	29.8
		39.30					
		36.07					
0.064		26.26	22.86	0.614	14.0		
		22.10					
		20.23					
		25.48	25.71			0.822	21.1
		26.56					
		25.10					

6.5.1.1 Tests without intermediate stitch welding

All of these specimens failed by elastic lateral-torsional buckling of the two members. As the members began to rotate, slipping of the members against one another was audible. The members bore on one other at one corner of the section, then moved apart at failure. Significant rotation was visible at loads much lower than the ultimate buckling capacity. At failure, the members had rotated away from each other more than 45° at mid-length. This rotation is depicted in Figure 6.15. A typical specimen under ultimate load is shown in Figure 6.16.

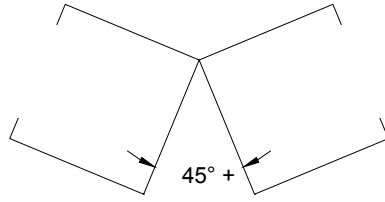


Figure 6.15 Deformed shape of paired members with no stitch welds

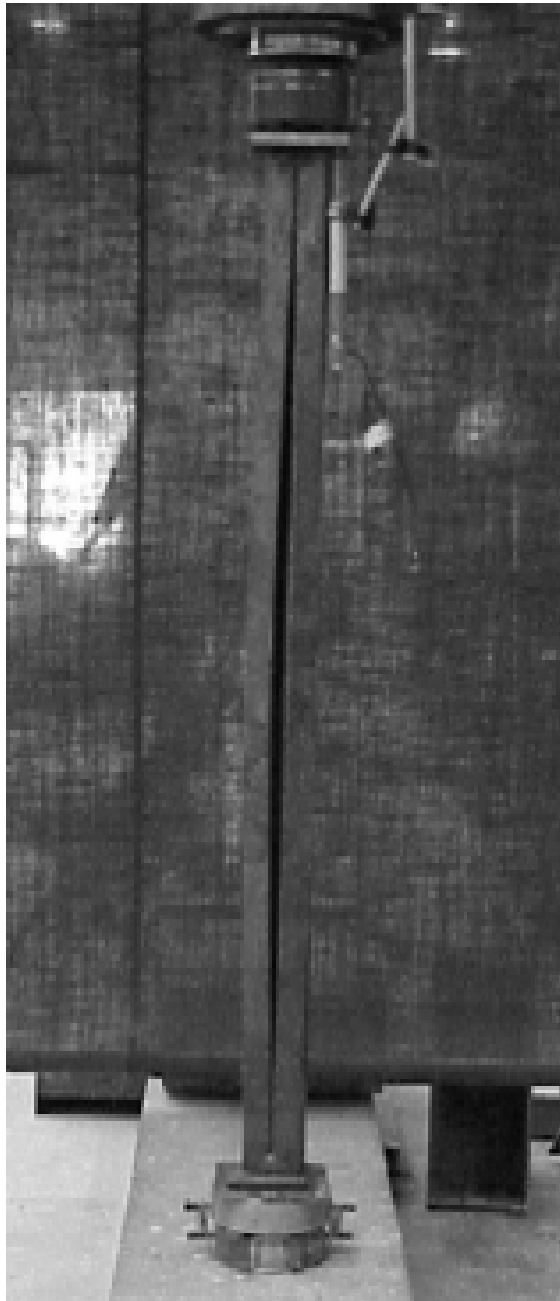


Figure 6.16 Buckling of typical specimen with no stitch welding

6.5.1.2 Tests with a stitch weld on one side at mid-length

Failure in these specimens was similar to the specimens without stitch welding, but it occurred at higher loads. The members rotated away from one another, but they were connected at the weld, so independent translation was restrained. This weld also restrained the rotation of the members to some degree. In some specimens, plastic deformation of the lip was observed around the weld. This deformation is shown in Figure 6.17. The specimens did translate out of plane similarly to the specimens without stitch welding. In most cases, large deflections and rotations were visible at loads much less than the ultimate failure load. In a few cases, buckling occurred suddenly.



Figure 6.17 Buckling of specimen with stitch welding on one side

6.5.1.3 Tests with stitch welds on one side at third points

The two specimens with 0.080 in. thick material failed in simple Euler buckling very similar to the specimens with a stitch weld on one side at mid-length. The two members rotated away from each other, and the point of maximum deflection and rotation of the members was at mid-length. The two specimens with 0.100 in. thick material failed in buckling of a shorter section. Approximately 12 in. at each end remained straight, and the central portion of the length buckled into a half sine wave. Again, the point of maximum deflection and rotation of the members was at mid-length

6.5.1.4 Tests with stitch welds on both sides at third points

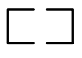

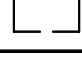
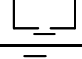
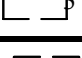
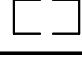

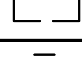

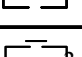

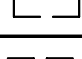
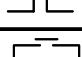
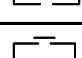
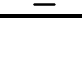
Both of these members initially went into double curvature. The sections between the ends and the welds buckled into half sine waves and the members rotated away from one another at the middle of this section. The center of the specimen, between the stitch welds, remained straight. One of the two specimens buckled and failed at this point. The other suddenly buckled in single curvature of the entire section, with plastic local buckling at mid length.

6.5.1.4 Comparison of Experimental and Theoretical Capacities

The experimental results were compared to theoretical values determined using the 2001 *AISI Specification* and the Direct Strength Method (Schafer 2002). Ultimate strengths were compared in all cases. These values are shown in Table

6.13 for the built-up sections. For the theoretical capacities K was taken as 0.5, the theoretical effective length factor, not 0.65 the recommended effective length factor. Theoretical capacities in red are unconservative when compared to the experimental results.

Table 6.13 Experimental vs. theoretical capacities

Thickness (in.)	Orientation	Ultimate Axial Capacity (k)		
		Experimental	AISI	DSM
0.100		34.63	29.8	27.7
		34.54	31.2	27.7
		38.56	37.9	44.2
		47.17	37.9	46.6
		54.24	39.9	46.6
0.080		20.40	24.7	20.0
		22.90	24.7	20.0
		30.77	31.2	33.4
		39.47	31.2	36.5
		27.72	32.7	33.4
		35.28	32.7	36.5
0.064		17.27	20.2	14.7
		18.15	20.3	14.7
		22.86	24.5	25.1
		25.71	24.5	28.6

The Direct Strength Method calculations were based on three finite strip analyses for each member thickness. The first analysis was of a single member without any special restraints. The second was of a single member with one corner of the cross-section restrained with springs against translation in the z direction and rotation. The third analysis was of a single member with two corners of the cross-section restrained against translation in the z direction and rotation.

For all cases, the critical local and distortional buckling stresses were determined from the first analysis. The critical global buckling stress was taken as the least of the global buckling load from the first analysis at a half wavelength equal to the distance between the stitch welds or the global buckling load from the appropriate restrained model with a half wavelength equal to the total member length. Figure 6.18 shows typical elastic buckling curves with these points indicated

The capacities predicted by the 2001 *AISI Specification* range from 20% greater than the experimental data (i.e. unconservative) to 36% less than the experimental data. Only one value predicted for the 0.100 in. thick material was unconservative, and the values became less conservative or more unconservative as the material thickness decreased to 0.080 and 0.064 in. This trend likely occurs because the *AISI Specification* requirements are based upon research with hot-rolled sections. Local and distortional buckling modes become more critical as the material thickness decreases, leading to unconservative analysis. It is important to

note that these provisions do not distinguish between stitch welds on one side of the member only and stitch welds on both sides.

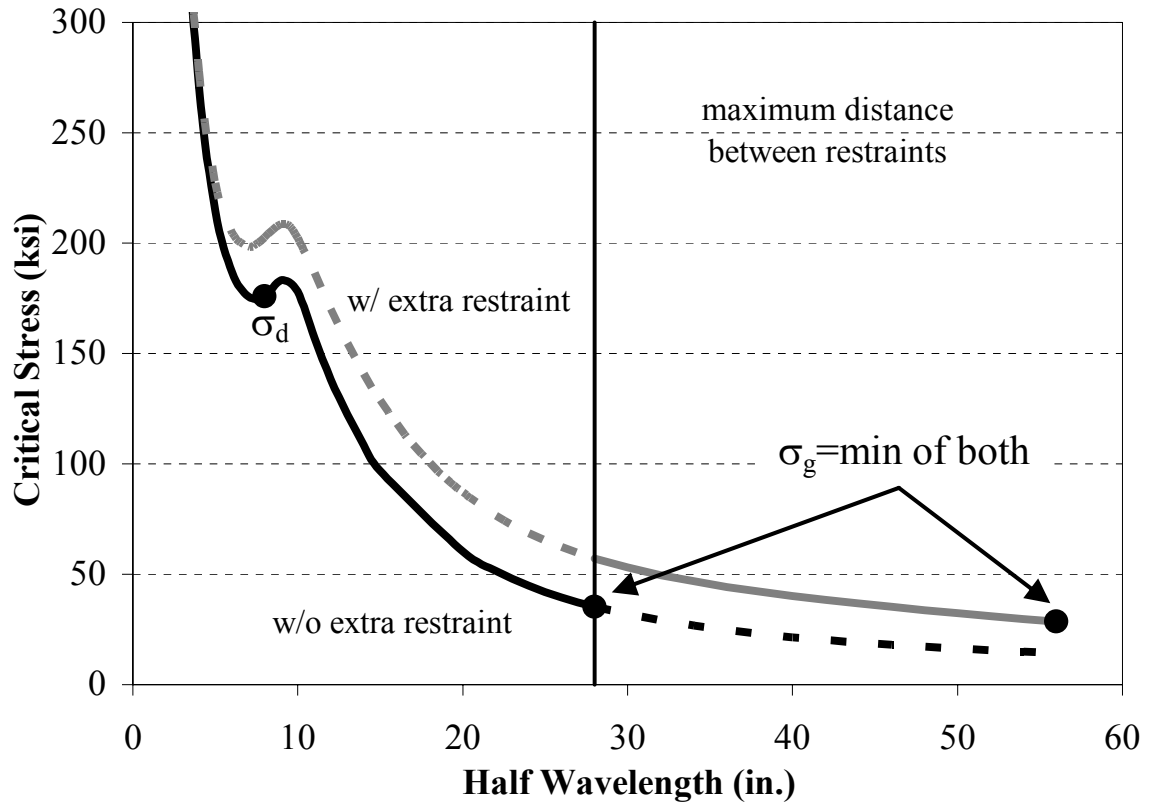


Figure 6.18 Typical elastic buckling curves used with DSM

The capacities predicted by the Direct Strength Method follow the AISI trend in most cases. The capacities predicted for the specimens without intermediate stitch welds were the most conservative. This may be due to difficulties in quantifying and modeling the restraints on the members. Friction between the members provides a larger portion of the total restraint in this case, leading to increased conservatism.

The procedure used to generate elastic buckling curves for the Direct Strength Method required an assumed stiffness for each spring. The values chosen were based upon the deformations observed in the laboratory. The opposing members keep one another from translating sideways during buckling, so a very large stiffness was selected for the translational springs. The rotational restraint at the connection is limited by the base metal, so the spring stiffness was chosen based on the limiting material thickness.

These springs estimated the effects of the intermediate welds connecting the members, but they did not account for the restraining effects of contact and friction between the members. This restraint could be modeled by applying relatively soft spring restraints to the "unrestrained" model used to determine the behavior of the section between the welds. However, quantifying the effects of friction and contact to determine the effective spring stiffness is difficult.

Chapter 7 Conclusions and Recommendations

7.1 Conclusions

7.1.1 Purlins

- Providing increased section stability at the brace point increases the axial capacity of a purlin.
- A standing seam roof system increases the section stability and therefore increases the axial capacity of a strut purlin.
- Currently, no method gives accurate design capacities for deep Zee cold-formed strut purlins that are laterally restrained by a standing seam roof system.
- Providing mid-length external bracing increases the axial capacity of a strut purlin significantly. This indicates that global buckling modes and interactions between global buckling modes and local or distortional modes are important.
- Global bracing always improves the axial capacity for cold-formed strut purlins.
- The axial capacity of a braced purlin is sensitive to the rigidity of the bracing. A bracing system that is infinite or perfectly rigid will result in a higher axial capacity than a system with finite or limited stiffness. A bracing system with finite stiffness will result in a higher capacity when compared to a non braced system.

- None of the methods studied in this research (DSM 2004, AISI 2002 & 2005, and Fisher 1993) consider the strut purlin as a part of the roof system. Modeling the restraint provided by the roof system is critical to accurately predicting the capacity of the strut purlins for design.
- The design method in the 2002 *AISI Specification* is not dependable when applied to deep strut purlins attached to a standing seam roof because it is conservative when no lateral restraint is provided and highly unconservative when lateral restraint is provided.
- In the sections tested, Schafer's Direct Strength Method (2004) is highly sensitive to the critical half wavelength of a member in global buckling. In the long span sections used in these tests, small variations in the critical wavelength can result in a significant change in the capacity due to the controlling global buckling mode.
- Part (a) of Fisher's (1993) alternate approach for calculating the capacity of strut purlins attached to standing seam panels does not account for global buckling issues. Part (b) requires the tested capacity of a representative section. As such, its utility for deep Zee cold-formed strut purlins fails to predict the capacity accurately.
- The global buckling mode is very important in long span strut purlins.
- The design method described in the 2004 Supplement to the *AISI Specification* is unconservative except when the bracing is extremely rigid.

7.1.2 Built-up Members

- A pair of built-up members achieves a higher stress than a single member before buckling occurs. This occurs for all double member tests even when the members are connected only at their extreme ends. Friction between the members provides some restraint and stability against out-of-plane translation and rotation.
- Built-up members welded together at mid-length have a higher ultimate capacity than specimens welded together at the ends only. This small length of stitch welding provided on one or both sides provides significant restraint against rotation of the members. Welding on only one side provides a surprisingly large degree of restraint, and welding on both sides provides more restraint than welding on one side only.
- Providing stitch welds between members at their third points instead of at mid-length does not consistently increase the capacity of the specimen. This may be because the first buckling mode of the members is a single half sine wave over the entire length of the member. Welding the specimens together at mid-length provides restraint against rotation at the point of maximum out of plane deflection and rotation, while welding at the third points does not.
- For built-up members, the 2001 *AISI Specification* provides reasonable estimates of capacity for relatively compact members, but it tends to be unconservative for members with slender elements.

- The Direct Strength Method (2004) provides overly conservative estimates of capacity for built-up members, probably because of difficulties in quantifying restraints provided by interactions between the members.

7.2 Recommendations

7.2.1 Purlins

- The design method in the 2002 *AISI Specification* should not be extended to include deep Zee purlin sections. Improved reliable design procedures, possibly incorporating the theory behind the Direct Strength Method, are needed.
- Additional research needs to be pursued with a larger variety of deep Zee purlin sections and specimen lengths attached to standing seam roof systems. This will aid in developing a method for predicting axial load capacity of longer and deeper sections as a cold-formed system rather than individual members.
- Additional study is required to determine the amount of restraint provided by the roof panel through standing seam clips to the purlin strut. This can be done by using more than one screw per clip and by varying the clip and the clip spacing.
- The effect of external lateral restraint on the capacity of deep Zee purlin struts should be studied in order to determine the increase in capacity provided by

this restraint and to find ways to provide better lateral restraint in building roof systems.

- A thorough investigation of the amount of lateral restraint provided by sag angles and edge beam or eave struts in a roof system is needed.
- An investigation of the effect of section stability on axial and bending capacity of deep Zee strut purlins is needed.
- Development of improved internal bracing between the purlins in a roof system will help address the serviceability issue of large lateral deflections
 - NOTE: An improved internal diaphragm bracing system has developed out of this work and is presently being tested.

Preliminary tests suggest an increase in bending capacity by 10 to 18% and the elimination of all need to brace to the eave strut is possible.

7.2.2 Built-up Members

- Additional study is needed to fully understand the interaction between members of slender built-up sections with discrete connections.
- Additional study is needed to fully understand the boundary conditions of axially loaded built-up members and their implications on the effective length factor, K .
- Development of an improved design procedure is needed.

- The current (2002) *AISI Specification* needs restrictions placed on the discrete intermediate connections or the boundary conditions to avoid grossly unconservative designs.

References

American Institute of Steel Construction (AISC), *Manual of Steel Construction - Load and Resistance Factor Design*, Third Edition (2001), Washington, DC.

American Iron and Steel Institute (AISI), *North American Specification for the Design of Cold-Formed Steel Structural Members 2001 Edition* (2002). Washington, DC.

American Iron and Steel Institute (AISI), *North American Specification for the Design of Cold-Formed Steel Structural Members 1996 Edition* (1997). Washington, DC.

American Iron and Steel Institute (AISI), *Commentary on North American Specification for the Design of Cold-Formed Steel Structural Members: 2001 Edition* (2002). Washington, DC.

American Iron and Steel Institute (AISI), *A Guide For Designing with Standing Seam Roof Panels: Design Guide CF97-1*. August 1997. Washington, DC.

Aslani, F., and Goel, S.C., (1991) *Analytical criterion for buckling strength of built-up compression members*, Engineering Journal of the American Institute of Steel Construction, Volume 28, Issue 4, 4th quarter, p 159-168

Bjorhovde, R. (1972), *Deterministic and Probabilistic Approaches to the Strength of Steel Columns*, Ph.D. Dissertation, Lehigh University, Bethlehem, PA, May.

Bjorhovde, R. (1988), *Columns: From Theory to Practice*, Engineering Journal, AISC, Vol. 25, No. 1, 1st Quarter, pp 21-34

Bleigh, F. (1952), *Buckling Strength of Metal Structures*, McGraw-Hill, pp 176-179

Brueggen, B.L. (2004). "Strength and Serviceability Issues of Cold-Formed Steel Joists", University of Oklahoma.

Davies, J.M. (2000). "Recent research advances in cold-formed steel structures", *Journal of Constructional Steel Research*, 55(1-3), 267-288.

Dimos, P. and Sudharmapal, A.R. (1990), "Cold-Formed Steel Z-Sections with Sloping Edge Stiffeners under Axial Load", *Journal of Structural Engineering*, Vol. 116, No.2, 392-405

Euler, L., (1744) "Methodus inveniendi lineas curvas maximi minimive proprietate gaudentes, sive solutio problematis isoperimetrici lattissimo sensu accepti; Additamentum 1, De curvis elasticis" (A method for finding curved lines enjoying properties of maximum or minimum, or solution of isoperimetric problems in the broadest accepted sense; Appendix 1, The elastic curve) Lausanne & Geneve, Switzerland

Fisher, J.M., Kaehler, R.C. and Glaser, N.J., (1993). "Axial Load Capacity of Sheeted Cold-Formed C and Z Members", Report CF 93-2, American Iron and Steel Institute, Washington, D.C.

Galambos, T.V. (editor) (1998) "Guide to Stability Design Criteria for Metal Structures", Fifth Edition, John Wiley & Sons, Inc., New York, New York

Hancock, G. J. (2003). "Cold-formed Steel Structures", *Journal of Constructional Steel Research*, 59(4), 473-487

Hancock, G.J., Murray, M. Thomas and Ellifritt, S. Dane (2001). "Cold-formed Steel Structures to the AISI Specification. Marcel Dekker, Inc. New York, Basel.

Hatch, J., Easterling, W.S. Murray, T.M., "Strength Evaluation of Strut-Purlins". (1991) Report No. CE/VPI-ST90/08, Virginia Polytechnic Institute and State University, Blacksburg, VA.

King, L.W., Translation of the Code of Hammurabi, *Internet Ancient History Source Book*, <http://www.fordham.edu/halsall/ancient/hamcode.html>

LaBoube, R.A., & Yu, W.W. (1998). "Recent research and developments in cold-formed steel framing", *Thin-Walled Structures*, 32(1-3), 19-39.

Rondal, J. (2000). "Cold-formed steel members and structures- General report", *Journal of Constructional Steel Research*, 55, 155-158

Schafer, B.W. (2002). "Design Manual for the Direct Strength Method of Cold-Formed Steel Design – Draft," Final Report to the American Iron and Steel Institute, Washington, D.C., available at www.ce.jhu.edu/bschafer/direct_strength.

Schafer, B.W. (2005) Personal discussion on Built-up Member Provisions. Annual Stability Conference, Structural Stability Research Council, Montreal, Quebec, April 2005.

Sherman, D.R. & Yura, J.A., (1998) *Journal of Constructional Steel Research*, volume 46, Issue 1, page 470 April-June 1998

Simaan, A. and Pekoz, T. (1976). "Diaphragm Braced Members and Design of Wall Studs", *Journal of The Structural Division*, ASCE, Vol.102, No. ST1, 77-93

Tide, R.H.R. (1985), *Reasonable Column Design Equations*, Proceedings 1985 Annual Technical Session, Structural Stability Research Council, April, Cleveland, OH, Lehigh University, Bethlehem, Pennsylvania

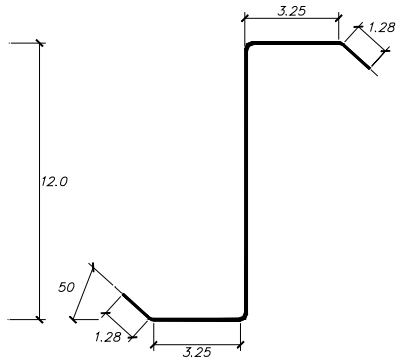
Toney, Pat (2004) Personal discussion on Cold-formed steel. Star Building Systems, Oklahoma City, Oklahoma.

Willis, C.T., Wallace, B. (1990), "Behavior of Cold-Formed Steel Purlins under Gravity Loading." *Journal of Structural Engineering*, ASCE 116 No. 8,

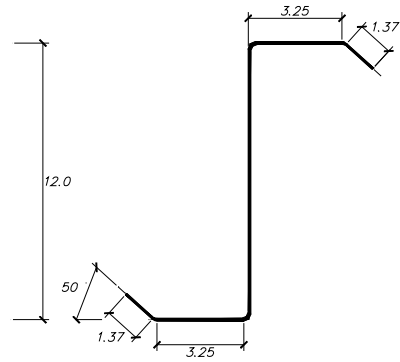
APPENDIX A - Section Properties of Purlin Test Specimens

Appendix A

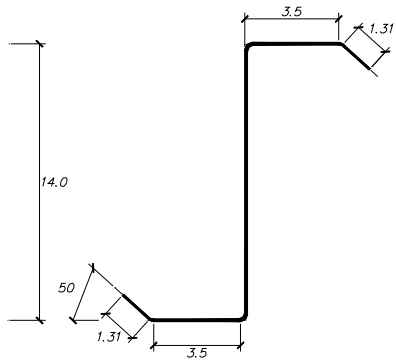
Section Properties of Test Specimens



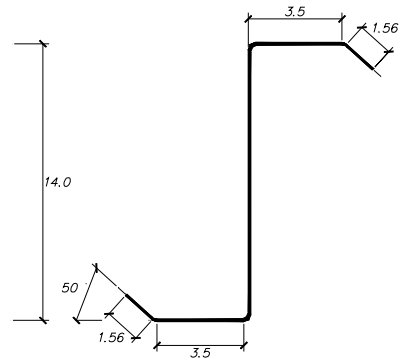
12Z080



12Z100



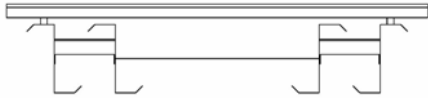
14Z080



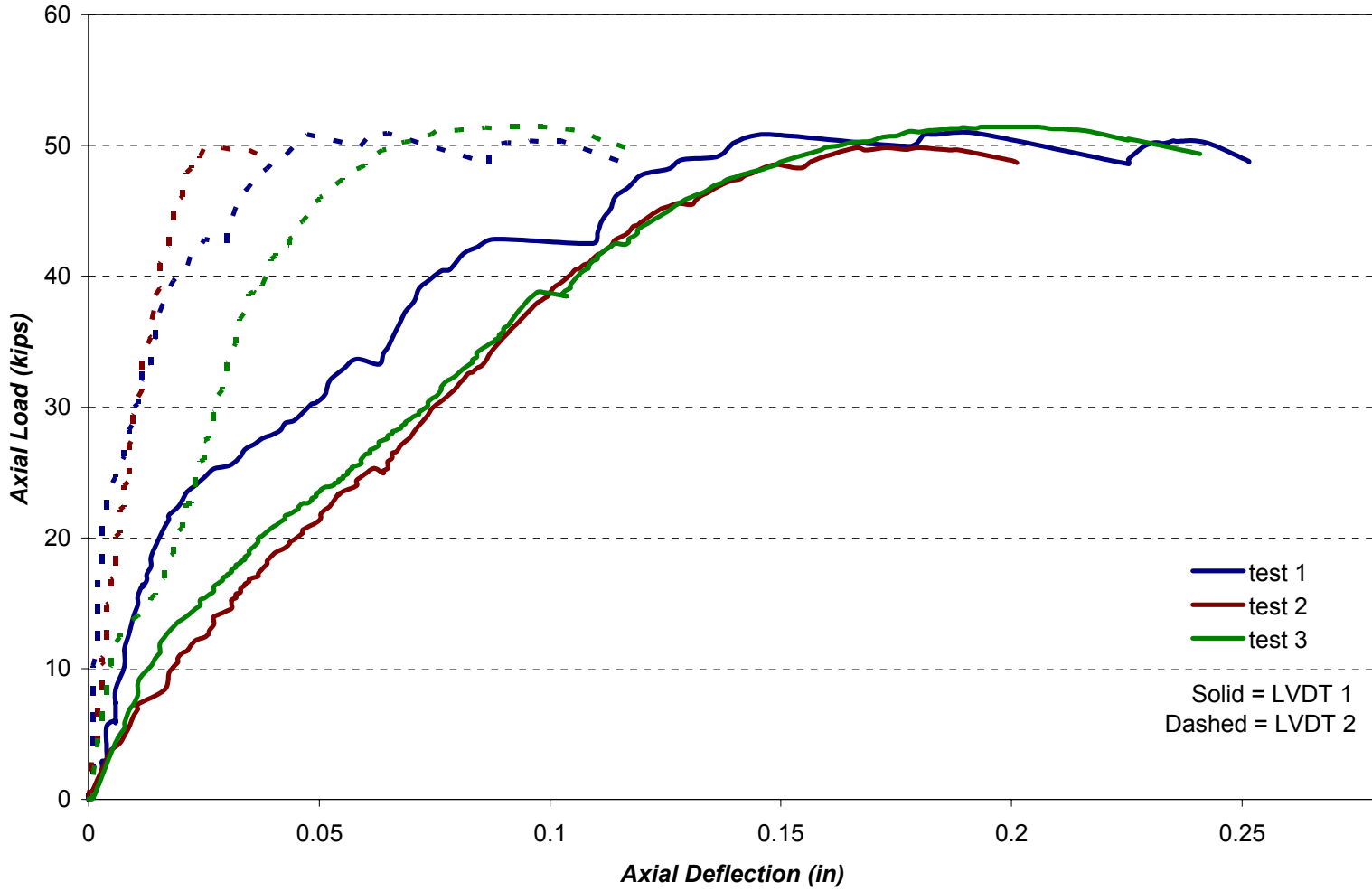
14Z134

All dimensions are in inches

APPENDIX B - Purlin Axial Load Vs Axial Deflection Plots



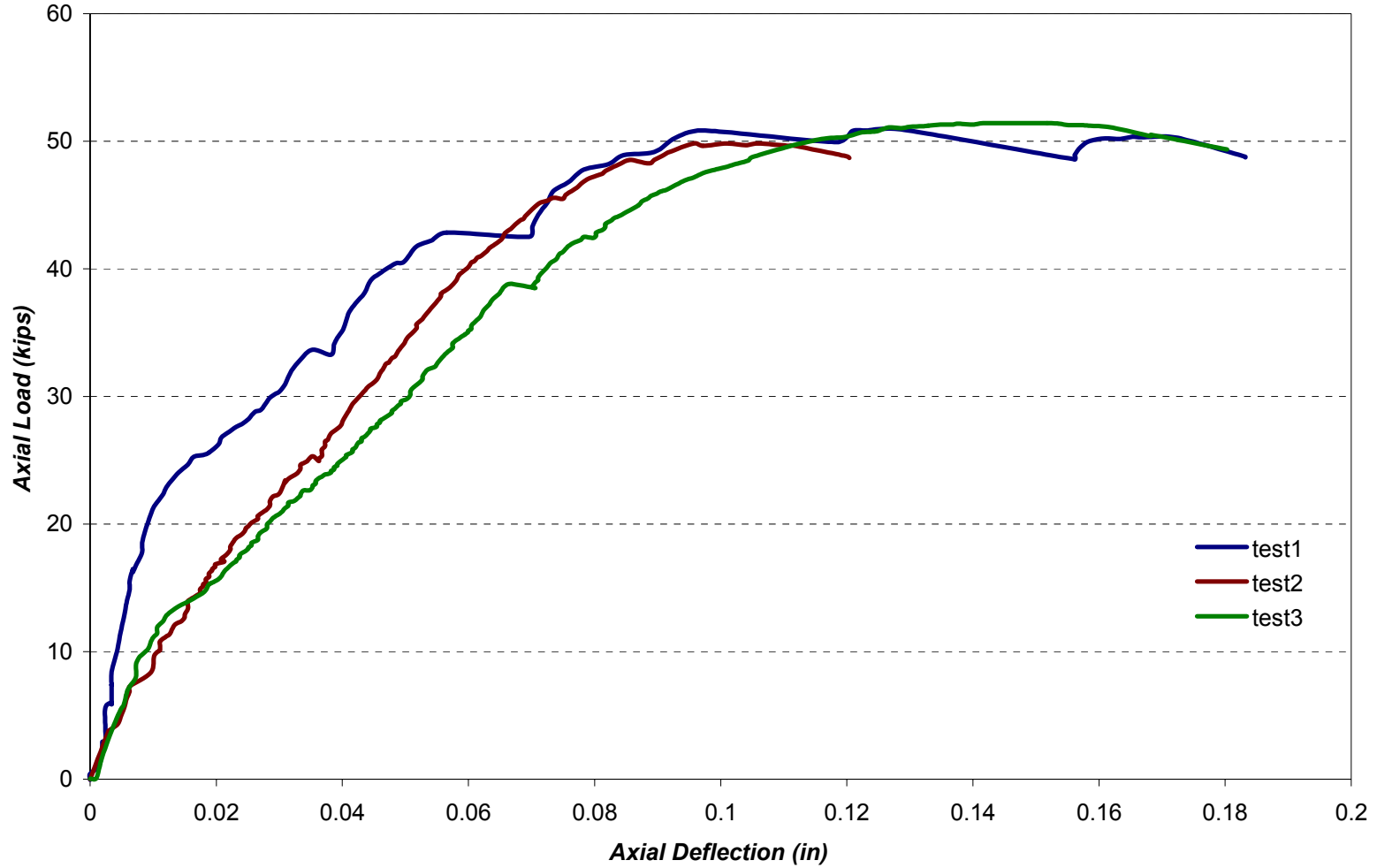
**12" deep 0.080" thick
4 Purlin tests with roof panel**



**12" deep 0.080" thick
4 Purlin tests with roof panel
Average LVDT 1&2**

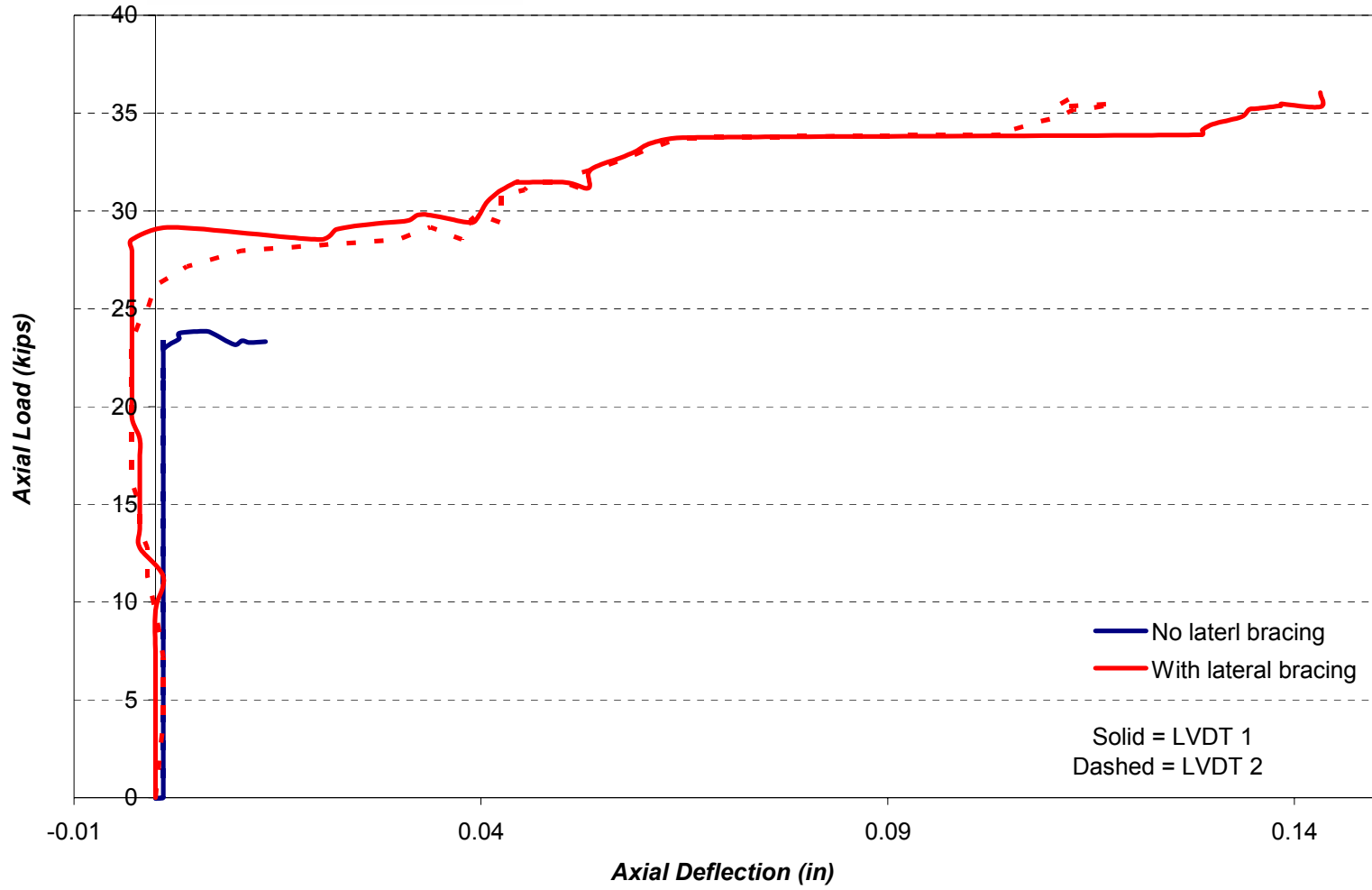


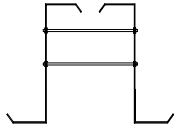
164



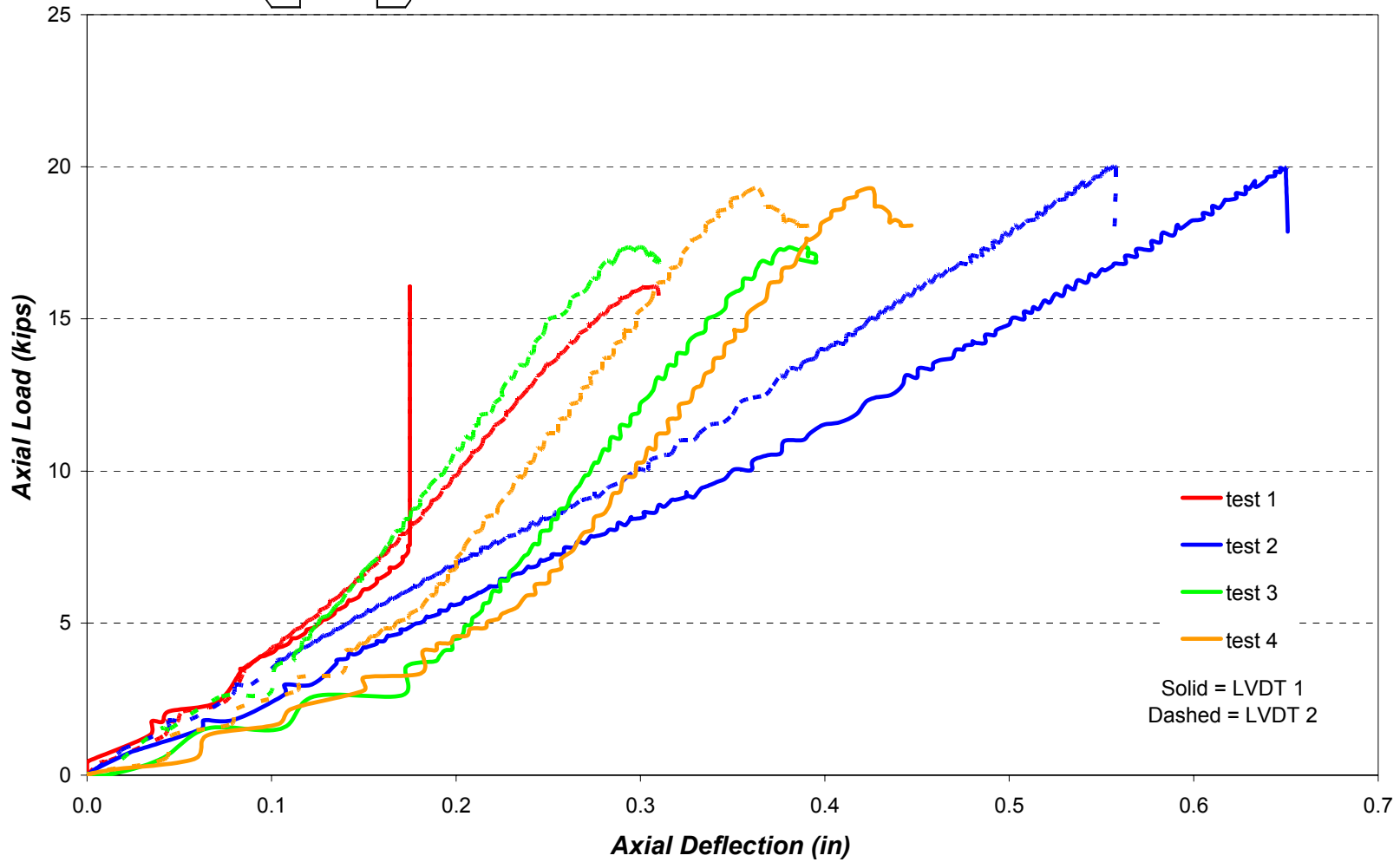


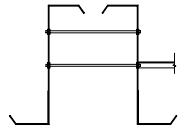
**12" deep 0.080" thick
2 Purlin tests with roof panel**





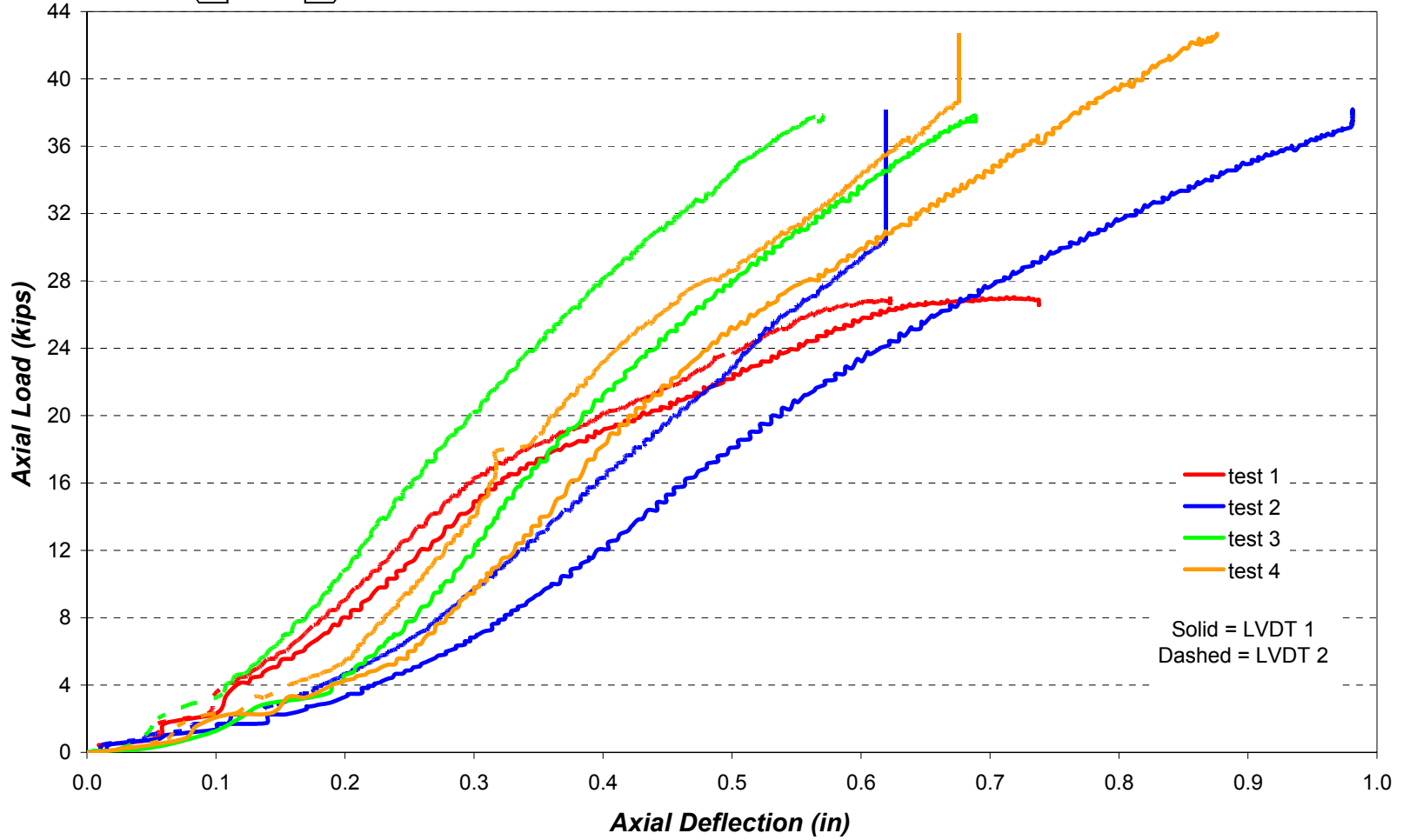
12" deep 0.080 thick
2 Purlin tests w/o Restraint or roof panel





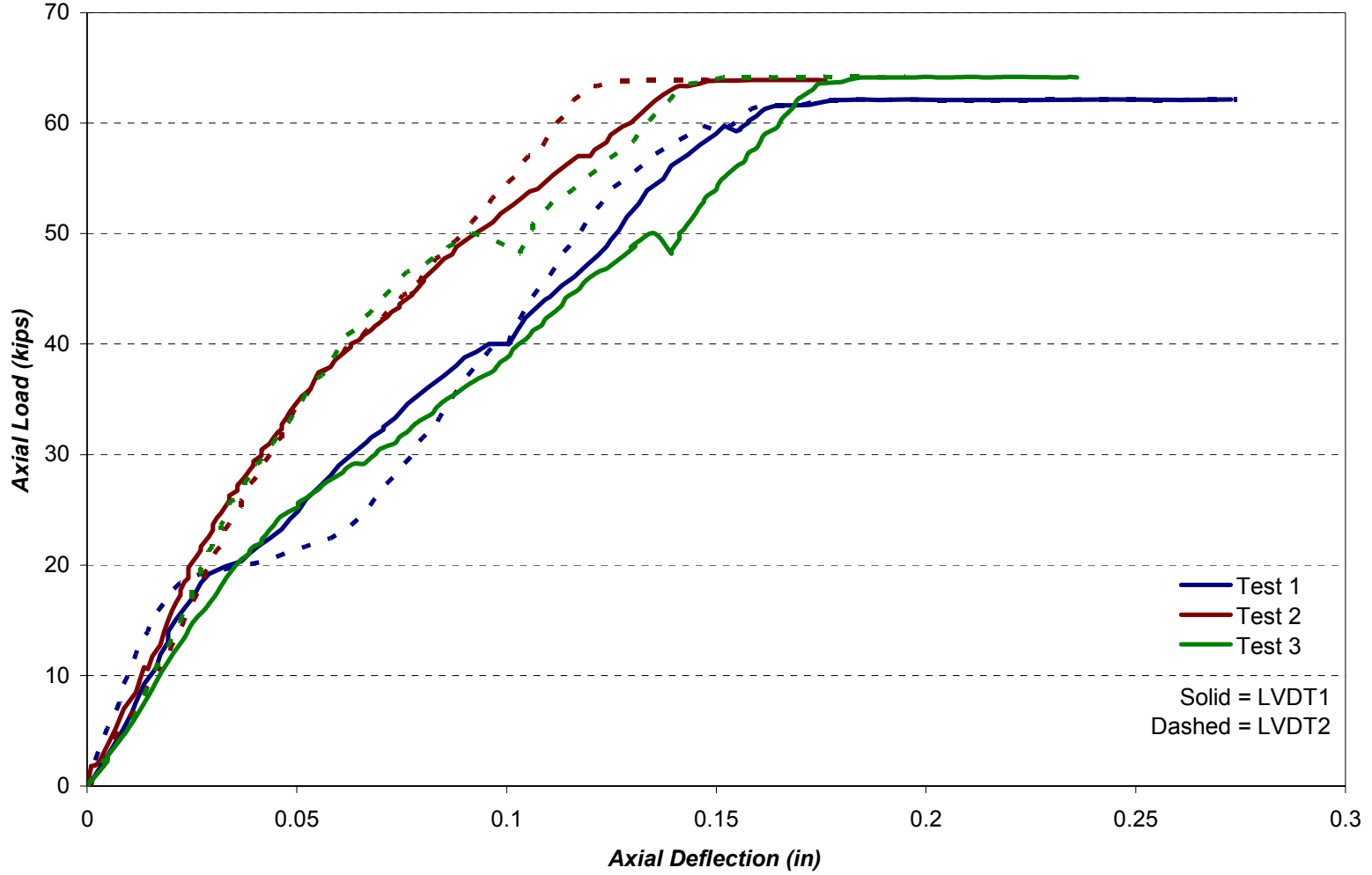
12" deep 0.080 thick
2 Purlin tests w/o roof panel but w/ Restraint

167

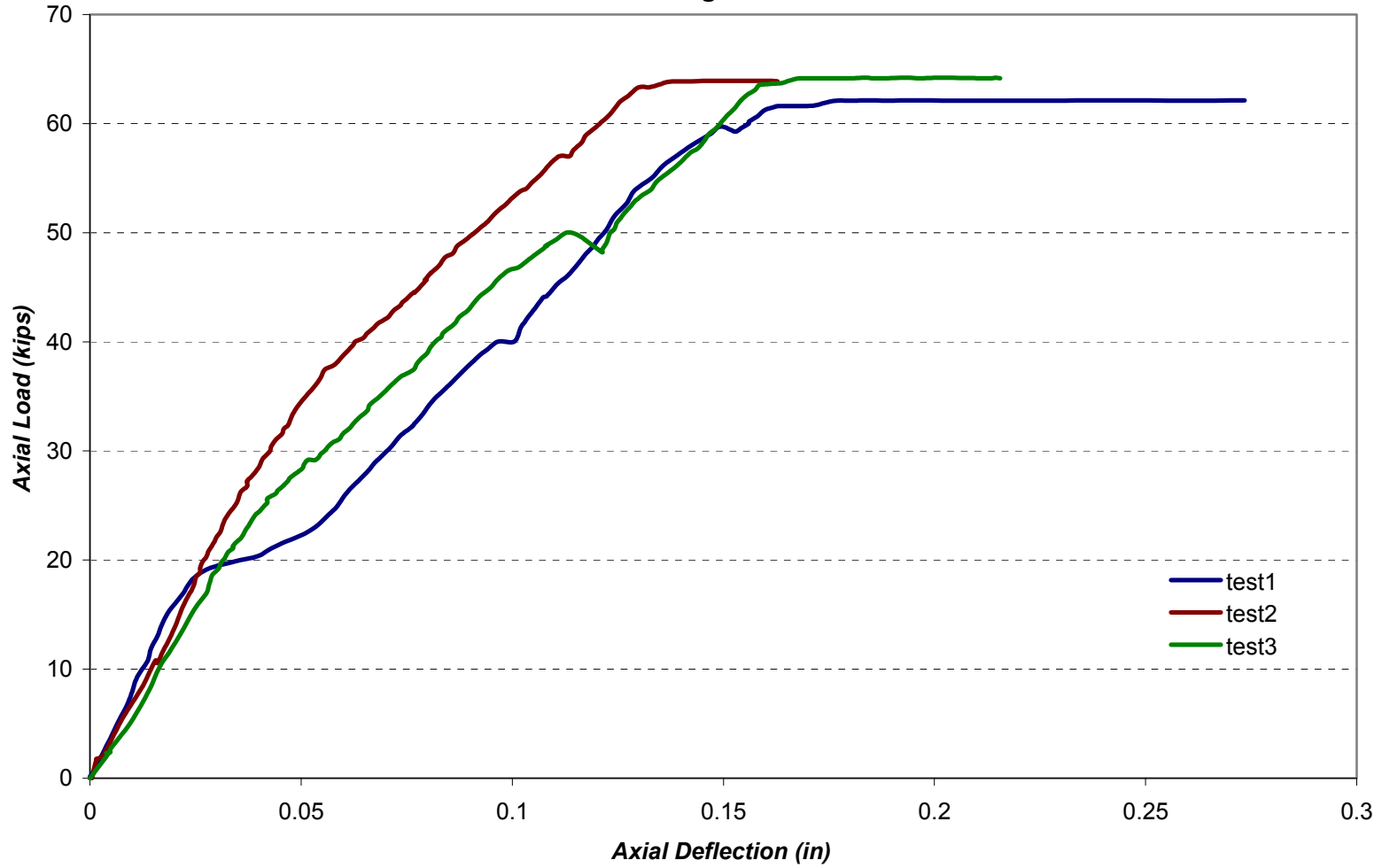




12" Deep Purlins 0.100" Thick
4 Purlin tests with roof panel



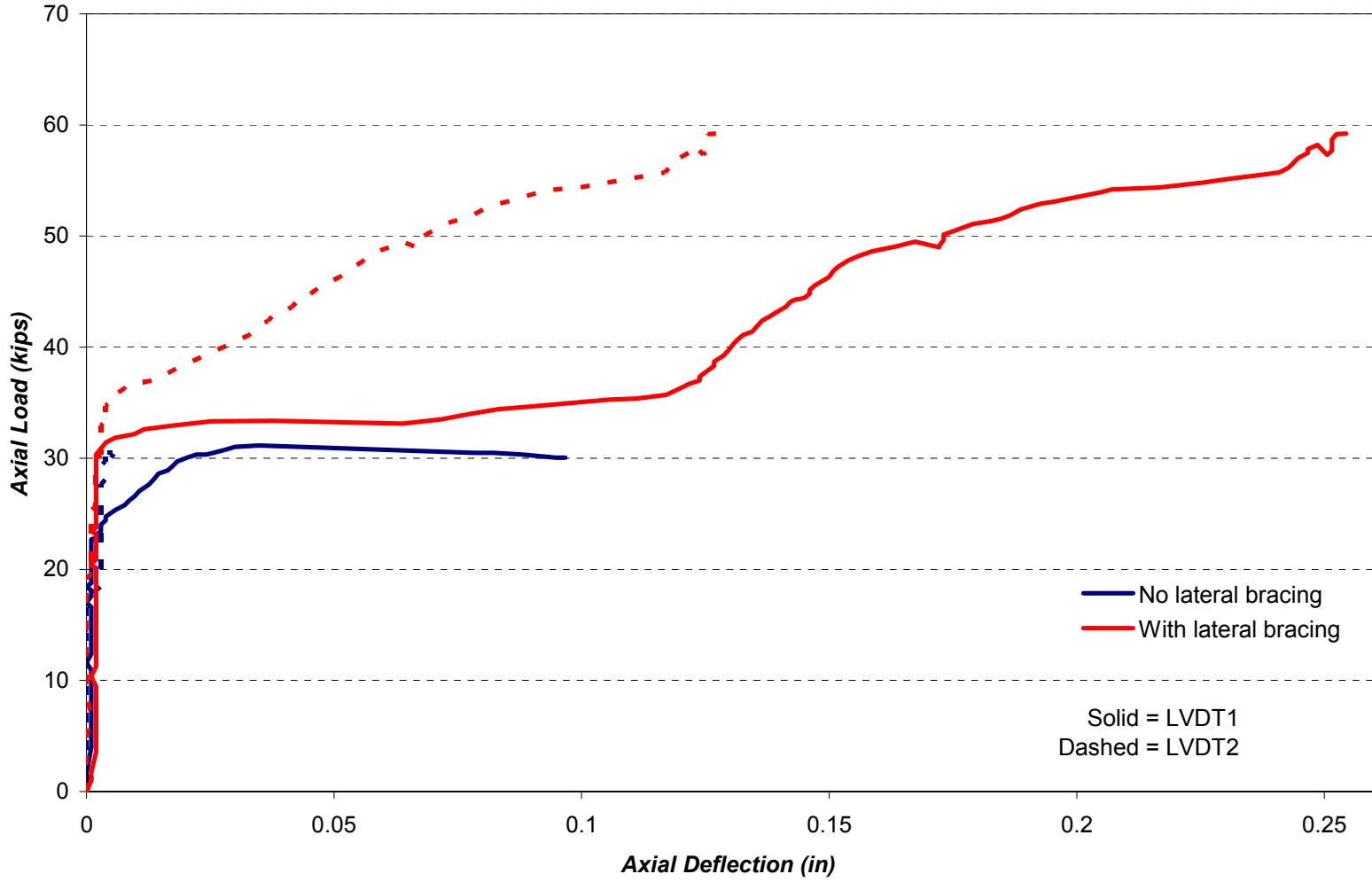
**12" deep 0.100" thick
4 Purlin tests with roof panel
Average LVDT 1&2**

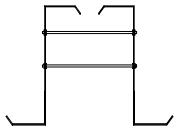


**12" Deep Purlins 0.100" Thick
2 Purlin tests with roof panel**



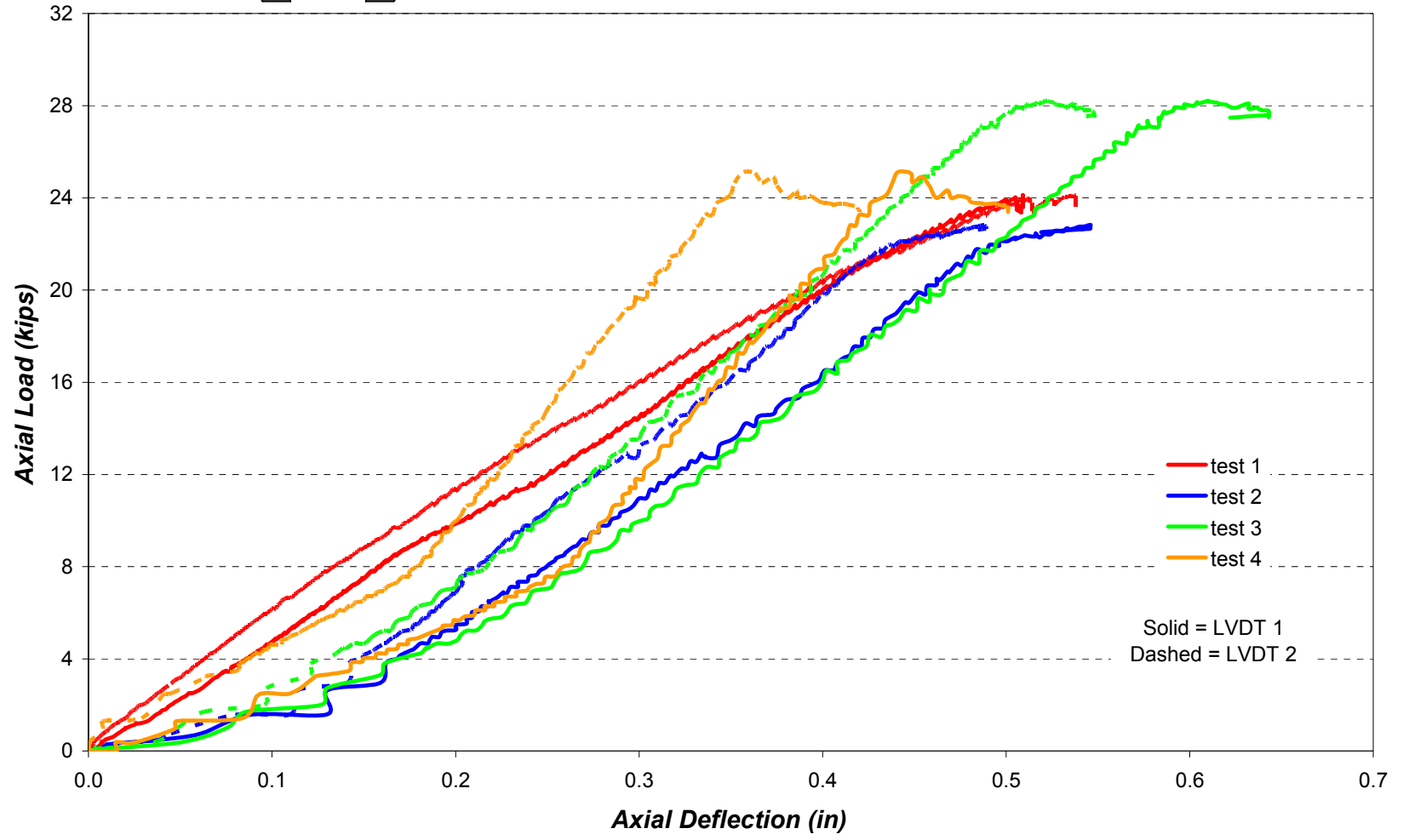
170

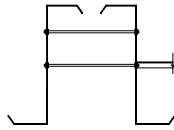




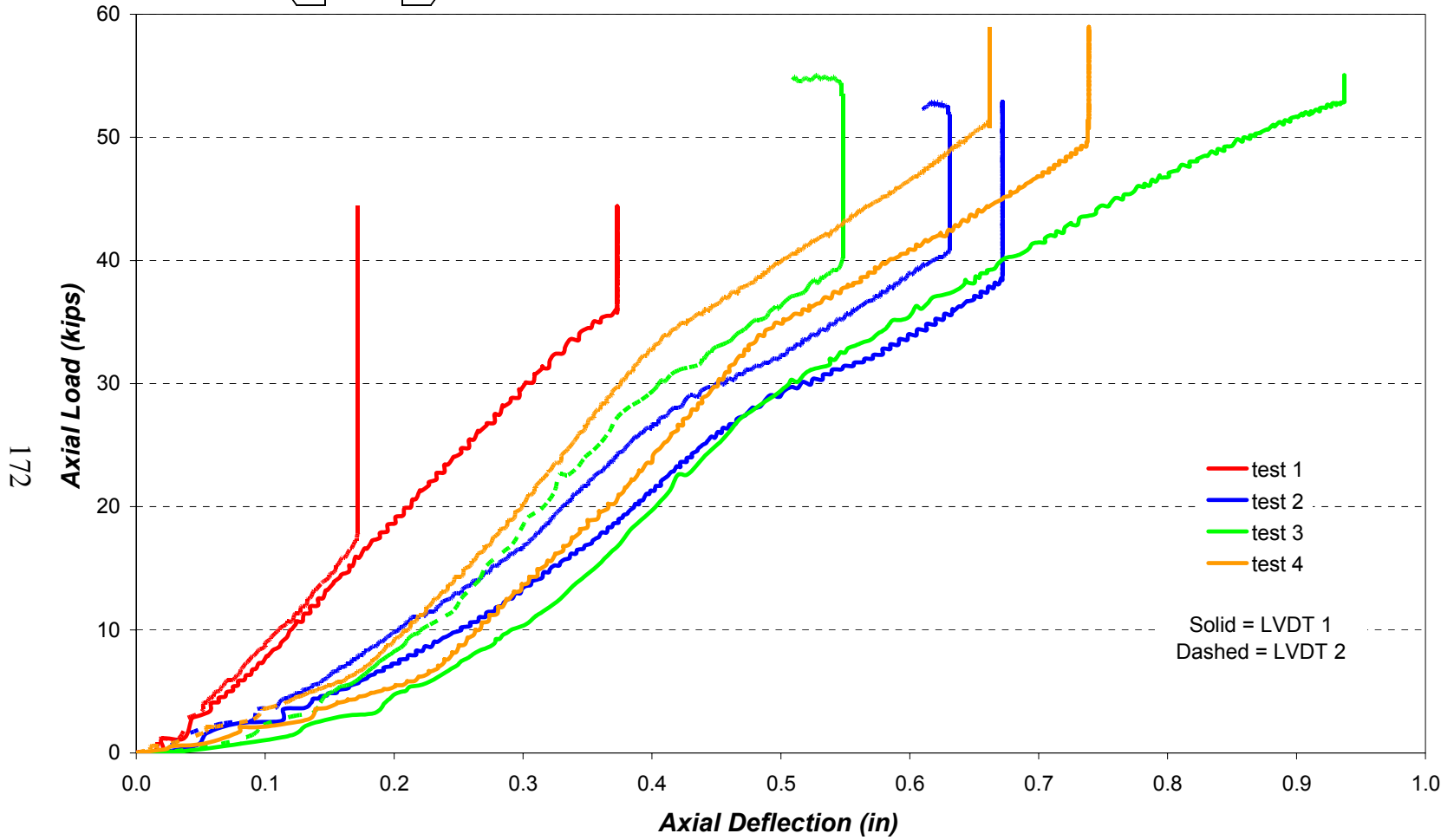
12" deep 0.100
2 Purlin tests w/o Restraint or roof panel

171

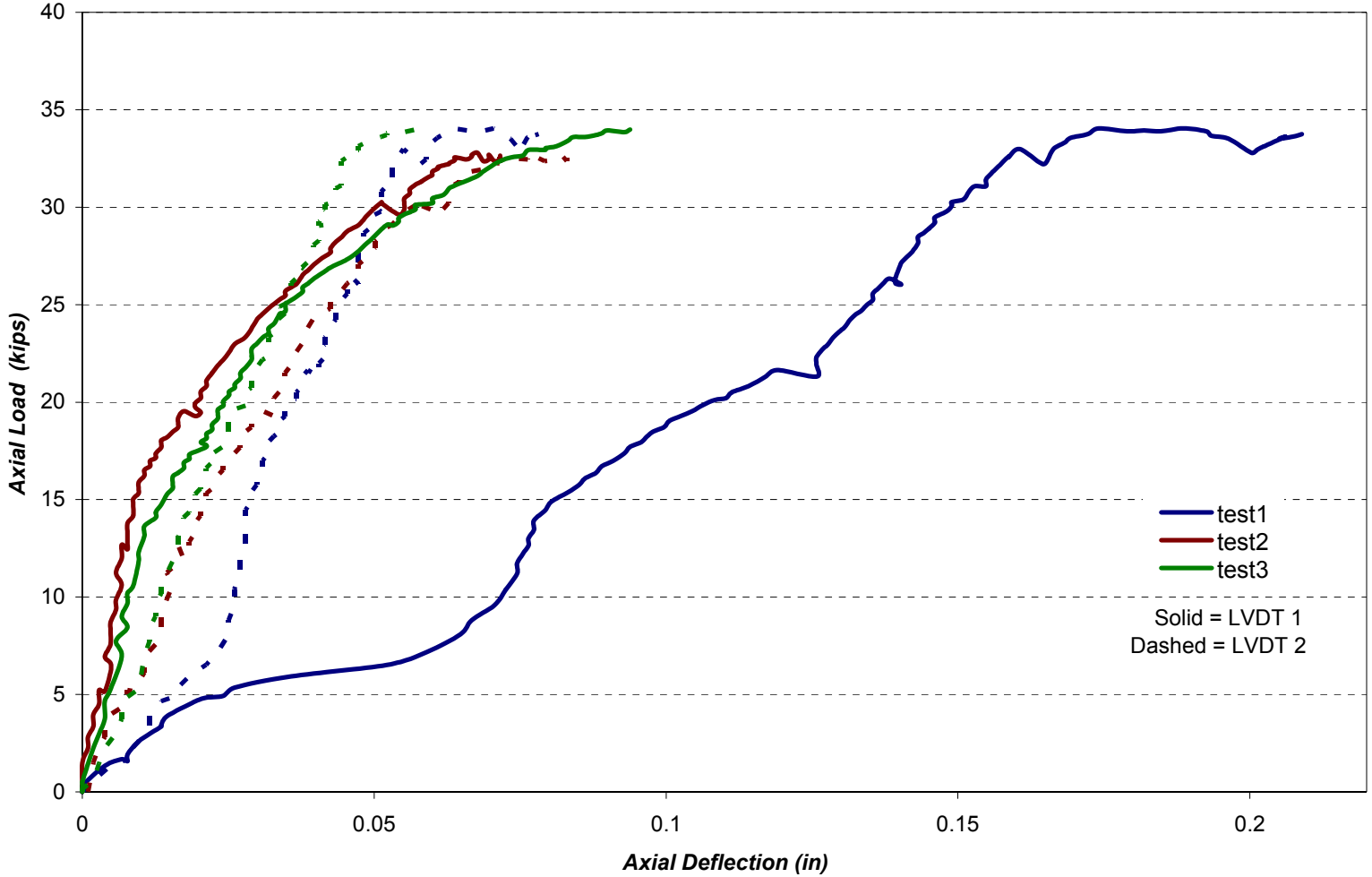




12" deep 0.100
2 Purlin tests w/o roof panel but w/ Restraint

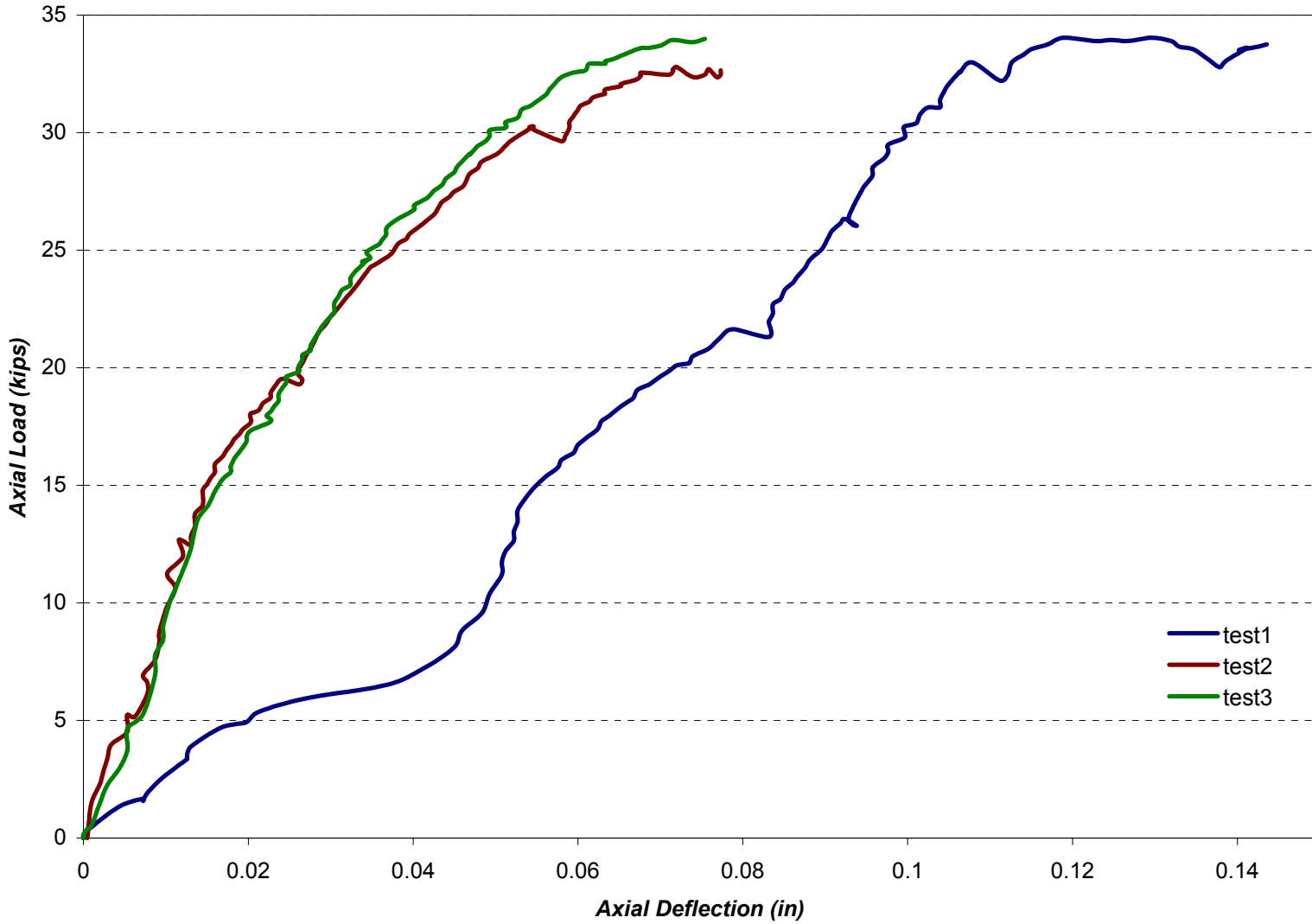


14" deep 0.080" thick
4 purlin tests with roof panel





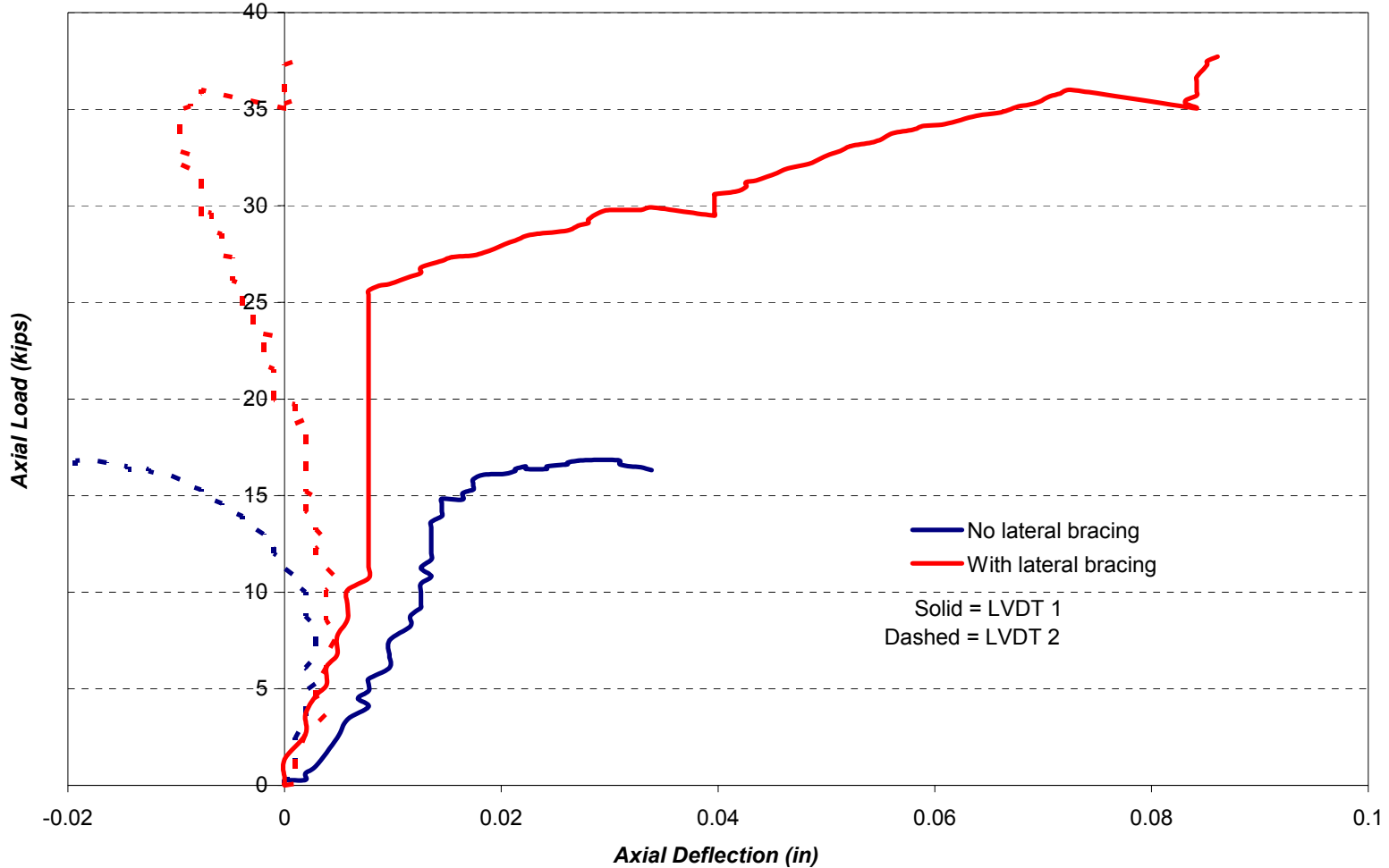
14" Deep 0.080" thick
4 purlin tests with roof panel
Average LVDT 1&2

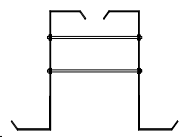


14" deep 0.080 thick
2 Purlin tests with roof panel

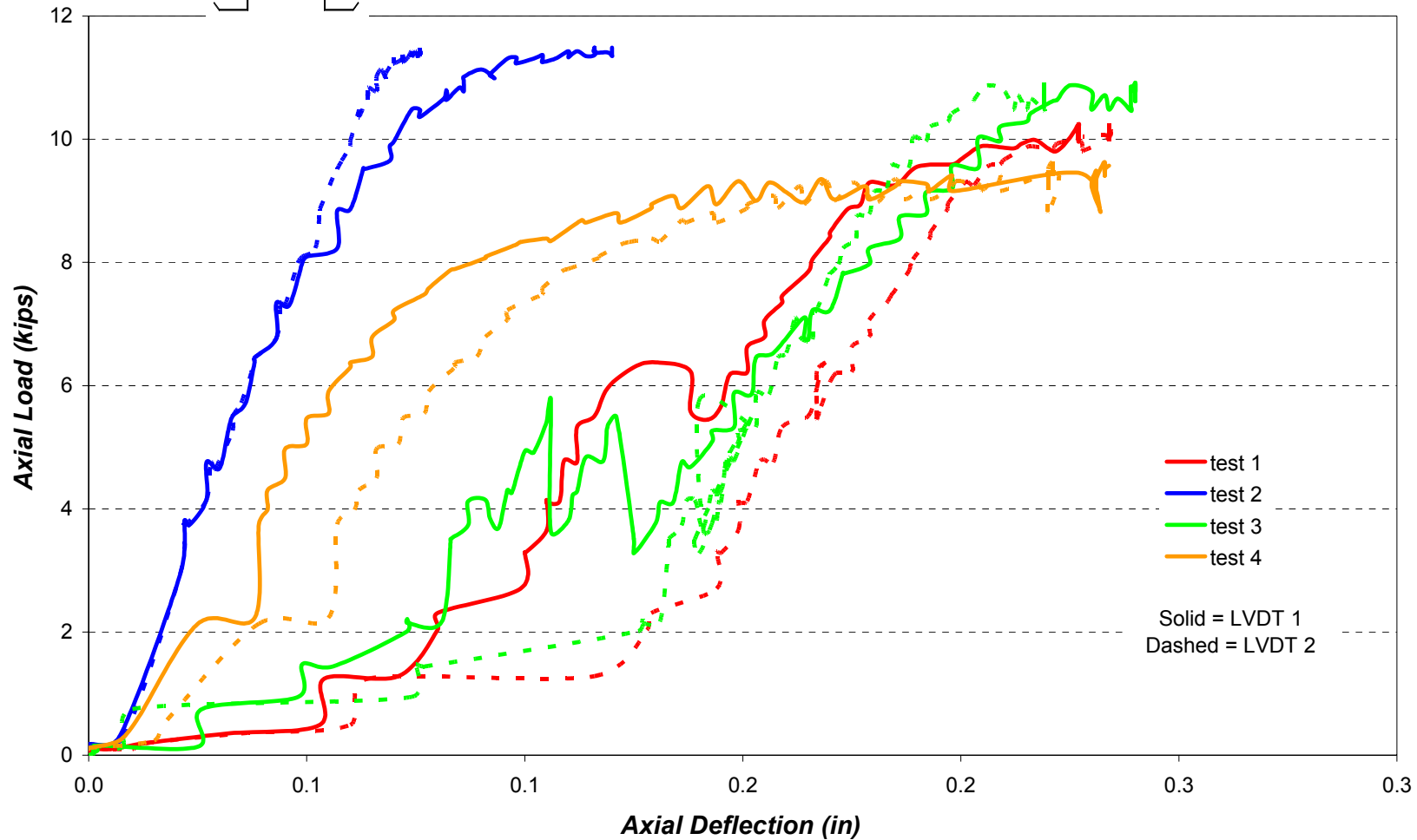


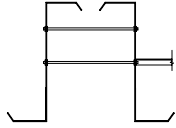
175





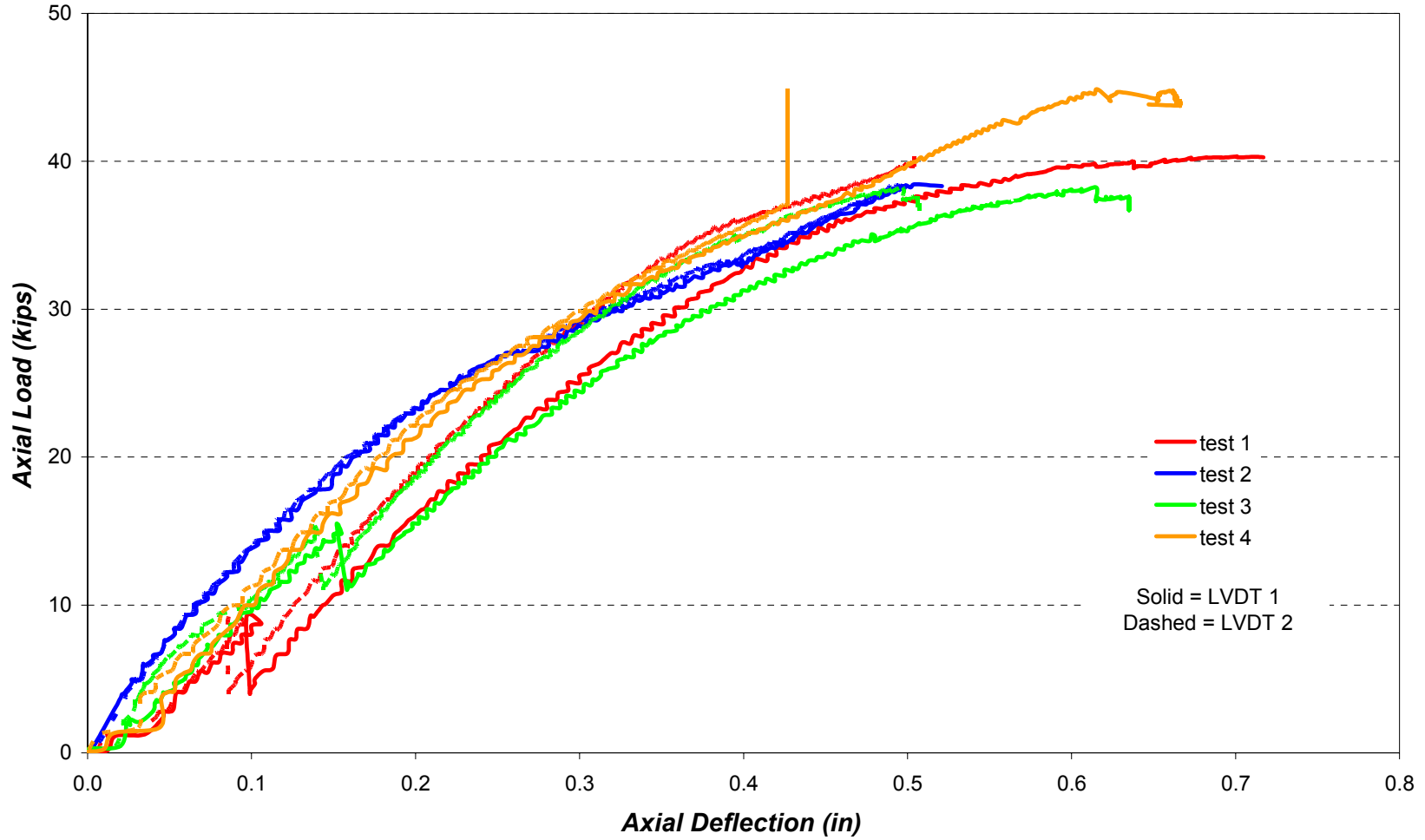
14" deep 0.080 thick
2 Purlin tests w/o Restraint or roof panel



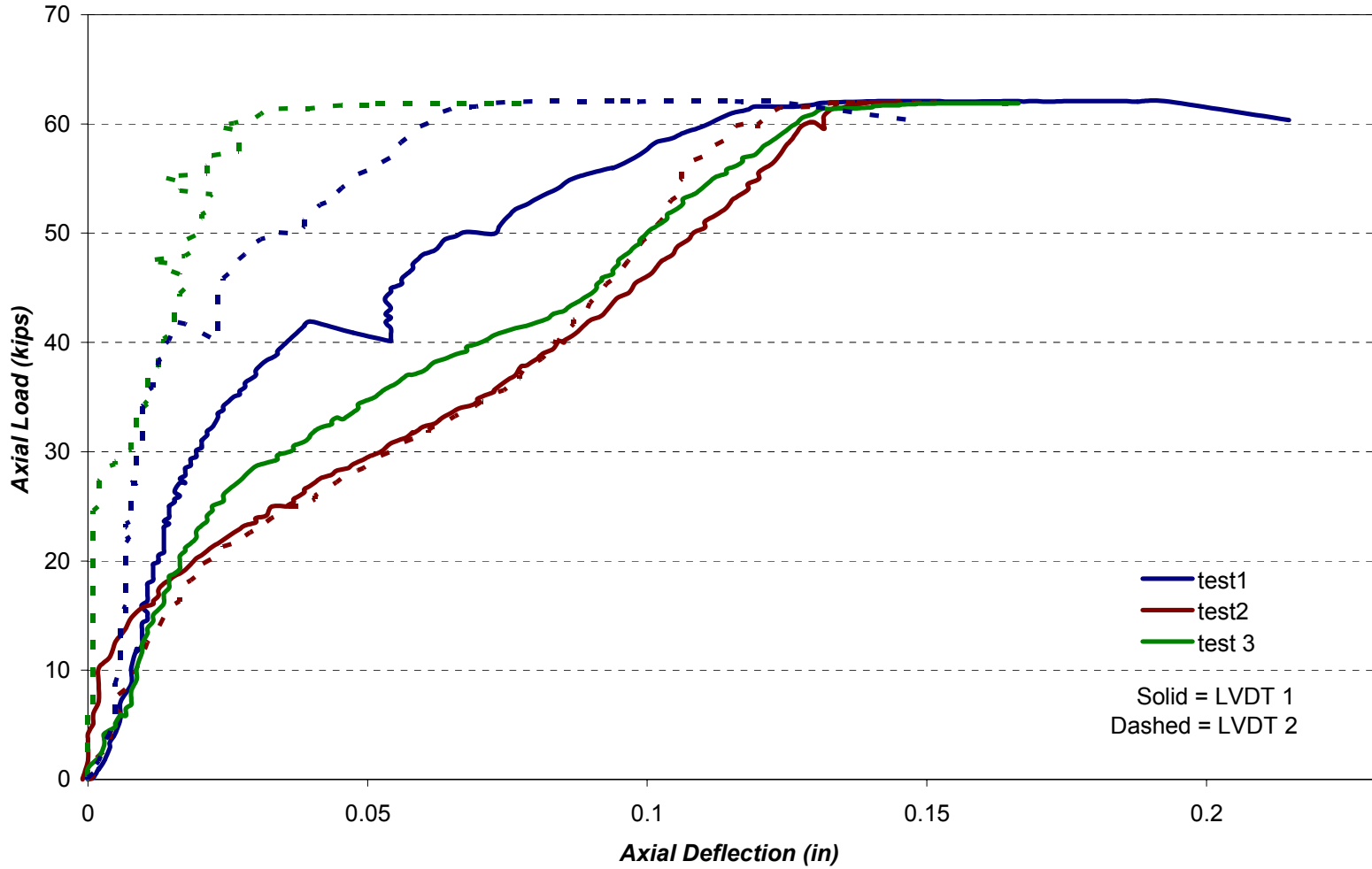


14" deep 0.080 thick
2 Purlin tests w/o roof Panel but w/ Restraint

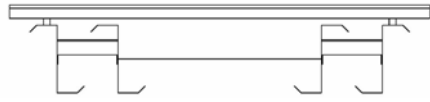
177



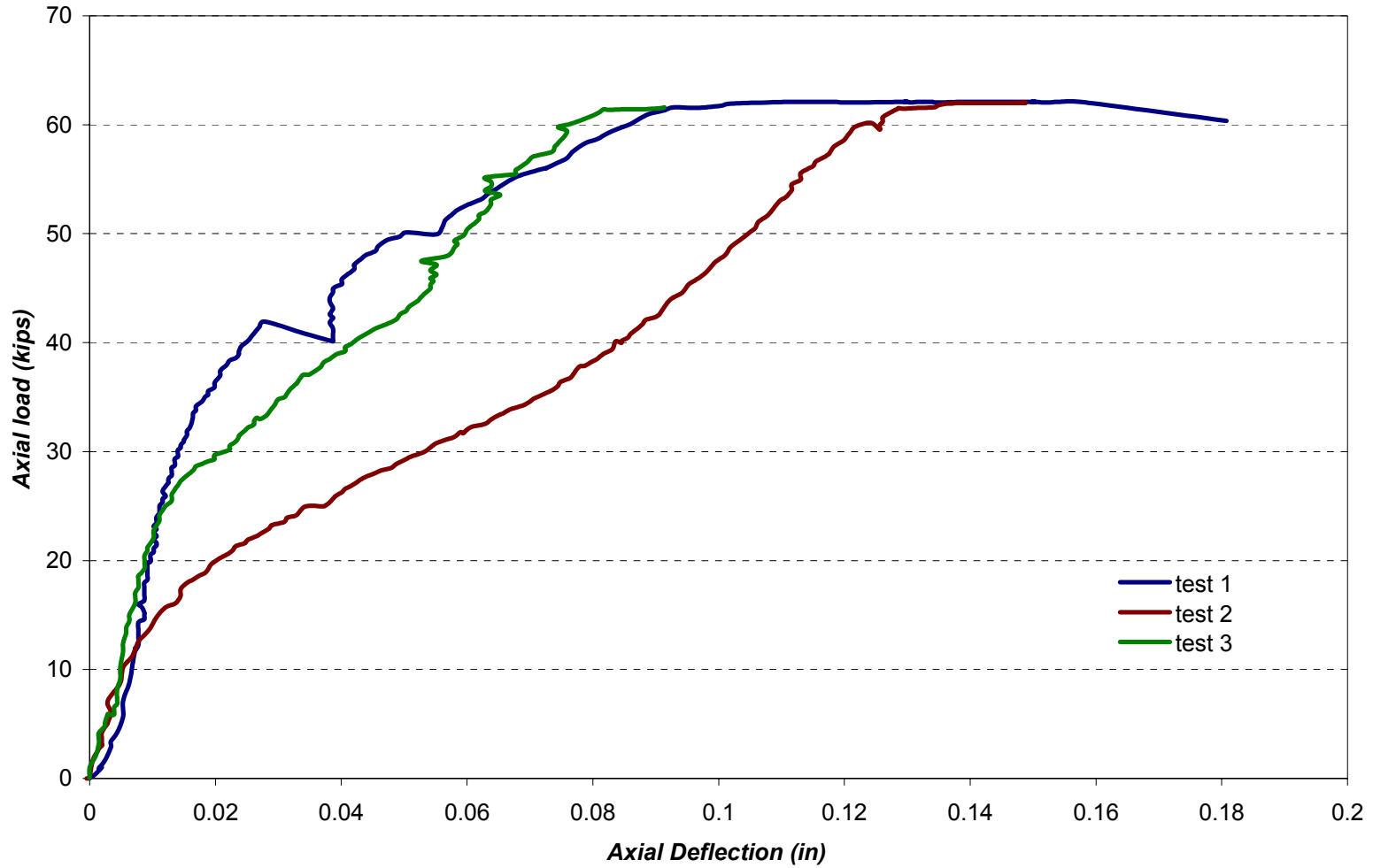
14" deep 0.134" thick
4 purlin tests with roof panel



14" deep 0.134" thick purlins
4 Purlin tests with roof panel
Average LVDT 1&2



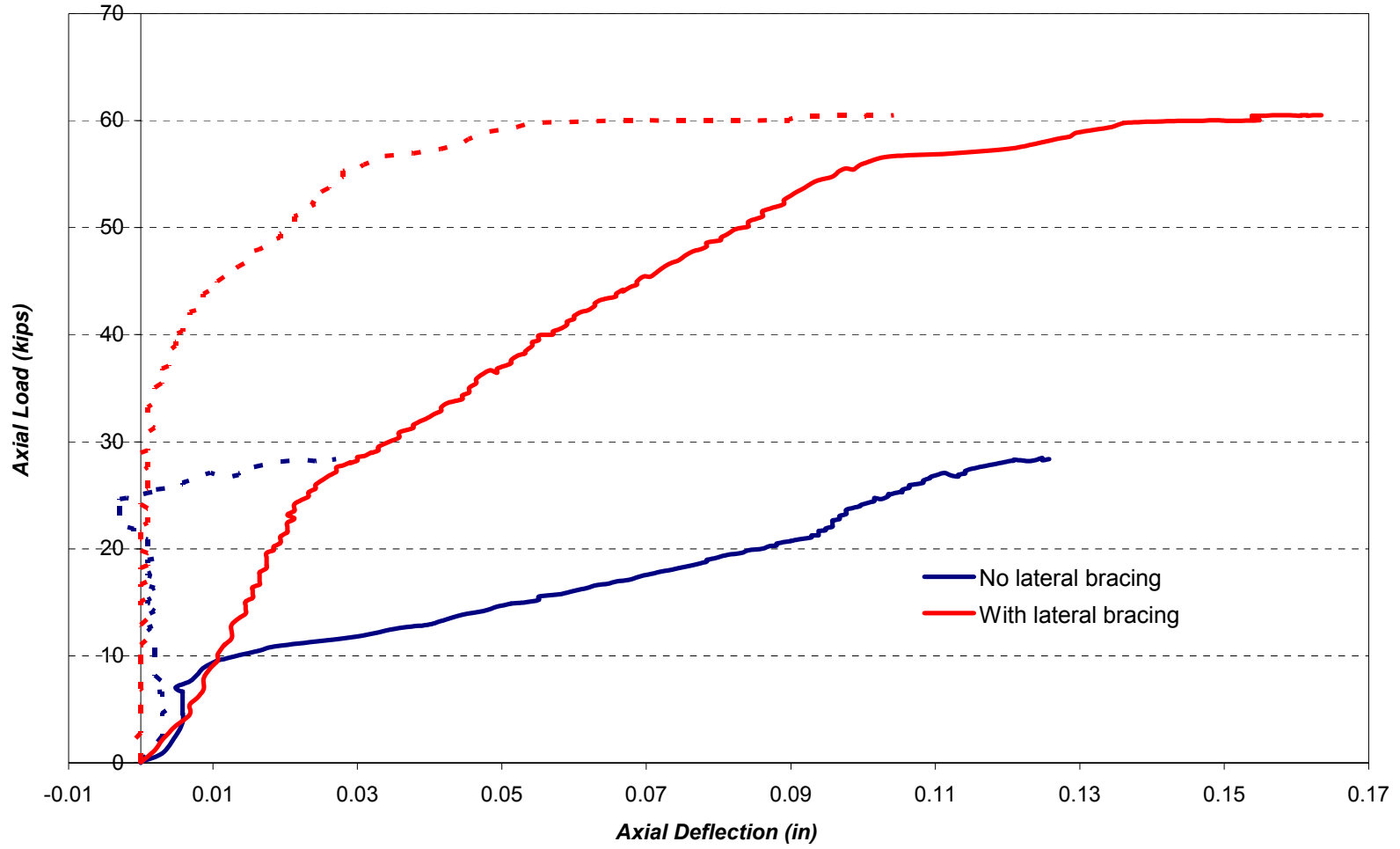
179

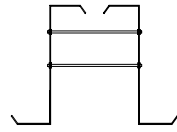


**14" Deep 0.134" thick
2 Purlin tests with roof panel**



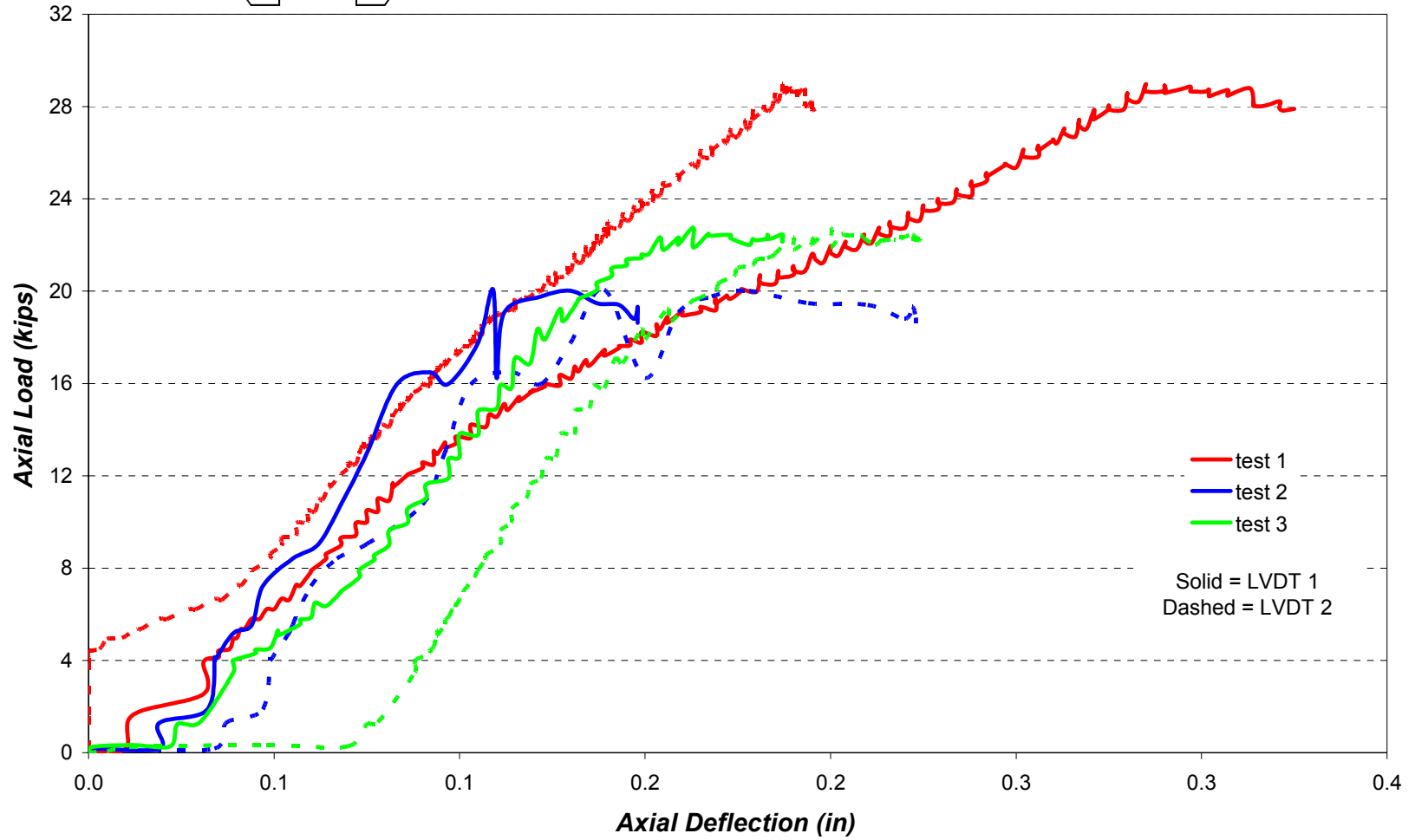
180

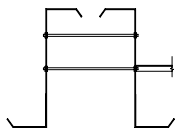




14" deep 0.134 thick
2 Purlin tests w/o Restraint or roof panel

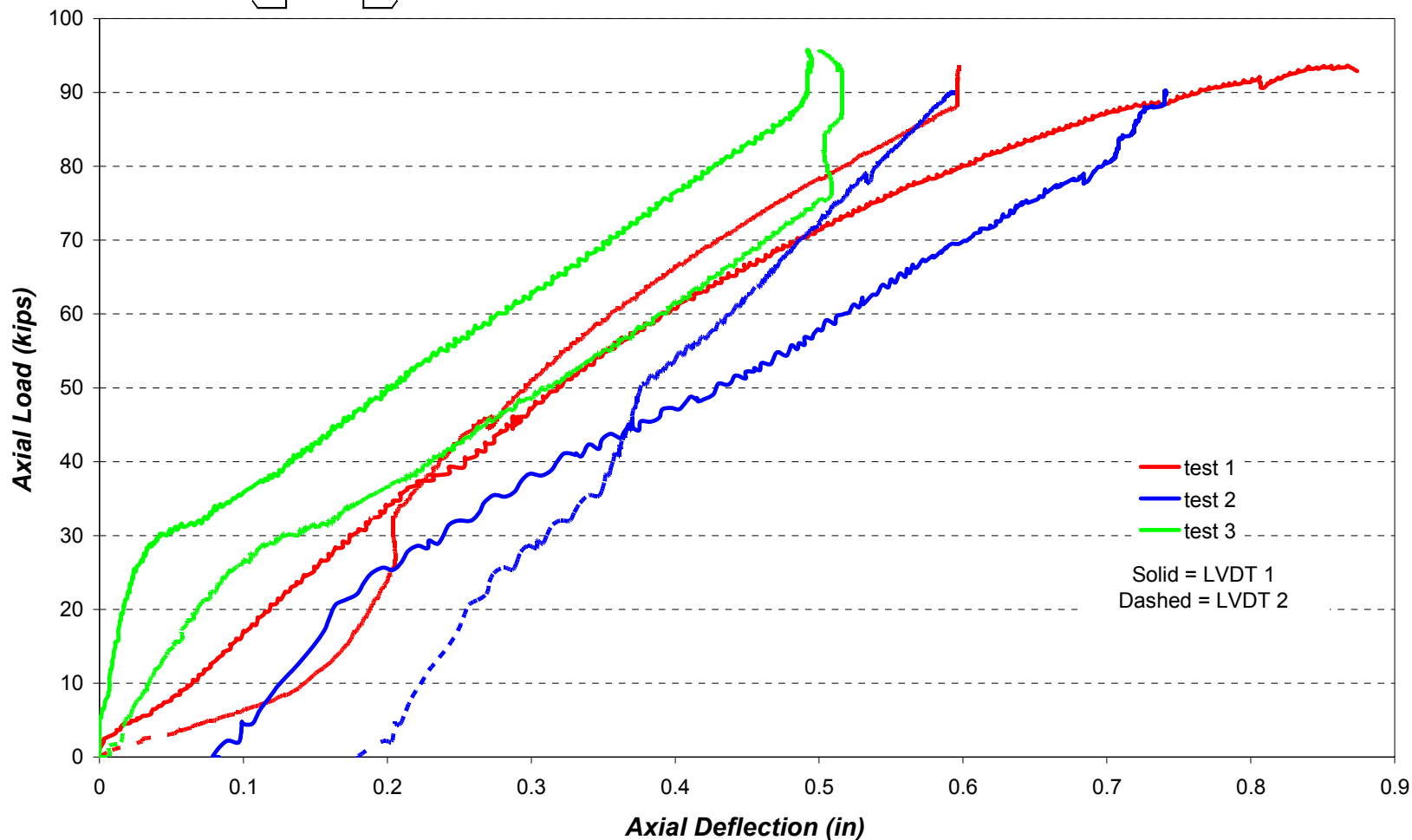
181



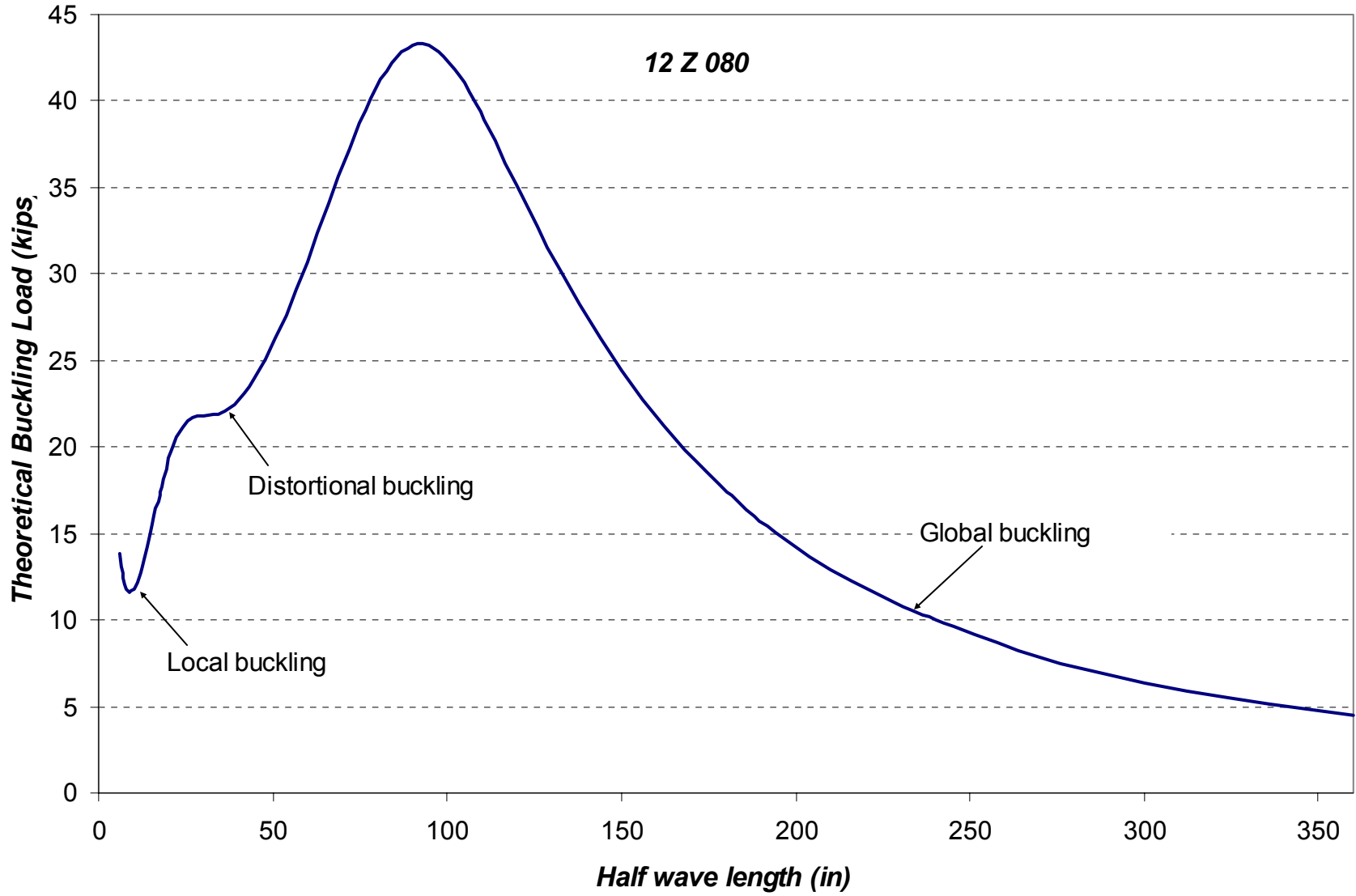


14" deep 0.134 thick
2 Purlin tests w/o roof panel but w/ Restraint

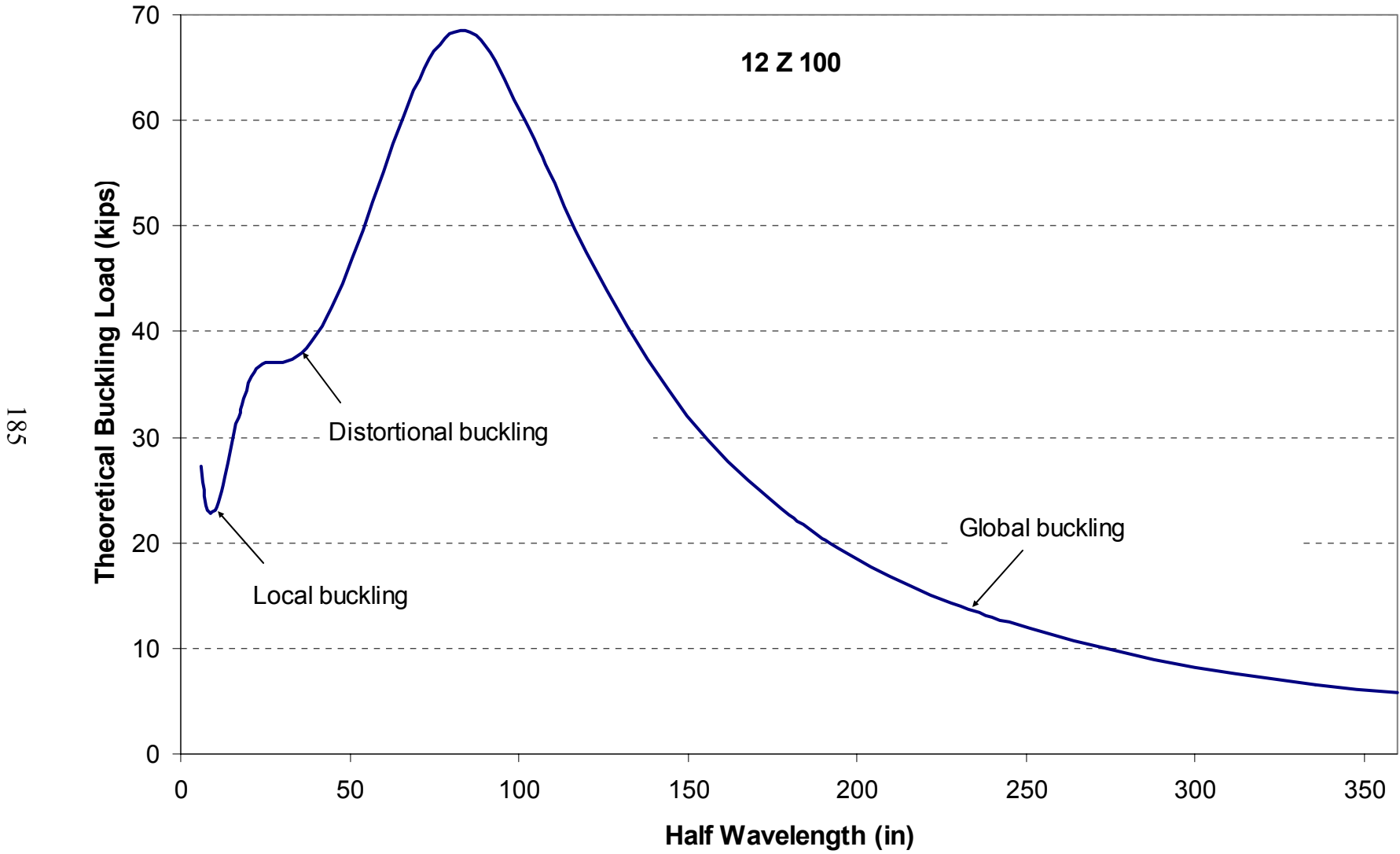
182

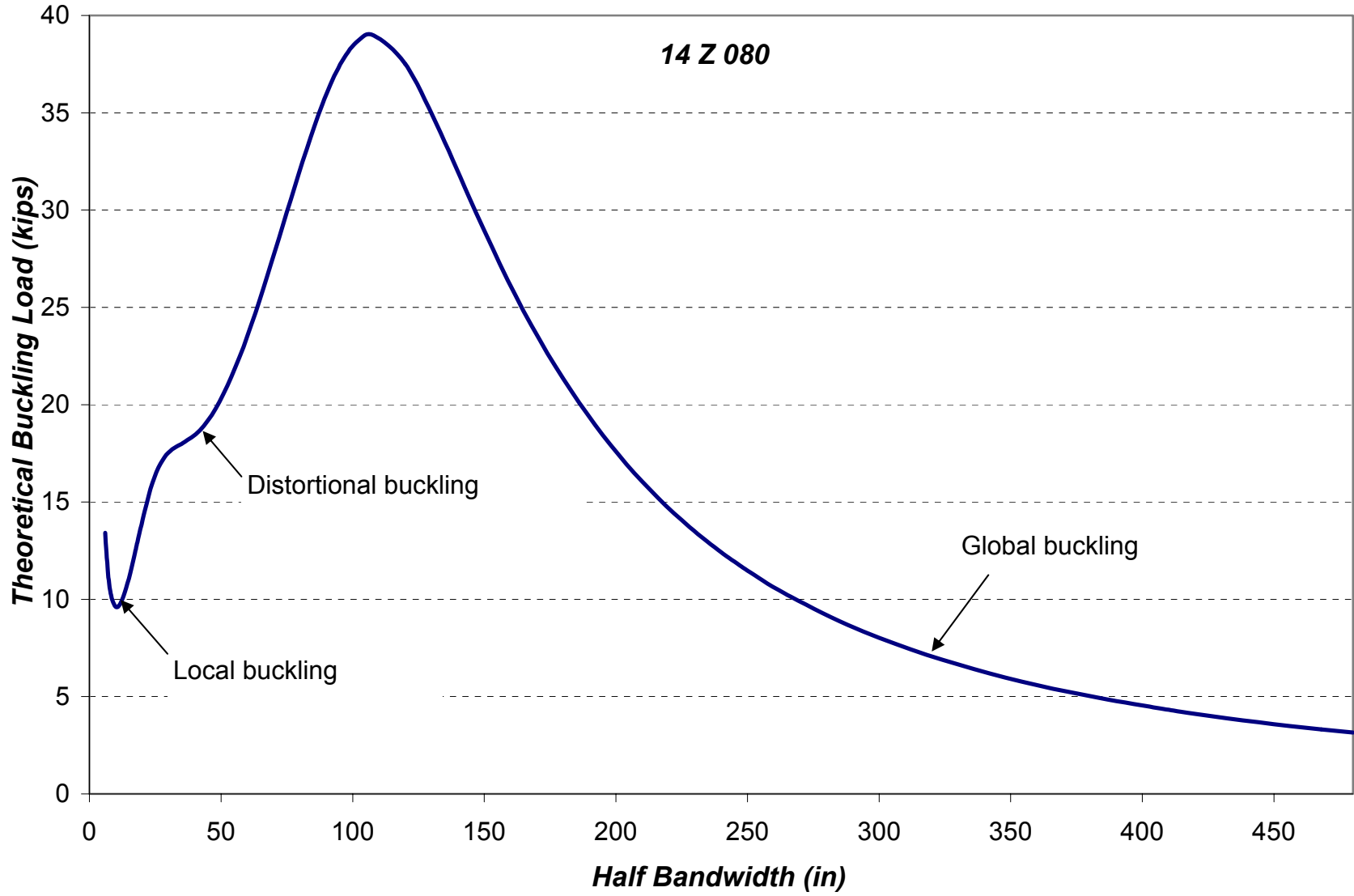


APPENDIX C - Purlin Direct Strength Method Plots

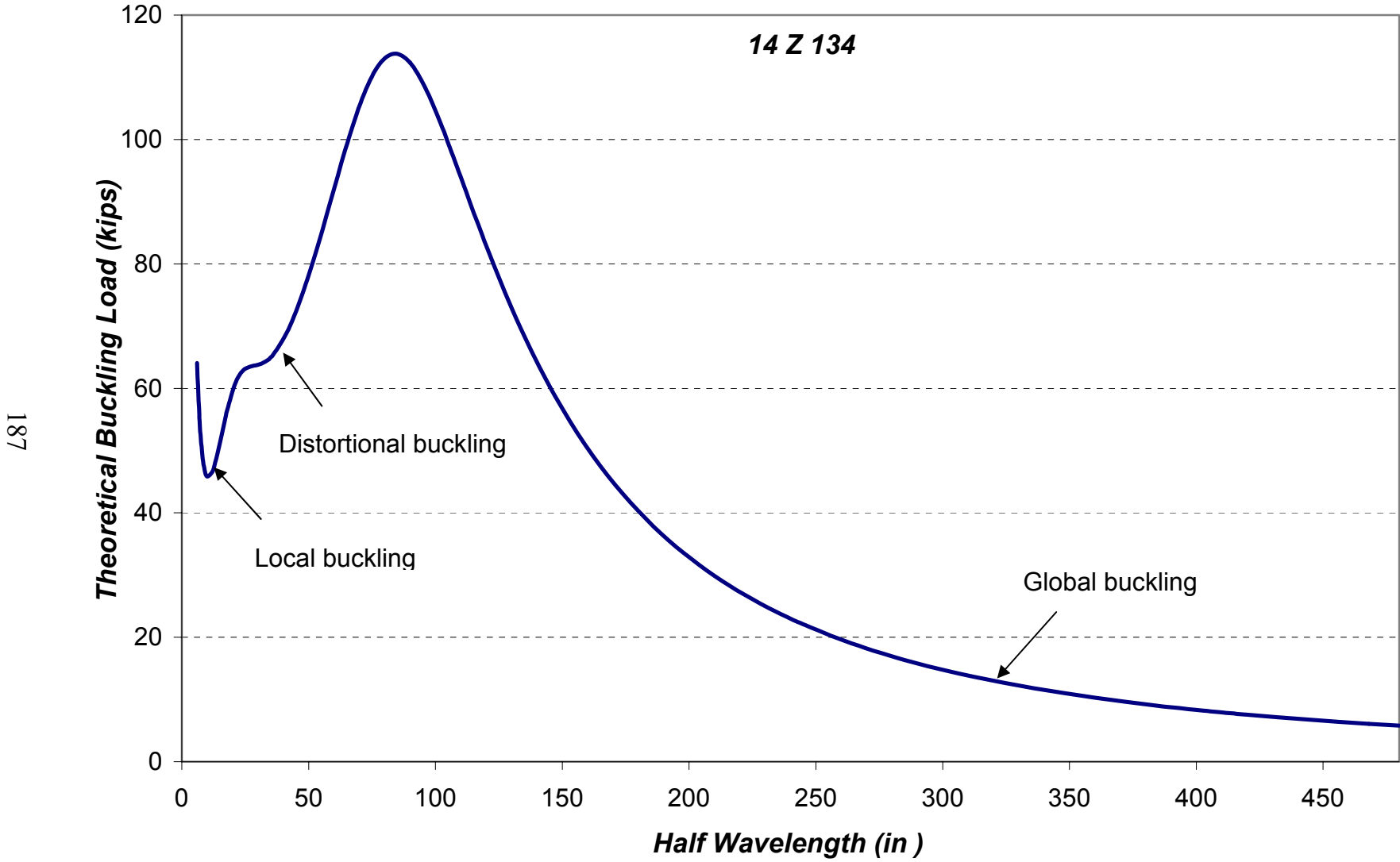


12 Z 100





14 Z 134



187

APPENDIX D - Purlin AISI Effective Method Capacity Calculation

CFS Version 4.11
 Section: Section 1.sct
 Zee 12x3.25x1.25x0.08

Axial Capacity - 2001 AISI Specification - US (LRFD)

Test Specimen 12Z080 (Laterally Unrestrained)

Design Parameters:

Lx	30.000 ft	Ly	30.000 ft	Lt	30.000 ft
Kx	0.6500	Ky	0.6500	Kt	0.6500
Cbx	1.0000	Cby	1.0000	ex	0.0000 in
Cmx	1.0000	Cmy	1.0000	ey	0.0000 in
Braced Flange: None		Moment Reduction, R: 0.0000			

Loads:	P	Mx	Vy	My	Vx
	(k)	(k-in)	(k)	(k-in)	(k)
Entered	0.000	0.000	0.000	0.000	0.000
Applied	0.000	0.000	0.000	0.000	0.000
Strength	6.720	53.831	6.074	47.571	14.103

Effective section properties at applied loads:

Ae	1.64096 in ²	Ixe	34.648 in ⁴	Iye	4.254 in ⁴
		Sxe (t)	5.7747 in ³	Sye (l)	1.0598 in ³
		Sxe (b)	5.7747 in ³	Sye (r)	1.0598 in ³

Interaction Equations

AISI Eq. C5.2.2-1 (P, Mx, My)	0.000 + 0.000 + 0.000 = 0.000 <= 1.0
AISI Eq. C5.2.2-2 (P, Mx, My)	0.000 + 0.000 + 0.000 = 0.000 <= 1.0
AISI Eq. C3.3.2-1 (Mx, Vy)	0.000 + 0.000 = 0.000 <= 1.0
AISI Eq. C3.3.2-1 (My, Vx)	0.000 + 0.000 = 0.000 <= 1.0

$$P_n = \frac{P}{\Phi} = \frac{6.720}{0.85} = 7.91(k)$$

CFS Version 4.11
 Section: Section 2.sct
 Zee 12x3.25x1.37x0.1

Axial Capacity - 2001 AISI Specification - US (LRFD)

Test Specimen 12Z100 (Laterally Unrestrained)

Design Parameters:

Lx	30.000 ft	Ly	30.000 ft	Lt	30.000 ft
Kx	0.6500	Ky	0.6500	Kt	0.6500
Cbx	1.0000	Cby	1.0000	ex	0.0000 in
Cmx	1.0000	Cmy	1.0000	ey	0.0000 in
Braced Flange: None		Moment Reduction, R: 0.0000			

Loads:	P	Mx	Vy	My	Vx
	(k)	(k-in)	(k)	(k-in)	(k)
Entered	0.000	0.000	0.000	0.000	0.000
Applied	0.000	0.000	0.000	0.000	0.000
Strength	9.506	72.387	11.904	64.923	17.445

Effective section properties at applied loads:

Ae	2.0684 in ²	Ixe	43.569 in ⁴	Iye	5.631 in ⁴
		Sxe (t)	7.2616 in ³	Sye (l)	1.3799 in ³
		Sxe (b)	7.2616 in ³	Sye (r)	1.3799 in ³

Interaction Equations

AISI Eq. C5.2.2-1 (P, Mx, My)	0.000 + 0.000 + 0.000 = 0.000 <= 1.0
AISI Eq. C5.2.2-2 (P, Mx, My)	0.000 + 0.000 + 0.000 = 0.000 <= 1.0
AISI Eq. C3.3.2-1 (Mx, Vy)	0.000 + 0.000 = 0.000 <= 1.0
AISI Eq. C3.3.2-1 (My, Vx)	0.000 + 0.000 = 0.000 <= 1.0

$$P_n = \frac{P}{\Phi} = \frac{9.506}{0.85} = 11.18(k)$$

CFS Version 4.11
 Section: Section 3.sct
 Zee 14x3.5x1.31x0.08

Axial Capacity - 2001 AISI Specification - US (LRFD)

Test Specimen 14Z080 (Laterally Unrestrained)

Design Parameters:

Lx	40.000 ft	Ly	40.000 ft	Lt	40.000 ft
Kx	0.6500	Ky	0.6500	Kt	0.6500
Cbx	1.0000	Cby	1.0000	ex	0.0000 in
Cmx	1.0000	Cmy	1.0000	ey	0.0000 in
Braced Flange: None		Moment Reduction, R: 0.0000			

Loads:	P	Mx	Vy	My	Vx
	(k)	(k-in)	(k)	(k-in)	(k)
Entered	0.000	0.000	0.000	0.000	0.000
Applied	0.000	0.000	0.000	0.000	0.000
Strength	4.915	44.014	5.167	52.472	15.357

Effective section properties at applied loads:

Ae	1.85056 in ²	Ixe	52.314 in ⁴	Iye	5.229 in ⁴
		Sxe (t)	7.4735 in ³	Sye (l)	1.2154 in ³
		Sxe (b)	7.4735 in ³	Sye (r)	1.2154 in ³

Interaction Equations

AISI Eq. C5.2.2-1 (P, Mx, My)	0.000 + 0.000 + 0.000 = 0.000 <= 1.0
AISI Eq. C5.2.2-2 (P, Mx, My)	0.000 + 0.000 + 0.000 = 0.000 <= 1.0
AISI Eq. C3.3.2-1 (Mx, Vy)	0.000 + 0.000 = 0.000 <= 1.0
AISI Eq. C3.3.2-1 (My, Vx)	0.000 + 0.000 = 0.000 <= 1.0

$$P_n = \frac{P}{\Phi} = \frac{4.915}{0.85} = 5.78(k)$$

CFS Version 4.11
 Section: Section 4.sct
 Zee 14x3.5x1.56x0.134

Axial Capacity - 2001 AISI Specification - US (LRFD)

Test Specimen 14Z134 (Laterally Unrestrained)

Design Parameters:

Lx	40.000 ft	Ly	40.000 ft	Lt	40.000 ft
Kx	0.6500	Ky	0.6500	Kt	0.6500
Cbx	1.0000	Cby	1.0000	ex	0.0000 in
Cmx	1.0000	Cmy	1.0000	ey	0.0000 in
Braced Flange: None		Moment Reduction, R: 0.0000			

Loads:	P	Mx	Vy	My	Vx
	(k)	(k-in)	(k)	(k-in)	(k)
Entered	0.000	0.00	0.000	0.00	0.000
Applied	0.000	0.00	0.000	0.00	0.000
Strength	10.202	86.27	24.481	105.15	25.057

Effective section properties at applied loads:

Ae	3.1419 in ²	Ixe	88.325 in ⁴	Iye	9.709 in ⁴
		Sxe (t)	12.618 in ³	Sye (l)	2.189 in ³
		Sxe (b)	12.618 in ³	Sye (r)	2.189 in ³

Interaction Equations

AISI Eq. C5.2.2-1 (P, Mx, My)	0.000 + 0.000 + 0.000 = 0.000 <= 1.0
AISI Eq. C5.2.2-2 (P, Mx, My)	0.000 + 0.000 + 0.000 = 0.000 <= 1.0
AISI Eq. C3.3.2-1 (Mx, Vy)	0.000 + 0.000 = 0.000 <= 1.0
AISI Eq. C3.3.2-1 (My, Vx)	0.000 + 0.000 = 0.000 <= 1.0

$$P_n = \frac{P}{\Phi} = \frac{10.202}{0.85} = 12.00(k)$$

CFS Version 4.11
 Section: Section 5.sct
 Zee 12x3.25x1.28x0.08

Axial Capacity - 2001 AISI Specification - US (LRFD)

Test Specimen 12Z080 (Laterally Restrained)

Design Parameters:

Lx	6.0000 ft	Ly	6.0000 ft	Lt	6.0000 ft
Kx	1.0000	Ky	1.0000	Kt	1.0000
Cbx	1.0000	Cby	1.0000	ex	0.0000 in
Cmx	1.0000	Cmy	1.0000	ey	0.0000 in
Braced Flange: None		Moment Reduction, R: 0.0000			

Loads:	P	Mx	Vy	My	Vx
	(k)	(k-in)	(k)	(k-in)	(k)
Entered	0.000	0.00	0.000	0.00	0.000
Applied	0.000	0.00	0.000	0.00	0.000
Strength	32.712	241.40	6.074	47.80	14.103

Effective section properties at applied loads:

Ae	1.64576 in ²	Ixe	34.768 in ⁴	Iye	4.330 in ⁴
		Sxe (t)	5.7947 in ³	Sye (l)	1.0737 in ³
		Sxe (b)	5.7947 in ³	Sye (r)	1.0737 in ³

Interaction Equations

AISI Eq. C5.2.2-1 (P, Mx, My)	0.000 + 0.000 + 0.000 = 0.000 <= 1.0
AISI Eq. C5.2.2-2 (P, Mx, My)	0.000 + 0.000 + 0.000 = 0.000 <= 1.0
AISI Eq. C3.3.2-1 (Mx, Vy)	0.000 + 0.000 = 0.000 <= 1.0
AISI Eq. C3.3.2-1 (My, Vx)	0.000 + 0.000 = 0.000 <= 1.0

$$P_n = \frac{P}{\Phi} = \frac{32.712}{0.85} = 38.48(k)$$

CFS Version 4.11
 Section: Section 6.sct
 Zee 12x3.25x1.37x0.1

Axial Capacity - 2001 AISI Specification - US (LRFD)

Test Specimen 12Z100 (Laterally Restrained)

Design Parameters:

Lx	6.0000 ft	Ly	6.0000 ft	Lt	6.0000 ft
Kx	1.0000	Ky	1.0000	Kt	1.0000
Cbx	1.0000	Cby	1.0000	ex	0.0000 in
Cmx	1.0000	Cmy	1.0000	ey	0.0000 in
Braced Flange: None		Moment Reduction, R: 0.0000			

Loads:	P	Mx	Vy	My	Vx
	(k)	(k-in)	(k)	(k-in)	(k)
Entered	0.000	0.00	0.000	0.00	0.000
Applied	0.000	0.00	0.000	0.00	0.000
Strength	46.740	334.50	11.904	64.92	17.445

Effective section properties at applied loads:

Ae	2.0684 in ²	Ixe	43.569 in ⁴	Iye	5.631 in ⁴
		Sxe (t)	7.2616 in ³	Sye (l)	1.3799 in ³
		Sxe (b)	7.2616 in ³	Sye (r)	1.3799 in ³

Interaction Equations

AISI Eq. C5.2.2-1 (P, Mx, My)	0.000 + 0.000 + 0.000 = 0.000 <= 1.0
AISI Eq. C5.2.2-2 (P, Mx, My)	0.000 + 0.000 + 0.000 = 0.000 <= 1.0
AISI Eq. C3.3.2-1 (Mx, Vy)	0.000 + 0.000 = 0.000 <= 1.0
AISI Eq. C3.3.2-1 (My, Vx)	0.000 + 0.000 = 0.000 <= 1.0

$$P_n = \frac{P}{\Phi} = \frac{46.740}{0.85} = 54.99(k)$$

CFS Version 4.11
 Section: Section 7.sct
 Zee 14x3.5x1.31x0.08

Axial Capacity - 2001 AISI Specification - US (LRFD)

Test Specimen 14Z080 (Laterally Restrained)

Design Parameters:

Lx	9.0000 ft	Ly	9.0000 ft	Lt	9.0000 ft
Kx	1.0000	Ky	1.0000	Kt	1.0000
Cbx	1.0000	Cby	1.0000	ex	0.0000 in
Cmx	1.0000	Cmy	1.0000	ey	0.0000 in
Braced Flange: None		Moment Reduction, R: 0.0000			

Loads:	P	Mx	Vy	My	Vx
	(k)	(k-in)	(k)	(k-in)	(k)
Entered	0.000	0.00	0.000	0.00	0.000
Applied	0.000	0.00	0.000	0.00	0.000
Strength	26.553	254.38	5.167	53.45	15.357

Effective section properties at applied loads:

Ae	1.85056 in ²	Ixe	52.314 in ⁴	Iye	5.229 in ⁴
		Sxe (t)	7.4735 in ³	Sye (l)	1.2154 in ³
		Sxe (b)	7.4735 in ³	Sye (r)	1.2154 in ³

Interaction Equations

AISI Eq. C5.2.2-1 (P, Mx, My)	0.000 + 0.000 + 0.000 = 0.000 <= 1.0
AISI Eq. C5.2.2-2 (P, Mx, My)	0.000 + 0.000 + 0.000 = 0.000 <= 1.0
AISI Eq. C3.3.2-1 (Mx, Vy)	0.000 + 0.000 = 0.000 <= 1.0
AISI Eq. C3.3.2-1 (My, Vx)	0.000 + 0.000 = 0.000 <= 1.0

$$P_n = \frac{P}{\Phi} = \frac{26.553}{0.85} = 31.24(k)$$

CFS Version 4.11
 Section: Section 8.sct
 Zee 14x3.5x1.56x0.134

Axial Capacity - 2001 AISI Specification - US (LRFD)

Test Specimen 14Z134 (Laterally Restrained)

Design Parameters:

Lx	9.0000 ft	Ly	9.0000 ft	Lt	9.0000 ft
Kx	1.0000	Ky	1.0000	Kt	1.0000
Cbx	1.0000	Cby	1.0000	ex	0.0000 in
Cmx	1.0000	Cmy	1.0000	ey	0.0000 in
Braced Flange: None		Moment Reduction, R: 0.0000			

Loads:	P	Mx	Vy	My	Vx
	(k)	(k-in)	(k)	(k-in)	(k)
Entered	0.000	0.00	0.000	0.00	0.000
Applied	0.000	0.00	0.000	0.00	0.000
Strength	57.085	512.82	24.481	106.80	25.057

Effective section properties at applied loads:

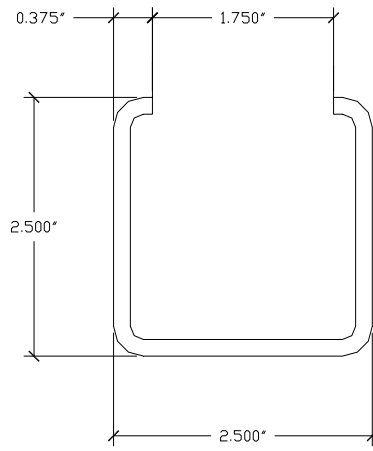
Ae	3.1419 in ²	Ixe	88.325 in ⁴	Iye	9.709 in ⁴
		Sxe (t)	12.618 in ³	Sye (l)	2.189 in ³
		Sxe (b)	12.618 in ³	Sye (r)	2.189 in ³

Interaction Equations

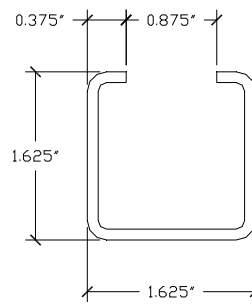
AISI Eq. C5.2.2-1 (P, Mx, My)	0.000 + 0.000 + 0.000 = 0.000 <= 1.0
AISI Eq. C5.2.2-2 (P, Mx, My)	0.000 + 0.000 + 0.000 = 0.000 <= 1.0
AISI Eq. C3.3.2-1 (Mx, Vy)	0.000 + 0.000 = 0.000 <= 1.0
AISI Eq. C3.3.2-1 (My, Vx)	0.000 + 0.000 = 0.000 <= 1.0

$$P_n = \frac{P}{\Phi} = \frac{57.085}{0.85} = 67.16(k)$$

APPENDIX E - Section Properties of Built-up Test Specimens

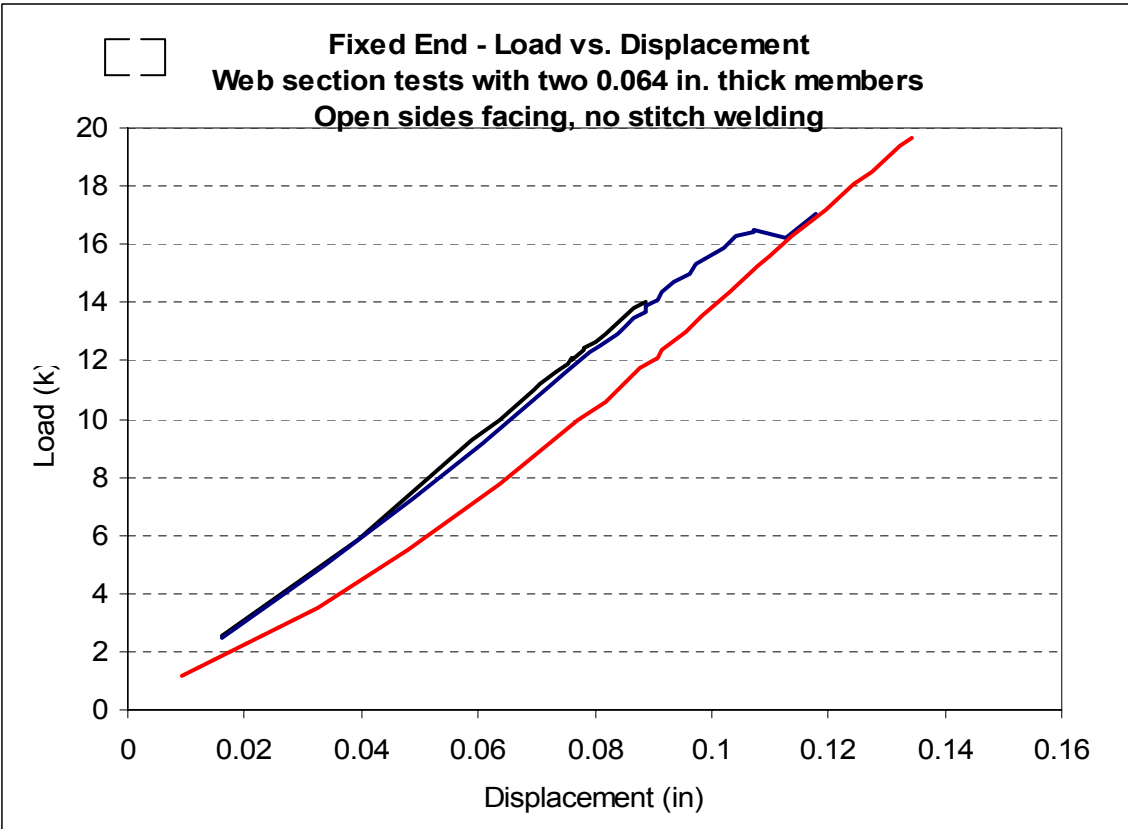
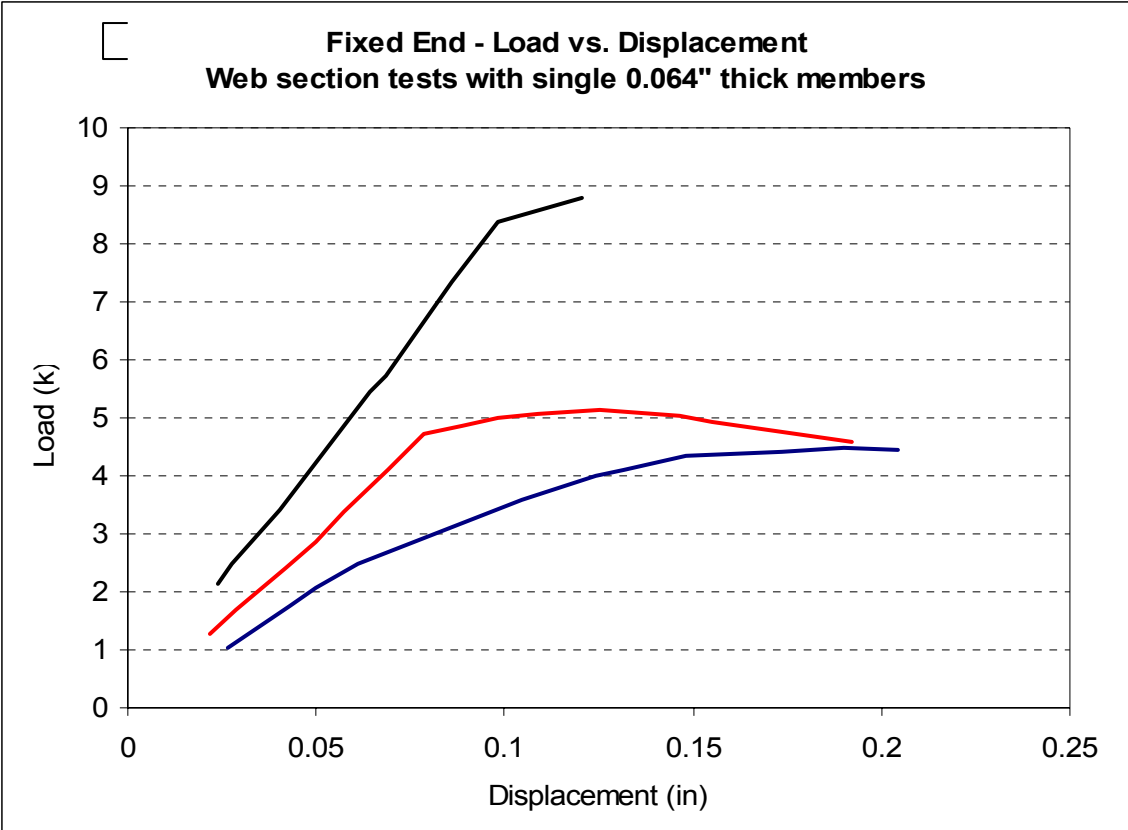


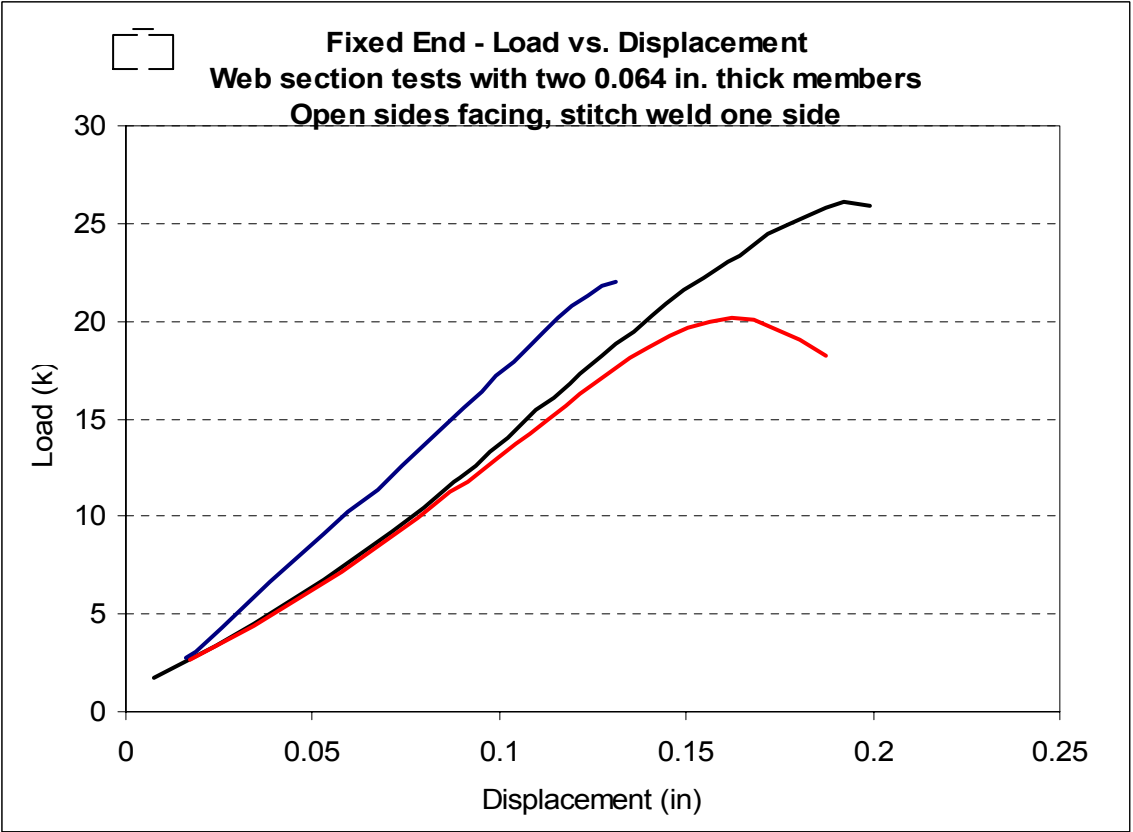
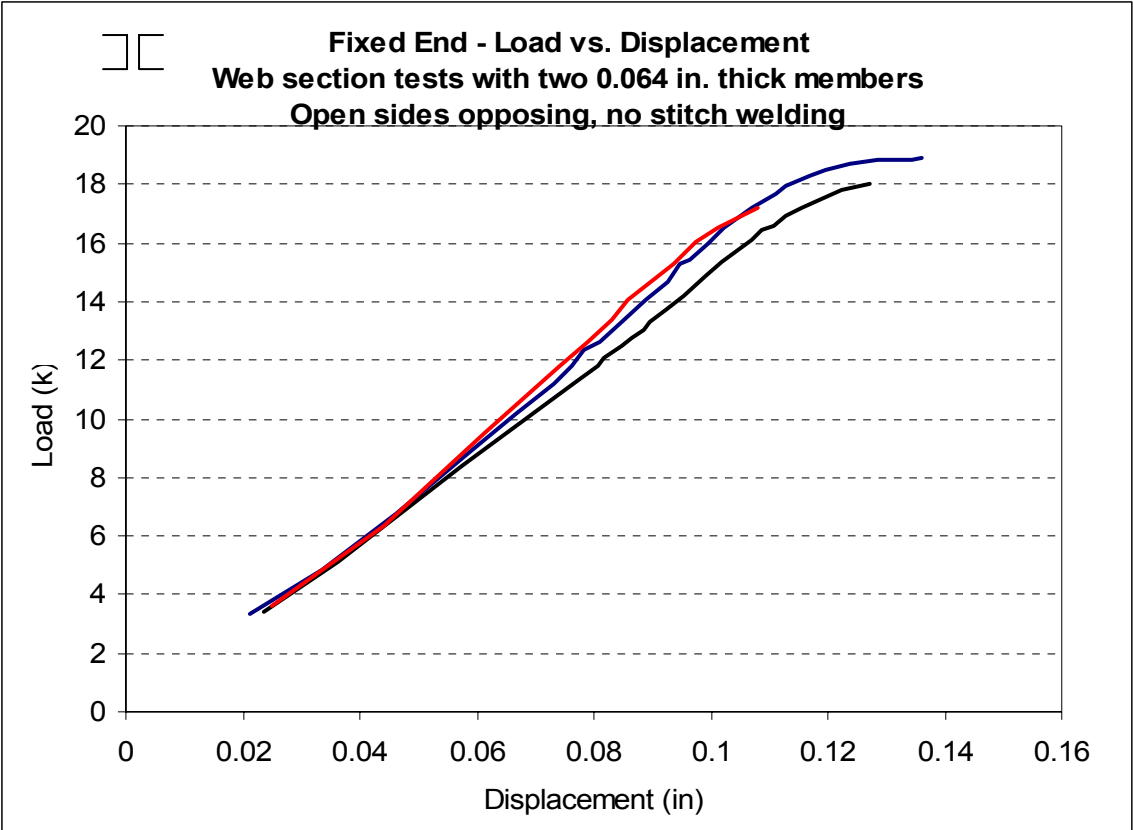
2 1/2" WEB

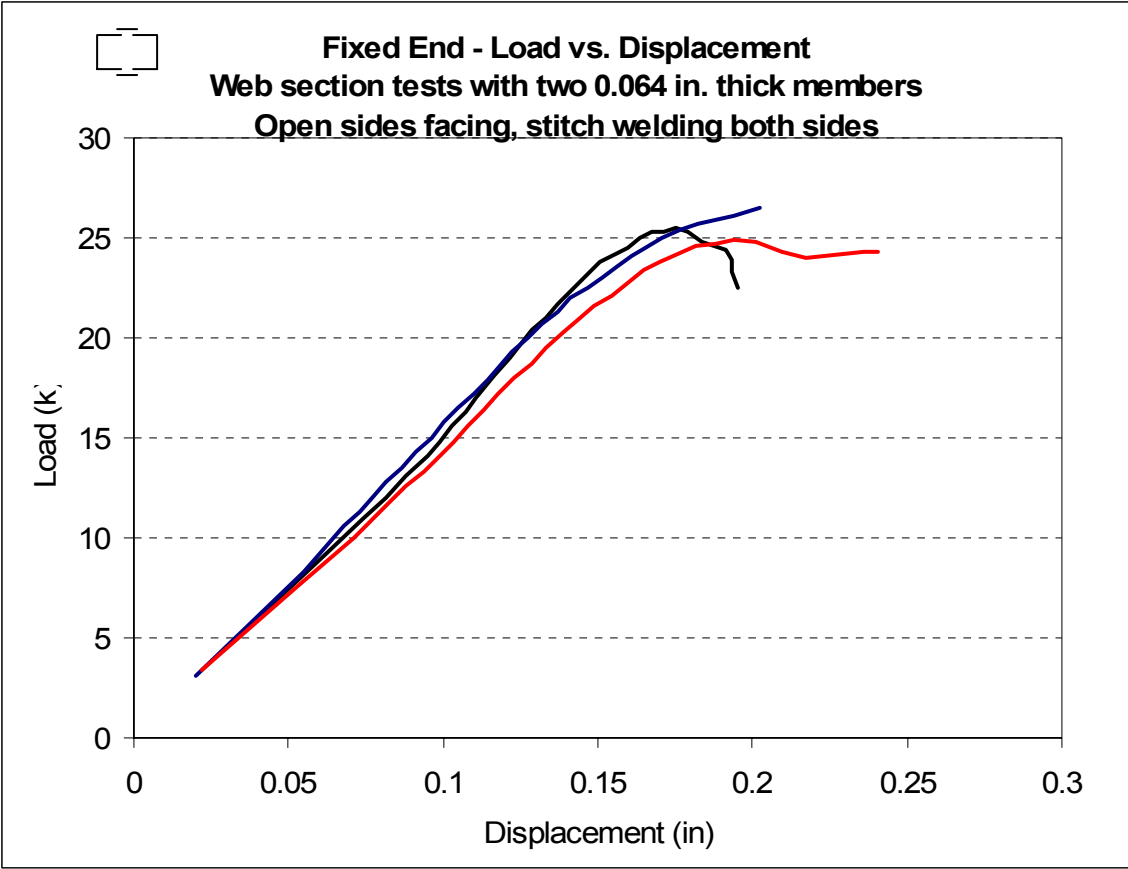


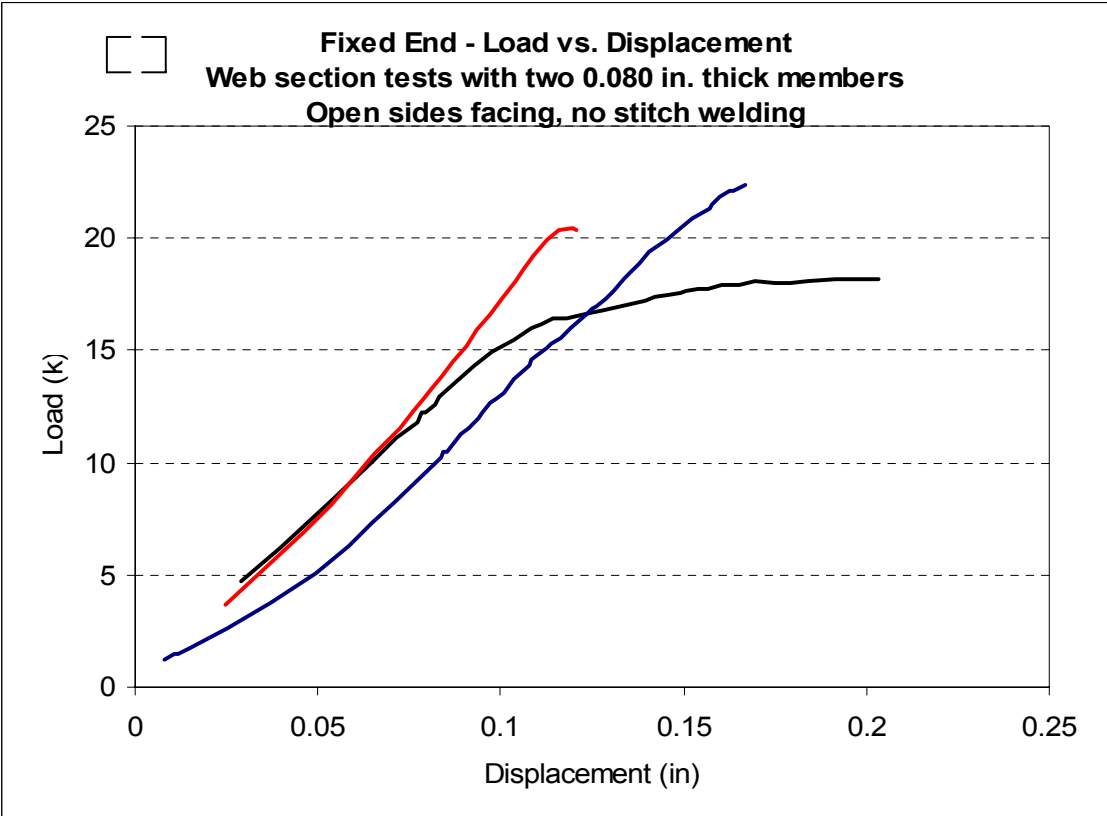
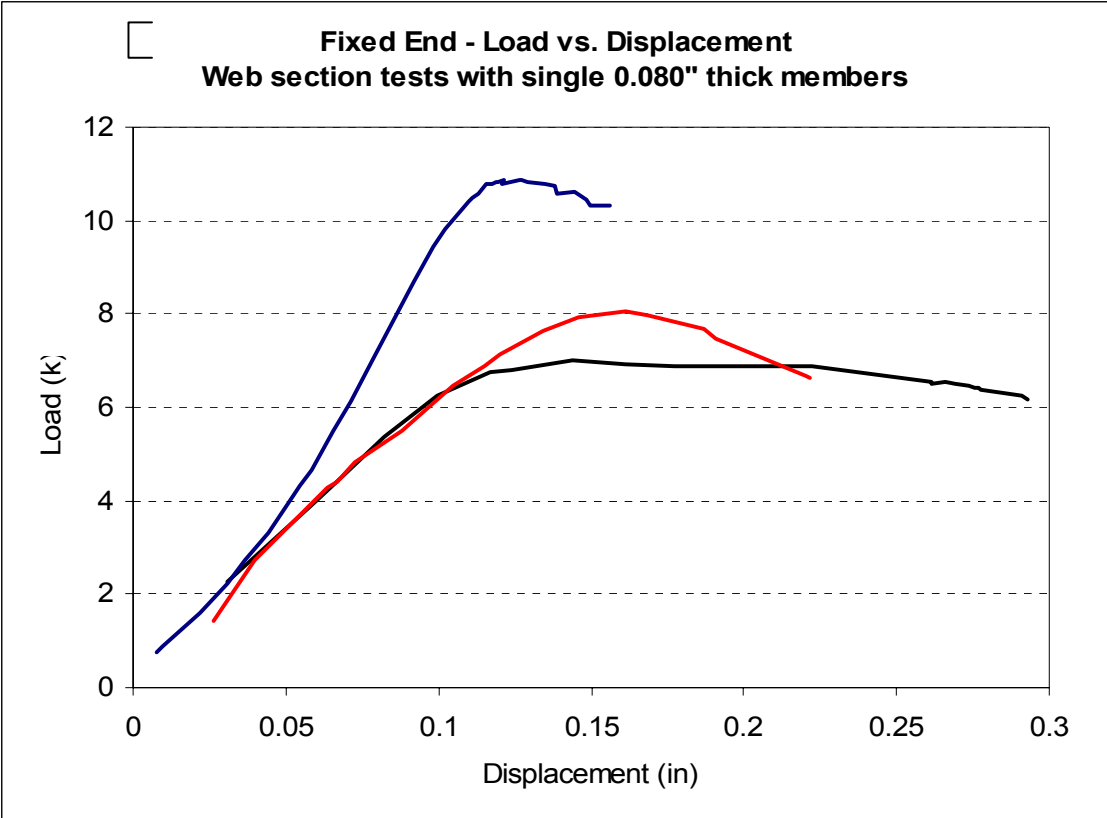
1 5/8" WEB

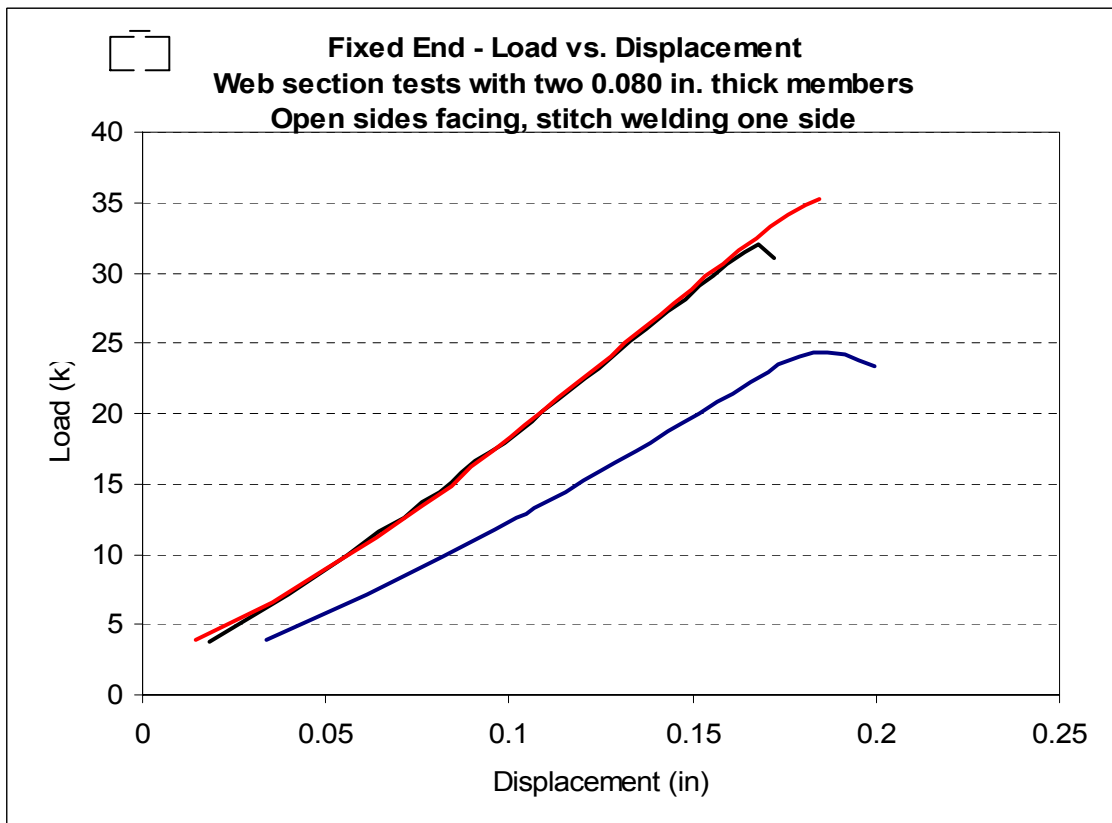
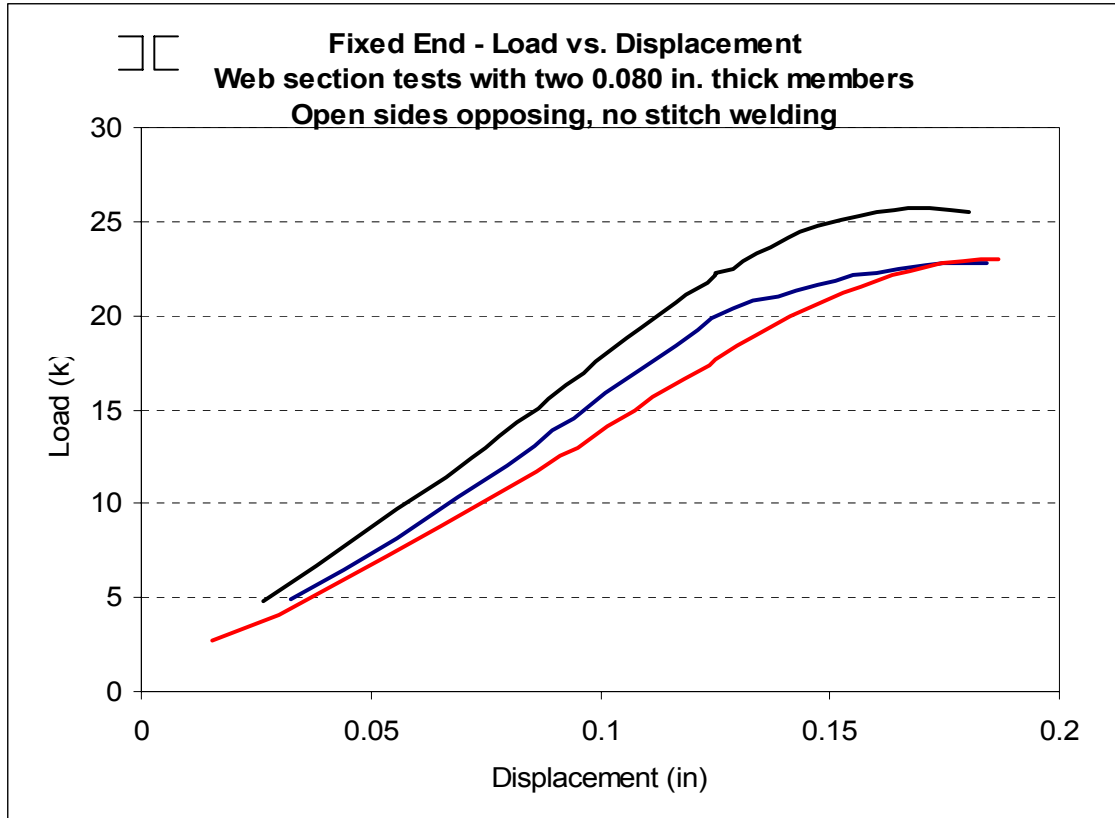
**APPENDIX F - 55" – 1 5/8" Built-up Member, Fixed End,
Load vs. Deflection Plots**

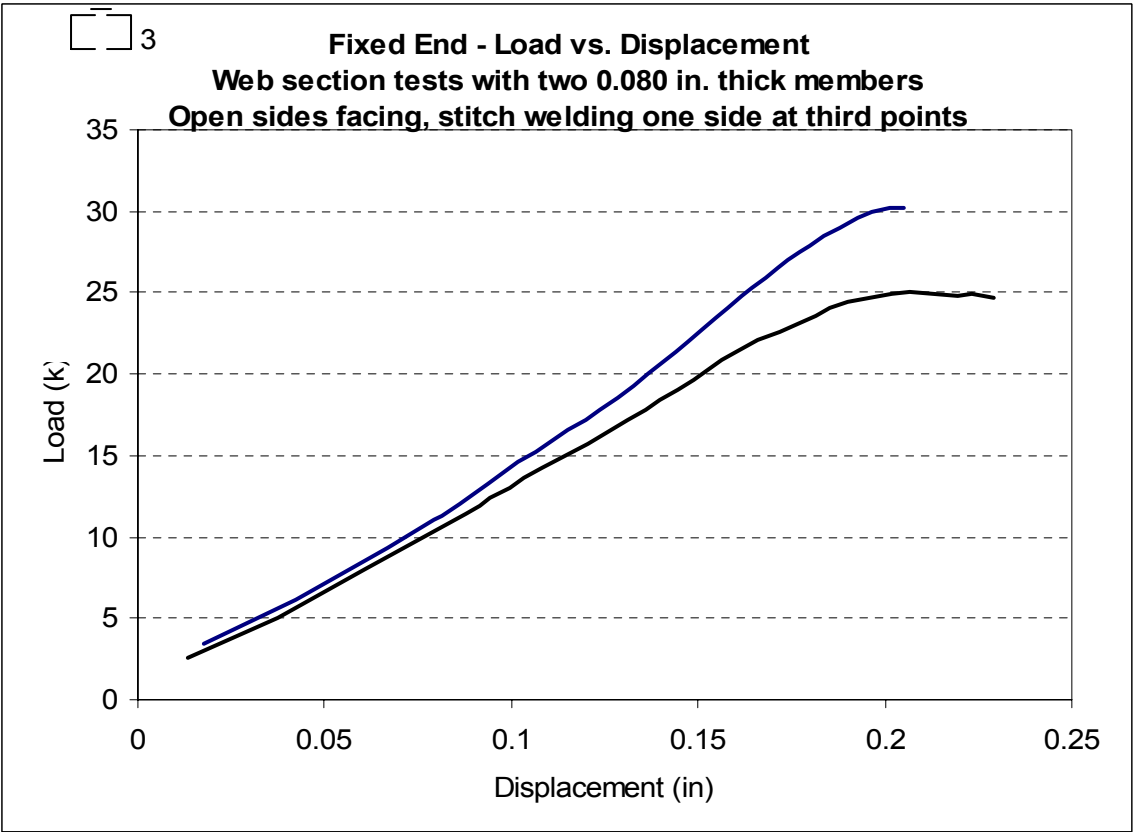
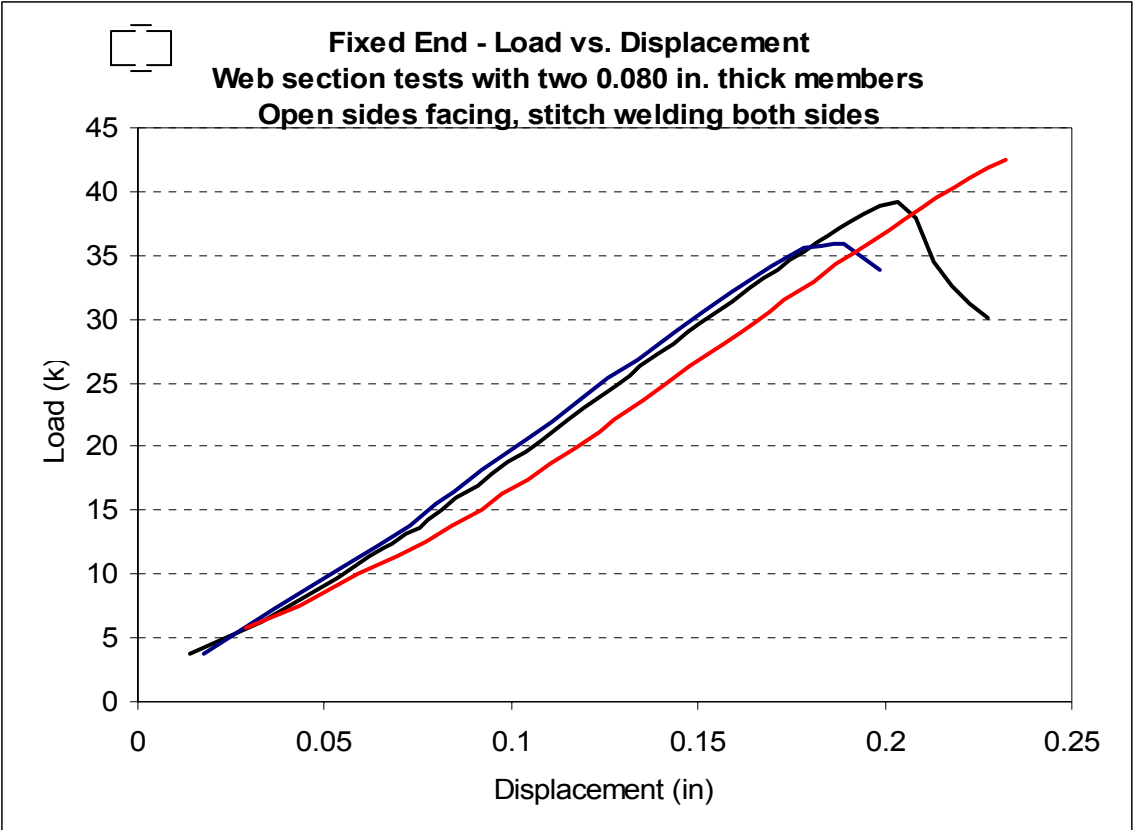


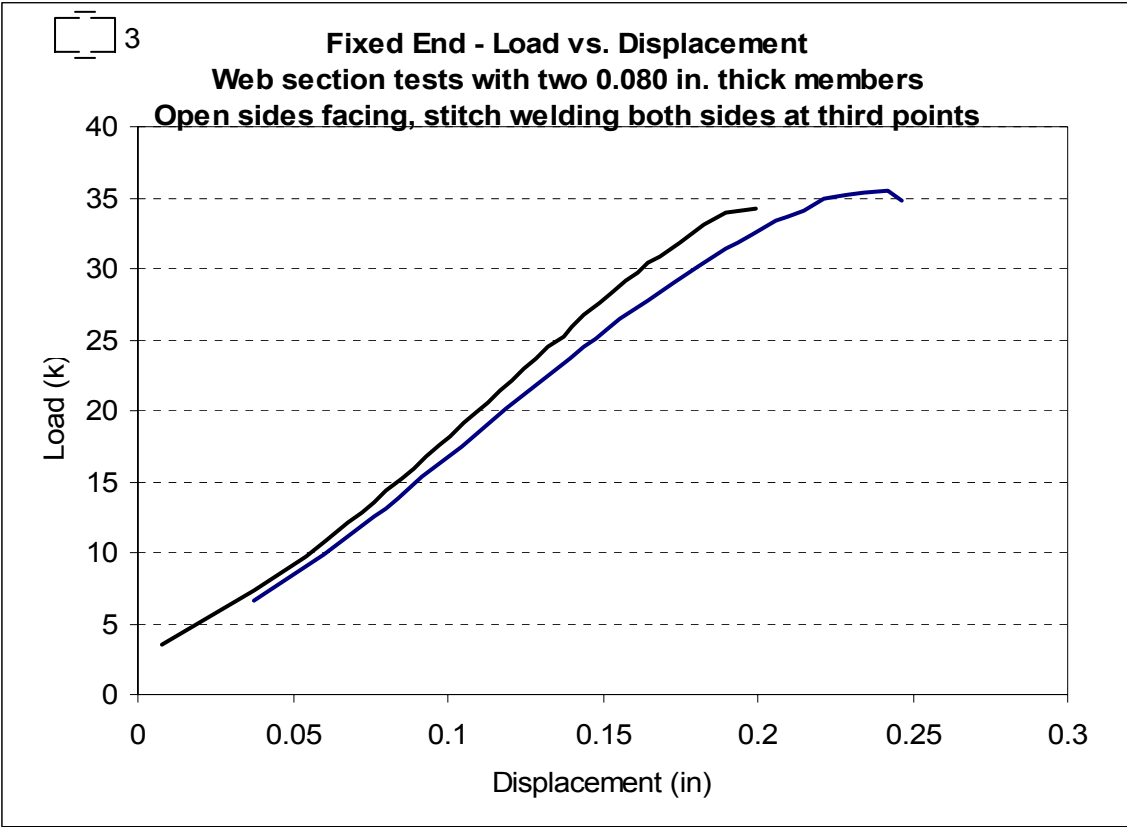


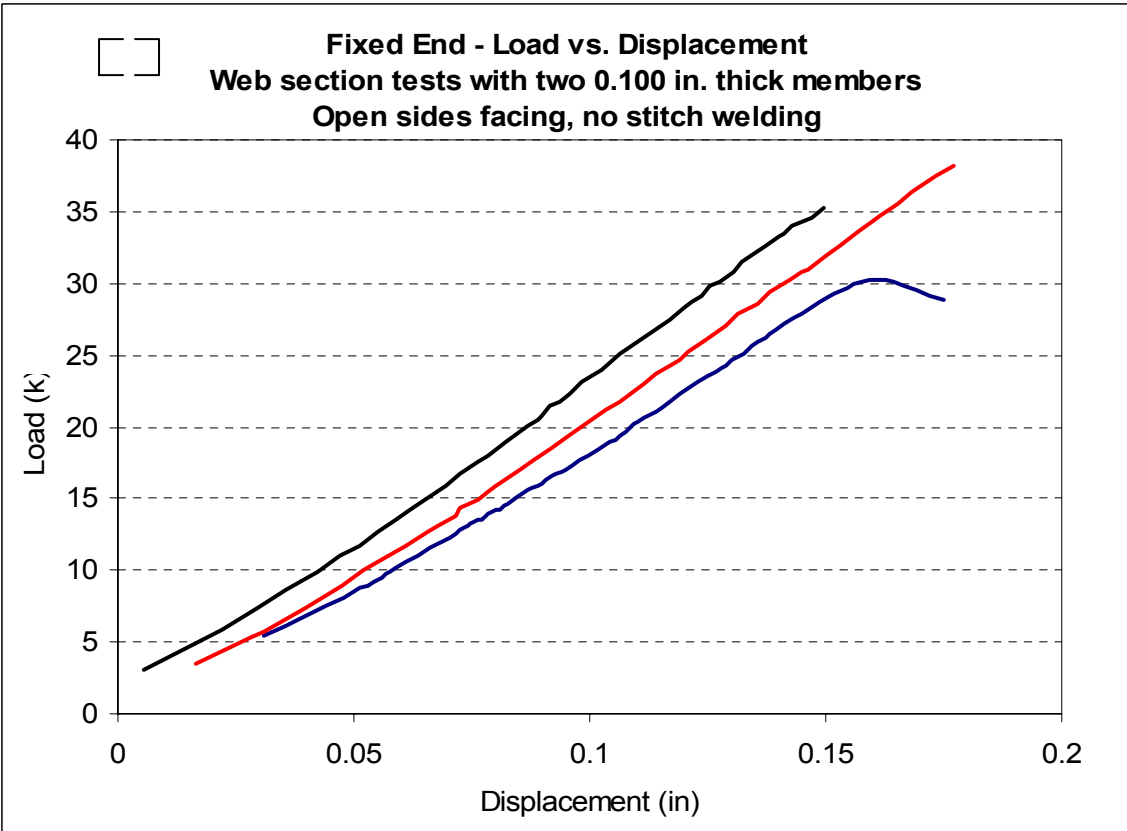
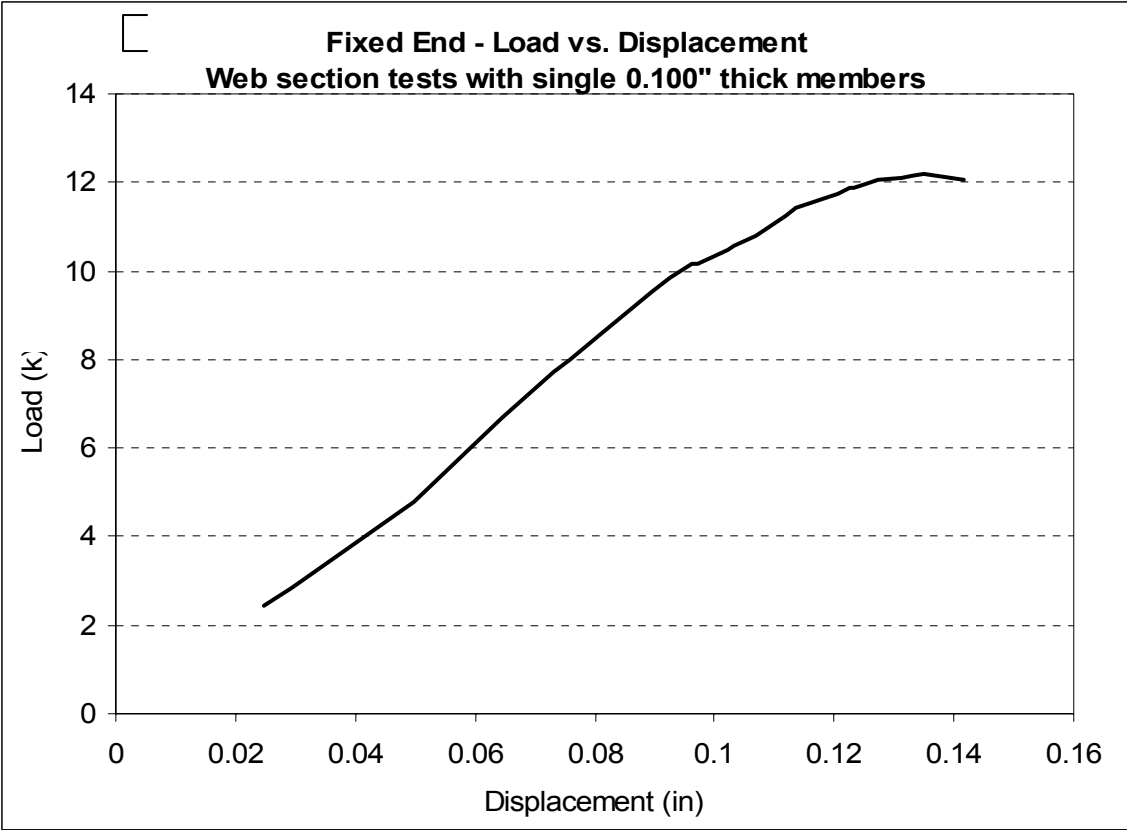


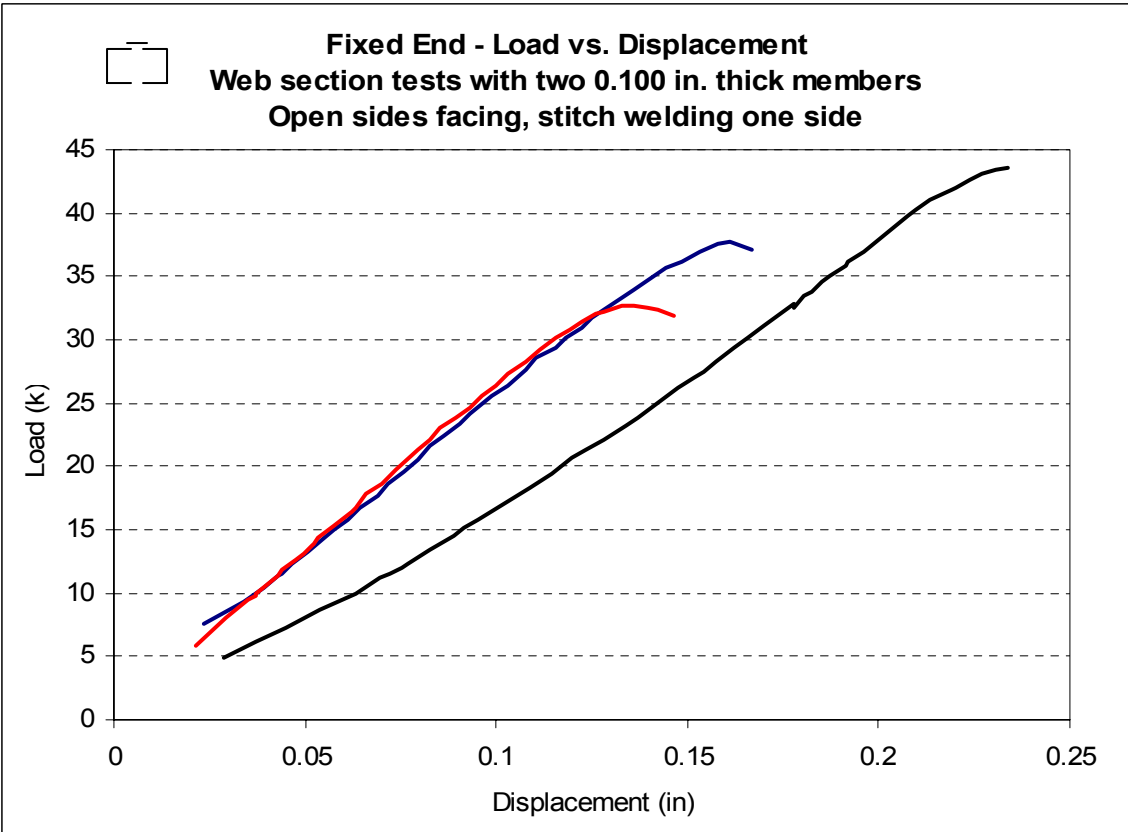
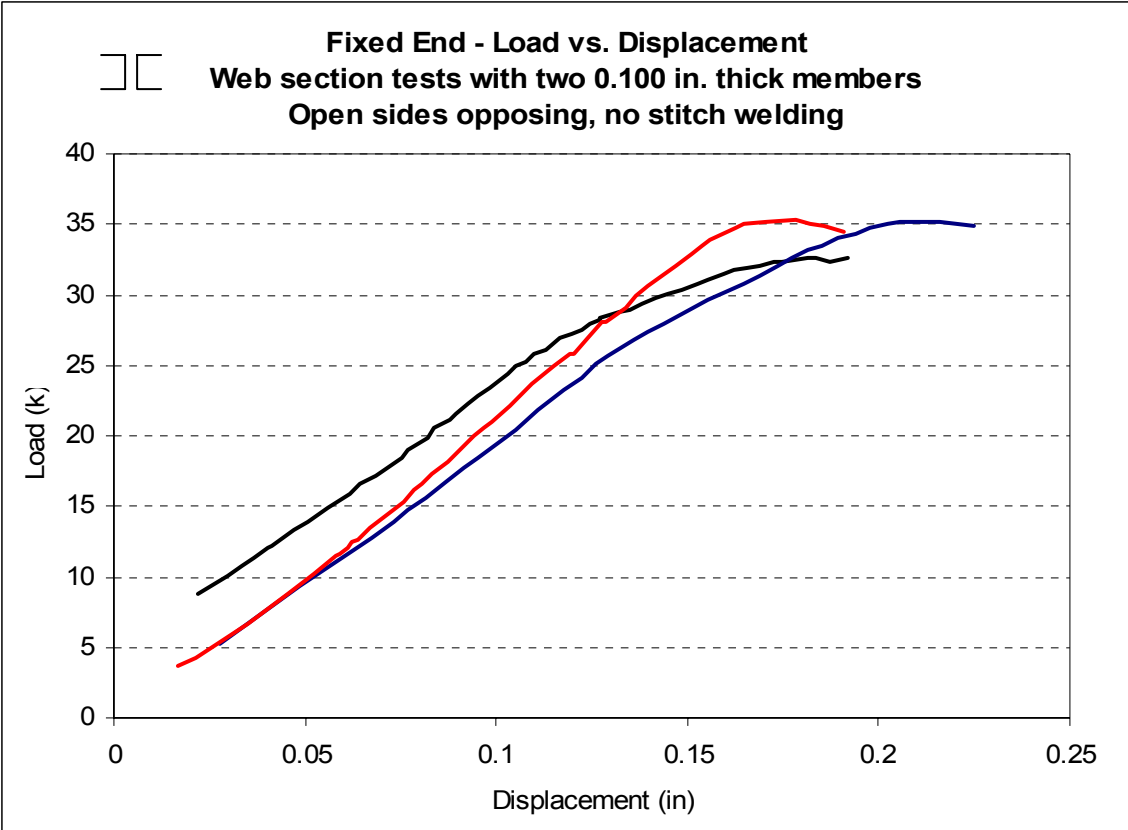


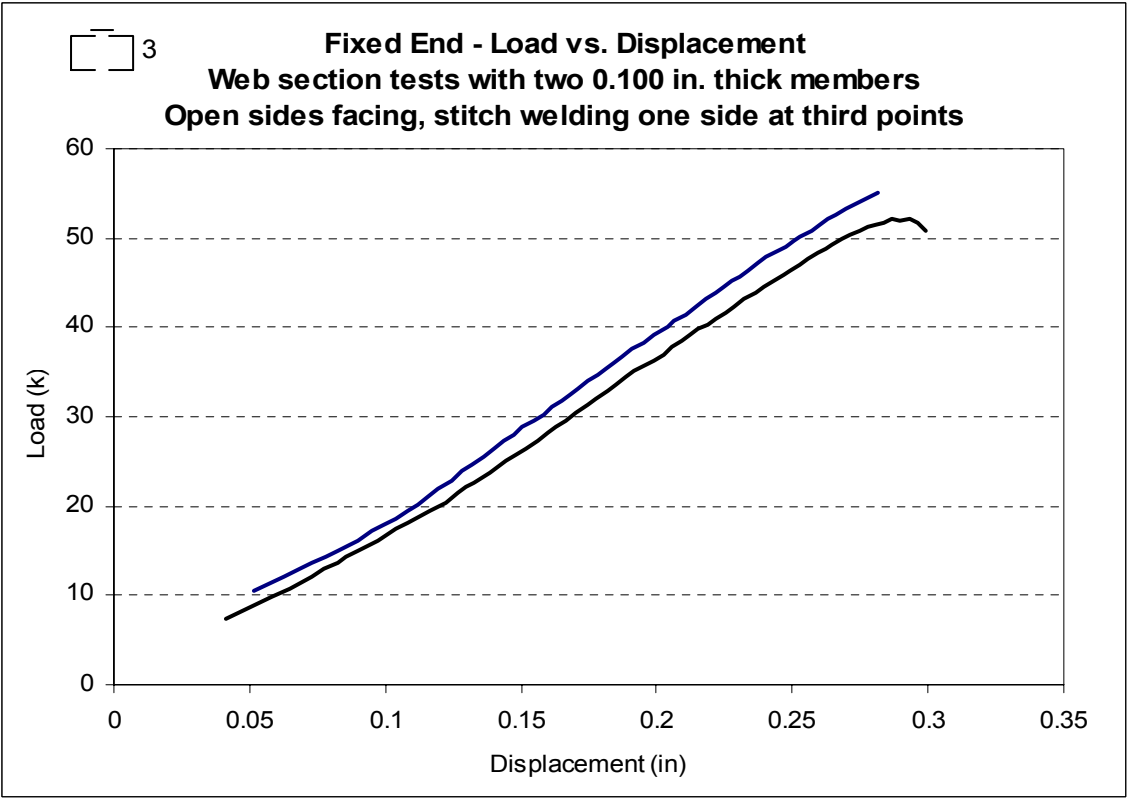
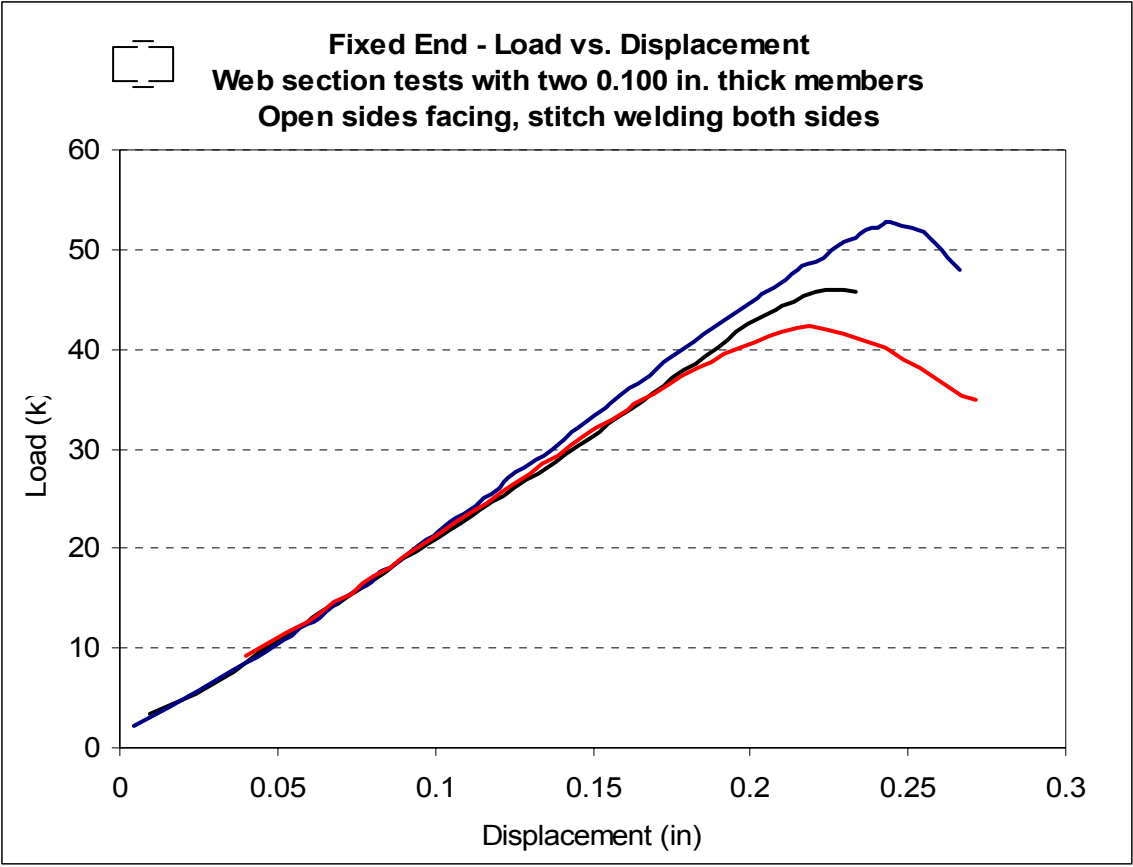




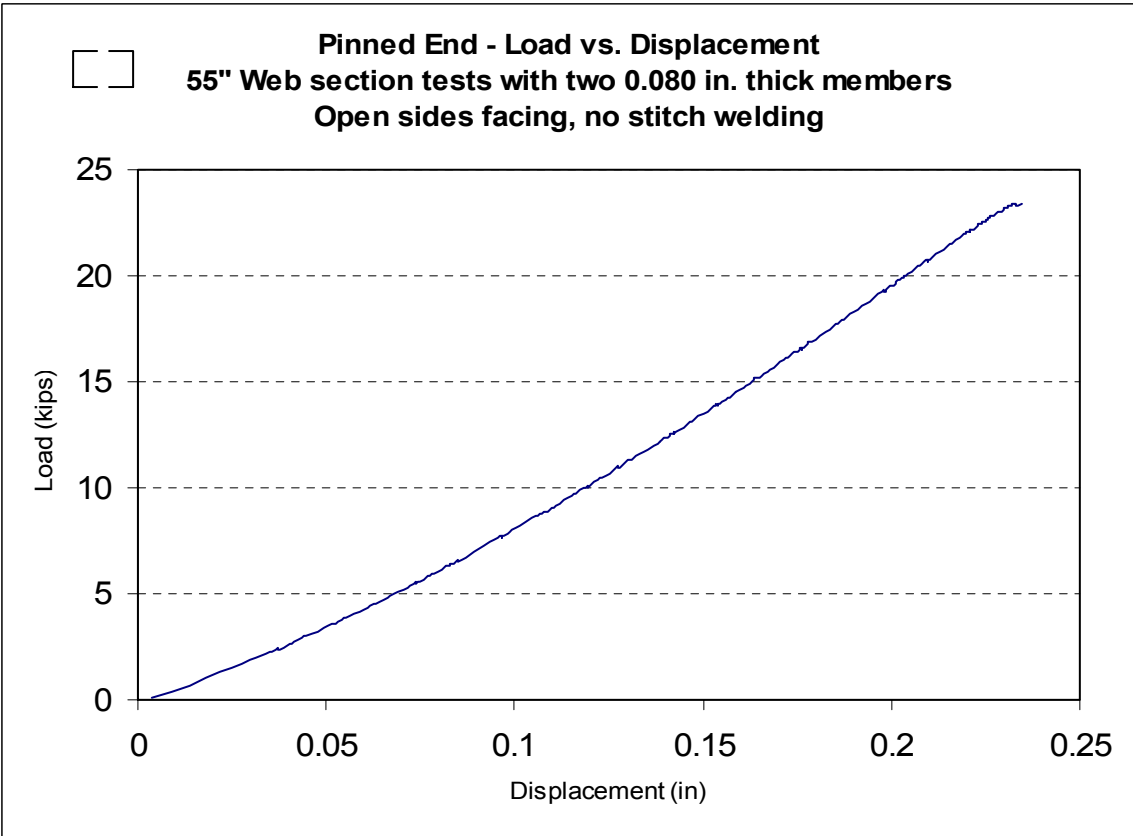
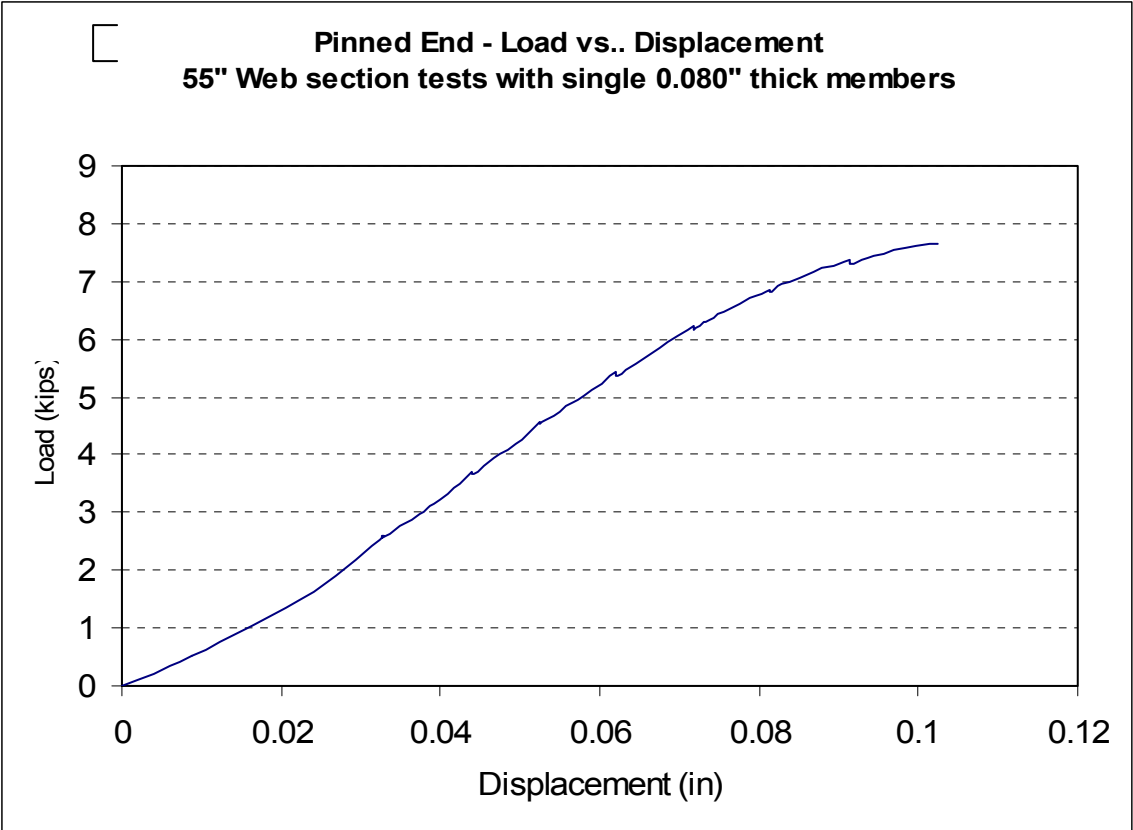


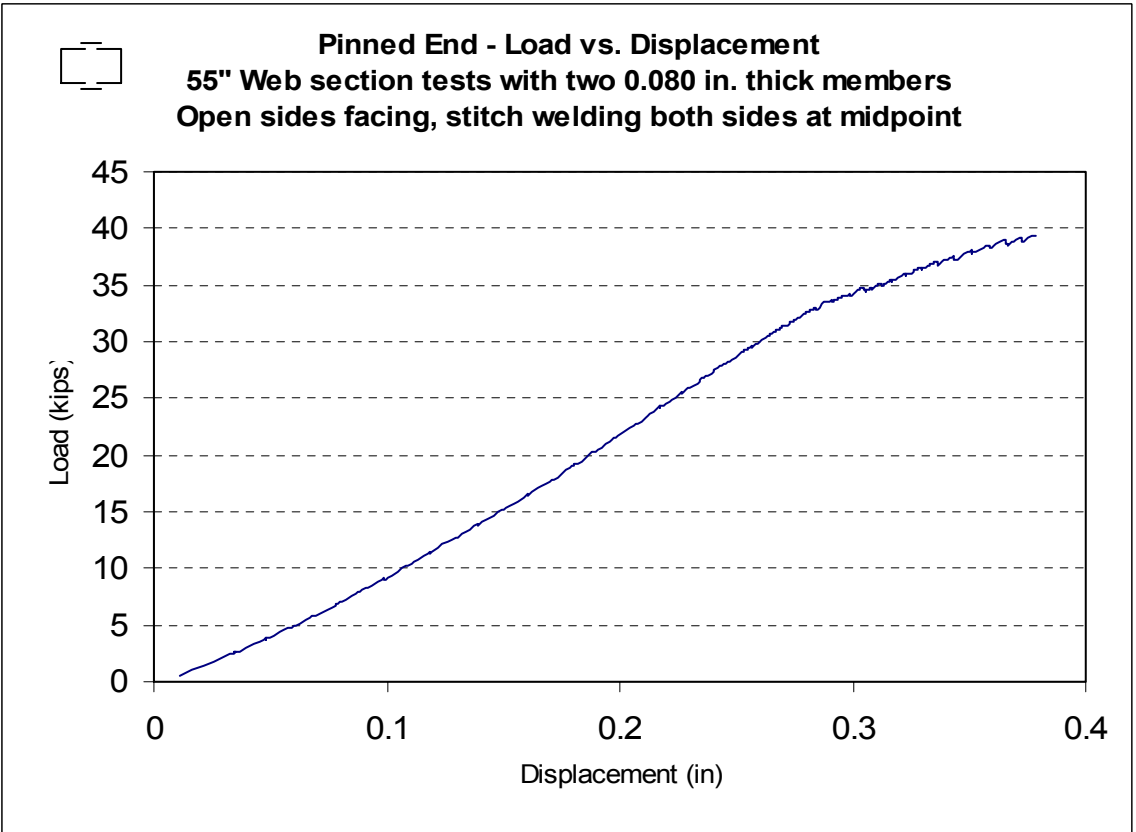
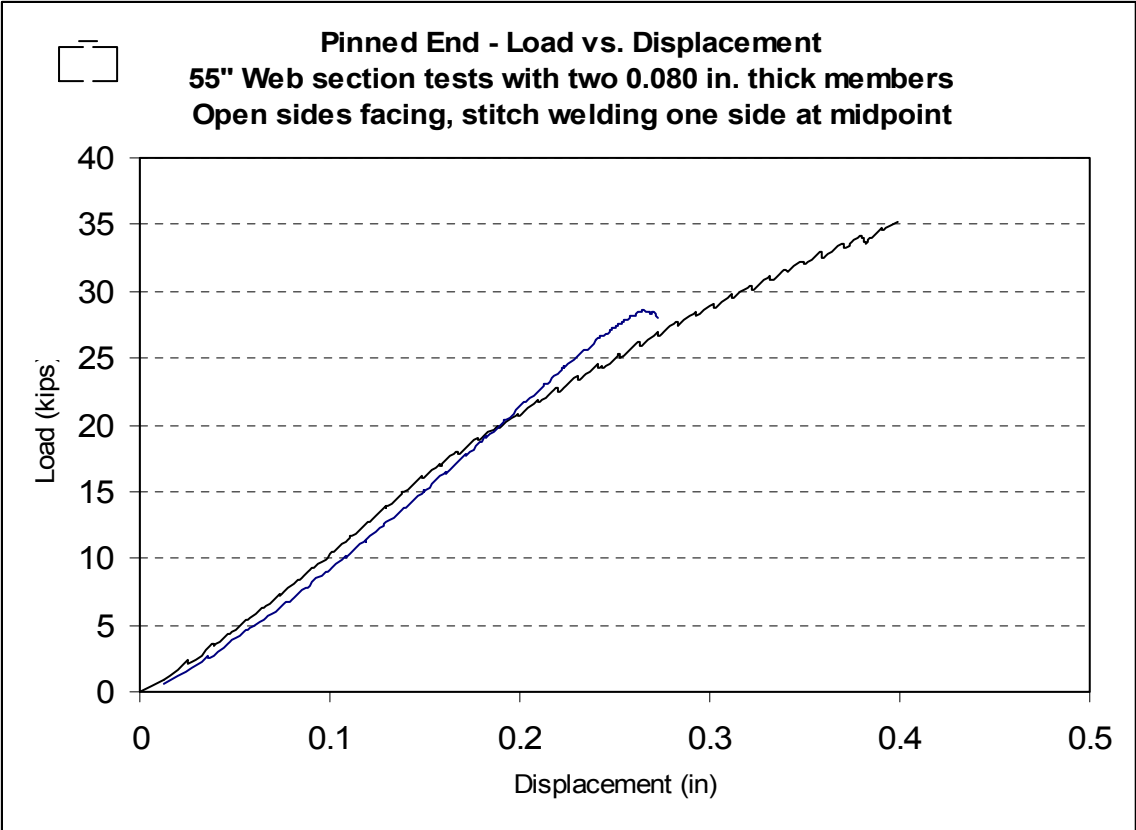


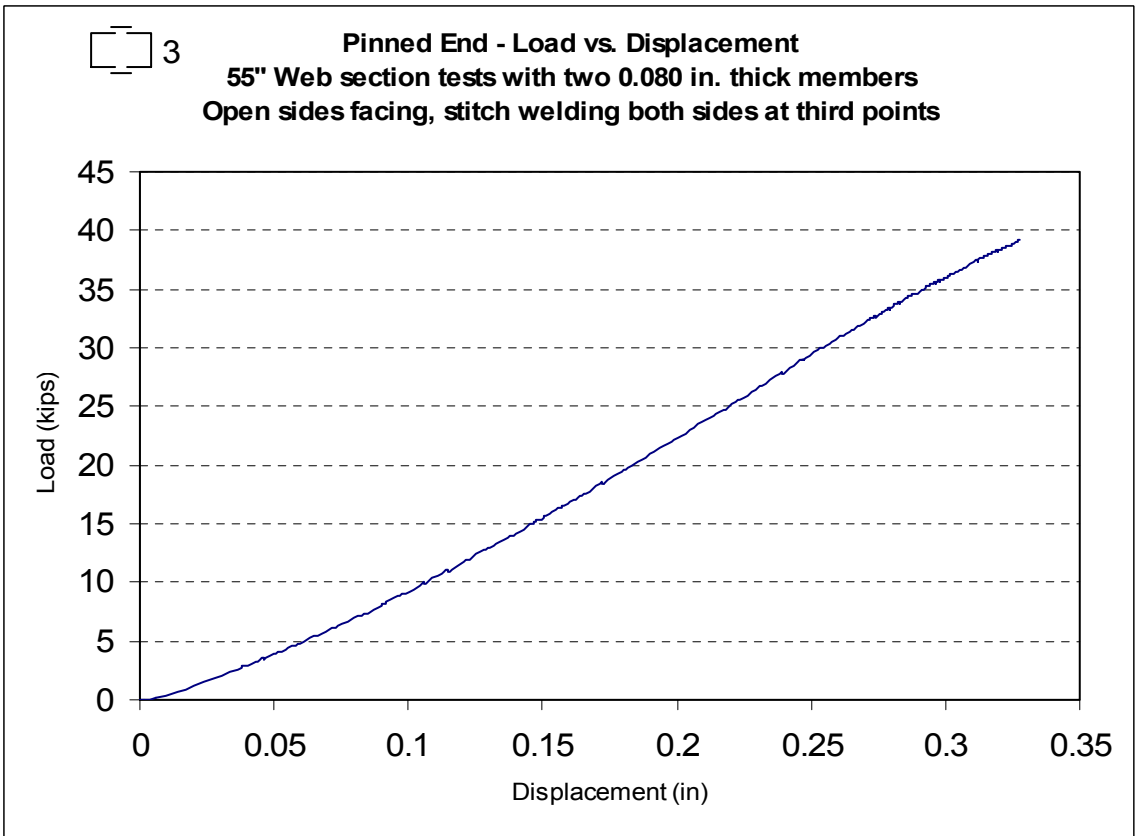
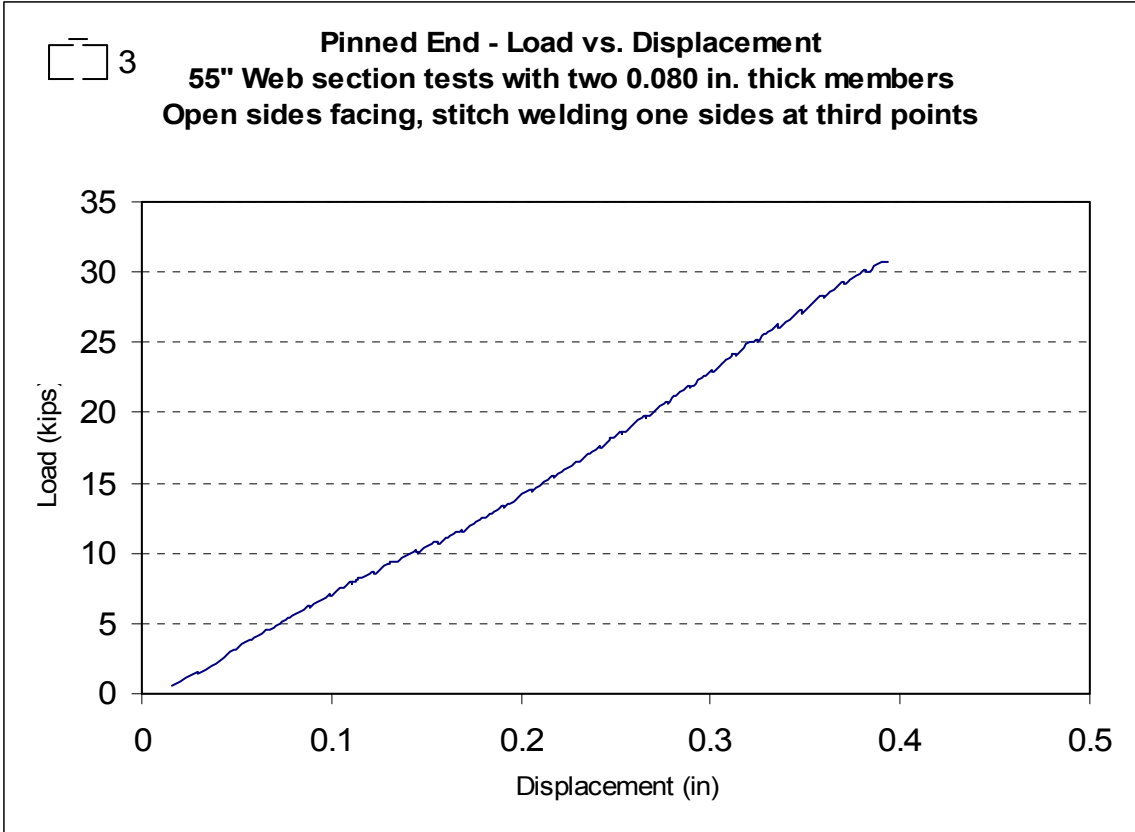


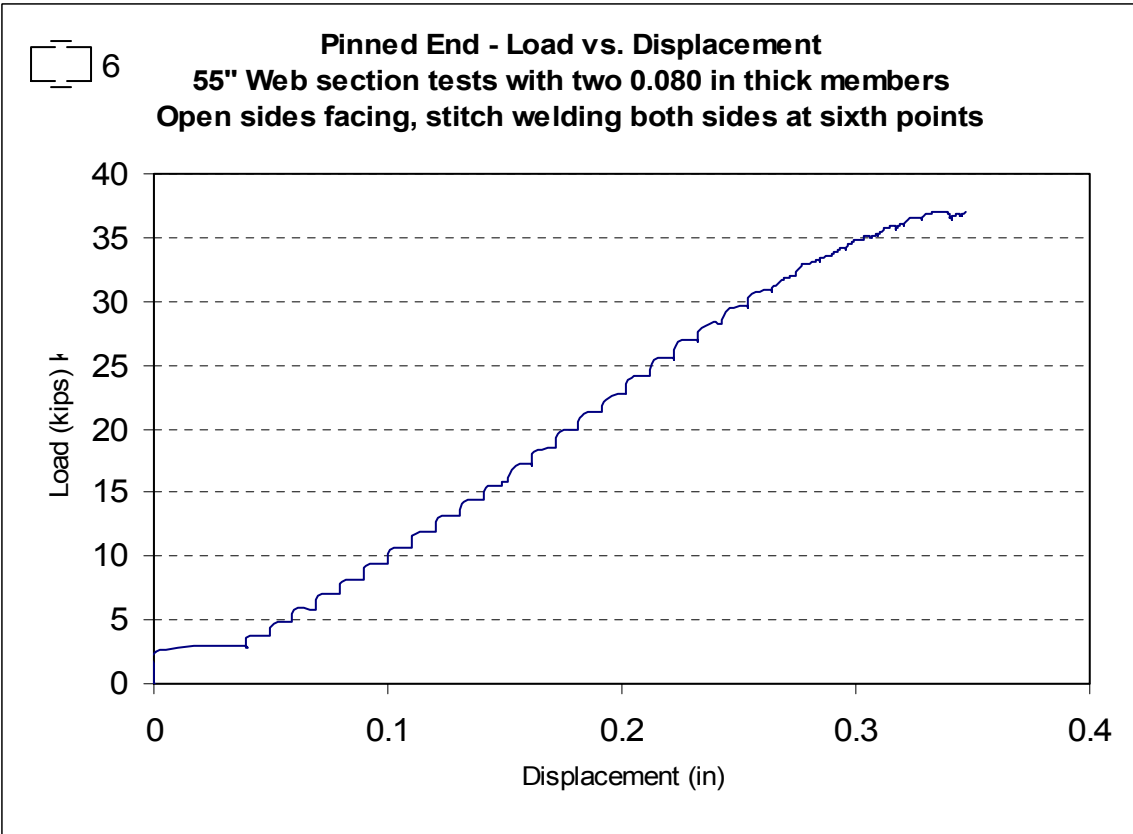
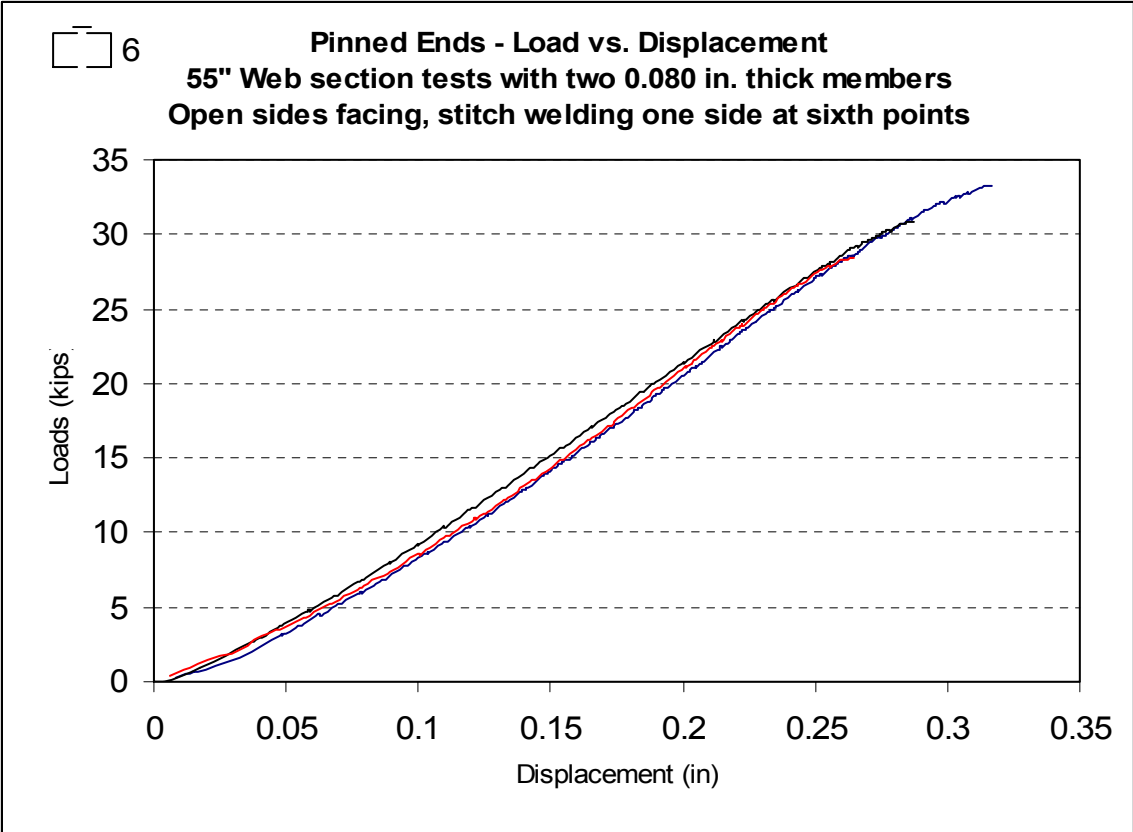


**APPENDIX G - 55" – 1 5/8" Built-up Member, Pinned End
Load vs. Deflection Plots**

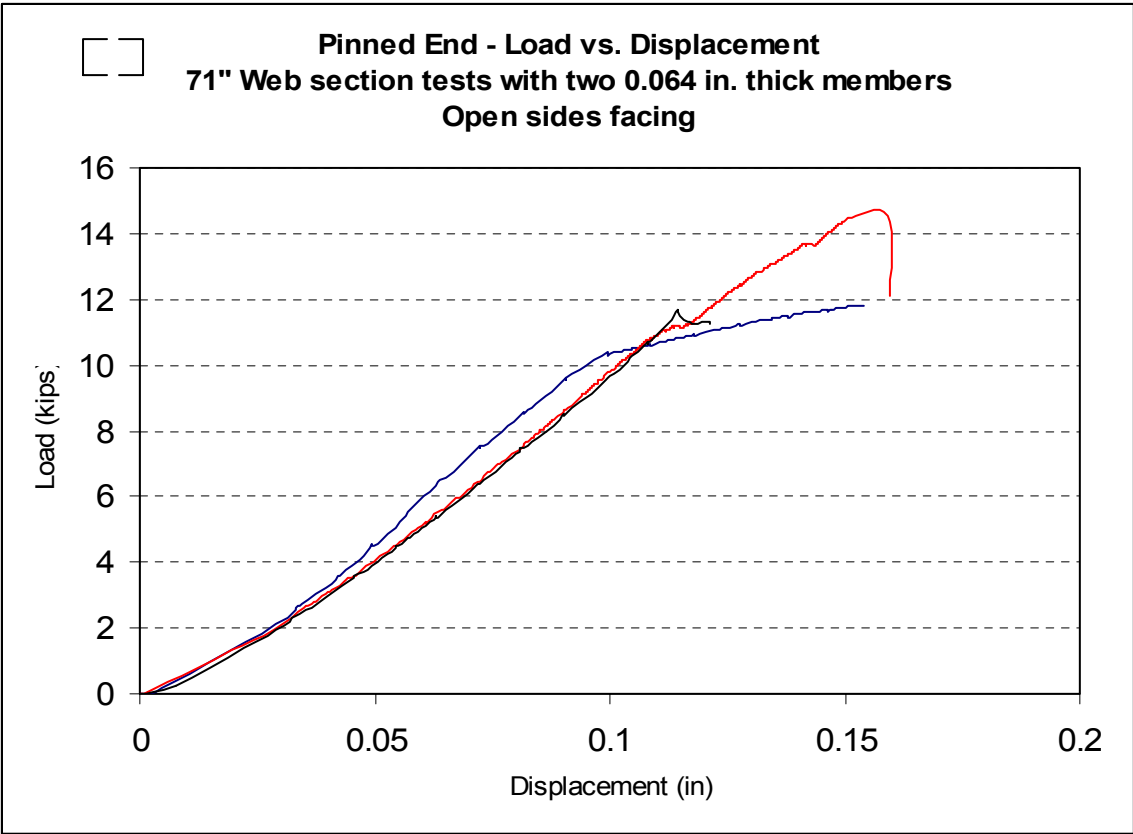
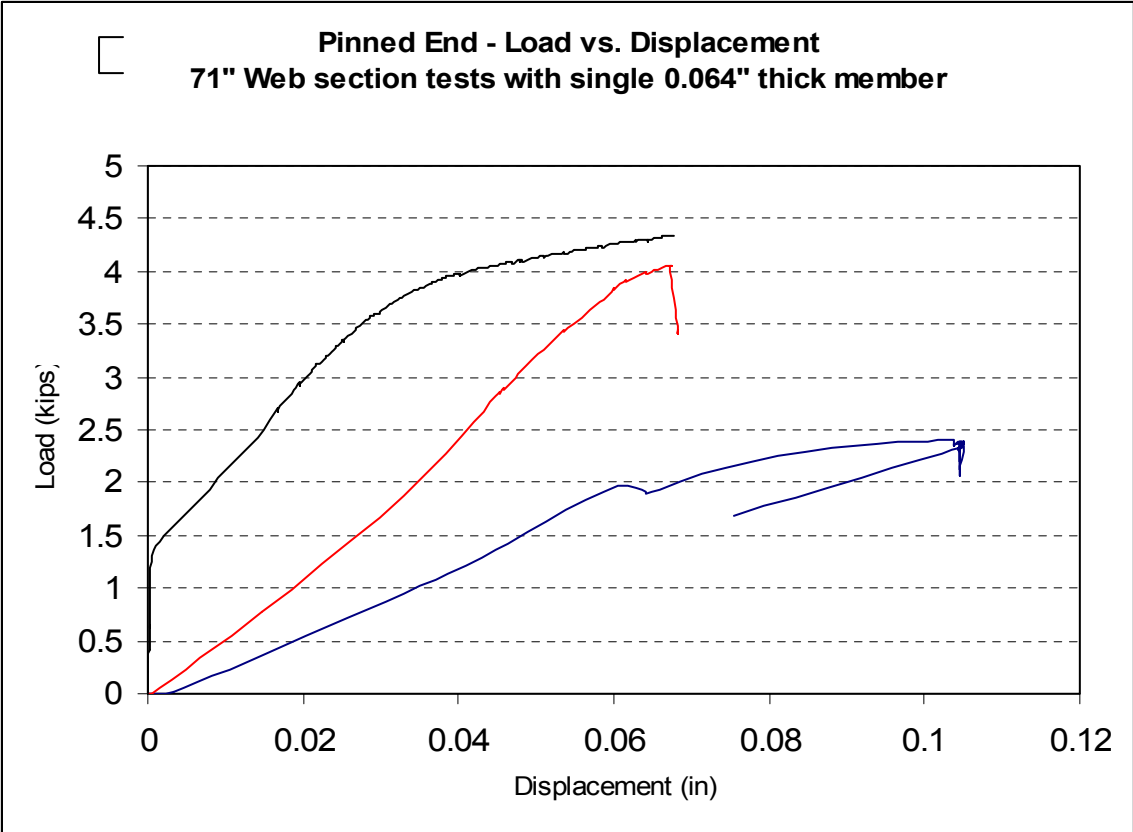


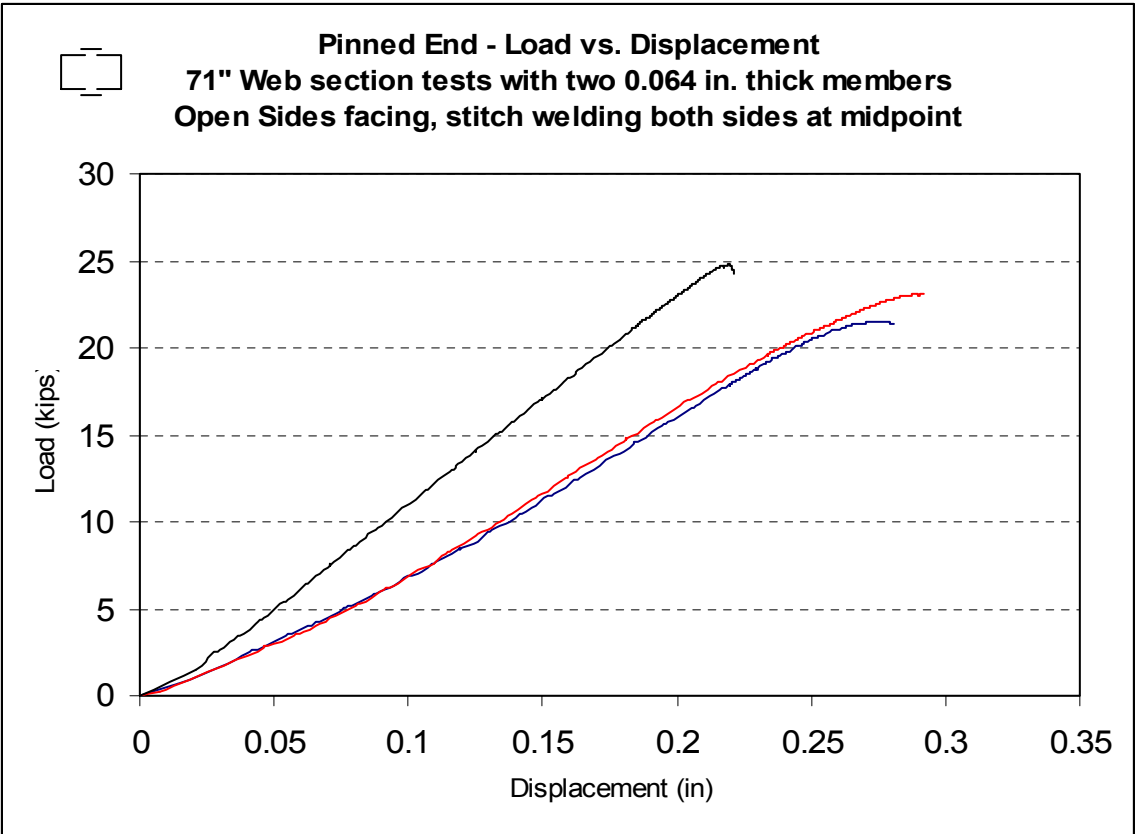
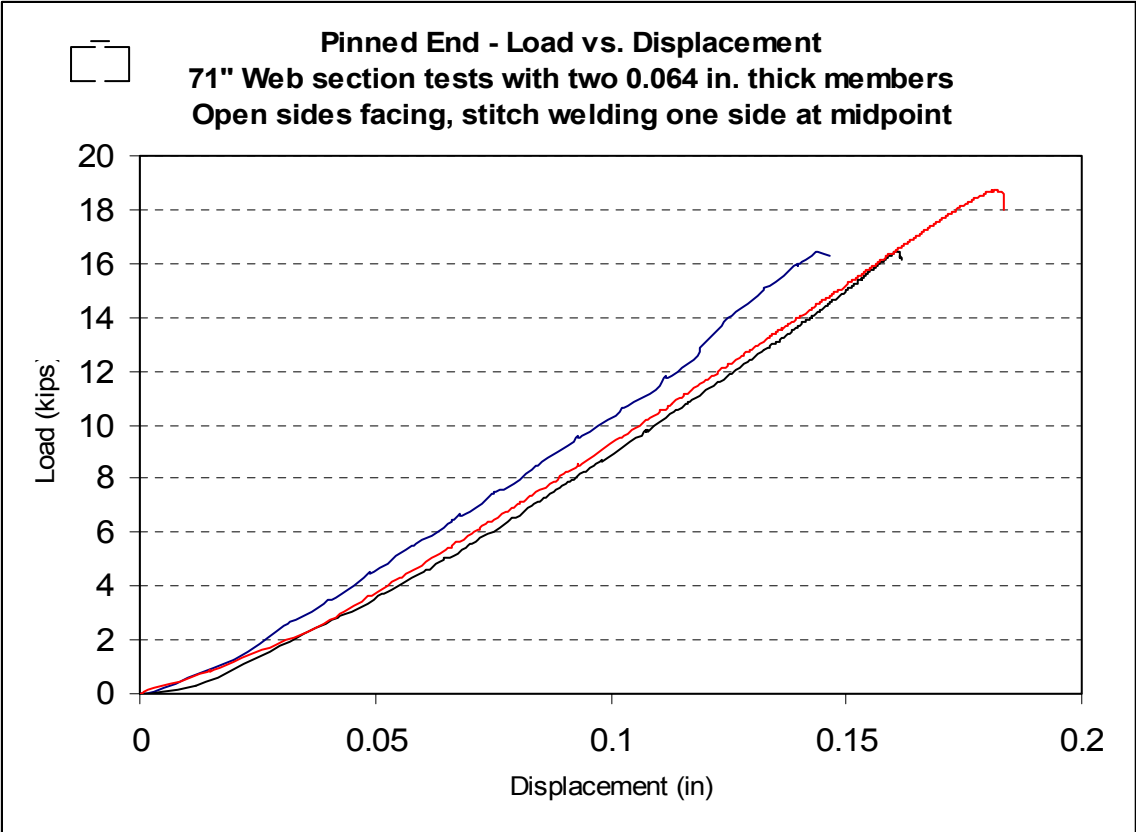


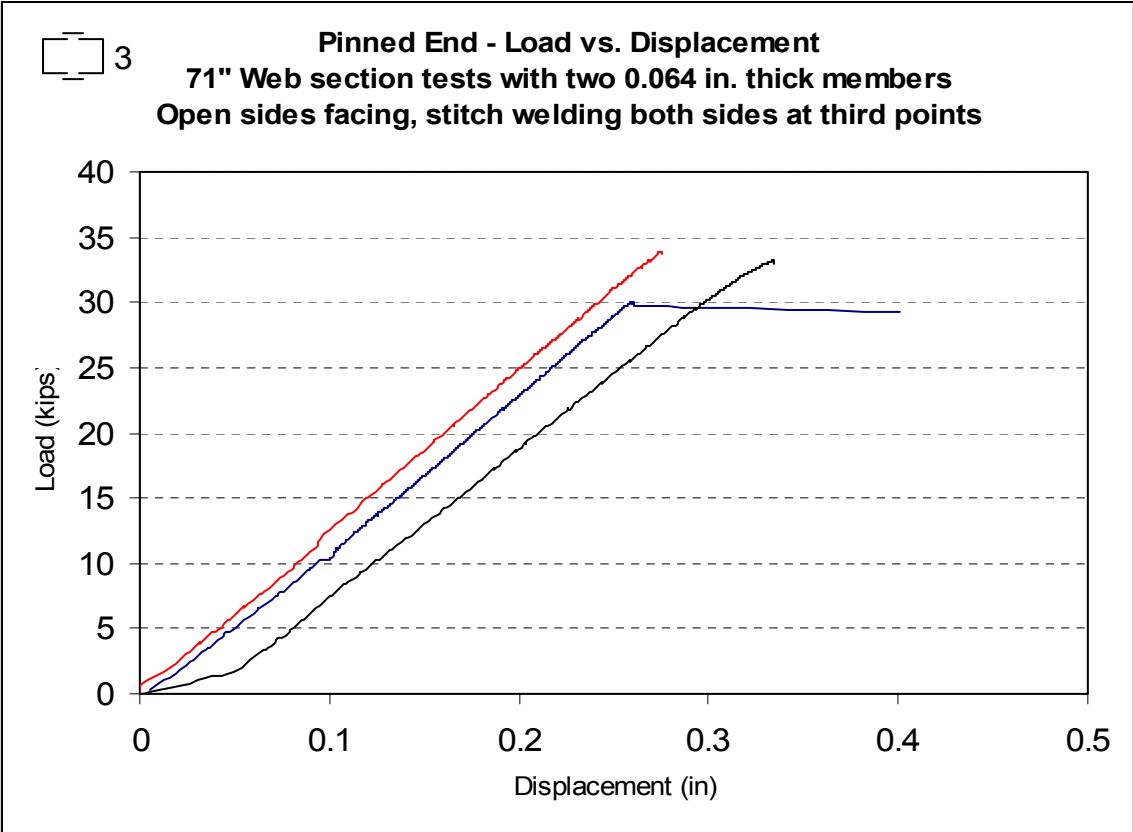
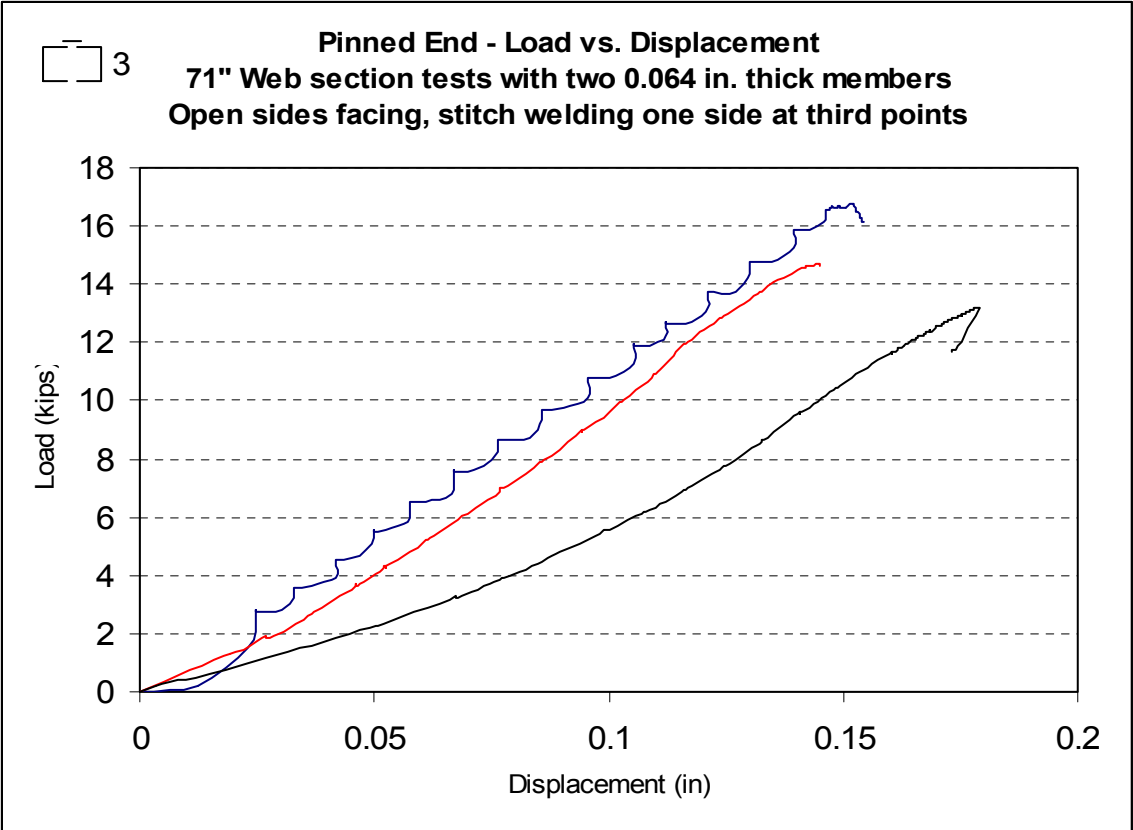


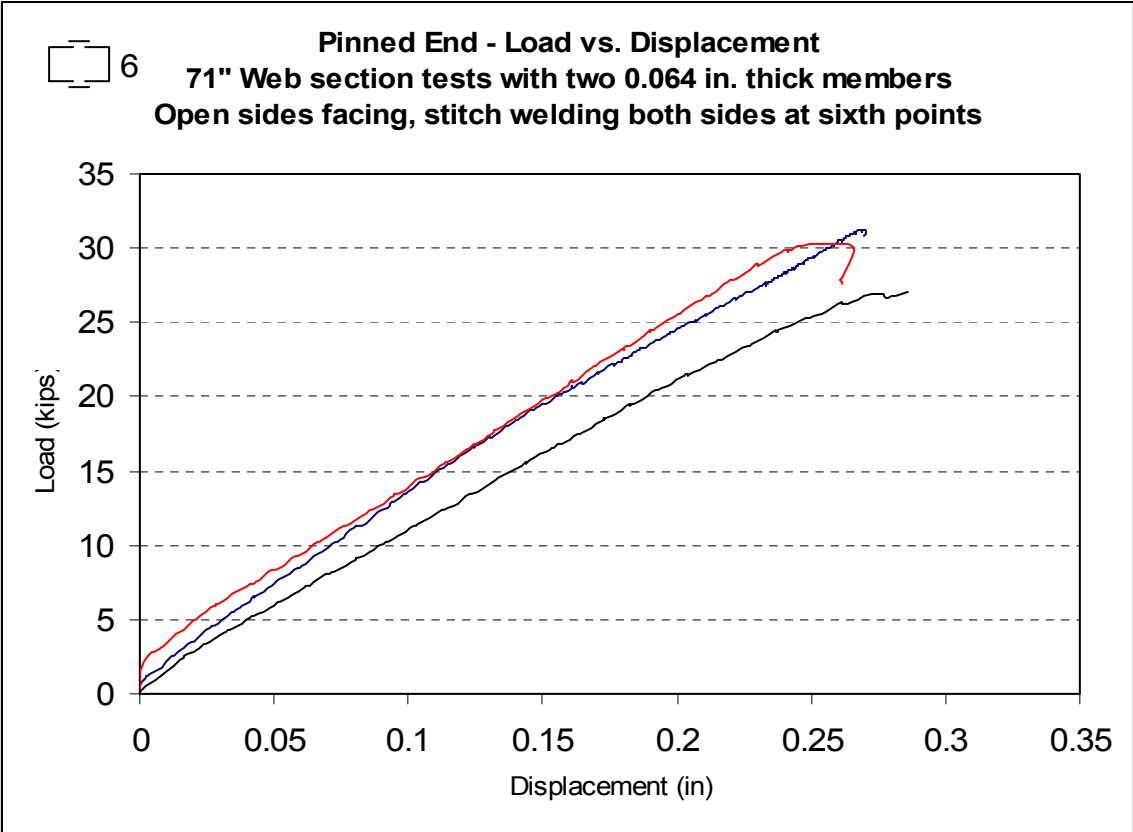
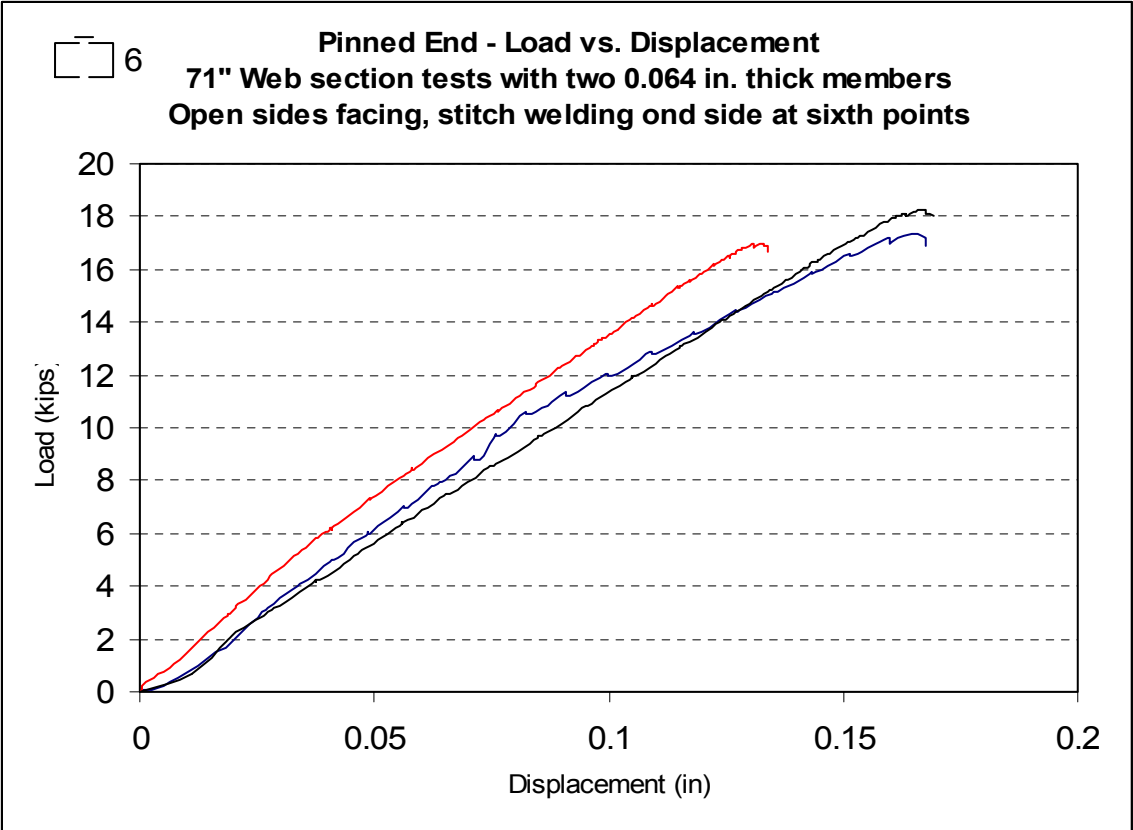


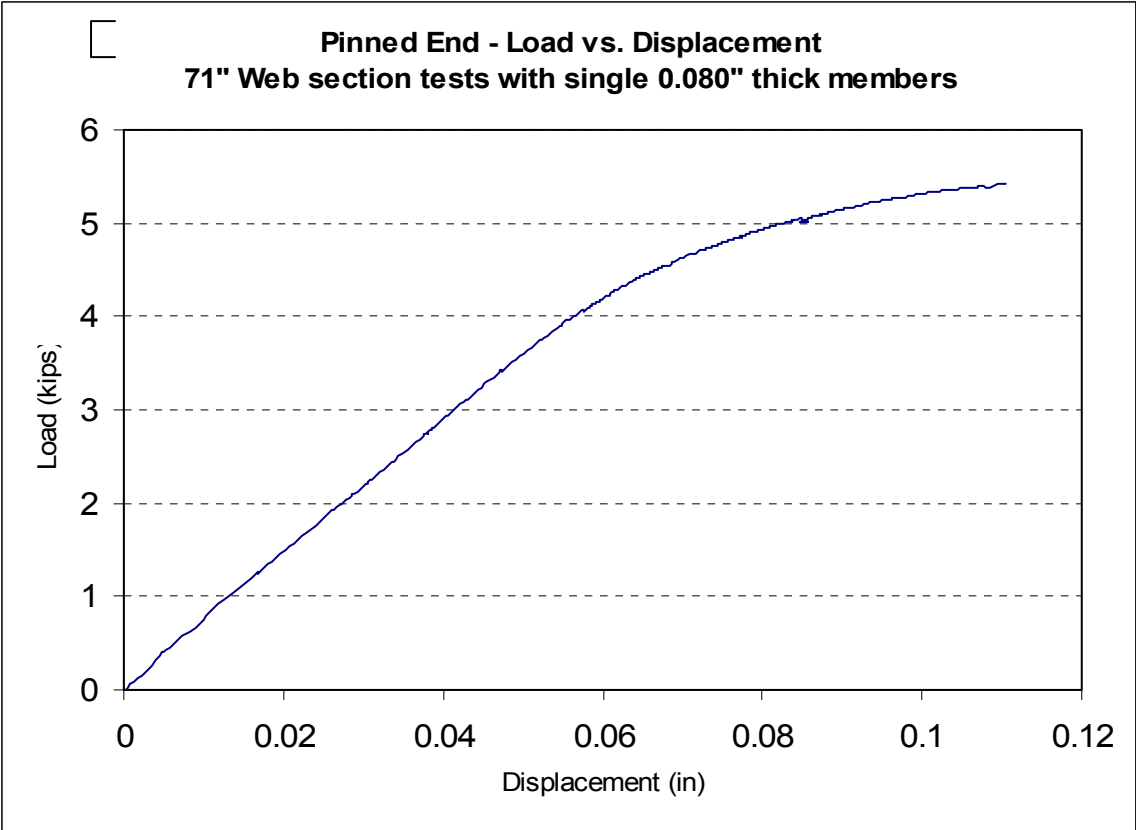
**APPENDIX H - 71" – 1 5/8" Built-up Member, Pinned End
Load vs. Deflection Plots**

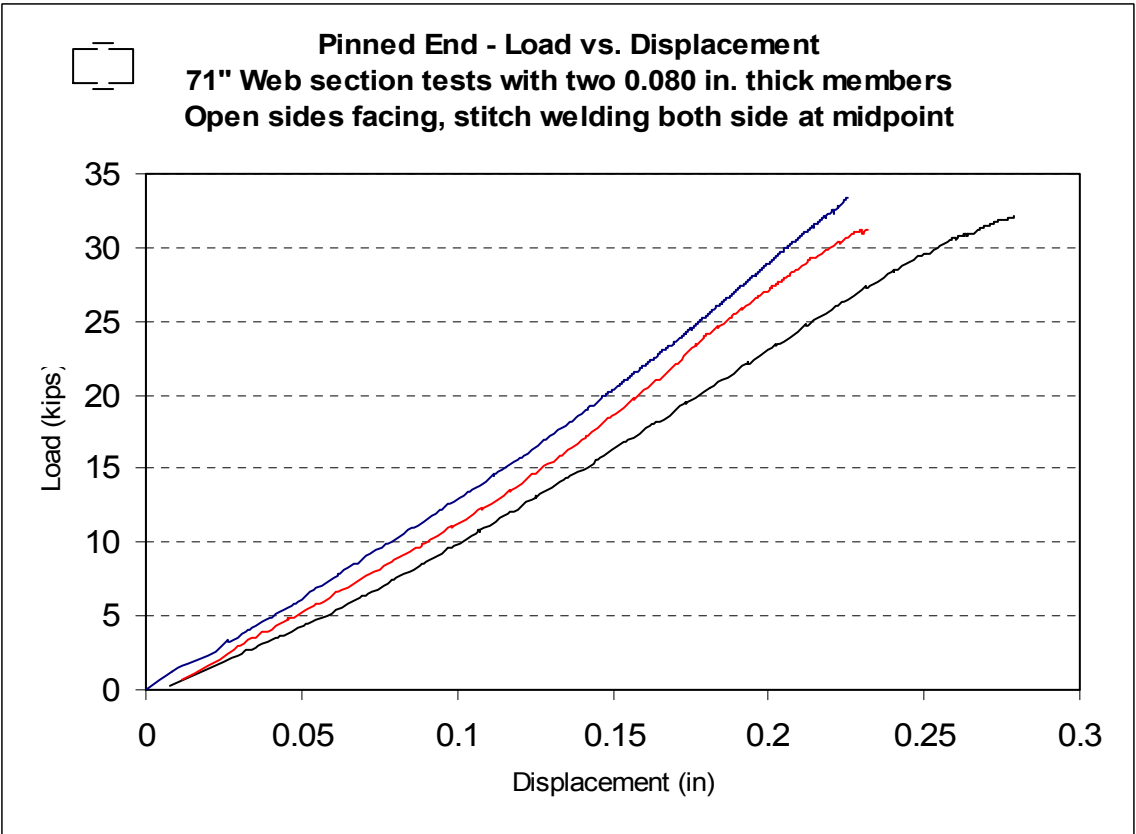
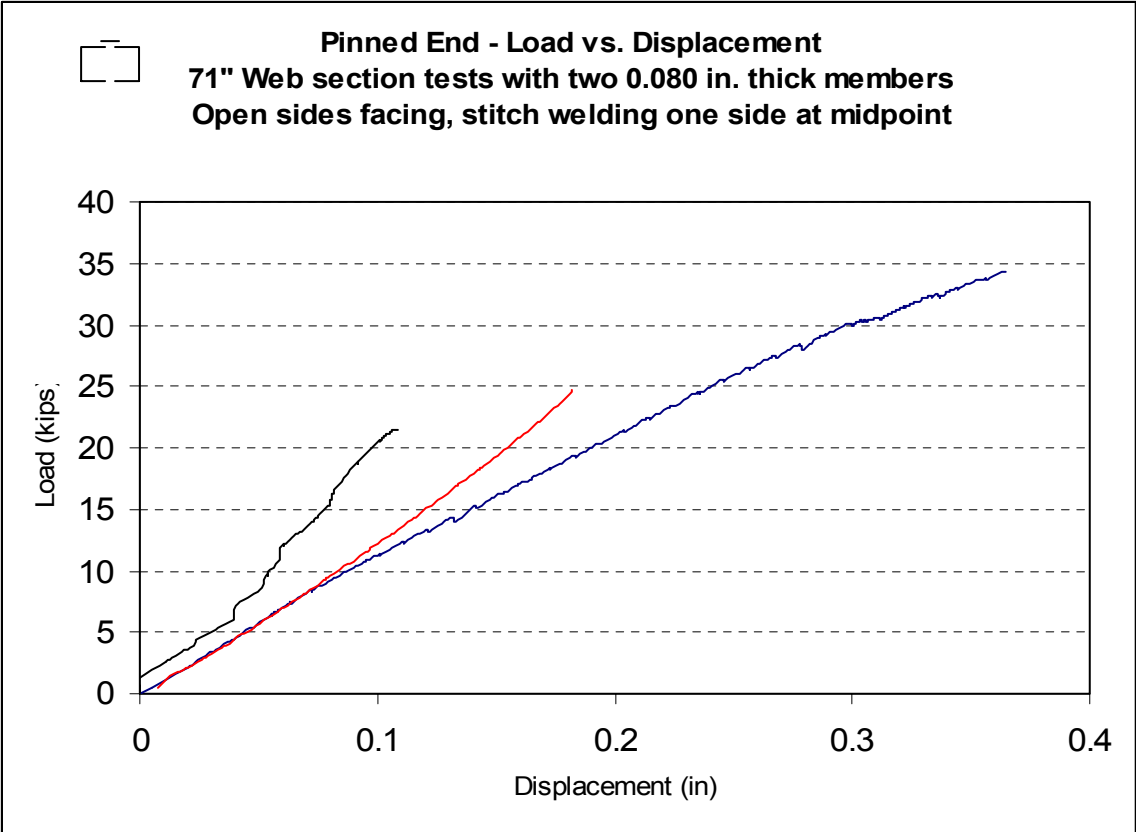


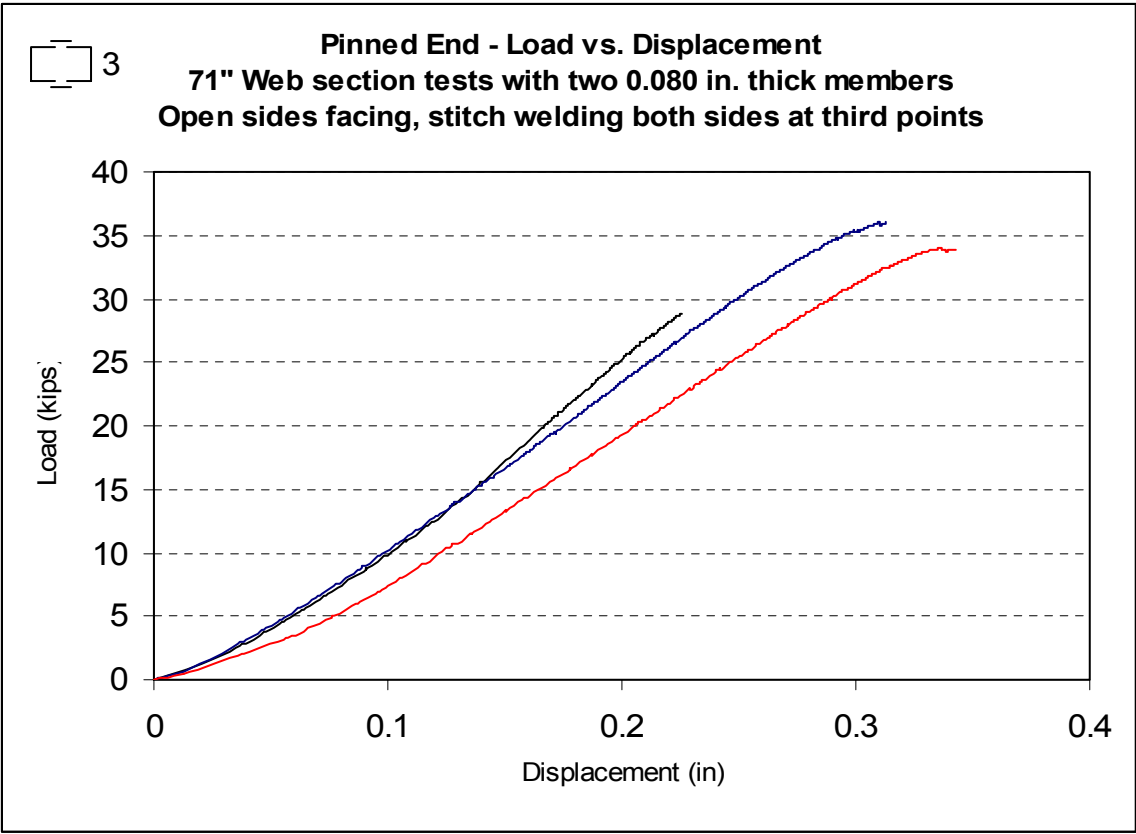
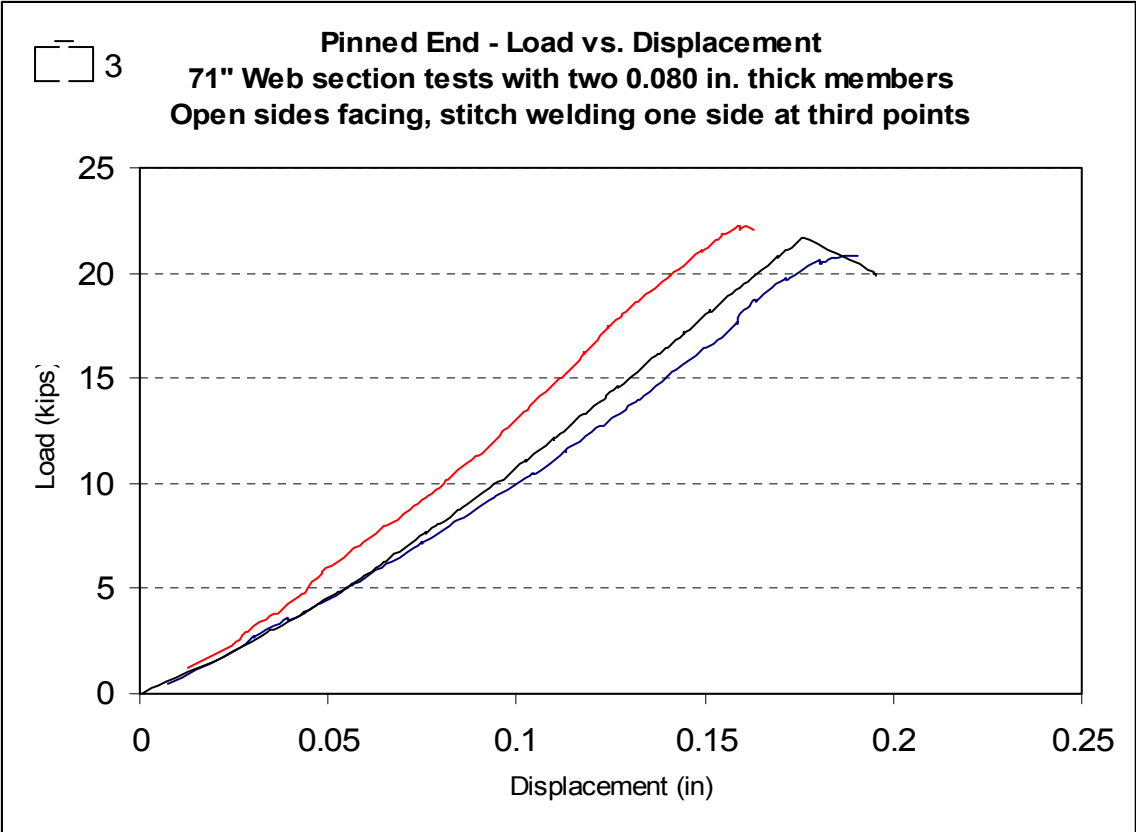


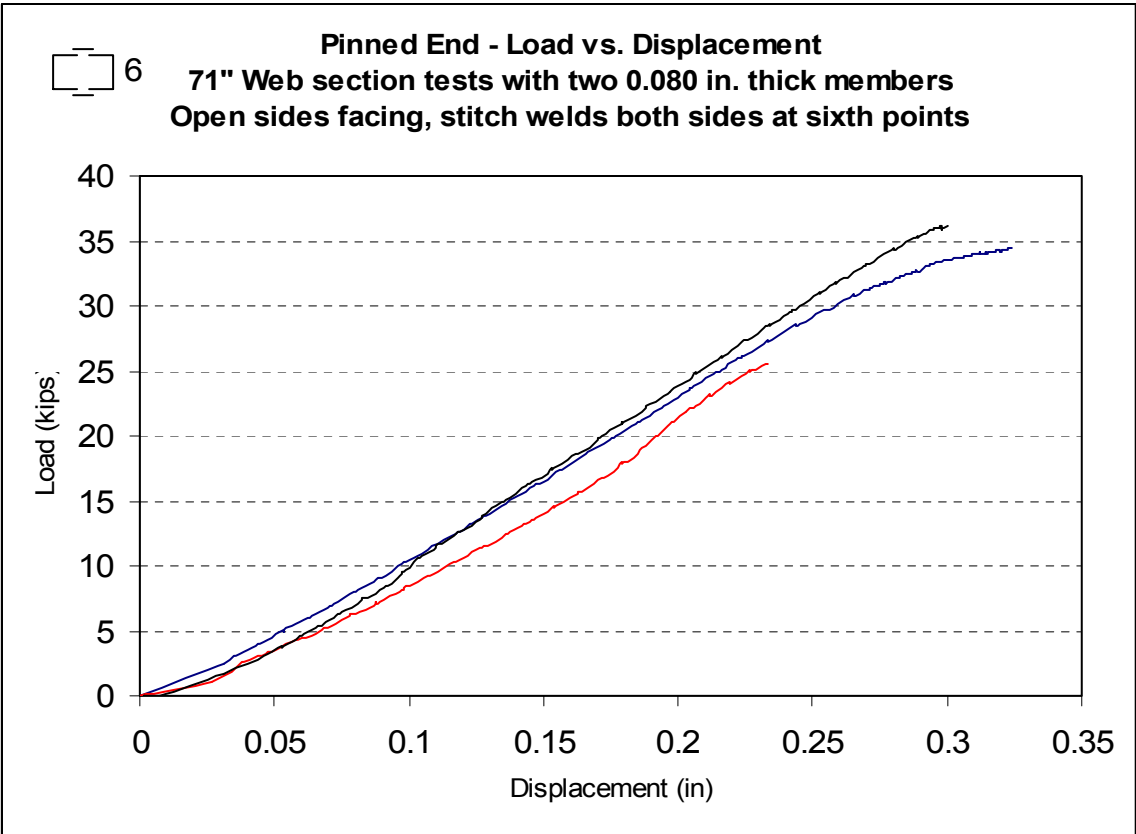
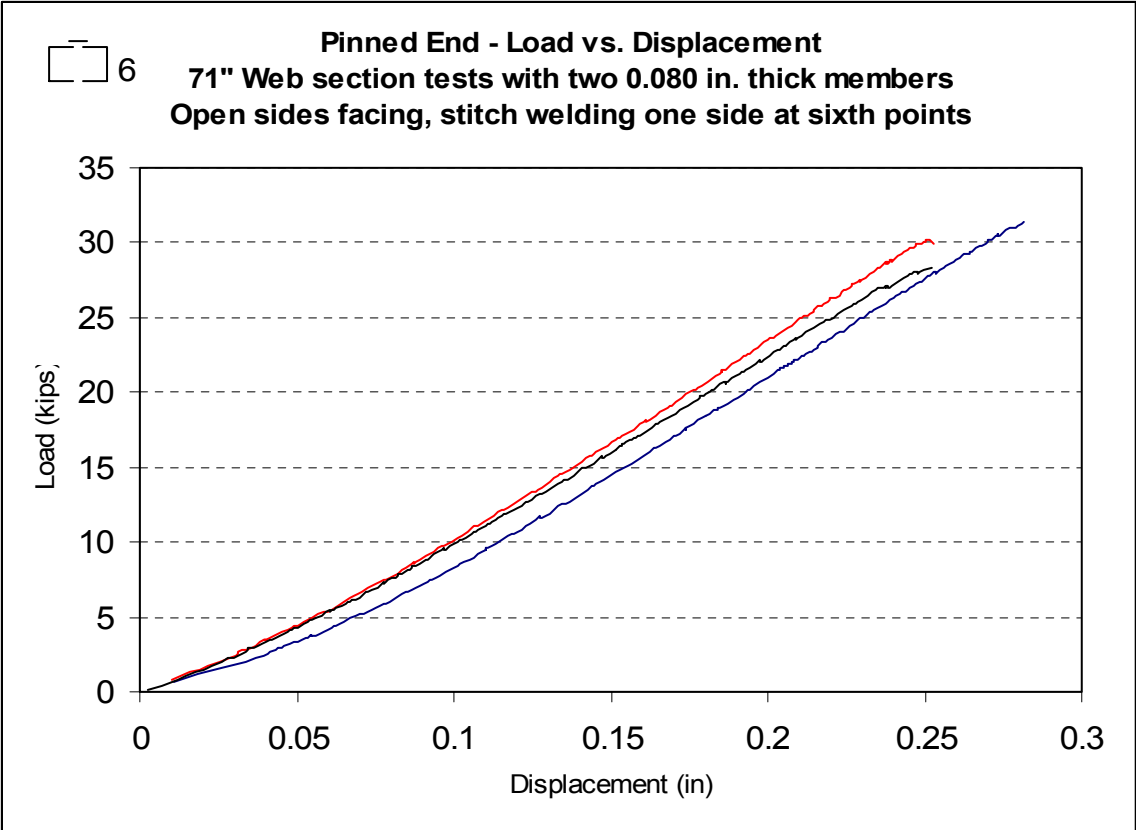


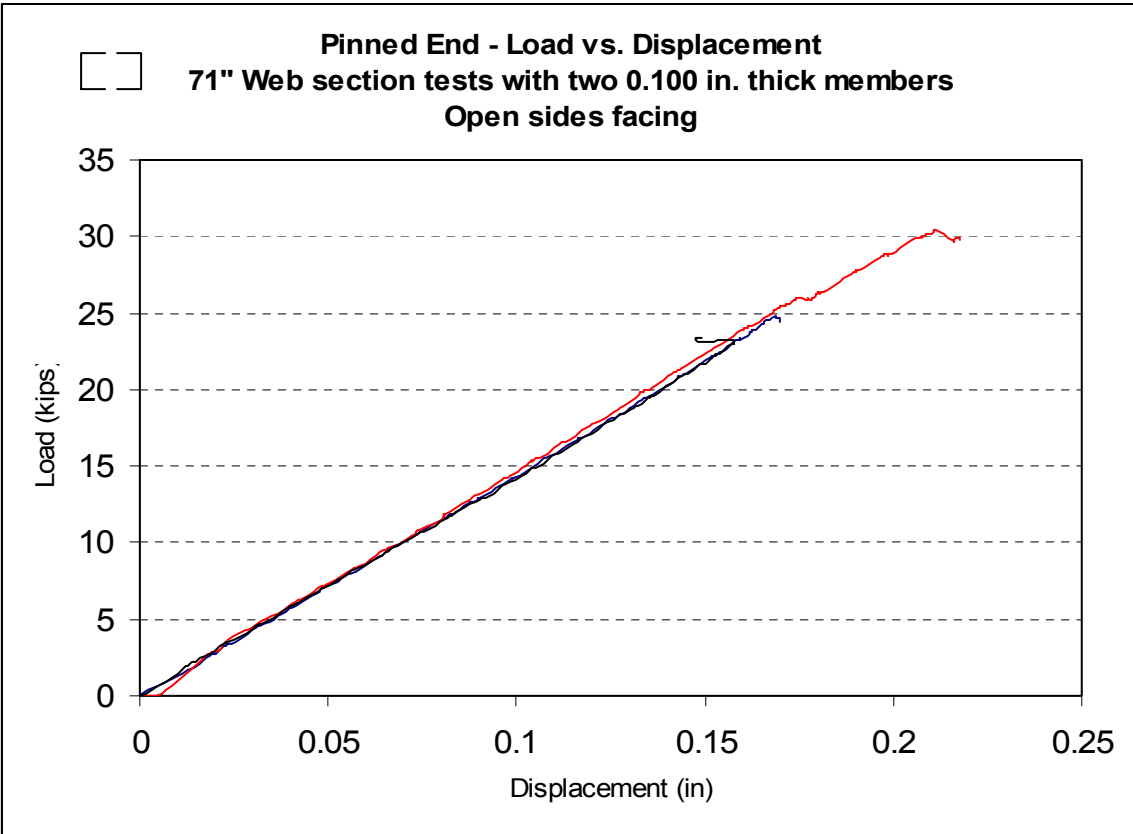
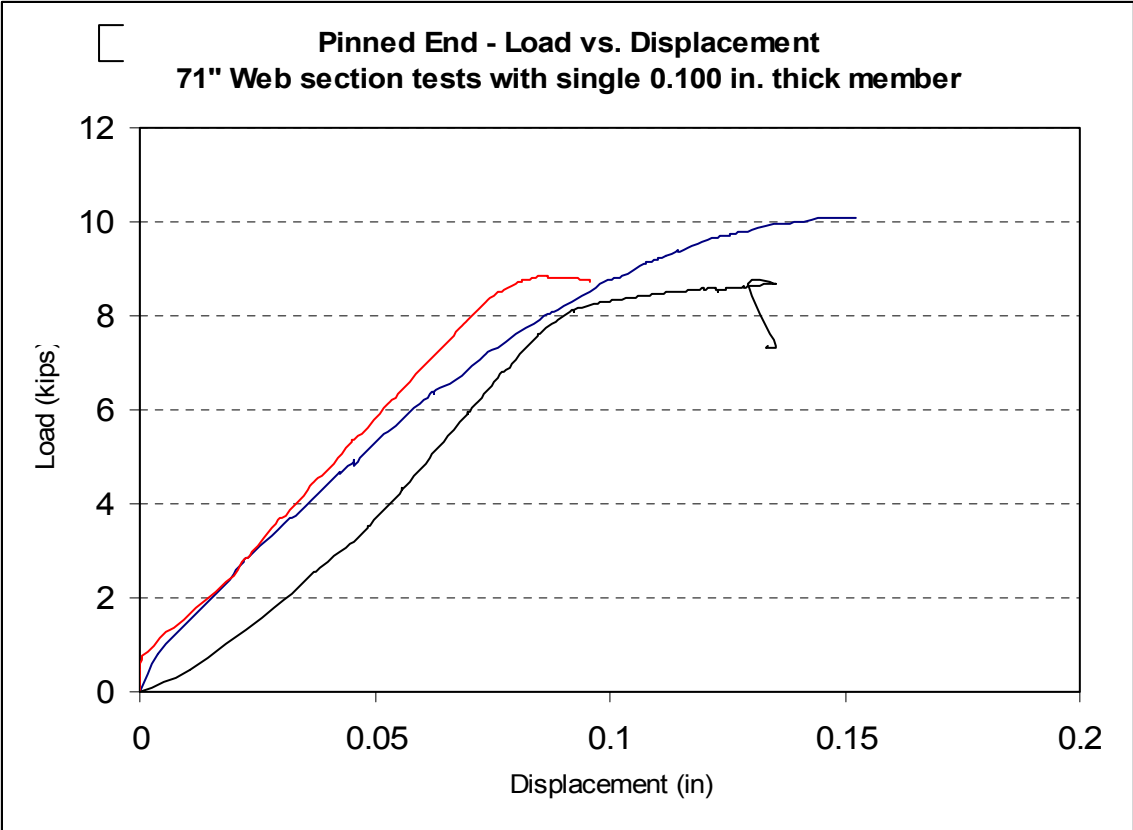


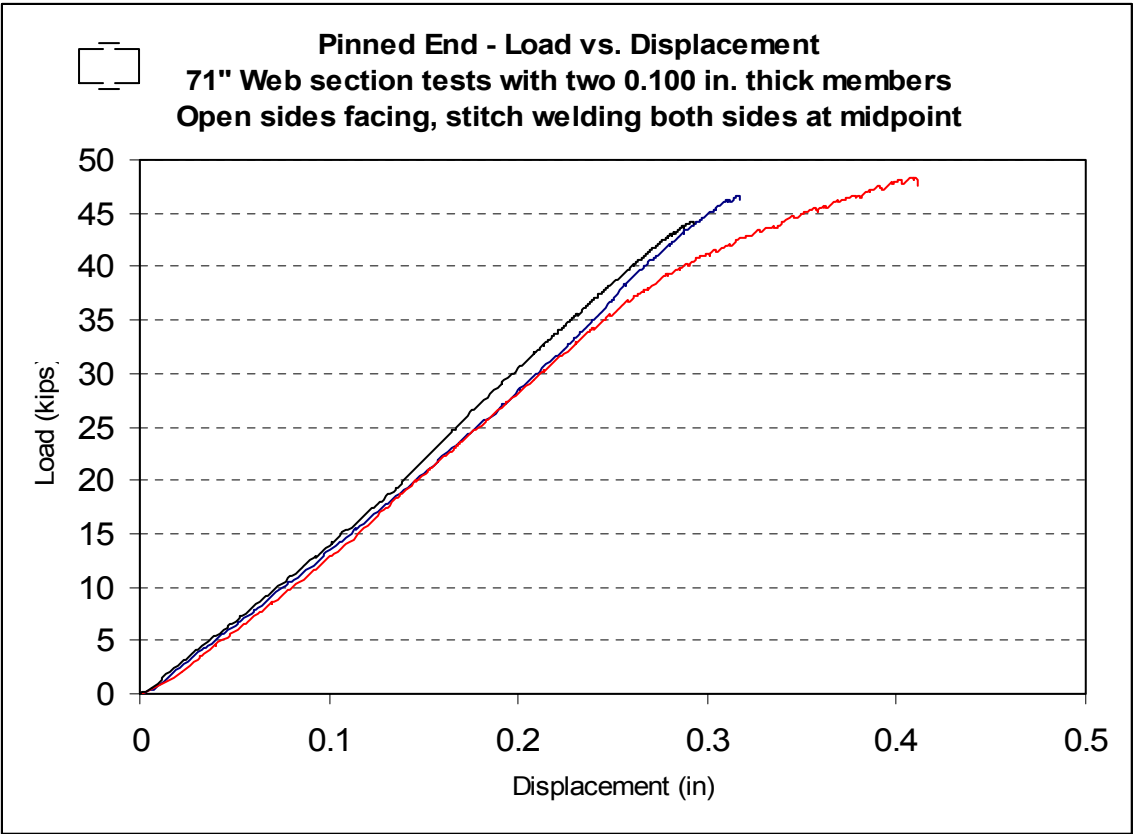
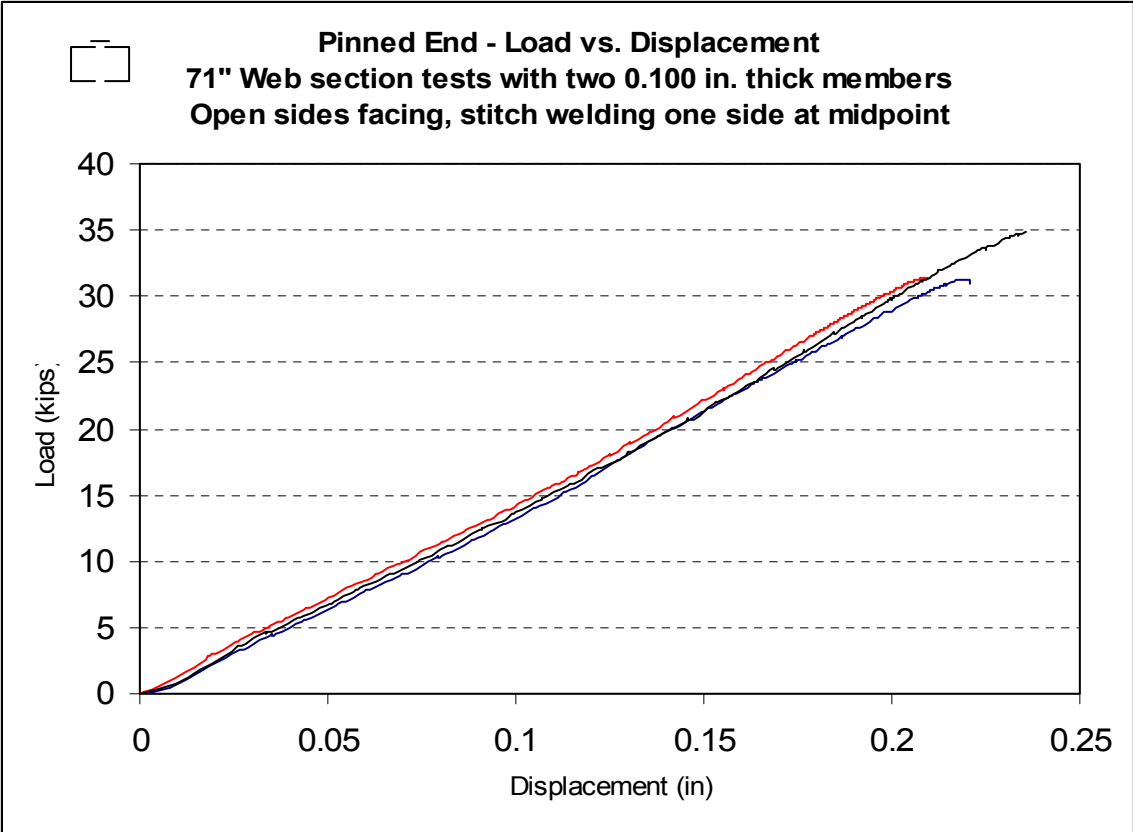


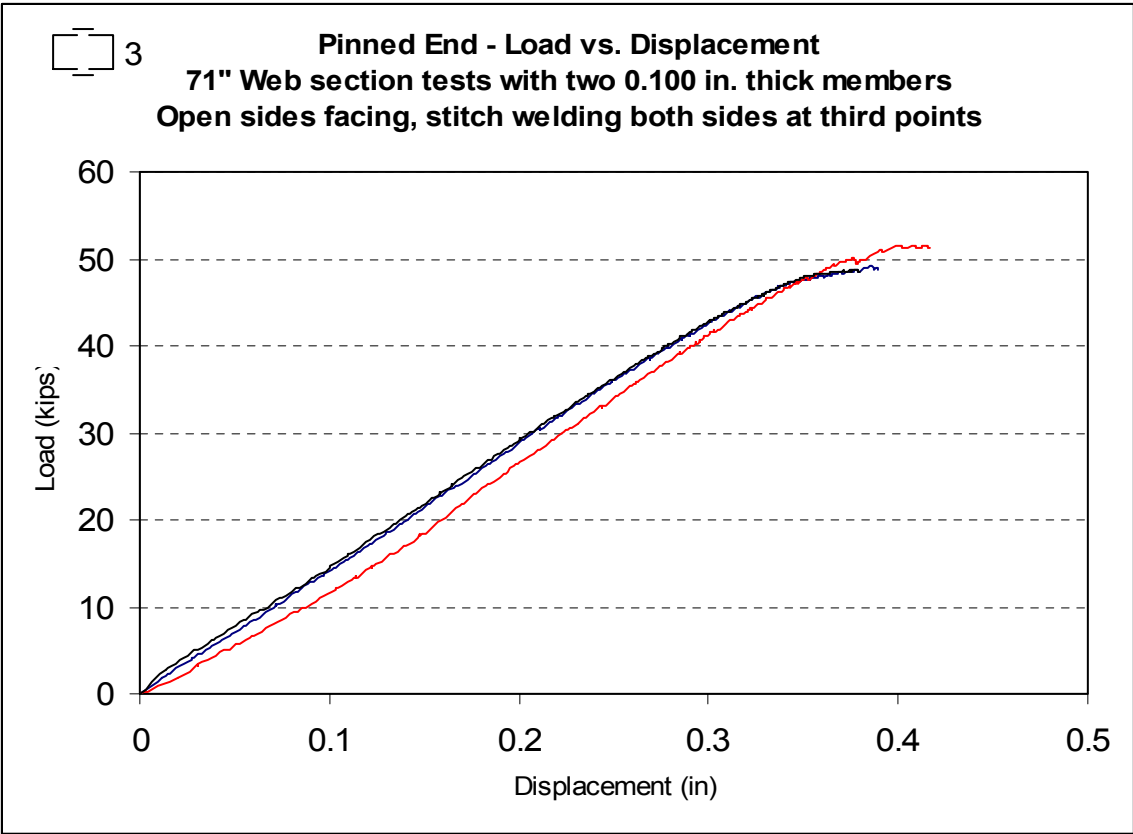
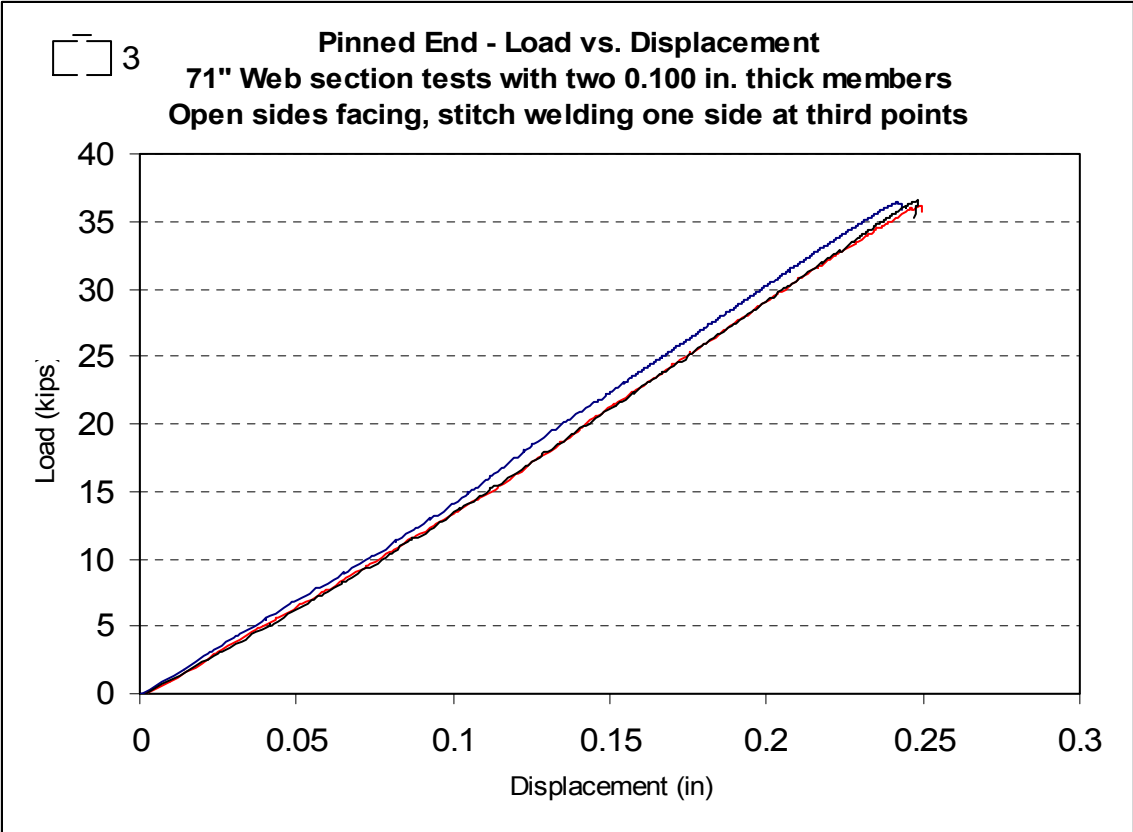


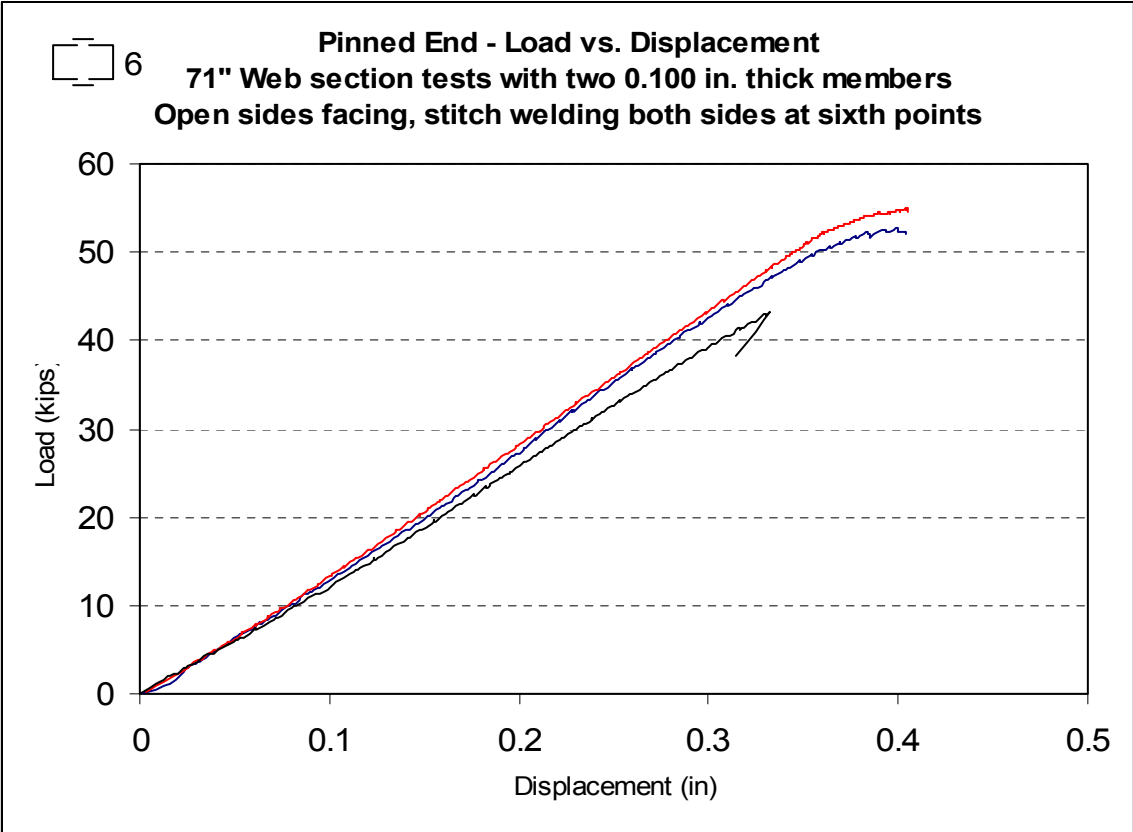
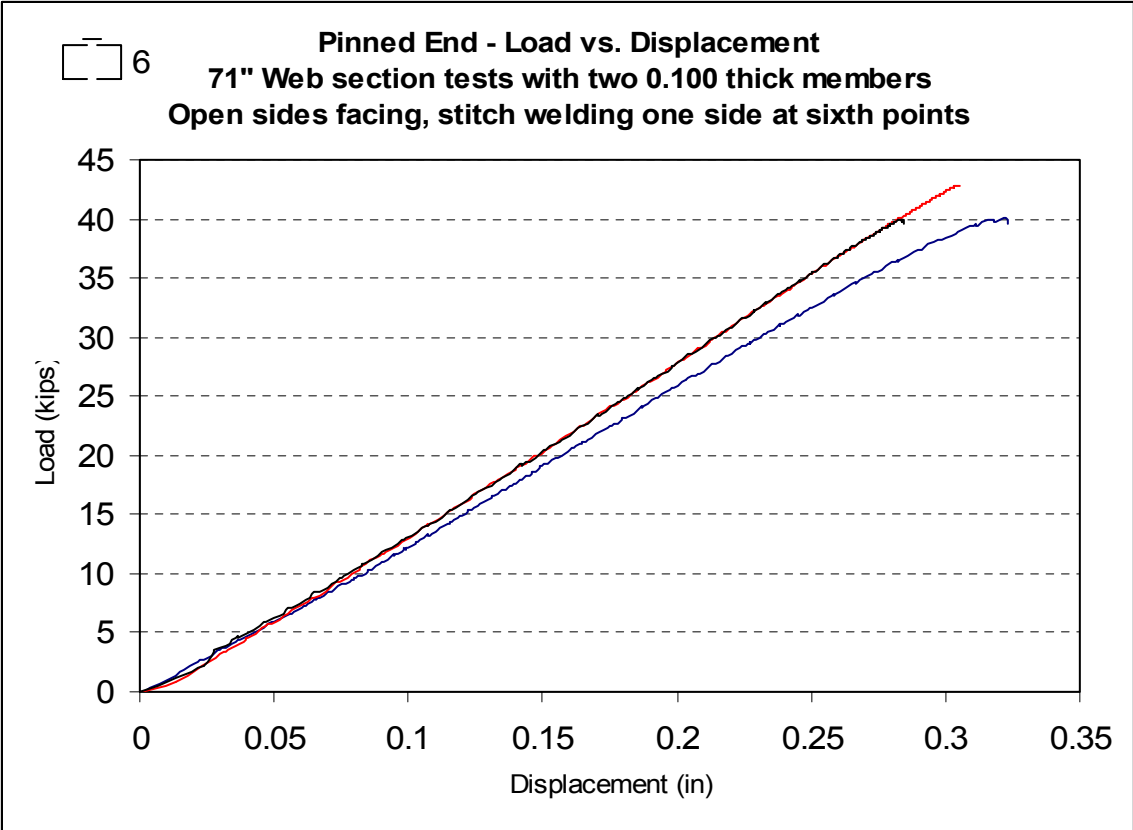












**APPENDIX I - 71" – 2 ½" Built-up Member, Pinned End
Load vs. Deflection Plots**

